



This work is protected by copyright and other intellectual property rights and duplication or sale of all or part is not permitted, except that material may be duplicated by you for research, private study, criticism/review or educational purposes. Electronic or print copies are for your own personal, non-commercial use and shall not be passed to any other individual. No quotation may be published without proper acknowledgement. For any other use, or to quote extensively from the work, permission must be obtained from the copyright holder/s.

**Volatile biomarkers emitted by cell cultures:  
headspace analysis using selected ion flow tube  
mass spectrometry, SIFT-MS**

---

**Thomas W. E. Chippendale**

Submitted for the Degree of Doctor of Philosophy

October 2012

Keele University

## Abstract

The work presented in this thesis was initiated in order to develop a non-invasive real-time gas phase analytical technique, based on selected ion flow tube mass spectrometry (SIFT-MS), for monitoring the progression of human cell cultures and the detection of microbial contamination in such cultures by monitoring and quantifying the emitted volatile compounds.

Fundamental SIFT experiments were performed to characterise the reactions of the SIFT-MS precursor ions ( $\text{H}_3\text{O}^+$ ,  $\text{NO}^+$  and  $\text{O}_2^{+\bullet}$ ) with several volatile compounds of potential value to biological research; a necessity for their quantification. The work has resulted in new methods for the quantification acetaldehyde and  $\text{CO}_2$  in gaseous samples.

The compounds present in the headspace of sealed cultures of six human cell types were analysed by SIFT-MS, the key finding being their consumption of the toxic volatile compound acetaldehyde from the media. Further experiments involved the addition of the enzyme aldehyde dehydrogenase inhibitors diethylaminobenzaldehyde and disulfiram to cultures of hepG2 (hepatocellular carcinoma) cells, when it was observed that consumption of acetaldehyde from the cultures/headspace was reduced, and in some cases, acetaldehyde was even produced due to the actions of the cellular alcohol dehydrogenase enzyme. Furthermore, the solvent dimethylsulphoxide was reduced to dimethylsulphide by the cells, which is known to occur *via* the enzyme methionine sulfoxide reductase. This process was retarded by the ALDH inhibitors.

The use of SIFT-MS for the detection of microbial infection in mammalian cell cultures was also explored. The volatile compounds emitted by *E. coli* (strain JM109), into the gas phase above two different culture media, were analysed using SIFT-MS. Further, the progression of a culture of this bacterium was monitored continuously over a 4-hour period. The findings of this research were then applied to the study of human cell cultures intentionally infected by *E. coli* bacterium, including cultures contained in a 1L bioreactor.

**Key words:** selected ion flow tube mass spectrometry; SIFT-MS; carbon dioxide; acetaldehyde; dimethyl sulphide; mesenchymal stem cells; aldehyde dehydrogenase; methionine sulfoxide reductase; *Escherichia coli*; microbial contamination

## Acknowledgements

First of all, I am extremely grateful to Professor David Smith for the constant advice and encouragement he has offered throughout the duration of this project, not least in the writing of this thesis. It is not possible to put into words how much he has improved my understanding of science in general, but I hope it will suffice to say that it has been an enormous privilege and pleasure to have worked with him, and his complete dedication to science has been of great inspiration throughout. I would also like to acknowledge that he participated in the vast majority of the SIFT-MS experimental work that is reported in this thesis.

His long-time colleague, and fellow pioneer of the SIFT-MS technique, Professor Patrik Španěl, has also offered a great deal of thoughtful advice during his visits Keele, for which I am grateful. I have been fortunate also to have been able to work with him on various experiments, some of which are reported in this thesis and have also resulted in several publications. I would like thank him particularly for arranging a short stay with his Mass Spectrometry research group at the J. Heyrovský Institute in Prague, which was an educational and enjoyable experience.

I am also grateful to my principal supervisor, Professor Alicia El Haj, who was always available when I was in need of direction or advice, particularly on the biological aspects of the project. I would also like to thank her specifically for encouraging me to participate in several conferences, including the Termis Meeting in Granada; for organising the bioreactor project (see Chapter 7); and for giving me the opportunity to contribute to a chapter in the book *Comprehensive Biotechnology*.

I am also grateful to have had the opportunity to collaborate with Dr. Josep Sulé-Suso and his group during this project and to participate in numerous experiments and discussions with them. I would also like to thank the other staff, post-doctoral researchers and PhD students at the Institute, particularly Bin Hu, who has been a great source of discussion and advice throughout this project, and initiated the work shown in Chapter 5.

Finally, I would like to acknowledge the advice and education on various issues that was given by my co-supervisors Professor Chris Hewitt and Dr. Karen Coopman of Loughborough University, particularly in the early stages of the project, as well as the useful discussion held with my fellow student Qasim Rafiq.

This project is a part of the EPSRC's Doctoral Training Centre (DTC) initiative.

## Contents

### List of Tables - 4 -

### List of Figures - 7 -

## 1. Introduction - 10 -

### 1.1. Motivations for the study - 11 -

### 1.2. Monitoring large scale cell cultures: current techniques and the PAT Initiative - 11 -

### 1.3. Gas/vapour phase analysis: cell culture applications - 13 -

#### 1.3.1. SIFT-MS, PTR-MS and GC-MS - 13 -

#### 1.3.2. Mammalian cell cultures - 15 -

#### 1.3.3. Microbial cell cultures - 16 -

### 1.4. Summary remarks - 17 -

## 2. Overview of the SIFT and SIFT-MS techniques - 18 -

### 2.1. Principle of operation - 18 -

#### 2.1.1. The SIFT technique - 18 -

#### 2.1.2. SIFT-MS for the quantification of trace gas compounds in humid air - 21 -

#### 2.1.3. Modes of operation - 22 -

#### 2.1.4. Sampling methods - 24 -

### 2.2. Applications of SIFT-MS: breath analysis studies - 25 -

#### 2.2.1. "Breath acetone concentration; biological variability and the influence of diet" - 25 -

#### 2.2.2. "Determination of the deuterium abundances in water from 156 to 10,000 ppm by SIFT-MS" - 28 -

## 3. SIFT ion chemistry studies in preparation for SIFT-MS analyses - 31 -

### 3.1. Introduction to the studies - 31 -

#### 3.1.1. SIFT-MS ion chemistry - 31 -

#### 3.1.2. "Selected ion flow tube, SIFT, studies of the reactions of $H_3O^+$ , $NO^+$ and $O_2^+$ with some biologically active isobaric compounds in preparation for SIFT-MS analyses" [107] - 33 -

#### 3.1.3. "Minimising the effects of isobaric product ions in SIFT-MS quantification of acetaldehyde, dimethyl sulphide and carbon dioxide" [108] - 34 -

### 3.2. Experimental - 37 -

#### 3.2.1. Compounds - 37 -

#### 3.2.2. SIFT analysis - 37 -

### 3.3. Analysis of MW 86u and 88u compounds: results and discussion - 38 -

#### 3.3.1. Binary rate coefficients for the MW 86u and 88u VOCs - 38 -

#### 3.3.2. Product ion distributions for reactions of MW 86u and 88u VOCs with $H_3O^+$ , $NO^+$ and $O_2^{+\bullet}$ - 39 -

### 3.4. Concurrent analyses of $CO_2$ , AA and DMS: results and discussion - 47 -

#### 3.4.1. Analysis of AA in the presence of $CO_2$ and DMS - 48 -

#### 3.4.2. Analysis of DMS in the presence of $CO_2$ and AA - 50 -

#### 3.4.3. Analysis of $CO_2$ in the presence of AA and DMS - 50 -

### 3.5. Summary remarks - 53 -

## 4. Headspace analyses of human cell cultures - 55 -

### 4.1. Materials and methods - 55 -

#### 4.1.1. Cell culture in tissue culture flasks - 55 -

#### 4.1.2. Cell culture in spinner flasks using microcarriers - 56 -

#### 4.1.3. Sample preparation - 56 -

#### 4.1.4. Headspace analysis - 57 -

#### **4.2. Results and discussion - 58 -**

- 4.2.1. Analysis of the headspace of cell culture media and supplements - 58 -
- 4.2.2. Interpretation of SIFT-MS mass spectra derived from the headspace of static cells cultures - 61 -
- 4.2.3. Quantification of VOCs present in the headspace of static cell cultures - 64 -
- 4.2.4. Effects of overnight incubation on cell viability - 66 -
- 4.2.5. Spinner flask cell cultures - 67 -

#### **4.3. Summary remarks - 69 -**

### **5. Acetaldehyde and dimethyl sulphoxide metabolism by cultured human cells - 71 -**

#### **5.1. Introduction. - 71 -**

- 5.1.1. Aldehyde dehydrogenase (ALDH) and the detoxification of acetaldehyde (AA) by human cells - 71 -
- 5.1.2. Methionine sulphoxide reductase A (MsrA) and the reduction of dimethyl sulphoxide (DMSO) in human cells - 73 -

#### **5.2. Experimental procedures - 75 -**

- 5.2.1. Theoretical model of AA metabolism - 75 -
- 5.2.2. Cell culture and application of ALDH inhibitors - 76 -
- 5.2.4. Headspace analysis - 77 -
- 5.2.5. Viability assay - 77 -

#### **5.3. Results - 78 -**

- 5.3.1. AA metabolism by hepG2 cells: theoretical and experimental results - 78 -
- 5.3.2. Neat AA added to hepG2 cell cultures - 80 -
- 5.3.3. Analysis of the culture medium headspace - 80 -
- 5.3.4. Inhibition of AA metabolism using DEAB and DSF - 81 -
- 5.3.5. Detection of DMSO reduction by human cells - 83 -
- 5.3.6. Inhibition of DMSO metabolism using ALDH inhibitors - 84 -
- 5.3.7. Headspace analysis of hMSC cultures treated with ALDH inhibitor compounds. - 85 -
- 5.3.8. Assessment of cell viability in hepG2 and hMSC cultures - 86 -

#### **5.4. Discussion - 88 -**

### **6. Headspace analyses of *Escherichia coli* cell cultures - 90 -**

#### **6.1. Experimental - 90 -**

- 6.1.1. Culture of *E. coli* cells and preparation for SIFT-MS headspace analyses - 90 -
- 6.1.2. Headspace analysis - 91 -

#### **6.2. Results - 92 -**

- 6.2.1. *E. coli* cultured in lysogeny broth - 92 -
- 6.2.2. *E. coli* cultured in high glucose DMEM - 94 -
- 6.2.3. Real-time monitoring of *E. coli* culture growth in DMEM medium - 96 -

#### **6.3. Summary and concluding remarks - 100 -**

### **7. Identification of microbial contamination in mammalian cell cultures using headspace analysis techniques - 102 -**

#### **7.1. Introduction - 102 -**

#### **7.2. Experimental - 103 -**

- 7.2.1. Sample preparation for headspace analysis - 103 -
- 7.2.2. Bioreactor culture using the CELL-tainer bioreactor® system - 103 -
- 7.2.3. Culture of *E. coli* (JM109) cells - 104 -
- 7.2.4. Gas/vapour phase analysis by SIFT-MS - 104 -

#### **7.3. Results - 105 -**

- 7.3.1. Bacterial and fungal infections in mammalian cell cultures - 105 -
- 7.3.2. Intentional *E. coli* infection of a bioreactor culture of human cells - 108 -

#### **7.4. Summary and discussion - 112 -**

**8. Summary, concluding remarks and recommendations for further work - 113 -**

*8.1. Summary - 113 -*

*8.2. Concluding remarks - 115 -*

*8.3. Suggestions for further work - 117 -*

*8.4 List of publications - 118 -*

*8.4.1. Book chapter - 118 -*

*8.4.2. Published journal articles - 119 -*

*8.4.3. Articles in press - 119 -*

**9. Bibliography - 120 -**

**Appendix A. .... Publications - 129 -**

*A1. Breath acetone concentration; biological variability and the influence of diet - 129 -*

*A2. Determination of the deuterium abundances in water from 156 to 10,000 ppm by SIFT-MS - 139 -*

*A3. Selected ion flow tube, SIFT, studies of the reactions of  $H_3O^+$ ,  $NO^+$  and  $O_2^+$  with some biologically active isobaric compounds in preparation for SIFT-MS analyses - 148 -*

*A4. Minimising the effects of isobaric product ions in SIFT-MS quantification of acetaldehyde, dimethyl sulphide and carbon dioxide - 158 -*

*A5. A study of enzymatic activity in cell cultures via the analysis of volatile biomarkers - 168 -*

*A6. Time-resolved selected ion flow tube mass spectrometric quantification of the volatile compounds generated by *E. coli* JM109 cultured in two different media - 178 -*

**Appendix B. .... Typical operating conditions of the SIFT-MS instrument - 189 -**

## List of Tables

- Table 1.** List of some modern analytical techniques and reported applications for the *in situ* monitoring of mammalian cell cultures. Adapted from Teixeira *et al.* [12]. - **12** -
- Table 2.** List of the primary (non-hydrated) product ion types derived from the reactions between different types of volatile reactant molecules and the SIFT-MS precursor ions,  $\text{H}_3\text{O}^+$  and  $\text{NO}^+$ . Reactions with the  $\text{O}_2^+$  precursor ion are not included because they tend to result in less predictable breakdown (fragmentation) patterns. Adapted from Smith and Španěl, 2011[36]. - **32** -
- Table 3.** SIFT-MS kinetics database entries for the quantification of carbon dioxide and acetaldehyde using the  $\text{H}_3\text{O}^+$  precursor ion [144, 146], and for the quantification of dimethyl sulphide using  $\text{NO}^+$  [80, 117], as derived prior to the present studies. These are displayed in the format compatible with the SIFT-MS software, with the  $m/z$  values of the precursor and product ions listed, followed by the calculated/experimentally-derived rate coefficient and f correction-factor. Further explanation about the f-factors can be found in Španěl *et al.*, 2006 [75]. - **36** -
- Table 4.** Rate coefficients (k), in units of  $10^{-9} \text{ cm}^3 \text{ s}^{-1}$ , for the reactions of  $\text{H}_3\text{O}^+$ ,  $\text{NO}^+$  and  $\text{O}_2^+$  with four isobaric compounds of molecular mass (m) 88u, and four of molecular mass 86u. The calculated collisional rate coefficients ( $k_c$ ) are presented in square brackets (same units as k). The polarisabilities ( $\alpha$ ) and permanent dipole moments ( $\mu$ ) [147], used to calculate  $k_c$  according to the formula derived by Su and Chesnavich [74], are also indicated for each compound. - **39** -
- Table 5.** The molecular formulae and  $m/z$  values of the product ions formed from the reactions of  $\text{H}_3\text{O}^+$ ,  $\text{NO}^+$  and  $\text{O}_2^+$  with eight VOCs, four with molecular weights (MW) of 86u and four of 88u, along with their branching ratios in percent, %. The primary product ions are given in bold, with the hydrates in parentheses, and unique product ions and underlined (see text). Ionisation energies of each compound in electron volts, are given in italics [131]. The data were obtained from the analyses of aqueous solutions of each compound, the approximate molar concentrations of which are also given. - **40** -
- Table 6.** Derived values of the humidity-independent association efficiency coefficients ( $A_{\text{eff}}$ ) and three-body rate coefficients (kMH +) for the formation of hydrates of the protonated compounds indicated, as formed by ligand switching and three-body association. Further information is given in the text. - **45** -
- Table 7.** SIFT-MS kinetics library entries presented in the format required in order to the SIFT-MS software to perform on-line calculations of the concentrations of diacetyl and acetoin using the  $\text{H}_3\text{O}^+$  or  $\text{NO}^+$  precursor ions. - **46** -
- Table 8.** SIFT-MS kinetics library entries for the determination of the concentrations of acetaldehyde (AA) and dimethyl sulphide (DMS) in humid samples using  $\text{H}_3\text{O}^+$  and  $\text{NO}^+$  reagent ions. Further explanation in text. - **49** -
- Table 9.** SIFT-MS kinetics library entries for the determination of the concentrations of  $\text{CO}_2$  in the presence of AA and DMS in humid samples using  $\text{H}_3\text{O}^+$  and  $\text{NO}^+$  reagent ions. - **51** -
- Table 10.** Summary of the human cell types used in the study, including the base media and supplements. Substance abbreviations are listed below the table. - **55** -
- Table 11.** The headspace concentrations, given in parts-per-billion by volume (*ppbv*) of various volatile compounds present in samples of neat DMEM (0%), DMEM with 10% v/v FBS, and neat FBS (100%), following a sealed incubation period of around 16 hours at 37°C. The analyses were performed using SIFT-MS operated in MIM mode using  $\text{H}_3\text{O}^+$ . - **60** -
- Table 12.** The headspace concentrations, given in parts-per-billion by volume (*ppbv*) of various volatile compounds present in samples of distilled water ( $\text{dH}_2\text{O}$ ), a 1 g/L glucose solution in water, neat DMEM (0%), DMEM with 10% v/v FBS, and neat FBS (100%), following a sealed incubation period of around 16 hours. Separate samples were incubated at either 37 °C or 70°C, as indicated, but all were held at 37°C during headspace analyses, which were performed using SIFT-MS operated in MIM mode using  $\text{H}_3\text{O}^+$  precursor ions. The DMEM and FBS samples analysed in these experiments originate from batches different from those that were analysed in [41]. - **60** -
- Table 13.** Single SIFT-MS measurements of the concentrations of methanol, acetaldehyde (AA), carbon dioxide, ethanol and acetone, given in parts-per-billion by volume (*ppbv*), in the headspaces of varying numbers of six different human cell types and one embryonic chick femur cell, ECFC, type. All analyses were



performed by operating SIFT-MS in MIM mode, employing  $\text{H}_3\text{O}^+$  as precursor ions. Details of these cells can be found in Table 10. All samples contained typical liquid and headspace volumes of 50mL and 100mL respectively, and measurements were performed following an overnight (16 hours) incubation period. The water vapour levels were between 3.5 and 4.5% in all experiments. - 65 -

**Table 14.** Concentrations of several volatile compounds (given in parts-per-billion by volume, *ppbv*) measured in the headspace of samples containing 50mL of complete DMEM medium alone (see Table 10), and medium containing approximately 25 million human mesenchymal stem cells, hMSCs. The analyses first took place following the usual overnight (~16 hours) incubation period, and then following a further 24 and 48 hours, as indicated. - 66 -

**Table 15.** Concentrations of methanol, acetaldehyde (AA), ethanol and acetone measured in the headspace of Cytodex-1 microcarriers contained in 15mL of PBS at a concentration of 2 g/L. - 68 -

**Table 16.** List of cell types whose emitted vapour compounds have previously been analysed using the gas phase analysis techniques SIFT-MS, PTR-MS and GC-MS. The effects of these cells on the AA level measured in the headspace relative to their respective medium controls are indicated. - 74 -

**Table 17.** Michaelis-Menton constants ( $K_M$ ) and maximum reaction velocities ( $V_{\max}$ ) for alcohol dehydrogenase- and aldehyde dehydrogenase- (ALDH-) mediated oxidation reactions of ethanol and acetaldehyde respectively.  $K_M$  values are given as liquid concentrations (M), as presented in the literature, and then converted to gas phase concentrations (*ppbv*), assuming the system is sealed and that Henry's Law applies. - 75 -

**Table 18.** List of the variables and starting conditions used to formulate the theoretical model of acetaldehyde (AA) consumption/production by hepG2 and CALU-1 cell culture headspaces *via* the ethanol metabolism pathway. The starting gas phase concentration AA for the CALU-1 experiments was obtained from [41] and that for the hepG2 cells were derived from averaging the experimental data derived in this study. The starting ethanol concentrations Henry's law coefficients ( $K_H$ ) for ethanol and AA at, obtained from [151, 156], were used to derive the apparent liquid phase concentrations at 37°C. - 76 -

**Table 19.** The concentrations of AA, given in *ppbv*, measured in the headspace of hepG2 cells which initially contained varying quantities of AA. The initial AA concentrations are the values measured above the media alone, following the same incubation period as the cells, and the final concentrations are those measured when  $2(10^7)$  cells were additionally present. The decline in AA concentration measured in the headspace was then used to calculate the rate of AA consumption per cell by applying the Henry's Law coefficient at 37°C [151]. - 80 -

**Table 20.** Single measurements of the concentrations of several common volatile compounds measured in the headspace of samples of non-treated (NT) DMEM medium, as well as medium containing 0.1% v/v DMSO (~14,000  $\mu\text{M}$ ) alone and with dissolved DEAB (200  $\mu\text{M}$ ) and DSF (20  $\mu\text{M}$ ). The mean and coefficient of variation (CV) are indicated for each compound. - 81 -

**Table 21.** The concentrations of AA, acetone and DMS, in parts-per billion by volume (*ppbv*), measured in the headspace above samples containing ~ $2(10^6)$  hepG2 cells in 25mL of DMEM medium, following resuscitation from liquid nitrogen and varying numbers of post-thaw PBS-washes. The concentrations of these compounds in the medium headspace when no cells are present are given in *italics*. - 83 -

**Table 22.** Concentrations of AA and DMS, given in parts-per-billion by volume (*ppbv*), measured in the headspace above typically  $5(10^6)$  hMSCs in 10mL of medium containing the ALDH inhibitor compounds DEAB and DSF. In this case the cells were pre-treated with the inhibitors for 24 prior to their transfer to the glass bottles which were incubated for a further 16 hours whilst sealed. Also shown are the concentrations of AA and DMS measured in the headspace of samples of non-treated (NT) cells and samples containing 0.1 v/v (~14,000  $\mu\text{M}$ ) DMSO solvent, without inhibitor compounds. The concentrations of AA and DMS measured in the medium alone, without cells were  $89 \pm 37$  and  $6 \pm 4$  *ppbv* respectively. - 86 -

**Table 23.** List of the precursor ions and the primary product ions together with their mass-to-charge ratio ( $m/z$ ) and those of their hydrates, as used for the compound analyses reported in this chapter. The importance of the selection of the precursor for the analysis of each compound is highlighted by the two studies of isobaric compound and isobaric product ions, as given in Chapter 3. Noted in parentheses in the right column are the  $m/z$  values of the  $^{34}\text{S}$  isotopologue ions, which constitute about 4.2% of the total signal for a particular compound per sulphur atom. - 92 -

**Table 24.** Concentrations of various compounds (in parts-per-billion by volume, *ppbv*) as measured by SIFT-MS in the headspace above different concentrations of growing cultures of *E. coli* JM109 in LB. The bacteria

were first cultured overnight in shaker flasks containing LB, resulting in a highly concentrated “stock” cell suspension. A volume of this suspension, indicated in the top row of the table, was then added to bottles containing fresh LB medium, so that the final volume was always 25mL. - 94 -

**Table 25.** Concentrations of various compounds (in parts-per-billion by volume, *ppbv*) as measured by SIFT-MS in the headspace above *E. coli* cultures in DMEM medium. The volume of concentrated “stock” *E. coli* suspension (in LB) added to the DMEM (final volume 25mL), is indicated in the top row of the table (see text). These *E. coli*/DMEM suspensions were incubated at 37°C without agitation in sealed 150mL glass bottles for around 16 hours prior to the analysis. - 96 -

**Table 26.** The concentrations (in *ppbv*) of some selected volatile compounds measured in the headspace above clean DMEM medium (10% v/v FBS, 2mM L-glutamine) and DMEM infected with the bacterium *C. testosteroni*. The data are shown in the paper presented in Appendix A7 [190]. - 108 -

**Table 27.** Typical values for selected working parameters of the *Profile 3* SIFT-MS instrument used throughout this study. - 136 -

## List of Figures

**Figure 1.** Block diagram summarising the layout of this thesis, with each of the blocks indicating the content of a chapter. - 10 -

**Figure 2.** Schematic of the *Profile 3* SIFT-MS instrument, as was used throughout this research. Key dimensions are indicated, and further details can be found in Table 17 in Appendix B. Adapted from Smith & Španěl, 2011 [36]. - 18 -

**Figure 3.** (a) An example  $\text{H}_3\text{O}^+$  spectrum showing the count rates of the ions detected by the downstream mass spectrometer of the SIFT-MS instrument during a direct breath exhalation, obtained using the Full Scan (FS) mode. The precursor ions used in the analysis and characteristic product ions, formed from the reactions of some common breath compounds with the  $\text{H}_3\text{O}^+$  precursor ions, are labelled. (b) A Multiple Ion Monitoring (MIM) mode profile, obtained using the  $\text{H}_3\text{O}^+$  precursor ion, showing the absolute concentrations of ethanol, acetone and acetaldehyde, given in parts-per-billion by volume (*ppbv*) present in two breath samples, which were directly exhaled into the instrument. The water vapour level is also given in % units, 1% being equivalent to  $10^7$  *ppbv*. The portion of each exhalation from which the concentration was derived is indicated by the shaded dashed boxes. The concentrations of the compounds analysed in the laboratory air, which was sampled before, between and after the breath exhalations, are as follows: water vapour 1.72%; acetaldehyde 4 *ppbv*; ethanol 621 *ppbv*; acetone 24 *ppbv*. - 23 -

**Figure 4.** (a) and (b): Histogram plots showing the distributions of breath acetone for two individuals (A and B respectively), measured using SIFT-MS employing the  $\text{H}_3\text{O}^+$  precursor ion over a period of several weeks during the mornings (post-breakfast). The mean values and their standard deviations (SD), and the median values are given in parts-per-billion by volume (*ppbv*). (c): Plot showing the dependence of the time of day on the concentrations of acetone measured in the breath exhalations of volunteers A (open circles) and B (filled circles). Adapted from Španěl *et al.*, 2011 [88]. - 27 -

**Figure 5.** SIFT-MS mass spectrum (ion counts per second, *c/s*, against mass to charge ratio, *m/z*) showing the presence of the isotopologues of the trihydrate of the  $\text{H}_3\text{O}^+$  ions, the relative count rates of which can provide the D/H ratio in water vapour. The derived values of  $R_{\text{liq}}$  (see text) for the spectral distributions, derived from analyses of the headspace of three deuterated water vapour samples, are given in parts-per-million by volume (*ppmv*). The scan was performed over a limited *m/z* range in order to obtain accurate analyses of the third  $\text{H}_3\text{O}^+$  hydrate, *viz.*  $\text{H}_3\text{O}^+(\text{H}_2\text{O})_3$ , and its isotopologues, as indicated. The third hydrate of  $\text{H}_3\text{O}^+$  present at *m/z* 73 and the isotopologues present at *m/z* 74 and 75 are labelled. - 29 -

**Figure 6.** Semi-logarithmic plot showing the count rates (in counts-per-second, *c/s*) of the primary (non-hydrated) precursor ions:  $\text{H}_3\text{O}^+$  (closed circles),  $\text{NO}^+$  (grey circles) and  $\text{O}_2^+$  (open circles), which were simultaneously injected into the flow tube of the SIFT-MS instrument in the presence of ethyl acetate vapour, introduced at varying flow rates (see text). - 38 -

**Figure 7.** SIFT-MS ‘composite’ mass spectra (ion counts-per-second, *c/s*, against mass-to-charge ratio, *m/z*), obtained using (a)  $\text{H}_3\text{O}^+$ ; and (b)  $\text{NO}^+$  precursor ions, showing the combined analyses of samples of  $\text{CO}_2$ , AA and DMS in humid air. - 48 -

**Figure 8.** Change of the relative count rate of  $\text{NO}^+\text{CO}_2$  with the humidity of the sample due to the ligand-switching reactions that occur with  $\text{H}_2\text{O}$ . The power law indicated can be used to account for this change and is implemented in the latest versions of *Profile 3* SIFT-MS software (Trans Spectra Limited, UK) using library entries presented in Table 9. - 52 -

**Figure 9.** SIFT-MS FS mode spectra (ion counts-per-second, *c/s*, against mass-to-charge ratio, *m/z*) of the headspaces of 50mL of DMEM supplemented with FBS (10%), antibiotic-antimycotic (1%) and L-glutamine (2mM), obtained using (a)  $\text{H}_3\text{O}^+$ ; (b)  $\text{NO}^+$ ; and (c)  $\text{O}_2^+$  precursor ions. The precursor and product ions are indicated with open and closed bars respectively. - 59 -

**Figure 10.** SIFT-MS mass spectra (ion counts-per-second, *c/s*, against mass-to-charge ratio, *m/z*) obtained using the  $\text{H}_3\text{O}^+$  precursor ion showing the headspace of glass bottles containing (a) DMEM medium (10% FBS, 1% antibiotic-antimycotic, 2mM L-glutamine) alone (repeated from Figure 9a for comparison); and (b) the same medium containing  $1(10^8)$  human mesenchymal stem cells (hMSCs) following 16-hours incubation at  $37^\circ\text{C}$ . Each of the labelled compounds are present in both spectra, but are indicated in separate spectra for clarity. - 62 -

**Figure 11.** Principal component analysis (PCA) plot (principal component 1 against principal component 2) showing the analysis of the data obtained from SIFT-MS mass spectra, derived from the headspace analyses of samples of DMEM alone, and DMEM containing hMSCs. The PCA analysis is based on the peak heights contained in spectra that were obtained using (a)  $\text{H}_3\text{O}^+$  and (b)  $\text{NO}^+$  precursor ions, over the  $m/z$  range of 10-120. - **63** -

**Figure 12.** Microscopy images (10x) showing hepG2 hepatocellular carcinoma cells following application of the Cellstain double stain, with live cells stained green and the nuclei of dead cells stained red. The samples were analysed (a) prior to and (b) following overnight incubation at  $37^\circ\text{C}$  inside sealed glass bottles. The images are adapted from [157]. - **67** -

**Figure 13.** The cell numbers measured over the course of a 24-day spinner flask culture (100mL working volume) of hMSCs attached to Cytodex-1 surface microcarriers (7 g/L). - **68** -

**Figure 14.** Plot showing the concentrations of AA, in parts-per-billion by volume (*ppbv*) measured in the headspace of (a) varying numbers of hepG2 cells in 15mL DMEM media and (b) CALU-1 cultures in 50mL of media in a study published prior to the start of the present project [41], following 16 hours incubation at  $37^\circ\text{C}$ . In both cases, the open circles indicate AA concentrations derived from SIFT-MS analyses while the solid lines represent the concentrations of AA predicted by a model based on Michaelis-Menton enzyme kinetics. In addition, the predicted concentrations of ethanol in the vapour phase are plotted using dashed lines (plotted on a different y-axis in (a)). The model assumes that the hepG2 cells each contain 6000 molecules of ALDH and 5000 molecules of ADH, and the CALU-1 cells each contain no ALDH and 1500 molecules of ADH. Note the logarithmic scale on the x-axis. Other assumptions and important values are listed in Table 2 and Table 3. - **79** -

**Figure 15.** Plots showing the mean AA concentrations ( $N=2$ ), given in parts-per-billion by volume (*ppbv*), measured in the headspace of cell cultures against (a) the DEAB concentration in the culture media; and (b) the cell number. In (a), each of the samples contained  $1.5(10^7)$  hepG2 cells, and all of the liquid samples were 15mL in volume. The short-dashed line in (a) indicates the concentration of AA that was measured in the liquid headspace. In (b) 20  $\mu\text{M}$  DSF (closed circles) is used as an inhibitor of ALDH, as well as 200  $\mu\text{M}$  DEAB. In both plots, the long-dashed lines are “eye ball” variations, following the experimental points. - **82** -

**Figure 16.** Plots showing the mean DMS concentrations ( $N=2$ ), given in parts-per-billion by volume (*ppbv*), measured in the headspace of hepG2 cell cultures against (a) the DEAB concentration in the culture media; and ((b) & (c)) the cell number. Note the changes in scales on the x-axes. - **85** -

**Figure 17.** Confocal microscopy images of hepG2 cells, following application of the Cellstain double stain, obtained (a) prior to and (b-d) following overnight incubation inside sealed glass bottles. The live cells are stained green while the nuclei of dead cells are stained red. The cells in (a) and (b) were not treated with ALDH inhibitors, whereas in (c) and (d) 200 $\mu\text{M}$  DEAB and 20 $\mu\text{M}$  DSF were added to the contained medium respectively. The results of ATPLite assays conducted on hepG2 (e); and hMSC (f), are also shown. The results were obtained following culture under normal conditions (non-treated; NT) or following 16 hours of treatment with 0.1% v/v DMSO, or with ALDH inhibitors: DEAB or DSF. The inhibitor concentrations are indicated on the x-axis where appropriate. The data is presented as the mean  $\pm$  standard error ( $N=8$ ). - **87** -

**Figure 18.** SIFT-MS spectra (ion counts-per-second, *c/s*, against mass-to-charge ratio,  $m/z$ ) obtained using  $\text{H}_3\text{O}^+$  precursor ions for the analysis of the headspace of (a) 25mL of LB culture medium and (b) a highly concentrated suspension of *E. coli* in LB following overnight incubation at  $37^\circ\text{C}$ . Only the major compounds are indicated. Dimethyl disulphide is identified by the abundance ratio of its characteristic isotopologue ions at  $m/z$  95 and 97 (see text). - **93** -

**Figure 19.** SIFT-MS mass spectra (ion counts-per-second, *c/s*, against mass-to-charge ratio,  $m/z$ ) obtained using  $\text{H}_3\text{O}^+$  precursor ions for the analysis of the headspace of (a) 25mL of DMEM supplemented with 10% v/v FBS and 2mM L-glutamine; and (b) 24mL of the same medium with 1mL of highly concentrated *E. coli* cells in LB medium following overnight incubation at  $37^\circ\text{C}$  inside sealed 150mL glass bottles. Also identified are the characteristic product ions of the compounds indicated. - **95** -

**Figure 20.** Plots showing the concentrations of water vapour, methanol, ethanol, acetaldehyde, hydrogen sulphide, methanethiol, acetone and propanol as they were monitored *via* real time SIFT-MS analyses above an open *E. coli* JM109 culture in a medium consisting largely of DMEM. The analyses were performed simultaneously using  $\text{H}_3\text{O}^+$  precursor ions. - **99** -

**Figure 21.** Schematic diagram of the CELL-tainer<sup>®</sup> bioreactor bag, displaying the gas inlet and exhaust lines and the sampling point for the hypodermic needle which was coupled directly to the SIFT-MS sampling line. - 105 -

**Figure 22.** SIFT-MS mass spectra (ion counts-per-second, *c/s*, against mass-to-charge ratio, *m/z*) each obtained using H<sub>3</sub>O<sup>+</sup> precursor ions showing the analyses of the compounds present in the headspace above (a) RPMI media infected with fungal cells; (b) DMEM:Ham's F-12 media infected with fungal cells; and (c) DMEM media infected with bacteria. The major volatile compounds that are elevated above typical culture media levels are indicated, with the measured concentrations given in parts-per-billion by volume (*ppbv*). - 106 -

**Figure 23.** SIFT-MS spectra (counts-per-second, *c/s*, against mass-to-charge ratio, *m/z*) obtained using H<sub>3</sub>O<sup>+</sup> precursor ions for the analysis of the headspace of (a) DMEM medium supplemented with 10% v/v FBS and 2mM L-glutamine; and (b) the same medium that had become infected with the bacterium *C. testosteroni*, contained inside sealed glass bottles. The major compounds and their product ions are indicated. Dimethyl disulphide (DMS) is again identified by the abundance ratio of its characteristic isotopologue ions at *m/z* values of 95 and 97, and hydrated isotopologue ions at *m/z* 113 and 115. The spectra are adapted from the paper presented in Appendix A7 [190]. - 107 -

**Figure 24.** SIFT-MS spectra (counts-per-second, *c/s*, against mass-to-charge ratio, *m/z*) obtained using H<sub>3</sub>O<sup>+</sup> precursor ions for the analysis of the sealed gas/vapour phase inside a sealed CELL-tainer<sup>®</sup> bioreactor bag containing 500mL of DMEM (10% FBS, 1% antibiotic-antimycotic, 2mM L-glutamine) and Cytodex-1 microcarrier beads at a concentration of 2 g/L, in the absence of human and microbial cells. - 109 -

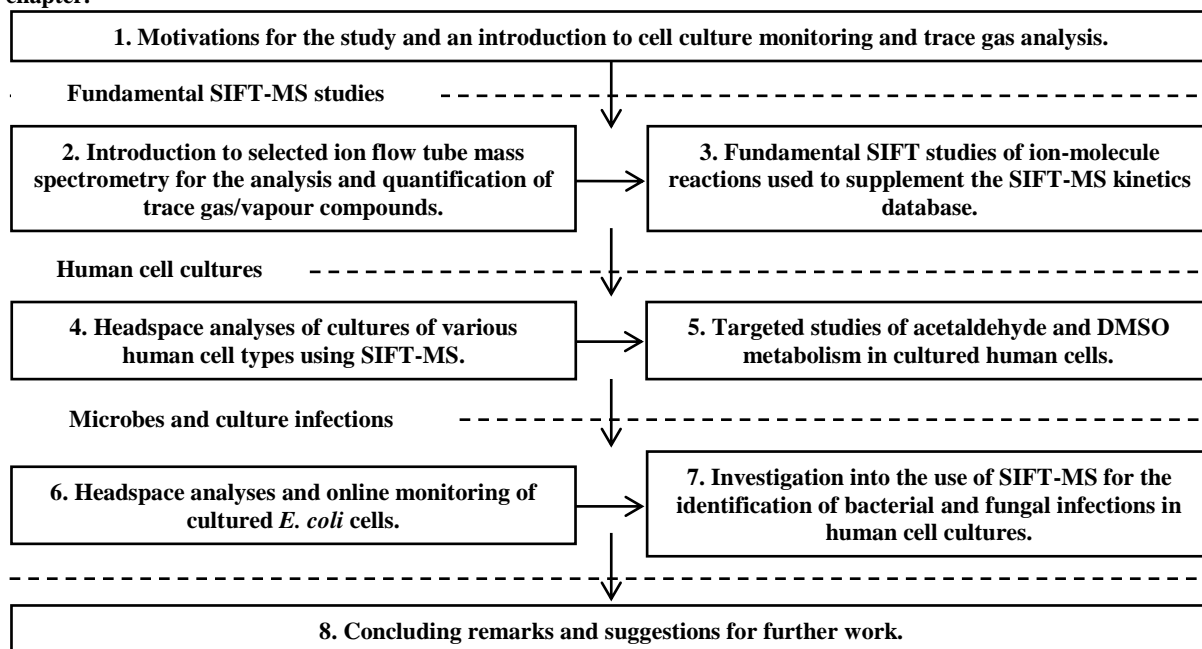
**Figure 25.** Cell counts of the hMSCs attached to the Cytodex-1 microcarrier beads present in the DMEM media of a CELL-tainer<sup>®</sup> bioreactor; obtained using the colourimetric assay, WST-8 (*N*≥6). - 109 -

**Figure 26.** Plot showing the online measurements of pH and the dissolved oxygen concentration inside a CELL-tainer<sup>®</sup> bioreactor bag containing hMSCs attached to Cytodex-1 microcarriers and *E. coli* JM109 in 1L of DMEM medium (10% FBS, 1% antibiotic-antimycotic, 2mM L-glutamine), and the headspace concentrations of ammonia, hydrogen sulphide, acetaldehyde and ethanol measured in the off-gas of the bioreactor culture at time intervals, without disturbing the culture, using SIFT-MS. Methanethiol was also detected and quantified, but the results are not shown for clarity (see text). On the x-axis is plotted the time, in hours, from which the 1L hMSC culture was intentionally infected with 40mL of stock *E. coli* JM109 bacteria (~5(10<sup>10</sup>) cells). - 111 -

## 1. Introduction

The following explanation of the thesis structure is given in reference to the block diagram presented in Figure 1, which, following the present Introduction section, displays the work as 3 separate but related areas of study. This begins with an introduction to selected ion flow tube mass spectrometry (SIFT-MS) and the analytical techniques involved, as well as some breath analysis studies (Chapter 2). This work was furthered by studying some of the ion-molecule reactions upon which quantitative SIFT-MS analyses are based (Chapter 3). This involved some unusual challenges and added some new biologically-relevant volatile compounds to the SIFT-MS database of compounds which can be identified and accurately quantified using this technique.

**Figure 1. Block diagram summarising the layout of this thesis, with each of the blocks indicating the content of a chapter.**



The focus then shifts to the analysis of the compounds present in the headspaces of some cultured human cell types (Chapter 4). During the course of these studies, it also became possible to analyse some specific metabolic processes, *viz.* the metabolism of toxic acetaldehyde and of the cryopreservant dimethyl sulphoxide in a human hepatocellular carcinoma cell line and human mesenchymal stem cells (Chapter 5). As part of the overall goals of the work, it was also desirable to develop headspace analysis methods to identify the presence of undesirable cells, particularly microbes which commonly infect routine cell cultures, and could prevent healthy integration of implanted cells or tissue. This is addressed first by studies of cultured *E. coli* cells, which also involved the first attempts at online monitoring of cultured cells for an extended period (several hours) using SIFT-MS (Chapter 6), and then in studies of mammalian cell cultures which were infected with

microbes, both for smaller- and larger- scale cultures (Chapter 7). Finally some concluding remarks and suggestions for further work are presented (Chapter 8).

### **1.1. Motivations for the study**

The present study was initiated with the goal of developing a new application for the established trace gas analysis technique, selected ion flow tube mass spectrometry (SIFT-MS), *viz.* monitoring the headspaces of large scale human cell cultures in real time; specifically of cells of importance to the field of regenerative medicine. The condition of the cells is of particular importance in this field because they may be applied directly to the body of a patient in the treatment of a particular disease. Characteristics such as viability, proliferative status and differentiation potential of the applied cells and the presence of unwanted cell types could affect the success of the treatment. The application of SIFT-MS, a real time, vapour phase analysis instrument, for the non-invasive, online monitoring of cell cultures applicable to regenerative medicine is therefore a desirable prospect, particularly if it could be used to indicate the aforementioned culture characteristics.

The remainder of this chapter reviews some of the methods currently used to monitor cell cultures, particularly at large scale, as well as the developing technologies, including gas/vapour phase analysis techniques, which may find utility in this area in the future.

### **1.2. Monitoring large scale cell cultures: current techniques and the PAT Initiative**

Large-scale cell culture processes form an important step in the commercial production of numerous biological substances, including foods, insecticides, organic chemicals and compounds of medical importance, such as antibiotics, vaccines and therapeutic proteins [1, 2]. The expansion of mammalian, microbial, insect or plant cells for these purposes are usually carried out in stirred-tank-type bioreactors, which may exceed 10<sup>5</sup> litres in volume [2]. As mentioned above, similar culture methods may also be employed in the production of future regenerative medicine therapies, and there is a growing literature on the subject [3-7]. In addition, the development of specialised bioreactors for the production of tissue-engineered constructs is also an expanding field [8-10].

In order for bioreactor-derived biological products to be commercially successful, the methods of production must be cost-efficient and able to meet the demands of the appropriate regulatory bodies. Techniques for monitoring and controlling the contents of these bioreactors are extremely important in satisfying these requirements. Industrial large scale cell cultures are routinely monitored using sterile *in situ* probes, which can

provide quantitative online measurements of process variables; commonly pH, temperature, headspace pressure and the dissolved oxygen concentration in liquid media [1, 2]. Feedback control loops are also commonly implemented so that automated responses are induced to ensure that the process variables remain within predetermined parameters. However, samples must also be removed from the culture in order to perform important offline analyses of variables including the cell number and medium composition [2]. Instruments may incorporate automated sampling systems to obtain samples of cells and media from a bioreactor at set time points. The Bioprofile FLEX (Nova Biomedical Corp.) is one such example, which can measure important culture parameters such as the number of cells, the partial pressures of headspace carbon dioxide and oxygen, and the concentrations of important dissolved species such as glucose, glutamine, ammonium ions and lactate ions [11].

**Table 1. List of some modern analytical techniques and reported applications for the *in situ* monitoring of mammalian cell cultures. Adapted from Teixeira *et al.* [12].**

Method	Comment	Cell line	Monitored components	Ref.
Near-infrared spectroscopy	Broad peaks; chemometrics needed for interpretation	CHO	Recombinant protein, Glc, Gln, Amm, Lac	[13]
		CHO	Glc, Gln, Amm, Lac	[14]
		HEK	Viable cells, Glc, Gln, Amm, Lac, pH	[15]
Mid-infrared spectroscopy	Higher resolution but costly hardware than near-IR; chemometrics needed for interpretation	CHO	Glc, Lac	[16]
2D fluorometry	Broad peaks; chemometrics needed for interpretation	NS0	Recombinant GFP	[17]
		BHK	Viable cells, recombinant protein	[18]
Dielectric spectroscopy	Only for biomass	CHO	Viable cells	[19]
		Hybridoma	Viable cells	[20]
Raman spectroscopy	At-line calibration required for quantification.	CHO	Viable cells, Glc, Gln, Amm, Lac, glutamate	[21]
Electronic nose	Off-gas monitoring; chemometrics needed for interpretation	CHO	Viable cells, recombinant protein	[22]

**Abbreviations:** CHO – Chinese hamster ovary; HEK – human embryonic kidney; NS0 – mouse myeloma; BHK – baby hamster kidney; Glc- glucose; Gln- glutamine; Amm- ammonia; Lac- lactate; GFP- green fluorescent protein. The hybridoma cell line is a fusion of normal mouse cells with mouse cancer cells [20].

These methods for monitoring large-scale cell cultures are well established and accurate, however, they are inherently invasive and some environmental changes cannot be detected in real time. These limitations mean that production processes cannot be easily optimised, and in the biopharmaceutical industry, any significant changes often have to be fully validated with new clinical trial procedures at great expense to the company [12]. These extra costs hinder improvements to production processes, and consequently such processes are very often run at low efficiencies [12, 23]. This has led to the introduction of the FDA-led Process Analytical Technology (PAT) initiative in 2004, which encourages companies to adopt modern analytical techniques for on- or at-line monitoring of cell culture, and other processes involved in the production of biological products [24]. Some of the technologies that have been studied as potential PATs are displayed in Table 1. The major benefit for companies adopting PATs into their production processes is the potential for continuously collecting data which



can be used to justify post-approval proposals for process changes, thereby helping to avoid some of the significant expenses that may be incurred if a new clinical trial becomes necessary [12].

Similar PAT-type techniques have also been applied to the analysis of cells and tissues of interest to regenerative medicine, which are not included in Table 1. Examples include the use of dielectric spectroscopy for monitoring neural differentiation of human mesenchymal stem cells (**hMSCs**) [25], and the determination of the viable numbers of stem cells cultured on microcarrier beads [26]. Fourier transform infrared spectroscopy and Raman spectroscopy have also been used to distinguish between multipotent hMSCs and pluripotent human embryonic stem cells [27] and a sophisticated multi-channel sensor system was reportedly used to monitor the progression of a haematopoietic stem cell culture [28]. In addition, magnetic resonance spectroscopy has been used for monitoring the growth, metabolism and viability of a tissue-engineered bioartificial liver [29]. Studies such as these demonstrate that key data can be obtained rapidly and non-invasively using spectroscopic techniques, which could enable the quality of a cultured batch of cells to be assessed and for timely decisions/interventions to be made in order to alter the condition of the culture.

### **1.3. Gas/vapour phase analysis: cell culture applications**

The analysis of gaseous samples is commonly performed using spectroscopic/mass spectrometric techniques or devices consisting of one or many electronic nose-type (electrochemical) sensors. Numerous applications have been demonstrated for these techniques including atmospheric monitoring [30, 31], the detection of explosives [32], analysis of foods [33] and breath analysis for disease diagnosis [34]. Relevant to the work described in this thesis, as mentioned above, there is a growing movement towards the use of advanced, non-invasive monitoring methods for cell culture processes relevant to biotechnology and regenerative medicine.

This section will begin with descriptions of three of the common gas/vapour phase mass spectrometry-based analysis techniques, these being the most relevant to the studies presented in this thesis. The application of these and other techniques to the analysis and online monitoring of the gas/vapour phase above culture cells will be discussed with reference to the published literature.

#### **1.3.1. *SIFT-MS, PTR-MS and GC-MS***

Selected ion flow tube mass spectrometry (**SIFT-MS**) is the analytical technique which is central to the present study. The underlying principles of SIFT-MS will be discussed in Chapters 2 and 3, and have been reviewed extensively previously [35, 36], but the essential points are described here. The instrument operates by

introducing a sample gas/vapour into a flowing helium carrier gas, where it is chemically ionized by a precursor ion species ( $\text{H}_3\text{O}^+$ ,  $\text{NO}^+$  or  $\text{O}_2^{+\bullet}$ ), generating product ions that are characteristic of the neutral sample compounds. The absolute concentrations of the **trace** volatile compounds, mostly volatile organic compounds (**VOCs**) that are present in the gaseous sample are calculated based on the count rates of the detected precursor and product ions. This method of analysis allows analyses of gaseous samples to be performed in real time, even of single breath exhalations [35, 36], obviating the requirement for sample collection. It is important to note that the major components of air, *viz.*  $\text{N}_2$ ,  $\text{O}_2$ , Ar etc., do not react with the chosen precursor ions, which have been selected for this reason.

A similar technique, known as proton-transfer reaction mass spectrometry (**PTR-MS**) has also been employed in the analysis of cell culture headspaces. This technique differs from SIFT-MS mainly because it employs greatly enhanced concentrations of, typically,  $\text{H}_3\text{O}^+$  precursor ions in order to perform the chemical ionisation procedure, and contains a drift tube that applies a voltage to the contained flowing ions [31, 37]. The main advantage of this set-up is an increased sensitivity, to parts-per-trillion by volume (*pptv*) levels for some compounds [36]. The major disadvantage is the increased levels of product ion fragmentation which occur in the drift tube, which increase false compound identification and the probability of overlapping product ions, resulting in false concentration measurements [36]. Also, the use of only  $\text{H}_3\text{O}^+$  precursor ions prevents the analysis of compounds which will not react or do so very slowly with  $\text{H}_3\text{O}^+$ , such as methane and carbon disulphide. The latter potential problem has been addressed recently with the development of PTR-MS instruments that also use  $\text{NO}^+$  or  $\text{O}_2^+$  sources [38].

Gas chromatography mass spectrometry (**GC-MS**) operates in an entirely different manner to SIFT-MS and PTR-MS. In short, a gaseous sample is introduced into a carrier gas of the GC-MS instrument that flows into a narrow capillary column that contains a stationary phase to which the VOCs bind. This column is located inside an oven which is used to gradually raise the temperature in a controlled manner, in order to elute the analyte compounds. The eluted compounds, separated by their elution time, are immediately detected downstream by a mass spectrometer that identifies each eluted VOC. Thus, the ion counts/abundance of each eluted VOC against time is obtained. The elution/retention time of each particular VOC is related to the physical/chemical properties of the molecule, as well as the physical/chemical properties of the stationary phase (commonly a silicon-containing polymer), and the experimental conditions (temperature profile, flow rate). Thus, one of the major benefits of GC-MS is that eluted compound identification is aided by two key pieces of information, *viz.* the elution time, and the obtained mass spectrum [39]. Sensitivity at the *pptv* level is possible,

but quantification is performed with reference to standard samples of the compound of interest, making quantitative measurements relatively time consuming. As a result, GC-MS is not a real time gas phase analytical technique.

### 1.3.2. *Mammalian cell cultures*

SIFT-MS has previously been employed in the analyses of the headspace of cultured human lung cell lines, including the first analyses of the gas/vapour phase above the lung cancer cell lines CALU-1 and SK-MES in 2003 [40]. The analyses were performed by suspending the cells in the relevant culture media, contained inside in glass bottles, which were purged of the laboratory air, sealed and incubated at 37°C for 16 hours. Both the CALU-1 and SK-MES cell types were found to produce the toxic compound acetaldehyde (AA) in proportion to the cell number; a result which was confirmed for the CALU-1 cells in a study published in 2009, while two additional non-tumourigenic lung cell lines, *viz.* NL20 epithelial cells and recently immortalised 35FL121 Tel+ fibroblast cells. The former epithelial cells were found to produce AA whilst the latter fibroblast cells were seen to consume AA from their culture media [41]. In addition, rates of carbon dioxide production were obtained in this study for all 3 cell types, which were roughly proportional to the rate of cellular CO<sub>2</sub> production expected from the cells of the human body.

PTR-MS has also been used to perform headspace analyses, of tissue culture flasks containing several cancerous and non-cancerous lung cell lines as well as an immortalized retinal pigment epithelium cell line, hTERT-RPE1 [42]. These experiments found that a product ion with a mass-to-charge ratio ( $m/z$ ) of 45 was clearly lowered in mass spectra obtained from the headspace analyses of the cancerous cell cultures, but not in those of the non-cancerous cell types. This product ion was tentatively assigned to protonated AA, which resonates with the findings of the aforementioned SIFT-MS studies [40, 41]. However, the finding that the cancer cells consumed AA does contrast with the SIFT-MS studies.

Several studies of the vapours emitted from cultures of various tumourigenic cell types were also performed using GC-MS, including a study of the vapours emitted from the lung cancer cell line CALU-1, which in this case were cultured in a 100mL fermenter [43]. The experiments revealed that the AA concentration was reduced in the CALU-1 cells compared to medium controls, in contrast to the SIFT-MS studies. The cells were reported to consume three other aldehyde compounds, as well as some ketones, alkenes and acetonitrile, and emit four branched alkane compounds. The headspace compounds of some other cancerous and non-cancerous cell lines have been analysed in several GC-MS studies [44-47].

The aforementioned studies have largely been concerned with the analysis of cell culture headspace under static conditions, the major focus being more upon identifying the volatile biomarkers produced by different cell types, relating these to the presence of cancer cells which could ultimately be used for their detection in human breath, blood or urine. The cell types in question have little relevance to the culture of cells for biotechnology or regenerative medicine. Studies of the gas phase above cell cultures for such purposes are infrequent, possibly due to the lack of available volatile biomarkers of mammalian cell growth. Of course oxygen and carbon dioxide are major exceptions, and their concentrations have been measured in the off-gas of 2L bioreactor cultures of Chinese hamster ovarian (CHO) cells using online zirconium dioxide- and infrared-based sensors for process monitoring and control purposes [48]. The results compared favourably to those obtained using traditional *in situ* probes, and were used to derive oxygen uptake rates and carbon dioxide production rates.

### 1.3.3. *Microbial cell cultures*

SIFT-MS has been employed in the study of several medically important microbes, cultured under various conditions. These include the emissions produced by the bacteria *Pseudomonas aeruginosa* (PA) which are known to colonise the lungs of the majority of cystic fibrosis patients [49]. Concentrations of hydrogen cyanide (HCN) were found to be present in easily measurable quantities in the vapour phase above the majority of cultured PA strains derived from the sputum of cystic fibrosis patients when cultured on agar plates [49, 50], indicating that HCN could be an important biomarker for early detection of PA colonisation. Recently, a second major biomarker of many PA strains has been detected using GC-MS, *viz.* methyl thiocyanate, and quantified using both GC-MS and rapid SIFT-MS measurements [51]. In addition to these PA studies, the emissions from medically important fungi [52] and bacteria have been analysed using SIFT-MS, including a study of bacteria that commonly infect blood [53, 54] the urinary tract [55].

PTR-MS has been used to conduct headspace analyses of PA and *Streptococcus milleri*, cultured on agar [56], and in a separate study of 3 bacteria (*Escherichia coli*, *Shigella flexneri* and *Salmonella enterica*) and one yeast cell type (*Candida tropicalis*) [57]. In the latter study, the cells were cultured in liquid media, contained inside sealed bottles, with the headspace of which was regularly sampled for analysis. A similar pilot study has been reported using chemical ionisation mass spectrometry, a similar analytical technique to SIFT-MS, in which the count rates of selected ions related to numerous compounds, including bacterial metabolites acetoin, diacetyl and AA (see Chapter 3), were monitored in the off-gas of a 2L bioreactor culture of *Bacillus subtilis*

bacteria cells over a period of 600 minutes [58]. The concentrations of the metabolites were seen to increase and then decline over the culture period.

Aside from aforementioned study of the volatile compounds emitted by PA using SIFT-MS and GC-MS methods [51], there is an extensive literature relating to the use of GC-MS for the study of the VOCs emitted from cultured microbial cells, which is described in review articles [59, 60]. Studies of particular relevance to the present work include the application of GC-MS for the early identification of microbial infections by analysing the VOCs produced in cultures of another bacterium, *Leuconostoc mesenteroides*, which is used industrially for the production of dextrane [61]. Similar methods were applied to the microbial infection of microalgae cultures, in which statistical techniques were applied to the derived GC-MS data in order to rapidly identify the infection [62]. Also, GC-MS was used to detect the presence of several different microbial cells when added to an animal cell culture [63].

#### **1.4. Summary remarks**

Efforts to develop non-invasive online techniques for monitoring large scale cell cultures have increased with the introduction of the FDA's Process Analytical Technology (PAT) Initiative. Regenerative medicine is a growing research/clinical field, and such monitoring techniques are potentially of greater importance in the production of the cell-based therapies related to regenerative medicine. The studies reported in the literature suggest that gas/vapour analysis technologies could provide non-invasive methods of monitoring the progression of human cell cultures and/or identifying the presence of unwanted cell types, including microbial infections in real time. The work presented in this thesis explores the use of selected ion flow tube mass spectrometry (SIFT-MS) for this purpose.

## 2. Overview of the SIFT and SIFT-MS techniques

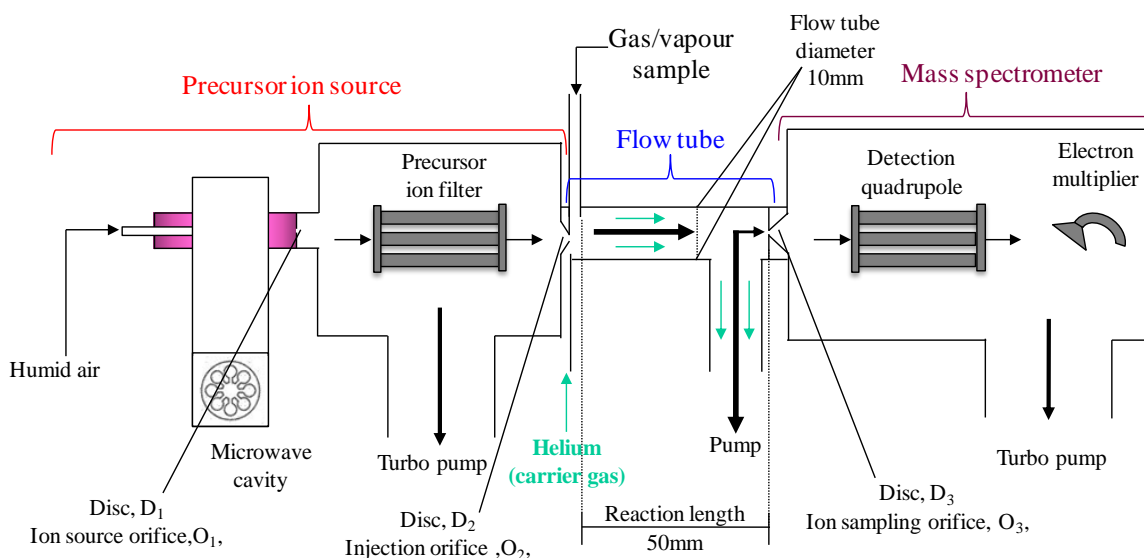
### 2.1. Principle of operation

The selected ion flow tube (SIFT) technique, was originally devised for the study of the kinetics of ion-molecule reactions, specifically the rate coefficients and the ion product distributions, primarily concerned with reactions that are considered to occur in the terrestrial atmosphere and cold interstellar clouds [64]. SIFT-MS is an extension of this technique, in which the underlying principles, and rate coefficients derived from SIFT experiments, are applied for the quantification of trace gas compounds in gaseous media; it is therefore useful to discuss the SIFT technique before moving on to SIFT-MS.

#### 2.1.1. The SIFT technique

The layout of a modern (*Profile 3*) SIFT-MS instrument, as is now used to perform SIFT experiments as well as SIFT-MS analyses at Keele University, is depicted in Figure 2. The following brief explanation of the SIFT technique, as well as SIFT-MS, will be given with reference to this figure; detailed descriptions are given in recent review papers [35, 36]. Also, the various dimensions and operating conditions of the specific instrument used throughout the studies presented in this thesis are summarised in Table 17, which is given in Appendix B.

**Figure 2.** Schematic of the *Profile 3* SIFT-MS instrument, as was used throughout this research. Key dimensions are indicated, and further details can be found in Table 17 in Appendix B. Adapted from Smith & Španěl, 2011 [36].



Considering that the SIFT is used to study ion-molecule reactions, a source of gaseous ions is required. In SIFT instruments, positive and negative ions are generated upstream by a gas discharge, and a quadrupole mass filter is used to select the ion specie of interest by its mass-to-charge ratio ( $m/z$ ) [65]. These selected ions,

termed precursor or reagent ions, are injected *via* a Venturi-type inlet orifice into the reaction flow tube, which contains an inert flowing carrier gas, usually helium, at a pressure of approximately 1 Torr [35, 36]. Upon entering the reaction flow tube, the swarm of cold ions form a Maxwellian velocity distribution according to the temperature of the carrier gas, typically 300K, and are convected along the flow tube by the helium carrier gas. A portion of the ions are sampled from the flow tube downstream via a pinhole orifice and enter the differentially pumped chamber of the analytical quadrupole mass spectrometer. The ions are separated according to their  $m/z$  values and detected and counted by an electron multiplier/pulse counting system [35, 36].

In order to determine the reaction rate coefficients and product ions formed in the reaction between a particular injected ion specie and a neutral analyte compound, denoted M, the latter is introduced into the reaction flow tube, either as a neat gas/vapour or diluted to a known concentration in an inert gas such as helium or nitrogen [36], through the sample inlet port of the instrument *via* a mass flow meter under controlled conditions. The ion/neutral reactions cause a decline in the precursor ion count rates as indicated by the downstream mass spectrometer/detection system, and the loss rate of the reagent ions is measured as a function of the flow rate of the analyte gas, which can be related to the number density of the analyte in the flow tube [36, 66]. The number of different product ions formed is dependent on the physical/chemical properties of the precursor ions and neutral compounds, as well as the humidity of the sample (further explanation and examples are given in Chapter 3), but often only one or two product ions result in significant (>1%) quantities [36]. The branching ratios of the product ions are determined at zero analyte flow in order to eliminate the potential distorting effect of secondary reactions of the product ions with the analyte gas [65].

In order to demonstrate the method used for the derivation of rate coefficients, it is useful to consider the following exothermic proton transfer reaction of  $\text{H}_3\text{O}^+$  precursor ions with M:



The following kinetics equation is then used to describe the time-decay of the number density of the  $\text{H}_3\text{O}^+$  precursor ions in the carrier gas,  $N_i$ :

$$\frac{dN_i}{dt} = - \left( N_i \cdot \frac{D_i}{\Lambda^2} \right) - (N_i \cdot k \cdot [M]) \quad (2)$$

The first term on the right side of this equation accounts for the diffusive loss of the precursor ions to the walls of the flow tube. This is characterised by the diffusion coefficient ( $D_i$ ) and the characteristic diffusion length ( $\Lambda$ ) which is dependent on the flow tube length and diameter [65, 67, 68]. The loss of precursor ions due to reaction (1) is described by the second term, where  $k$  is the rate coefficient for the reaction and  $[M]$  is the analyte molecule number density in the carrier gas. During analysis, the count rates of both the precursor ions

and product ions ( $\text{H}_3\text{O}^+$  and  $\text{MH}^+$  respectively) are monitored simultaneously at the downstream mass spectrometer at several different M flow rates [36, 66, 69]. Equation (2) can then be integrated in order to relate the count rate of  $\text{H}_3\text{O}^+$  precursor ions in the presence of M, denoted I, to the count rate in the absence of M, denoted  $I_0$  to give equation (3):

$$I = I_0 \cdot e^{-k \cdot [M]_t} = I_0 \cdot e^{-k \cdot [M] \frac{L+\epsilon}{v_i}} \quad (3)$$

Here,  $\epsilon$  is an end correction factor to the reaction length, L, which accounts for the mixing distance of the reactant gas to the carrier gas [36, 65, 66], and  $v_i$  is the linear velocity of the precursor ions along the flow tube. An absolute value of k can be derived from a semi-logarithmic plot of I against [M] [36]. Examples of this procedure are given in Chapter 3.

Obtaining k-values in this manner has been useful in the characterisation of reactions relevant to SIFT-MS trace gas analysis [70-72], but the method is dependent on the accurate measurement of the flow rate of M into the reaction flow tube, which is not always possible due to a lack of calibration data for flow meters, and the difficulties preparing accurate calibration mixtures caused by the sample adsorption of onto vessel surfaces, which occurs with most volatile organic compounds (VOCs) [36]. In order to bypass this problem, an alternative procedure has been adopted, which is based on the experimentally-justifiable assumption that exothermic proton transfer reactions, such as that shown in equation (1), occur at the gas kinetic (collisional) rate, characterised by the rate coefficient  $k_c$  [73]. It is possible to calculate  $k_c$  for such reactions provided the polarisability and dipole moment of the analyte molecule are known or can be estimated [74]. The hydronium ion,  $\text{H}_3\text{O}^+$ , is commonly used as a precursor ion for SIFT-MS analyses, and the  $k_c$ -values for its reactions with many organic compounds can thus be calculated when experimental data are difficult to obtain [36]. Two other precursor ions are commonly employed in SIFT-MS analyses, *viz.*  $\text{NO}^+$  and  $\text{O}_2^{+\bullet}$ , but it cannot be assumed that ion/neutral reactions involving these precursor ions will proceed at the gas kinetic rate, because the reaction processes sometimes proceed at less than unit efficiency [72]. In order to experimentally derive k-values for reactions involving these two ions, the three SIFT-MS precursor ion species:  $\text{H}_3\text{O}^+$ ,  $\text{NO}^+$  and  $\text{O}_2^{+\bullet}$ , are simultaneously injected into the flow tube, containing the carrier gas. The decay rates of the three precursor ions are then measured as the analyte gas/vapour is also introduced into the flow tube, which may be in the form of a dilute mixture in air at a known humidity. The relative decay rates of  $\text{NO}^+$  and  $\text{O}_2^{+\bullet}$  to that of  $\text{H}_3\text{O}^+$  will give proportional k-values for the reactions, relative to their respective  $k_c$  [36]. Several studies involving this method of deriving k-values for various compounds are presented in Chapter 3.



### 2.1.2. *SIFT-MS for the quantification of trace gas compounds in humid air*

SIFT-MS is an extension of the SIFT technique which allows the quantitative analyses of multiple trace gas/vapour compounds simultaneously, when present in dry or humid media. SIFT-MS experiments usually employ  $\text{H}_3\text{O}^+$ ,  $\text{NO}^+$  or  $\text{O}_2^{+\bullet}$  as precursor ions for the chemical ionisation of analyte compounds because these ions have been selected because they do not react significantly with the major components of air and breath, viz. nitrogen, oxygen, water, carbon dioxide and argon, but do react rapidly with most other compounds including most volatile organic compounds, VOCs. Thus, the precursor ions are not depleted significantly by an air sample and so the trace compounds can be analysed unhindered [35, 36].

It is clear from equations (2) and (3) that when the  $k$  is known for a reaction between an analyte molecule  $M$  and a particular precursor ion, then it is possible to determine the number density of the analyte molecules in the carrier gas  $[M]$ , by measuring the decline in the precursor ion count rate,  $I$ , as  $M$  flows into the carrier gas of the flow tube. If a mixture of analyte gases/vapours enter the flow tube then the reduction in  $I$  will reflect the net effect of all individual analyte gas/vapours, and quantitative analysis of the individual compounds present cannot be achieved by monitoring  $I$  only. However, if the analyte compounds each react to produce different product ions, then the count rates of these ions can also be monitored, allowing the individual compounds to be identified and quantified [35, 36]. This is an essential point which has allowed the development of SIFT-MS for the real-time detection and quantification of the trace gas compounds present in various complex mixtures, such as air and exhaled breath.

Given that only relative changes in the count rates of both the precursor and product ions are required for SIFT-MS analyses, it is important to consider that when the flow rate  $[M]$  of an analyte gas/vapour is small then the count rates of the product ions will be small and the fractional reduction in precursor ion counts will be immeasurably small (starting count rates of the precursor ions are typically between 1 and  $2(10^6)$  c/s). However, if the relatively low count rates of the product ions can still be accurately measured, then the number density of the characteristic product ions,  $[\text{MH}^+]_t$ , can be related to the number density of the precursor ions,  $[\text{H}_3\text{O}^+]$ , using equation (4), as follows:

$$[\text{MH}^+]_t = [\text{H}_3\text{O}^+] \cdot k \cdot [M] \cdot t \cdot D_e \quad (4)$$

As before,  $k$  is the reaction rate coefficient,  $[M]$  is the flow rate (number density) of the analyte molecules and  $t$  is the reaction time. The differential diffusion enhancement coefficient,  $D_e$ , additionally accounts for the mass-dependent rates at which the precursor and product ions diffuse to the walls of the reaction flow tube, affecting the relative number densities of the ions that reach the downstream ion sampling orifice to

the mass spectrometer (see Figure 2), thereby influencing quantitative analyses [75]. Another important consideration is the affects of mass discrimination against the heavier (larger  $m/z$ ) ions in the mass spectrometer. It happens that the opposing effects of differential diffusions and mass discrimination tend to cancel each other, but their combined effects must be incorporated in order to achieve accurate quantification of the concentrations of trace gas/vapour compounds by SIFT-MS analyses. These effects have been studied in detail previously [68, 76]. Further, the important involvement of the hydrated ions such as  $\text{H}_3\text{O}^+(\text{H}_2\text{O})_{1,2,3}$ ,  $\text{NO}^+(\text{H}_2\text{O})_{1,2}$  and  $\text{MH}^+(\text{H}_2\text{O})_{0,1}$ , is not considered in equation (4), but has been studied previously [77]. All of these factors are accounted for in the general equations, which allow the accurate derivation of  $[\text{M}]$  from the precursor and product ion count rates, and can be found in Španěl *et al.*, 2006 [75].

Calculating the concentration,  $C$ , of trace gas compound in a sample gas mixture requires the flow rates of the carrier gas and sample gas, denoted  $\phi_c$  and  $\phi_a$  respectively.  $C$  can then be calculated using equation (5):

$$C = [\text{M}] \cdot k_b \cdot \frac{T}{p} \cdot \frac{(\phi_c + \phi_a)}{\phi_a} \quad (5)$$

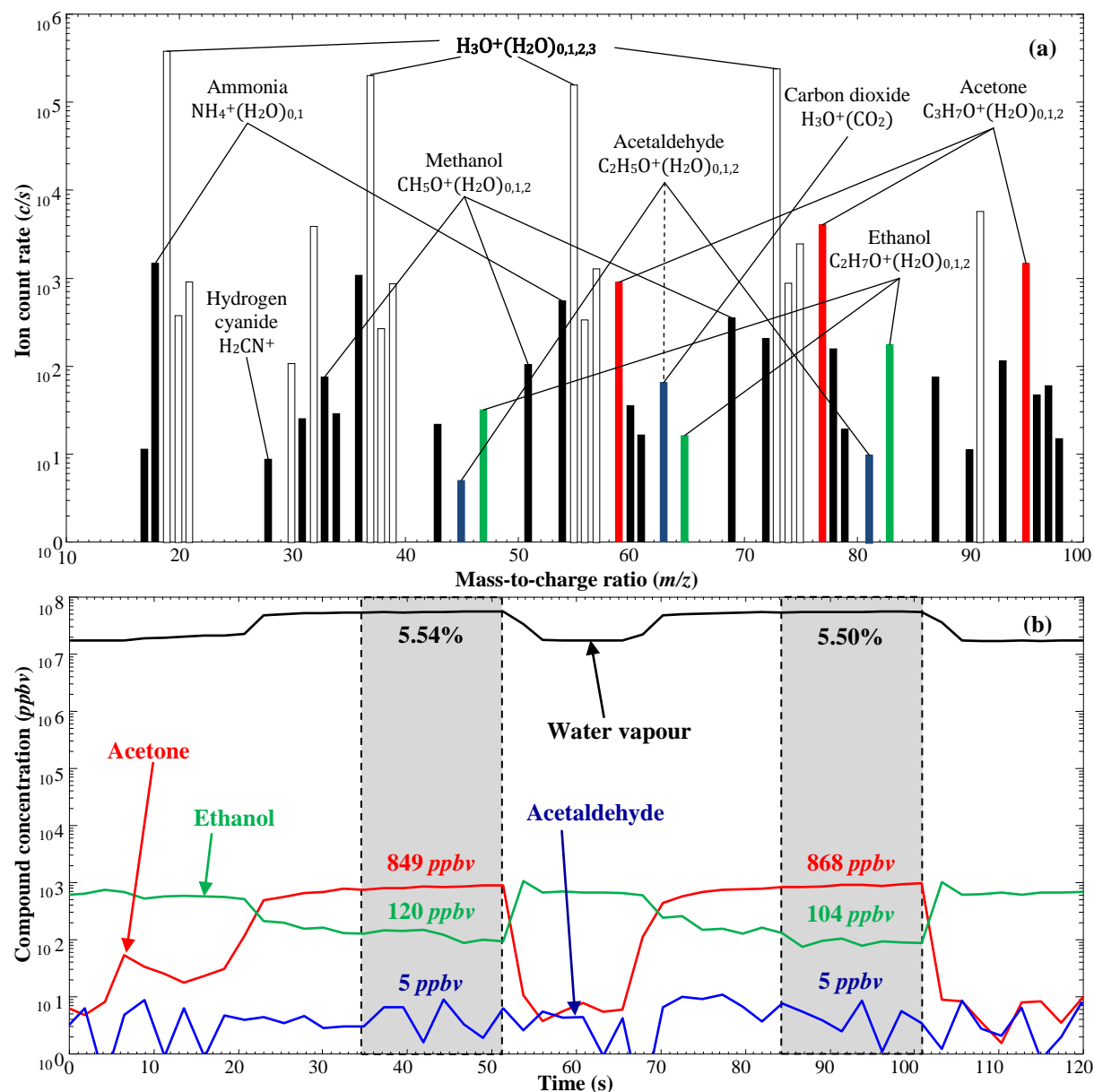
Here,  $k_b$  is the Boltzmann constant,  $T$  is the carrier gas temperature, and  $p$  is the total pressure inside the flow tube. Most of the variables in equations (4) and (5), as well as in the general equations for accurately deriving  $[\text{M}]$  [75], are either known constants, such as the flow tube dimensions, or are continuously monitored during the analysis, such as  $T$  and  $p$  (see Table 17 in the Appendix B for some typical values). These variables are incorporated into the SIFT-MS software which allows the real time quantification of particular trace gas compounds. Also, the rate coefficients for the reactions of these compounds with the precursor ions must be entered into a kinetics database, along with correction factors, denoted  $f$ , which can be used to account for specific kinetic processes which are sometimes necessary for accurate quantitative analyses.

The types of ion-neutral reactions that occur in SIFT-MS analyses are discussed in Chapter 3, including a list of some of the common product ions formed from  $\text{H}_3\text{O}^+$  and  $\text{NO}^+$  reactions in Table 2. Also some, now published, ion chemistry studies, which were undertaken to expand the kinetics database and involve some complicated analyses in which the product ions and values of  $k$  and  $f$  were derived for specific VOCs were derived, are detailed in Chapter 3.

### 2.1.3. Modes of operation

Two modes of operation can be utilised with SIFT-MS, *viz.* the Full Scan (**FS**) mode, and the Multiple Ion Monitoring (**MIM**) mode. These are described below in reference to the examples given in Figure 3.

Figure 3. (a) An example  $\text{H}_3\text{O}^+$  spectrum showing the count rates of the ions detected by the downstream mass spectrometer of the SIFT-MS instrument during a direct breath exhalation, obtained using the Full Scan (FS) mode. The precursor ions used in the analysis and characteristic product ions, formed from the reactions of some common breath compounds with the  $\text{H}_3\text{O}^+$  precursor ions, are labelled. (b) A Multiple Ion Monitoring (MIM) mode profile, obtained using the  $\text{H}_3\text{O}^+$  precursor ion, showing the absolute concentrations of ethanol, acetone and acetaldehyde, given in parts-per-billion by volume (*ppbv*) present in two breath samples, which were directly exhaled into the instrument. The water vapour level is also given in % units, 1% being equivalent to  $10^7$  *ppbv*. The portion of each exhalation from which the concentration was derived is indicated by the shaded dashed boxes. The concentrations of the compounds analysed in the laboratory air, which was sampled before, between and after the breath exhalations, are as follows: water vapour 1.72%; acetaldehyde 4 *ppbv*; ethanol 621 *ppbv*; acetone 24 *ppbv*.



In FS mode the downstream quadrupole mass spectrometer scans across a designated range of mass-to-charge ratios (*m/z*) for a chosen period of time, and the ion counts-per-second (*c/s*) are derived from the actual number of ion counts and the total sampling time for each *m/z* unit [36]. The output data is presented as a mass spectrum plot of *c/s* against *m/z*, an example of which is shown in Figure 3a. This method of data acquisition is

used for the determination of the product ions formed from the analysis of a particular VOC or an unknown mixture of compounds.

When operated in MIM mode the downstream mass spectrometer continuously accumulates only the ions relating to the selected  $m/z$  values of the precursor and product ions of interest. Combining these count rates with the flow tube pressure, temperature and other variables, including the necessary kinetics data for the ion-molecule reactions, enables the concentrations of desired compounds to be derived, as explained earlier, and monitored in real time. This can also be achieved in FS mode, but the use of MIM analyses increases the dwell time of the mass spectrometer on the desired ions, greatly increasing the accuracy of the measurements. An example MIM profile is shown in Figure 3b.

#### 2.1.4. *Sampling methods*

Analysis of gaseous compounds using SIFT-MS is simply achieved by opening the sample inlet port, allowing the air/gas/vapour sample to flow into the flow tube (see Figure 2) *via* the narrow capillary (0.2mm diameter) of the sampling arm. The capillary must be heated (typically to 70°C), in order to prevent condensation and adsorption of the analyte compounds, and calibrated to the correct flow rate so that accurate quantification of the individual compounds can be achieved, according to equations (4) and (5). As this narrow capillary is relatively short (<0.2m), a section of tubing with a wider internal diameter (0.5mm) connects it to the sample port, which does not restrict the flow rate significantly, and thus can be as long as 5m [78].

Breath exhalations through the mouth can be given directly into the instrument by exhaling at the entrance to the capillary [36]. Nose exhalations can be sampled in a similar manner, but should be aided by the use of a low flow pump [79, 80]. Alternatively, exhalations can be given into bags, which can then be sampled by puncturing with a hypodermic needle or by otherwise connecting the sampling arm to the bag contents. Headspace of bottles containing biological samples such as blood, urine or cultured microbial or mammalian cells can be sampled from sealed vessels by puncturing a septum using a hypodermic needle attached to the sampling arm. Upon introduction, the samples are immediately analysed, as described in previous sections. The rapid response of the instrument to the commencement and cessation of sampling is emphasised in the MIM analyses of two breath exhalations shown in Figure 3b.

## 2.2. Applications of SIFT-MS: breath analysis studies

SIFT-MS is capable of performing real time, quantitative analyses of numerous trace gas compounds simultaneously, in humid or dry air samples, with accuracy of typically parts-per-billion by volume (*ppbv*) levels. These features have frequently been exploited for the analysis of human breath samples, which can be delivered directly into the instrument, with the results immediately presented to the operator in the form shown previously in Figure 3. Numerous studies relating to the analysis of human breath by SIFT-MS for disease diagnosis physiological monitoring are present in the literature, including reference ranges for most common metabolites for significant cohorts of healthy volunteers [81-83], the detection of *Helicobacter Pylori* infection for the prevention of gastric ulcers [84], the early detection of *Pseudomonas aeruginosa* for the treatment of cystic fibrosis patients (see Chapter 1) [49-51], and the measurement of total body water in haemodialysis patients [85-87]. The non-invasive, real time, quantitative analyses that are possible using the SIFT-MS technique also have utility in other fields of study within the life sciences, including food sciences and environmental health and safety, references for which can be found in [36].

The majority of the work presented in this thesis relates to the use of SIFT-MS for the liquid headspace analysis of cultured human and/or bacterial cells. However, two studies were conducted as part of this thesis work, which relate to the use of breath analysis for clinical diagnosis and therapeutic monitoring, *viz.* the affects of diet on breath acetone [88], and the analysis of deuterium abundance in water vapour (this forming the basis for total body water measurements) [89]. The results of these studies have now been published, and so they are only summarised in the sections that follow; details are given in the published papers, copies of which can be found in Appendices A1 and A2.

### 2.2.1. “Breath acetone concentration; biological variability and the influence of diet”

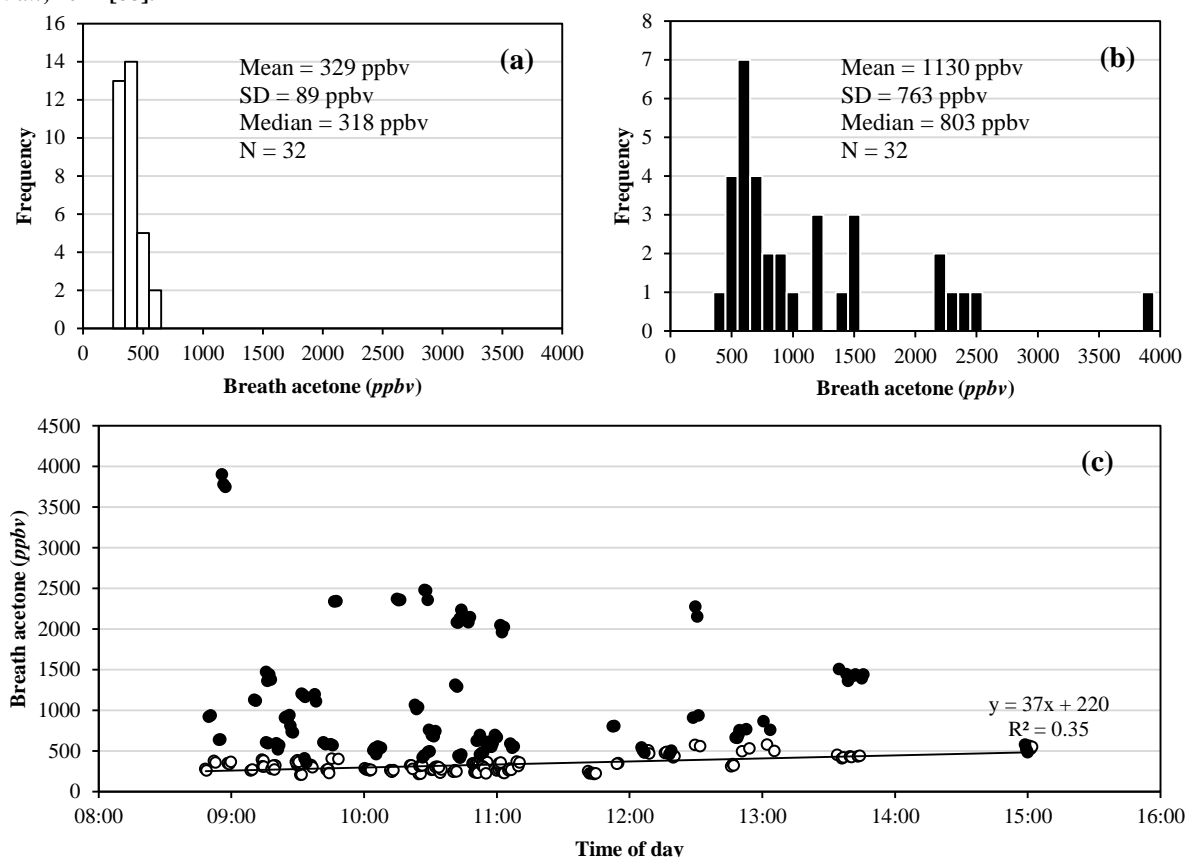
Acetone is the simplest ketone and a VOC which is present in the breath of all humans, as well as most mammals [90]. It is also emitted into the gas phase from human blood or urine, and is believed to be formed, at least in part, from acetyl coenzyme A *via* lipolysis, along with the other two ketone bodies acetoacetic acid and  $\beta$ -hydroxybutyric acid, usually termed acetoacetate and  $\beta$ -hydroxybutyrate [91]. The latter two compounds, however, do not appear so readily in the gas phase due to their tendency to dissociate into their ion forms in the bloodstream. Due to the volatility of acetone, and its relatively high concentration in the bloodstream, this VOC is easily detected in breath using SIFT-MS, and numerous studies of breath acetone have been conducted [81, 92, 93]. Elevated levels of breath acetone have commonly been observed in the exhaled breath of diabetes

sufferers, but increased blood acetone can be due to other factors, such as the length of the fasting period prior its measurement, and it is now well understood that breath acetone alone cannot be used as an indicator of diabetes [94-97]. The main purpose of this research mini-project was to address the unfortunate assumption that acetone alone can be an indicator of diabetes, which is still persists in the literature [98, 99], by providing further experimental support to the growing understanding that breath acetone concentrations can be influenced by a number of confounding factors even within the healthy population.

Exhaled breath was analysed directly with SIFT-MS as described in the ‘Sampling methods’ section earlier [35, 36], with quantitative data obtained using the MIM mode (see Figure 3b). Two SIFT-MS instruments were used to perform the studies which took place at Keele University and at the J. Heyrovský Institute in Prague. The ability of the instruments to accurately measure acetone concentrations was validated previously using standard mixtures [76]. All participants in the studies provided informed consent. Three experiments were reported which address some potential causes of variation in breath acetone concentration. These are summarised below:

(1) The acetone concentrations were measured in the breath exhalations of two healthy volunteers over a period of several weeks. The breath acetone distributions for volunteers A and B are shown in Figure 4a and 4b respectively. Clearly the distribution plot for volunteer A (70 years old male; body mass index (BMI) 25) is relatively narrow, while that of volunteer B (25 years old male; BMI 23) is much broader and more erratic. Neither individual believed that their diet was particularly variable during the course of these experiments. Figure 4c shows the breath acetone data plotted against the time at which the measurements took place for the two volunteers. As can be seen, for volunteer A there is a slow general increase in the breath acetone concentration over the several hours from the earliest measurements at around 08:45 towards lunchtime, which is due to a change in metabolic activity over the course of the morning, as the carbohydrates consumed for breakfast are depleted. However, for B there is such correlation, indicating that some other factors are behind the distribution shown in Figure 4b.

**Figure 4. (a) and (b): Histogram plots showing the distributions of breath acetone for two individuals (A and B respectively), measured using SIFT-MS employing the  $\text{H}_3\text{O}^+$  precursor ion over a period of several weeks during the mornings (post-breakfast). The mean values and their standard deviations (SD), and the median values are given in parts-per-billion by volume (ppbv). (c): Plot showing the dependence of the time of day on the concentrations of acetone measured in the breath exhalations of volunteers A (open circles) and B (filled circles). Adapted from Španěl *et al.*, 2011 [88].**



(2) Acetone concentrations were measured in the breath exhalations of eight healthy individuals (three males and five females; ages 18-42; BMI 24-32) following the consumption of a ketogenic meal. Baseline breath acetone concentrations were established for each individual using SIFT-MS in the evening prior to the experiment. Following an overnight fast (no breakfast) the breath acetone concentrations were measured again before each commenced a ketogenic diet (similar to the protocol used in [100]) which involved the consumption of 125g of whipping cream every 3h without protein supplement. The breath of each volunteer was analysed regularly over the course of around 7 hours. The breath acetone concentrations increased rapidly over the course of the day, with the final concentrations around a factor of 3 increased over that at the start of the day in all cases (figures shown in paper; see Appendix A1). The acetone increase showed no obvious correlation with BMI.

(3) The concentrations of acetone in the exhaled breath of two volunteers (28 years old female, BMI 26; 30 years old female, BMI 24) were measured using SIFT-MS over a period of 12 days, as they followed the low carbohydrate ketogenic diet that is commonly known as the Atkins diet (carbohydrate intake limited to  $20\text{g day}^{-1}$ , with only meat, fish, cheeses and vegetables allowed). Upon commencement of the diet, the breath acetone

concentrations immediately began to rise, and by day 2 had reached their approximate maxima. However, during the subsequent 10 days of the diet, breath acetone concentrations were highly varied for both subjects, but did remain approximately six to nine times above their pre-diet levels (figures shown in paper; see Appendix A1).

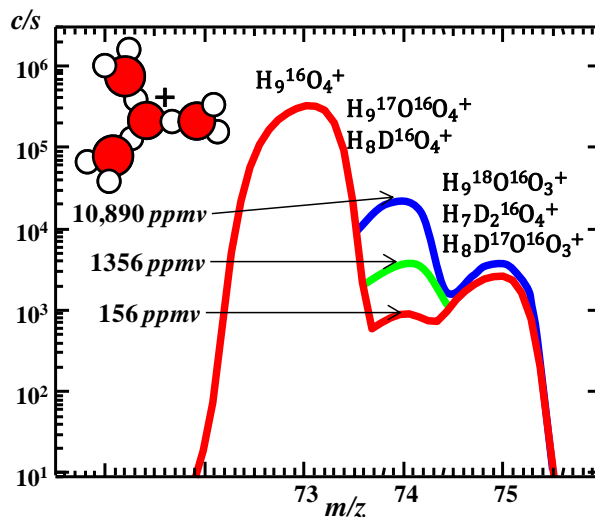
The results of this short study highlighted the breadth of inter-individual variation of acetone concentrations in exhaled breath, as well as that of intra-individual variation, at least in some cases. Further, the nutritional status/nature of the diet of an individual was shown to strongly influence breath acetone, with fasting, high fat and low carbohydrate diets all shown to cause elevations in the measured concentrations. These findings support the general sense of previous work. It should be noted that the apparent increase of breath acetone in diabetes sufferers, as indicated by a limited amount of data, is not greater than the diurnal increase that occurs in healthy people and by varying the diet. However, this does not necessarily imply that breath acetone variations could not be used by healthy individuals or diabetes sufferers, who can act as their own controls, to monitor control of their blood glucose. For screening for diabetes to be feasible, individuals would have to pay careful attention to their diet by stabilizing their nutritional input before breath analysis. Nevertheless, before the hypothesis that breath acetone can be used to diagnose and monitor diabetes can be totally abandoned, more studies on breath acetone in patients with both type-1 and type-2 diabetes are essential [101]. Such studies as these will also search for other breath metabolites (biomarkers), which, in combination with each other and acetone, might be more definite indicators of glycaemia [102].

#### 2.2.2. “Determination of the deuterium abundances in water from 156 to 10,000 ppm by SIFT-MS”

Over 10 years ago SIFT-MS [103] and flowing afterglow mass spectrometry (FA-MS) [104] techniques were developed for rapidly determining the deuterium (D) abundance in water vapour containing H<sub>2</sub>O, HDO and D<sub>2</sub>O molecules, which can then be related to the D abundance in the associated liquid water phase [104-106]. This has enabled the measurement of total body water *via* the analysis of HDO in breath following the ingestion of a known quantity of pure D<sub>2</sub>O, exploiting the isotope exchange that occurs between D<sub>2</sub>O and H<sub>2</sub>O molecules [85, 106]. However, these techniques were devised for the measurement of relatively low D abundances (<1000 ppmv) compared to those measured in the present study, and the underlying equations are not accurate when the abundance is >1000 ppmv due to the increased propensity for isotope exchange in which two H atoms can be exchanged by D atoms in the H<sub>3</sub>O<sup>+</sup>(H<sub>2</sub>O)<sub>3</sub> cluster (see Figure 5). The purpose of this work was to gain further understanding of D/H exchange in the H<sub>2</sub>O/HDO/D<sub>2</sub>O system and thereby to extend the use of the SIFT-MS and FA-MS analyses of the D abundance towards D/H ratios of 10,000 ppmv.



**Figure 5.** SIFT-MS mass spectrum (ion counts per second, *c/s*, against mass to charge ratio, *m/z*) showing the presence of the isotopologues of the trihydrate of the  $\text{H}_3\text{O}^+$  ions, the relative count rates of which can provide the D/H ratio in water vapour. The derived values of  $R_{1\text{liq}}$  (see text) for the spectral distributions, derived from analyses of the headspace of three deuterated water vapour samples, are given in parts-per-million by volume (*ppmv*). The scan was performed over a limited *m/z* range in order to obtain accurate analyses of the third  $\text{H}_3\text{O}^+$  hydrate, *viz.*  $\text{H}_3\text{O}^+(\text{H}_2\text{O})_3$ , and its isotopologues, as indicated. The third hydrate of  $\text{H}_3\text{O}^+$  present at *m/z* 73 and the isotopologues present at *m/z* 74 and 75 are labelled.



The measurement of the deuterium content in breath water vapour using SIFT-MS and FA-MS is based upon the ratio of the equilibrium ion densities at *m/z* 74 to *m/z* 75, which is denoted  $Q=[74]/[75]$ . The ions detected at these *m/z* values are composed of the isotopologues of the third water cluster of  $\text{H}_3\text{O}^+$ , as shown in Figure 5. The following equation has been used previously in routine FA-MS analyses [104, 105]:

$$Q = \frac{9R_1 + 4R_2}{4R_3} \quad (6)$$

Here  $R_2$  and  $R_3$  denote the known abundances of  $^{17}\text{O}$  (0.00387) and  $^{18}\text{O}$  (0.0198) respectively in ordinary water, and  $R_1$  denotes the abundance of D. In the present study, the  $R_1$  values were measured in the headspace ( $R_{1\text{vap}}$ ) of samples of known with a known liquid phase D abundance ( $R_{1\text{liq}}$ ). Using prepared mixtures of  $\text{D}_2\text{O}/\text{H}_2\text{O}$ , *i.e.* of known deuterium abundance, D/H, and accurate measurements using SIFT-MS, equation (6) was found to be accurate for  $R_1 < 0.001$  (*i.e.* for D abundances less than 1000 *ppmv*) according to an experimentally-derived plot of  $Q$  against  $R_{1\text{liq}}$  (the known liquid-phase D abundance), but when  $R_1$  exceeded 0.001, the results were inaccurate (see journal article in Appendix A2). Thus a correction factor was derived from a partial least squares fit of the experimental data points obtained from SIFT-MS data of the kind shown in Figure 5 as obtained for known mixtures of  $\text{D}_2\text{O}/\text{H}_2\text{O}$  that result in D/H ratios up to 10,000 *ppmv*, giving the following equation for  $R_1$  from experimentally measured  $Q$  values:

$$R_1 = \frac{4(R_3Q - R_2)/9}{1 - 0.0061(Q - 0.19)^2} \quad (7)$$

The numerator in this equation represents the solution of equation (6) with respect to  $R_1$  and the denominator is the parameterised correction factor obtained by a partial least squares fit of the data points, as mentioned (see article in Appendix A2). By applying this equation to Q data obtained in SIFT-MS experiments,  $R_{liq}$  values up to 10,000 *ppmv* can be determined, to a maximum uncertainty of around 3%.

### 3. SIFT ion chemistry studies in preparation for SIFT-MS analyses

#### 3.1. Introduction to the studies

The identification and accurate quantification of volatile compounds using SIFT-MS is based upon an understanding of the ion-molecule reactions that occur between the precursor ions ( $\text{H}_3\text{O}^+$ ,  $\text{NO}^+$  and  $\text{O}_2^{+\bullet}$ ) and the neutral analyte molecules (M) present in a gaseous sample, as discussed in detail in the previous chapter (see Section 2.1.2.). So that various volatile compounds can be analysed simultaneously in complex mixtures, numerous SIFT studies of ion-molecule reactions have been performed with the expressed purpose of characterising the essential reactions that are needed to extend the kinetics database library, which currently consists of over 250 volatile compounds, most of which are volatile organic compounds (VOCs), with molecular weights ranging from 17 to >200u. These studies have largely involved identifying the product ions formed from specific ion-molecule reactions, and then deriving the rate coefficients (k) for the reactions. However, quantification of some volatile compounds can be complicated by the presence of isobaric compounds or compounds that react with the precursor ions to form product ions that are isobaric, *i.e.* that have the same mass-to-charge ratio,  $m/z$ , as the product ions formed from M. Some examples of such complications are addressed in two SIFT-MS ion chemistry studies, which were published as a result of this work, namely:

- “Selected ion flow tube, SIFT, studies of the reactions of  $\text{H}_3\text{O}^+$ ,  $\text{NO}^+$  and  $\text{O}_2^+$  with some biologically active isobaric compounds in preparation for SIFT-MS analyses”. [107].
- “Minimising the effects of isobaric product ions in SIFT-MS quantification of acetaldehyde, dimethyl sulphide and carbon dioxide” [108].

These studies will be summarised in this chapter with reference to the full journal articles, copies of which are presented in Appendices A3 and A4.

##### 3.1.1. SIFT-MS ion chemistry

A list of the types of product ions that are commonly formed from  $\text{H}_3\text{O}^+$  and  $\text{NO}^+$  reactions with different types of analyte M is presented in Table 2. These are often predictable, particularly if the compound consists of a hydrocarbon chain or ring with a single functional group. As is shown in the table,  $\text{H}_3\text{O}^+$  reactions with M very often generate protonated analyte ions  $\text{MH}^+$ . This occurs in reactions where M has a proton affinity greater than that of water (691kJ/mol [109]), which is the case for most VOCs [36]. Crucially, these reactions invariably proceed at unit efficiency [36], *i.e.* where k is equal to the collisional rate coefficient  $k_c$ . This is a vitally

important aspect of the SIFT technique as  $k_c$  is usually calculable for reactions of M with  $\text{H}_3\text{O}^+$ , allowing  $k$  to be derived for the reactions of M with  $\text{NO}^+$  and  $\text{O}_2^{+\bullet}$  by relating the reduction of ion count rates of these precursor ions to that of  $\text{H}_3\text{O}^+$  when M is introduced. This is discussed in Chapter 2 and an example is given in the Results and discussion section of this chapter.

**Table 2. List of the primary (non-hydrated) product ion types derived from the reactions between different types of volatile reactant molecules and the SIFT-MS precursor ions,  $\text{H}_3\text{O}^+$  and  $\text{NO}^+$ . Reactions with the  $\text{O}_2^{+\bullet}$  precursor ion are not included because they tend to result in less predictable breakdown (fragmentation) patterns. Adapted from Smith and Španěl, 2011[36].**

Molecule (M)	$\text{H}_3\text{O}^+$ reactions	$\text{NO}^+$ reactions	Ref.
Alcohol	$\text{MH}^+$ ; $(\text{M} - \text{OH})^+$	$(\text{M} - \text{H})^+$ ; $(\text{M} - \text{OH})^+$	[110]
Diol	$\text{MH}^+$ ; $(\text{M} - \text{OH})^+$	$(\text{M} - \text{H})^+$ ; $(\text{M} - \text{OH})^+$	[111]
Ketone	$\text{MH}^+$	$\text{NO}^+\text{M}$ ; $\text{M}^{+\bullet}$	[112, 113]
Saturated aldehyde	$\text{MH}^+$ ; $(\text{M} - \text{OH})^+$	$(\text{M} - \text{H})^+$	[112, 114]
Unsaturated aldehyde	$\text{MH}^+$	$(\text{M} - \text{H})^+$ ; $\text{NO}^+\text{M}$	[112, 114]
Carboxylic acid	$\text{MH}^+$ ; $(\text{M} - \text{OH})^+$	$\text{NO}^+\text{M}$ ; $(\text{M} - \text{OH})^+$	[115]
Ester	$\text{MH}^+$ ; $(\text{M} - \text{OR})^+$	$\text{NO}^+\text{M}$ ; $(\text{M} - \text{OR})^+$	[115]
Ether	$\text{MH}^+$ ; $(\text{M} - \text{OR})^+$ ; $(\text{M} - \text{R})^+$	$(\text{M} - \text{H})^+$	[116]
Organosulphur	$\text{MH}^+$	$\text{M}^{+\bullet}$	[117]
Amine	$\text{MH}^+$ ; $(\text{M} - \text{H})^+$ ; $(\text{M} - \text{R})^+$	$\text{M}^{+\bullet}$ ; $(\text{M} - \text{H})^+$ ; $(\text{M} - \text{R})^+$	[118, 119]
Alkane	$\text{H}_3\text{O}^+\text{M}$	$(\text{M} - \text{H})^+$	[120]
Alkene	$\text{MH}^+$	$\text{M}^+$	[120, 121]
Monoterpene	$\text{MH}^+$ ; $(\text{M} - \text{R})^+$	$\text{M}^{+\bullet}$ ; $(\text{M} - \text{R})^+$	[122, 123]
Aliphatic halocarbon	$\text{MH}^+$ ; $\text{H}_3\text{O}^+\text{M}$ ; $(\text{M} - \text{X})^+$ ; $(\text{M} - \text{X})\text{OH}^+$	$(\text{M} - \text{X})^+$ ; $\text{M}^{+\bullet}$ ; $\text{NO}^+\text{M}$	[124, 125]
Aromatic hydrocarbon	$\text{MH}^+$	$\text{M}^{+\bullet}$	[120]
Aromatic halocarbon	$\text{MH}^+$ ; $(\text{M} - \text{X})^+$	$(\text{M} - \text{X})^+$ ; $\text{M}^{+\bullet}$ ; $\text{NO}^+\text{M}$	[124, 125]
Phenol	$\text{MH}^+$	$\text{M}^{+\bullet}$	[126]
$\text{H}_2\text{S}$ , $\text{HCN}$ , $\text{NH}_3$	$\text{MH}^+$	no reaction	[127-129]

The analyte molecules are denoted M and protonated molecules  $\text{MH}^+$ . Parent radical cations,  $\text{M}^{+\bullet}$ , and adduct ions,  $\text{NO}^+\text{M}$  and  $\text{H}_3\text{O}^+\text{M}$  are formed largely from charge transfer and ternary association reactions respectively [35, 130].

The reactions of  $\text{NO}^+$  with the molecule types presented in Table 2 are more varied. Charge transfer is one common reaction-type in which an electron is transferred from the molecule to the precursor ion, producing the parent radical cation  $\text{M}^{+\bullet}$ , and a nitric oxide molecule [36]. It is important to note that this can only occur when the ionisation energy of M is less than that of nitric oxide (9.26eV [131]). Other common reaction routes include hydride ion ( $\text{H}^-$ ) transfer, in which  $(\text{M} - \text{H})^+$  ions and  $\text{HNO}$  (nitroxyl) molecules are formed, and three-body  $\text{NO}^+$  association reactions, which form  $\text{NO}^+\text{M}$  product ions in the presence of the helium carrier gas.

The reactions of  $\text{H}_3\text{O}^+$  and  $\text{NO}^+$  with VOCs tend to form few (unhydrated) product ions, typically only one or two, which enables the quantification of multiple compounds simultaneously, facilitating the analysis of complex mixtures such as human breath or cell culture headspace [36]. The ionisation energy of molecular oxygen (12.06eV [131]) is greater than that of nitric oxide, and so  $\text{O}_2^{+\bullet}$  reactions typically occur *via* charge transfer. However, fragmentation commonly results from reactions with VOCs, and yields a greater number of product ions, which can complicate analyses of gas/vapour mixtures [36]. On the other hand,  $\text{O}_2^{+\bullet}$  is useful for the analysis of certain compounds which cannot be detected using  $\text{H}_3\text{O}^+$  and  $\text{NO}^+$ , such as  $\text{NO}$ ,  $\text{NO}_2$  [36] and

methane [132]. It is also a suitable ion for the quantification of ammonia, with which it reacts by charge transfer, forming  $\text{NH}_3^+$  [35, 36].

Considering that the major work presented in this thesis involves the analysis of biological samples, it is also important to recognise that these complex mixtures are often very humid, generally being incubated at  $37^\circ\text{C}$ , and saturated with an absolute water vapour content of around 6% (46 Torr). These elevated water vapour level result in partial conversion of the precursor ions to their hydrates,  $\text{H}_3\text{O}^+(\text{H}_2\text{O})_{1,2,3}$ ,  $\text{NO}^+(\text{H}_2\text{O})_{1,2}$  and  $\text{O}_2^+(\text{H}_2\text{O})_{1,2}$ , by sequences of three-body reactions [133]. These hydrated precursor ions can also react with M to produce hydrated product ions, such as  $\text{MH}^+(\text{H}_2\text{O})_{1,2,3}$  or  $\text{NO}^+\text{M}(\text{H}_2\text{O})$ . Such hydration reactions must be identified and accounted for in order for accurate quantification to be performed using SIFT-MS [36]; these will be discussed in later sections of this chapter.

### 3.1.2. *“Selected ion flow tube, SIFT, studies of the reactions of $\text{H}_3\text{O}^+$ , $\text{NO}^+$ and $\text{O}_2^+$ with some biologically active isobaric compounds in preparation for SIFT-MS analyses” [107]*

Distinguishing compounds of the same nominal molecular weight (MW) is a challenge in mass spectrometry, particularly when using SIFT-MS and similar techniques which do not involve the pre-separation of volatile compounds, as is the case with the widely-used gas chromatography mass spectrometry. One of the strengths of SIFT-MS for the analysis of complex mixtures is the ability to immediately switch between the use of  $\text{H}_3\text{O}^+$ ,  $\text{NO}^+$  and  $\text{O}_2^+$  for the chemical ionisation of the analyte compounds, which usually allows VOCs to be distinguished and simultaneously quantified, often when the compounds are isobaric [36]. An important study of this nature relating to the analysis of three isobaric VOCs with molecular weights (MW) of 60u, viz. propanol, acetic acid and methyl formate, has been published previously [134]. The results of this study included the identification of product ions specific to each of these VOCs, with propanol-specific product ions occurring in both  $\text{H}_3\text{O}^+$  and  $\text{NO}^+$  spectra, methyl formate-specific product ions only in  $\text{H}_3\text{O}^+$  spectra, and acetic acid-specific ions only in  $\text{NO}^+$  spectra [134].

A similar study is presented in this chapter, in which the reactions of four isobaric compounds with nominal MWs of 86u and four of 88u have been studied. The compounds of interest, their MWs and molecular formulae (structures may be viewed in Table 5), were as follows:

- MW 86u: 2,3-butanedione (**diacetyl**;  $\text{C}_4\text{H}_6\text{O}_2$ );  $\gamma$ -butyrolactone (**GBL**;  $\text{C}_4\text{H}_6\text{O}_2$ ); cyclopropane carboxylic acid ( $\text{C}_4\text{H}_6\text{O}_2$ ); allyl ethyl ether ( $\text{C}_5\text{H}_{10}\text{O}$ ).

- MW 88u: pyruvic acid ( $C_3H_4O_3$ ); n-butyric acid ( $C_4H_8O_2$ ); ethyl acetate ( $C_4H_8O_2$ ); 3-hydroxybutanone (**acetoin**;  $C_4H_8O_2$ ).

Acetoin and diacetyl are produced by bacterial cells [58] and are characteristic flavour compounds present in butter [135]. Acetoin is also emitted by biological substances, including ripe fruit, as are butyric acid and ethyl acetate [136-138]. Pyruvic acid, which commonly exists as the dissociated anion pyruvate when in solution, is an important compound in biochemistry. It is typically formed in mammalian cells from the breakdown of glucose *via* glycolysis, after which it may be used to produce energy, *via* the Krebs cycle or the formation of lactate, depending on the availability of oxygen, or it may enter another metabolic pathway [139]. Sodium pyruvate serves as an additional energy source in cell culture media, including Dulbecco's modified Eagle's medium (DMEM), which is featured prominently in later chapters. GBL is a natural component of wine [140] and acts as a prodrug for  $\gamma$ -hydroxybutyric acid *in vivo*, which has been shown to be an effective treatment for alcohol and heroin addictions [141]. However, GBL and  $\gamma$ -hydroxybutyric acid are also used as recreational drugs, which can be harmful and addictive [142]. It is clear that to be able to analyse these compounds by SIFT-MS would be of value; hence the reason for the study of the ion chemistry and the construction of kinetics database entries for them.

The SIFT-MS precursor ion-analyte molecule reactions have been reported previously for some of the above compounds in SIFT studies [112, 115, 116, 143], but these did not account for hydrated product ions. It is essential that these hydrates be included in the analysis in order for accurate quantification to be achieved, particularly when considering humid biological samples. Of the above eight compounds, those that had not been studied previously are cyclopropane carboxylic acid, pyruvic acid, and acetoin. This study was undertaken in order to enhance the SIFT-MS kinetics database so that these isobaric VOCs, each of which have some relevance in biology (with the exception of allyl ethyl ether), can be routinely identified and quantified in dry or humid samples. This work could be of importance to fields such as breath analysis, food science and botany, and could have some significance in the mammalian or microbial cell cultures, which are a major focus of this thesis.

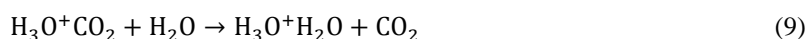
### 3.1.3. *“Minimising the effects of isobaric product ions in SIFT-MS quantification of acetaldehyde, dimethyl sulphide and carbon dioxide” [108]*

Quantification of volatile compounds with SIFT-MS requires knowledge of the rate coefficients for their reactions with the precursor ion. As mentioned above, the reactions usually occur at close to the collisional rate, with a rate coefficient ( $k_c$ ), which is typically of the order of  $10^{-9} \text{ cm}^3\text{s}^{-1}$ . However, there are numerous

exceptions, one of which is the reactions of carbon dioxide (CO<sub>2</sub>; mass 44u) molecules with H<sub>3</sub>O<sup>+</sup>, which is the most suitable precursor ion for CO<sub>2</sub> quantification by SIFT-MS. A method for quantifying CO<sub>2</sub> in humid air and exhaled breath has been described previously [144] which is based on the slow three-body association reactions with H<sub>3</sub>O<sup>+</sup>, in which adduct ions with mass-to-charge ratios (*m/z*) of 63 are formed as follows:



The H<sub>3</sub>O<sup>+</sup>CO<sub>2</sub> adduct ion is weakly bound relative to the hydrated hydronium precursor ion, H<sub>3</sub>O<sup>+</sup>H<sub>2</sub>O, and so carbon dioxide analysis is further complicated by rapid, exothermic ligand-switching reactions [145]:



Acetaldehyde (AA; C<sub>2</sub>H<sub>4</sub>O; MW 44u) reacts with H<sub>3</sub>O<sup>+</sup> to form primary protonated product ions with an *m/z* of 45, which also can hydrate to form C<sub>2</sub>H<sub>5</sub>O<sup>+</sup>(H<sub>2</sub>O) ions at *m/z* 63. This overlap creates an additional complication which must be corrected using the appropriate, calculated f-factors, as described in the aforementioned study [144], and shown in the kinetics database entry in Table 3. In turn, the H<sub>3</sub>O<sup>+</sup>CO<sub>2</sub>/C<sub>2</sub>H<sub>5</sub>O<sup>+</sup>(H<sub>2</sub>O) overlap also causes erroneously high AA measurements when both CO<sub>2</sub> and AA are present in the sample. A further potential problem for the accurate quantification of AA occurs when ethanol is also present, which is very often the case when analysing biological samples. This can arise due to the small quantities of O<sub>2</sub><sup>+</sup> ions (typically 1% of the total) which are inadvertently injected into the flow tube during H<sub>3</sub>O<sup>+</sup> analyses, and will react with ethanol largely by dissociative charge transfer, forming C<sub>2</sub>H<sub>5</sub>O<sup>+</sup> ions with *m/z* values of 45. Clearly, these overlap with the unhydrated, protonated AA product ions, which will lead to falsely high AA measurements, if not accounted for. Thus the levels of O<sub>2</sub><sup>+</sup> and ethanol are monitored during AA analyses, and the measurements are corrected using calculated f-factors [146]. The kinetics database entry used for AA concentration in the presence of CO<sub>2</sub> and ethanol is shown in Table 3.

AA was previously shown to react with NO<sup>+</sup> precursor ions largely by hydride ion transfer, as shown in equation (10) [112]:



Because reaction (10a) is relatively slow [112], any small contamination of *m/z* 43 ions will cause a comparatively large increase in the apparent AA concentration as measured utilizing reaction (10a). This will often occur as biological samples commonly contain acetone, and impurity O<sub>2</sub><sup>+</sup> ions will react with acetone to produce C<sub>2</sub>H<sub>3</sub>O<sup>+</sup> ions, also at *m/z* 43, which will interfere with AA quantification. Because of these potential complications, H<sub>3</sub>O<sup>+</sup> is the precursor ion of choice for AA quantification. As shown in reaction (10b) a second

minor product ion (25%) is also formed from the analysis of AA with  $\text{NO}^+$  product ions *via* slow three-body reactions, *viz.* the adduct ion  $\text{NO}^+\text{C}_2\text{H}_4\text{O}$  with an  $m/z$  of 74 (see Figure 7b). This has not been considered in previous studies of AA ion chemistry, but is considered in the present study. Carbon dioxide was also previously observed to react with  $\text{NO}^+$  by a slow three-body association reaction to form  $\text{NO}^+\text{CO}_2$ , which also has an  $m/z$  of 74 [145] (see Figure 7b). The analysis of this product ion as a second method of  $\text{CO}_2$  quantification is considered in this study.

**Table 3. SIFT-MS kinetics database entries for the quantification of carbon dioxide and acetaldehyde using the  $\text{H}_3\text{O}^+$  precursor ion [144, 146], and for the quantification of dimethyl sulphide using  $\text{NO}^+$  [80, 117], as derived prior to the present studies. These are displayed in the format compatible with the SIFT-MS software, with the  $m/z$  values of the precursor and product ions listed, followed by the calculated/experimentally-derived rate coefficient and  $f$  correction-factor. Further explanation about the  $f$ -factors can be found in Španěl *et al.*, 2006 [75].**

Carbon_dioxide( $\text{H}_3\text{O}^+$ )	Acetaldehyde( $\text{H}_3\text{O}^+$ )	Dimethyl_sulphide( $\text{NO}^+$ )
4 precursors	5 precursors	1 precursor
19 3.4e-15 1.0	19 3.7e-9 1.0	30 2.2e-9 1.0
37 3.4e-15 1.0	37 3.0e-9 1.0	1 product
55 3.4e-15 1.0	55 2.7e-9 1.0	62 1.0
73 3.4e-15 1.0	73 2.6e-9 1.0	
3 products	32 3.7e-9 1.0	
63 1.0	3 products	
45 -0.6	45 1.6	
81 -0.8	81 1.8	
	83 -100.5	

Dimethyl sulphide (**DMS**;  $\text{C}_2\text{H}_6\text{S}$ ; MW 62u) quantification can be performed using  $\text{H}_3\text{O}^+$  precursor ions, however this proceeds by protonation, forming  $\text{C}_2\text{H}_7\text{S}^+$  and its hydrate  $\text{C}_2\text{H}_7\text{S}^+(\text{H}_2\text{O})$  with  $m/z$  values of 63 and 81 respectively. Clearly these ions overlap in  $m/z$  with the product ions of the reactions of  $\text{H}_3\text{O}^+$  with  $\text{CO}_2$  and AA, as discussed (see Figure 7a), and so  $\text{H}_3\text{O}^+$  is often not usually suitable for DMS analysis. On the other hand,  $\text{NO}^+$  reacts rapidly with DMS by charge transfer, producing only  $\text{C}_2\text{H}_6\text{S}^+$  ions with  $m/z$  values of 62, and this is the preferred precursor ion for DMS analysis (see Table 3). In this case, there are few possibilities for overlaps with product ions formed from other volatile compounds, but one such compound is ethanthiol, which is isomeric with DMS [117]. This compound does charge transfer to generate overlapping  $m/z$  62 product ions, but also reacts partially by dissociative charge transfer and  $\text{NO}^+$ -association forming ions with  $m/z$  values of 29, 61 and 92, and so ethanthiol can be ruled out as a potential problem. Another potential problem may arise when oxygen is present in a sample to be analysed, since a three-body reaction can occur with  $\text{NO}^+$  in the presence of helium to form weakly bound adduct ions,  $\text{NO}^+\text{O}_2$ , which also appear at  $m/z$  62. In ambient air and human breath, molecular oxygen accounts for around 15-20% by volume, and under these conditions, the apparent concentration of DMS that is caused by the association reaction of  $\text{NO}^+$  with  $\text{O}_2$  would be around 10 *ppbv* [80], therefore actual DMS concentrations can be determined to reasonable accuracy in air and breath when they



exceed this value. Given that the oxygen concentration in biological samples, such as the cell cultures analysed in the work presented in later chapters, is unlikely to greatly exceed that present in human breath, the effects of oxygen on the apparent DMS concentration can be considered to be similarly small.

The presence of CO<sub>2</sub> and AA in a sample mixture does not prevent the quantification of DMS with NO<sup>+</sup>, but falsely high measurements of CO<sub>2</sub> and AA concentrations will be obtained using H<sub>3</sub>O<sup>+</sup> when DMS is present. As will be shown in later chapters, this can occur in cultured bacterial and human cells. Hence, the focus of this study was to address this problem by constructing new kinetics database entries so that these three compounds can be simultaneously quantified using SIFT-MS.

## 3.2. Experimental

### 3.2.1. Compounds

The two groups of four isobaric compounds (MW 86u and 88u), viz., 2,3-butanedione (diacetyl),  $\gamma$ -butyrolactone, cyclopropane carboxylic acid, allyl ethyl ether, pyruvic acid, n-butyric acid, ethyl acetate and 3-hydroxybutanone (acetoin), as well as acetaldehyde (AA) were all purchased from Sigma (UK) and the carbon dioxide from BOC (UK). Aqueous solutions were formulated inside 150mL glass bottles, when required, and sealed with rubber septa. The temperature of the samples was raised to 37°C using a water bath or incubator when required, although the experiments in which the MW 86u and 88u compounds were analysed took place with the samples kept at room temperature (20°C). DMS was obtained from culturing hepG2 hepatocellular carcinoma cells (see Chapters 4 and 5) in 25mL of a medium composed of Dulbecco's Modified Eagle's Medium (DMEM; Biosera, UK) with 10% v/v foetal bovine serum (Lonza, UK), 10 U/ml antibiotic-antimycotic (Biosera, UK), 2mM L-glutamine (Lonza, UK) and 0.1% v/v dimethyl sulphoxide (DMSO; Sigma, UK). Briefly, the cells were suspended in the media inside a sealed glass bottle and incubated overnight at 37°C. See Chapter 4 for more details on the cell culture process.

### 3.2.2. SIFT analysis

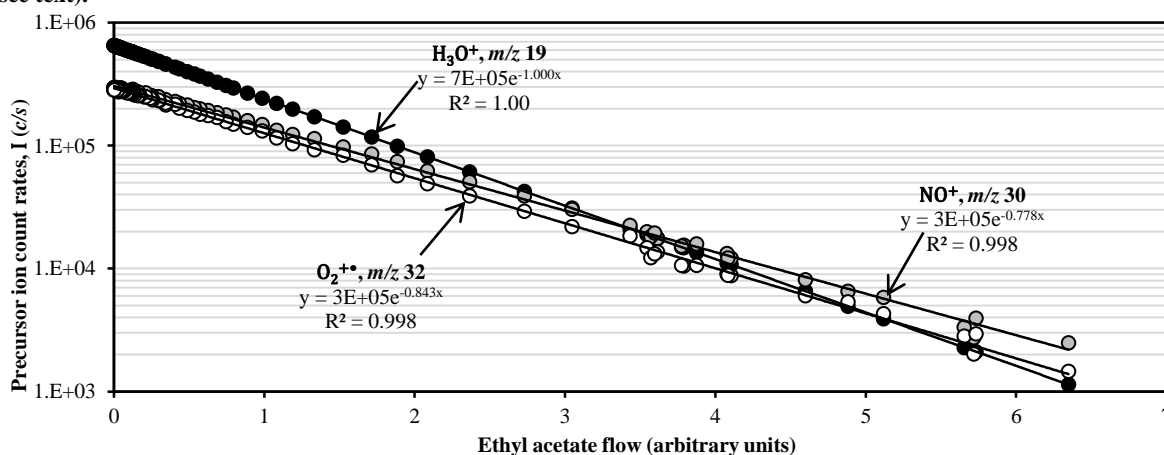
The SIFT technique and the *Profile 3* SIFT-MS instrument (Instrument Science, Crewe, UK) used to conduct the analyses were described in the previous chapter, and further details can be found in recent published review articles [35, 36]. The neat vapours of the MW 86u and 88u compounds could be sampled directly from their supplied containers by simply holding the solid or liquid sample compound close to the inlet of the sampling arm allowing the vapour to flow into directly to the flow tube of the SIFT-MS instrument (see Chapter 2).

### 3.3. Analysis of MW 86u and 88u compounds: results and discussion

#### 3.3.1. Binary rate coefficients for the MW 86u and 88u VOCs

In order to derive rate coefficients for the reactions of the MW 86u and 88u isobaric compounds with the available precursor ions, the resolution of the upstream mass quadrupole was reduced so that all three of the SIFT-MS precursor ions ( $\text{H}_3\text{O}^+$ ,  $\text{NO}^+$  and  $\text{O}_2^{+\bullet}$ ) were simultaneously injected into the flow tube. The sample vapour was then introduced through the sample port and the effective flow rate of the analyte molecules into the flow tube was lowered by simply moving the solid/liquid sample away from the opening of the sampling arm. This ensured a sufficiently large flow of the vapour to deplete the precursor ion count rates by at least one order of magnitude. The decline in the count rates (denoted  $I$ ) of the precursor ions were monitored in real time using the Multiple Ion Monitoring (MIM) mode, as described in Chapter 2. The effective analyte molecule flow could then be calculated from the reduction in the  $m/z$  19 ( $\text{H}_3\text{O}^+$ ) count rate ( $\text{flow} = \ln[I/I_0]$ ), and plotted on the x-axis against the count rates of  $m/z$  19,  $m/z$  30 ( $\text{NO}^+$ ) and  $m/z$  32 ( $\text{O}_2^{+\bullet}$ ). An example semi-logarithmic plot from which the decay rates for the reactions between the SIFT-MS precursor ions and ethyl acetate is shown in Figure 6.

**Figure 6.** Semi-logarithmic plot showing the count rates (in counts-per-second,  $c/s$ ) of the primary (non-hydrated) precursor ions:  $\text{H}_3\text{O}^+$  (closed circles),  $\text{NO}^+$  (grey circles) and  $\text{O}_2^{+\bullet}$  (open circles), which were simultaneously injected into the flow tube of the SIFT-MS instrument in the presence of ethyl acetate vapour, introduced at varying flow rates (see text).



The proton affinity of each of the VOCs analysed exceeds that of water ( $691\text{kJ mol}^{-1}$  [109]), and so all of the  $\text{H}_3\text{O}^+$  protonation reactions are exothermic and proceed according to their respective  $k_c$ -values. The  $k$ -values for these reactions can therefore be calculated according to the equations derived by Su and Chesnavich [74] when the polarisabilities ( $\alpha$ ) and molecular dipole moments ( $\mu$ ) are known or can be estimated (as was required for acetoin and pyruvic acid). The reduction in the  $\text{NO}^+$  and  $\text{O}_2^{+\bullet}$  count rates, relative to that of  $\text{H}_3\text{O}^+$ , as derived from the slopes of the semi-logarithmic plots such as in Figure 6, can then be used to calculate  $k$  for the

reactions of each compound, as a proportion of the calculated  $k_c(\text{H}_3\text{O}^+)$ . The calculated and experimentally-derived rate coefficients are given in Table 4.

**Table 4.** Rate coefficients ( $k$ ), in units of  $10^{-9} \text{ cm}^3\text{s}^{-1}$ , for the reactions of  $\text{H}_3\text{O}^+$ ,  $\text{NO}^+$  and  $\text{O}_2^+$  with four isobaric compounds of molecular mass ( $m$ ) 88u, and four of molecular mass 86u. The calculated collisional rate coefficients ( $k_c$ ) are presented in square brackets (same units as  $k$ ). The polarisabilities ( $\alpha$ ) and permanent dipole moments ( $\mu$ ) [147], used to calculate  $k_c$  according to the formula derived by Su and Chesnavich [74], are also indicated for each compound.

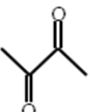
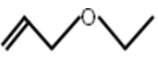
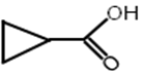
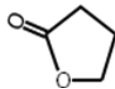
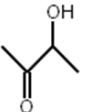
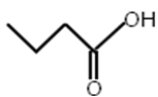
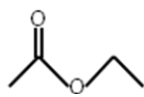
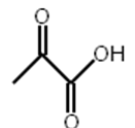
Compound	$m$ (u)	$\alpha$ ( $10^{-24} \text{ cm}^3$ )	$\mu$ (D)	$k$ [ $k_c$ ] ( $\text{H}_3\text{O}^+$ )	$k$ [ $k_c$ ] ( $\text{NO}^+$ )	$k$ [ $k_c$ ] ( $\text{O}_2^+$ )
2,3-butanedione (diacetyl)	86	8.2	0.0	[1.7]	1.4 [1.4]	1.5 [1.4]
Allyl ethyl ether		10.7	1.2	[2.5]	2.2 [2.1]	2.1 [2.0]
Cyclopropane carboxylic acid		10.0	1.8	[3.0]	2.1 [2.5]	2.4 [2.4]
$\gamma$ -butyrolactone		8.5	3.0	[4.1]	3.5 [3.4]	3.9 [3.3]
3-hydroxybutanone (acetoin)	88	8.8	2.6	[3.7]	3.0 [3.1]	3.4 [3.0]
n-butyric acid		10.0	1.8	[3.0]	2.4 [2.5]	2.6 [2.4]
Ethyl acetate		9.7	1.8	[2.9]	2.3 [2.4]	2.5 [2.4]
Pyruvic acid		6.6	2.3	[3.2]	2.1 [2.7]	2.8 [2.6]

As can be seen in Table 4, all of the reactions proceed according to rate coefficients that are close to  $k_c$ , *i.e.* at their maximum rates. The  $k$ -values are also in close agreement with those determined in previously published SIFT studies, *viz.* diacetyl [112], allyl ethyl ether [116],  $\gamma$ -butyrolactone [143], and ethyl acetate [115], as are the  $m/z$  values of the observed product ions for these reactions (see Table 5).

### 3.3.2. Product ion distributions for reactions of MW 86u and 88u VOCs with $\text{H}_3\text{O}^+$ , $\text{NO}^+$ and $\text{O}_2^+$

The product ion distributions for the reactions were derived from the headspace of aqueous solutions of the analyte VOCs, contained in sealed bottles. Mass spectra were produced by operating the SIFT-MS instrument in Full Scan (FS) mode. The  $m/z$  values of the formed product ions are given in Table 5, including those of the hydrated product ions which were generated because of the humidity of the samples. It should be noted that these experiments were performed with the samples held at room temperature; increasing the temperature/humidity increases the fractions of the hydrated product ions [77]. Some of the reaction mechanisms (see Table 2 and the “SIFT-MS ion chemistry” section earlier) relevant to the identification and quantification of these VOCs will be discussed below, in reference to Table 5.

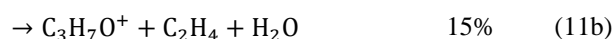
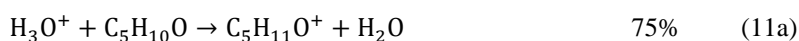
**Table 5.** The molecular formulae and  $m/z$  values of the product ions formed from the reactions of  $\text{H}_3\text{O}^+$ ,  $\text{NO}^+$  and  $\text{O}_2^+$  with eight VOCs, four with molecular weights (MW) of 86u and four of 88u, along with their branching ratios in percent, %. The primary product ions are given in bold, with the hydrates in parentheses, and unique product ions and underlined (see text). Ionisation energies of each compound in electron volts, are given in italics [131]. The data were obtained from the analyses of aqueous solutions of each compound, the approximate molar concentrations of which are also given.

MW	VOC	Physical state	H <sub>3</sub> O <sup>+</sup>	m/z			NO <sup>+</sup>	m/z			O <sub>2</sub> <sup>+</sup>	m/z		
86u	2,3-butanedione (diacetyl) C <sub>4</sub> H <sub>6</sub> O <sub>2</sub> 9.3 	Liquid BP 88 <sup>o</sup> C Solution 0.05M	C <sub>4</sub> H <sub>7</sub> O <sub>2</sub> <sup>+</sup>	100%	<b>87</b> (105, 123)		C <sub>4</sub> H <sub>6</sub> O <sub>2</sub> <sup>+</sup> NO <sup>+</sup> C <sub>4</sub> H <sub>6</sub> O <sub>2</sub>	75% 25%	<b>86</b> <b>116</b>		C <sub>2</sub> H <sub>3</sub> O <sup>+</sup> C <sub>4</sub> H <sub>6</sub> O <sub>2</sub> <sup>+</sup>	65% 35%	<b>43</b> <b>86</b>	
	Allyl ethyl ether C <sub>5</sub> H <sub>10</sub> O 9.6 <sup>†</sup> 	Liquid BP 66 <sup>o</sup> C Solution 0.01M	C <sub>5</sub> H <sub>11</sub> O <sup>+</sup> C <sub>3</sub> H <sub>7</sub> O <sup>+</sup> C <sub>2</sub> H <sub>5</sub> O <sup>+</sup>	75% 15% 10%	<b>87</b> (105) <u><b>59</b> (77, 95)</u> <u><b>45</b> (63, 81)</u>		C <sub>5</sub> H <sub>9</sub> O <sup>+</sup> C <sub>5</sub> H <sub>10</sub> O <sup>+</sup>	>95% <5%	<b>85</b> <b>86</b>		C <sub>3</sub> H <sub>6</sub> O <sup>+</sup> C <sub>5</sub> H <sub>10</sub> O <sup>+</sup> C <sub>3</sub> H <sub>5</sub> O <sup>+</sup> C <sub>3</sub> H <sub>5</sub> <sup>+</sup>	70% 15% 10% ≤5%	<b>58</b> (76, 94) <b>86</b> <u><b>57</b> (75)</u> <u><b>41</b></u>	
	Cyclopropane-carboxylic acid C <sub>4</sub> H <sub>6</sub> O <sub>2</sub> 10.6 	Liquid BP 183 <sup>o</sup> C Solution 0.5M	C <sub>4</sub> H <sub>7</sub> O <sub>2</sub> <sup>+</sup> C <sub>4</sub> H <sub>5</sub> O <sup>+</sup>	90% 10%	<b>87</b> (105, 123) <u><b>69</b></u>		NO <sup>+</sup> C <sub>4</sub> H <sub>6</sub> O <sub>2</sub> C <sub>4</sub> H <sub>5</sub> O <sup>+</sup>	60% 40%	<b>116</b> (134) <b>69</b>		C <sub>4</sub> H <sub>6</sub> O <sub>2</sub> <sup>+</sup> C <sub>4</sub> H <sub>5</sub> O <sub>2</sub> <sup>+</sup> C <sub>4</sub> H <sub>5</sub> O <sup>+</sup> C <sub>2</sub> H <sub>2</sub> O <sub>2</sub> <sup>+</sup> C <sub>3</sub> H <sub>6</sub> <sup>+</sup>	35% 20% 20% 15% 10%	<b>86</b> (104) <u><b>85</b> (103)</u> <u><b>69</b> (87)</u> <u><b>58</b> (76)</u> <b>42</b>	
	γ-butyrolactone (GBL) C <sub>4</sub> H <sub>6</sub> O <sub>2</sub> 10.3 	Liquid BP 206 <sup>o</sup> C Solution 0.5M	C <sub>4</sub> H <sub>7</sub> O <sub>2</sub> <sup>+</sup>	100%	<b>87</b> (105, 123)		NO <sup>+</sup> C <sub>4</sub> H <sub>6</sub> O <sub>2</sub>	100%	<b>116</b>		C <sub>2</sub> H <sub>2</sub> O <sup>+</sup> or C <sub>3</sub> H <sub>3</sub> <sup>+</sup> C <sub>4</sub> H <sub>6</sub> O <sub>2</sub> <sup>+</sup>	80% 20%	<b>42</b> (60) <b>86</b>	
88u	3-hydroxybutanone (acetoin) C <sub>4</sub> H <sub>8</sub> O <sub>2</sub> 9.4 <sup>‡</sup> 	Solid MP 15 <sup>o</sup> C Solution 0.2M	C <sub>4</sub> H <sub>9</sub> O <sub>2</sub> <sup>+</sup>	100%	<b>89</b> (107, 125)		NO <sup>+</sup> C <sub>4</sub> H <sub>8</sub> O <sub>2</sub> C <sub>2</sub> H <sub>5</sub> O <sup>+</sup> C <sub>4</sub> H <sub>8</sub> O <sub>2</sub> <sup>+</sup> C <sub>4</sub> H <sub>7</sub> O <sub>2</sub> <sup>+</sup>	80% 10% ≤5% ≤5%	<b>118</b> <u><b>45</b> (63, 81)</u> <b>88</b> <u><b>87</b> (105)</u>		C <sub>2</sub> H <sub>5</sub> O <sup>+</sup> C <sub>2</sub> H <sub>3</sub> O <sup>+</sup>	85% 15%	<b>45</b> (63, 81) <b>43</b>	
	n-butyric acid C <sub>4</sub> H <sub>8</sub> O <sub>2</sub> 10.2 	Liquid BP 163 <sup>o</sup> C Solution 0.02M	C <sub>4</sub> H <sub>9</sub> O <sub>2</sub> <sup>+</sup> C <sub>4</sub> H <sub>7</sub> O <sup>+</sup>	95% 5%	<b>89</b> (107, 125) <u><b>71</b></u>		NO <sup>+</sup> C <sub>4</sub> H <sub>8</sub> O <sub>2</sub> C <sub>4</sub> H <sub>7</sub> O <sup>+</sup>	80% 20%	<b>118</b> (136) <u><b>71</b></u>		C <sub>2</sub> H <sub>4</sub> O <sub>2</sub> <sup>+</sup> C <sub>3</sub> H <sub>5</sub> O <sub>2</sub> <sup>+</sup> C <sub>4</sub> H <sub>8</sub> O <sub>2</sub> <sup>+</sup> C <sub>2</sub> H <sub>3</sub> O <sup>+</sup>	85% 5% 5% ≤5%	<b>60</b> (78, 96) <u><b>73</b></u> <b>88</b> (106) <b>43</b>	
	Ethyl acetate C <sub>4</sub> H <sub>8</sub> O <sub>2</sub> 10.0 	Liquid BP 79 <sup>o</sup> C Solution 0.1M	C <sub>4</sub> H <sub>9</sub> O <sub>2</sub> <sup>+</sup>	100%	<b>89</b> (107)		NO <sup>+</sup> C <sub>4</sub> H <sub>8</sub> O <sub>2</sub>	100%	<b>118</b>		C <sub>2</sub> H <sub>5</sub> O <sub>2</sub> <sup>+</sup> C <sub>2</sub> H <sub>5</sub> O <sup>+</sup> C <sub>4</sub> H <sub>8</sub> O <sub>2</sub> <sup>+</sup> C <sub>2</sub> H <sub>3</sub> O <sup>+</sup>	40% 20% 20% 20%	<u><b>61</b> (79, 97)</u> <b>45</b> (63, 81) <b>88</b> (106) <b>43</b>	
	Pyruvic acid C <sub>3</sub> H <sub>4</sub> O <sub>3</sub> 9.9-10.4 	Liquid BP 165 <sup>o</sup> C Solution 2M	C <sub>3</sub> H <sub>5</sub> O <sub>3</sub> <sup>+</sup> C <sub>2</sub> H <sub>3</sub> O <sup>+</sup>	80% 20%	<b>89</b> (107, 125, 143) <u><b>43</b></u>		NO <sup>+</sup> C <sub>3</sub> H <sub>4</sub> O <sub>3</sub>	100%	<b>118</b> (136)		C <sub>2</sub> H <sub>3</sub> O <sup>+</sup>	100%	<b>43</b>	

<sup>†</sup> ionisation energy calculated from data presented in [148]; <sup>‡</sup> ionisation energy calculated from [149].

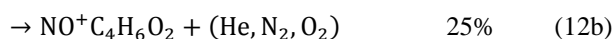
### 3.3.2.1. MW 86u compounds

The reactions of each of the four analyte compounds, denoted M, with  $\text{H}_3\text{O}^+$  proceed rapidly, with the protonated parent molecule,  $\text{MH}^+$ , being the dominant primary product ion in all cases. Each of these primary product ions forms a monohydrate and a dihydrate, with the exception of allyl ethyl ether, which forms just a monohydrate, as indicated in parentheses in Table 5. These hydrates are formed *via* three-body association reactions, which are discussed in a later section. Allyl ethyl ether undergoes the most complex reactions with  $\text{H}_3\text{O}^+$  of the four compounds, forming three different primary product ions:



All of the product ions are of the form  $\text{RO}^+$  which hydrate readily (see Table 5), with hydrocarbon molecules released in reactions (11b) and (11c). In the case of cyclopropane carboxylic acid, the primary protonated product ion partially dissociates to release  $\text{H}_2\text{O}$  and an ion of the form  $\text{RC}=\text{O}^+$ ; these do not usually form hydrated ions, as is the case here (see Table 5). Diacetyl and GBL do not dissociate after protonation, which is usually the case for ketones [112].

The processes involved in the reactions of the MW 86u compounds with  $\text{NO}^+$  are highly varied. Allyl ethyl ether reacts with  $\text{NO}^+$  almost entirely by hydride ion ( $\text{H}^-$ ) transfer, as is common with alkenes [121], whereas the single product formed from the reaction with GBL is the  $\text{NO}^+$  adduct ion,  $\text{NO}^+\text{C}_4\text{H}_6\text{O}_2$ , which does not hydrate significantly. Cyclopropane carboxylic acid reacts with  $\text{NO}^+$  primarily *via* the same mechanism, but there is an additional hydroxide ion transfer route, producing  $\text{C}_4\text{H}_5\text{O}^+$  ions and nitrous acid,  $\text{HNO}_2$ , molecules. The formed  $\text{RC}=\text{O}^+$  ions do not form hydrated ions, as above. Diacetyl is the only MW 86u compound analysed that reacts with  $\text{NO}^+$  primarily by charge transfer:



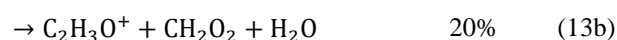
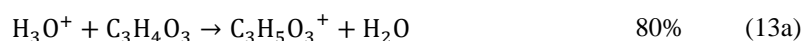
Route (12a) is energetically feasible because the ionisation energy of diacetyl (9.30eV) is very close to the recombination energy of  $\text{NO}^+$  (9.26eV). The calculated ionisation energy of allyl ethyl ether is slightly greater (9.6eV), and so reactions with  $\text{NO}^+$  are also seen to occur by charge transfer, but to a lesser extent (see Table 5). This relatively minor charge transfer product ion was not identified in the previously reported SIFT study in which the reaction of allyl ethyl ether with  $\text{NO}^+$  was analysed [116], possibly due to the overlap of the

charge transfer product ion ( $\text{C}_5\text{H}_{10}\text{O}^+$ ) with the carbon-13 isotopologue of the hydride ion transfer product ion ( $^{12}\text{C}_4^{13}\text{CH}_9\text{O}^+$ ).

The  $\text{O}_2^{+\bullet}$  reactions are all seen to proceed by charge transfer, producing the parent cation ( $\text{M}^+$ ), and at least one fragmentation product (see Table 5). An interesting observation can be made when considering the product ion at  $m/z$  of 42, formed in the reactions of  $\text{O}_2^{+\bullet}$  with both cyclopropane carboxylic acid and GBL. In the former reaction, the product ion must be  $\text{C}_3\text{H}_6^+$ , according to the molecular structure (see Table 5), but in the latter, the product ion could be either  $\text{C}_3\text{H}_6^+$  or  $\text{C}_2\text{H}_2\text{O}^+$ . Given that the ion forms hydrates, it is likely that  $\text{C}_2\text{H}_2\text{O}^+$  is the major product ion of the two, with neutral  $\text{C}_2\text{H}_4\text{O}$  molecules released. The resulting product ion distributions obtained for diacetyl and GBL are in good agreement with the previously published data [112, 143].

### 3.3.2.2. MW 88u compounds

As for the previous set of compounds, the reactions of  $\text{H}_3\text{O}^+$  with these four compounds proceed rapidly, with protonation again the dominant reaction route, and the protonated parent molecule,  $\text{MH}^+$ , the primary product ion in all cases. Only pyruvic acid forms a second significant primary product ion in reactions with  $\text{H}_3\text{O}^+$ :

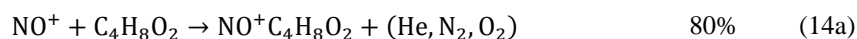


The neutral product ion formed *via* reaction route (13b) is most likely a formic acid molecule ( $\text{HCOOH}$ ). It is notable that a relatively concentrated pyruvic acid solution (2M; see Table 5) was required in order to generate a measurable headspace concentration of the compound. In order to enhance the headspace concentration further, the solution was acidified using the stronger hydrochloric acid. Surprisingly, this resulted in the formation of methanol, which is a compound that is easily measured by SIFT-MS using the  $\text{H}_3\text{O}^+$  precursor ion [110]. When the samples were again analysed 2 weeks later, having been kept the solution at room temperature, the pyruvic acid concentration had declined, while the methanol content had increased from around 200 *ppbv* to >10,000 *ppbv*. The mechanism of the conversion is not obvious from the structure of the pyruvic acid molecule.

Acetoin (3-hydroxybutanone) reacts with  $\text{H}_3\text{O}^+$  to produce a single primary product ion. Interestingly, this compound can exist either as a monomer (low melting point, coloured yellow) or as a dimer (higher melting point, white crystals). Operating SIFT-MS in the FS mode over a wide  $m/z$  range using both  $\text{H}_3\text{O}^+$  and  $\text{NO}^+$  clearly revealed the presence of both monomers and dimers in the headspace above the compound contained in a 150mL bottle. The more volatile monomer was gradually removed on vacuum pumping, leaving only the white

crystalline dimer. When the crystals were dissolved in water, analysis of the headspace revealed the presence of only the acetoin monomer, indicating that the dimer dissociates in aqueous solution. The data presented in Table 5 were obtained from the headspace of this solution. The product ions formed from the reactions of  $\text{NO}^+$  with n-butyric acid and ethyl acetate agree with the previously published SIFT study [115].

In each of the  $\text{NO}^+$  reactions, the major primary product ion is the adduct  $\text{NO}^+\text{M}$ , all of which form efficiently at, or close to,  $k_c$  (see Table 5) in three-body reactions which are mediated by the He carrier gas atoms and the major air molecules ( $\text{N}_2$ ,  $\text{O}_2$ , Ar). The most complex reaction occurs with acetoin:



The reaction route (14b) involves the abstraction of the  $\text{CH}_3\text{CO}$  group from the acetoin molecule (see Table 5). The minor reaction routes proceed *via* slightly endothermic mechanisms, *viz.* charge transfer (14c), which is only feasible due to the proximity of the ionisation energy of acetoin molecule (calculated as 9.4eV [148]) and the recombination energy of  $\text{NO}^+$  (9.26eV), and hydride ion ( $\text{H}^-$ ) transfer (14d). The minor reaction route that occurs in the reaction of  $\text{NO}^+$  with butyric acid proceeds by hydroxide ion ( $\text{OH}^-$ ) transfer, producing product ions of the form  $\text{RC}=\text{O}^+$ , which, again, do not hydrate. The hydride and hydroxide ion transfer reaction pathways are commonly seen to occur in  $\text{NO}^+$  reactions with organic compounds which contain an OH group [35, 115].

The reactions with  $\text{O}_2^{+\bullet}$  proceed predominantly *via* dissociative charge transfer, producing fragmentation ions. The simplest of these reactions occurs with pyruvic acid, where a single product ion is produced:

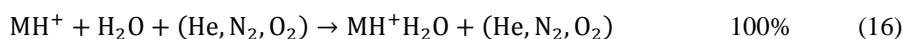


In reaction (15), the C-C bond between the two  $\text{C}=\text{O}$  groups is broken to produce the product ion at  $m/z$  43 and a formic acid molecule. The structure of the pyruvic acid molecule indicates that the product ion is  $\text{CH}_3\text{CO}^+$ , as shown, and this ion does not form hydrate ions under SIFT and SIFT-MS conditions [36]. This study also highlighted an error in the previously-published SIFT data, in which it was reported that ethyl acetate reacts with  $\text{O}_2^{+\bullet}$  to produce a fragment ion at  $m/z$  31 and does not form the parent molecule cation ( $\text{M}^+$ ), under the conditions of the SIFT experiments [115], which are somewhat different to those of the new SIFT-MS

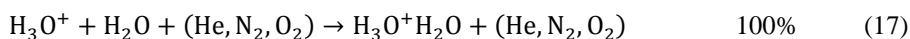
*Profile 3* instrument used in the present experiments. In this study, the fragment ion was not detected, and the ethyl acetate cation was present at a 20% level.

### 3.3.2.3. Hydration of the primary product ions $MH^+$ and $NO^+M$

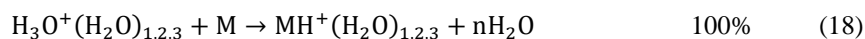
The importance of the hydration of the primary product ions has been alluded to previously in regard to the present study (see Section 3.1.1.), and the degree to which hydration occurs is dependent on the structure of the ion. The first step of hydration of protonated primary product ions (commonly formed from reactions with  $H_3O^+$ ) proceeds by the following three-body association reaction:



The primary and hydrated precursor ions,  $H_3O^+(H_2O)_{0,1,2,3}$ , should be dominant in SIFT-MS spectra, and the quantification of water vapour is based on the distribution of these four ions [133]. In the present experiments, the measured water vapour content was typically 1.5% when the compounds were analysed in air, and around 3% when analysed in solution. The initial three-body association reaction proceeds as follows:



The three-body rate coefficient for reaction (17) ( $K_{H_3O^+}$ ; also called  $k_3$  in the literature [107]) was determined to be  $6(10^{-28}) \text{ cm}^6\text{s}^{-1}$  at 298K in previous experiments [133]. The additional hydrated precursor ions, *viz.*  $H_3O^+(H_2O)_{2,3}$ , are formed *via* a sequence of similar reactions. Continuing from reaction (16), hydrated protonated product ions of the form  $MH^+(H_2O)$  can be formed *via* a second route, which is by ligand switching reactions between the  $H_3O^+(H_2O)_{1,2,3}$  cluster ions and M:



Considering that reactions (16), (17) and (18) occur concurrently during analysis, then the three-body rate coefficient ( $k_{MH^+}$ ) of hydration reaction (16) can be derived from the measured count rates of the ions. This is achieved by comparing the efficiencies of reactions (16) and (17), which are expressed by dimensionless association efficiency coefficient, denoted  $A_{\text{eff}}$  [77]. This value is obtained experimentally from the ratio of the count rates of  $MH^+$  to the total of the count rates of  $MH^+(H_2O)_{1,2,3}$ , which are taken relatively to a corresponding ratio for  $H_3O^+$  and its hydrates. The derivation of these coefficients has been described in detail previously [77, 150]. The value of  $A_{\text{eff}}$  for a particular compound, at a given concentration and flow rate into the SIFT flow tube, should be invariant with the sample humidity. This was validated in the present study by calculating the value of  $A_{\text{eff}}$  at the two different humidities at which the previously discussed experimental data was obtained, *viz.* 1.5% and 3%. The contribution of the switching reactions shown in equation (18) to  $A_{\text{eff}}$  is similarly expressed by a



dimensionless coefficient ( $S_{\text{eff}}$ ), which can be calculated assuming that (18) proceeds according to  $k_c$ , and has a typical value of 0.4 [77, 150]. Values for  $k_{\text{MH}^+}$  are then determined using the following relation:

$$k_{\text{MH}^+} = (A_{\text{eff}} - S_{\text{eff}})k_{\text{H}_3\text{O}^+} \quad (19)$$

The values of  $A_{\text{eff}}$  and  $k_{\text{MH}^+}$  for the 8 compounds analysed in this study are presented in Table 6.

**Table 6. Derived values of the humidity-independent association efficiency coefficients ( $A_{\text{eff}}$ ) and three-body rate coefficients ( $k_{\text{MH}^+}$ ) for the formation of hydrates of the protonated compounds indicated, as formed by ligand switching and three-body association. Further information is given in the text.**

MW	Compound	No. of functional groups	$A_{\text{eff}}^\dagger$	$k_{\text{MH}^+}$ ( $10^{-27} \text{ cm}^6 \text{ s}^{-1}$ ) $^\ddagger$
86	2,3-butanedione (diacetyl)	2	$7.2 \pm 0.1$	$4.1 \pm 0.1$
	Allyl ethyl ether	1	$6.2 \pm 0.1$	$3.5 \pm 0.1$
	Cyclopropane-carboxylic acid	2	$8.5 \pm 0.3$	$4.9 \pm 0.3$
	$\gamma$ -butyrolactone (GBL)	2	$4.9 \pm 0.3$	$2.7 \pm 0.3$
88	3-Hydroxybutanone (acetoin)	1	$1.8 \pm 0.1$	$0.8 \pm 0.3$
	n-butyric acid	2	$10.1 \pm 4.4$	$5.8 \pm 2.6$
	Ethyl acetate	1	$5.8 \pm 0.8$	$3.3 \pm 0.6$
	Pyruvic acid	3	$13.5 \pm 0.8$	$7.8 \pm 0.6$

$^\dagger$  Association efficiencies were calculated from experimental data, with the uncertainties resulting from the differences between the results obtained from analyses of the vapour of neat compounds and from the headspaces of aqueous solutions.

$^\ddagger$  Three-body association rate coefficients were estimated from  $A_{\text{eff}}$  using the theoretical maximum contribution of ligand-switching reactions [151] and an assumed value of  $k_{\text{H}_3\text{O}^+}$  (see text).

As mentioned, the value of  $k_{\text{H}_3\text{O}^+}$  is  $6(10^{-28}) \text{ cm}^6 \text{ s}^{-1}$  [133], and so the eight compounds will form hydrates more efficiently than the  $\text{H}_3\text{O}^+$  precursor ions. Production of  $\text{MH}^+$  hydrates is therefore inevitable, and erroneously low concentrations will be derived from SIFT-MS analyses unless these hydrated product ions, including dihydrates and trihydrates (see Table 5), are accounted for. The data presented in Table 5 indicate that the protonated product ions generated from the compounds with the greater number of active sites tend to hydrate more efficiently. Naturally, the best example of this is the protonated pyruvic acid, which adds a water molecule with the greatest efficiency, and the two protonated fatty acid molecules that have two active sites also hydrate relatively efficiently. On the other hand, the protonated ester, ether and ketones form hydrates with lesser efficiency.

As discussed earlier, only allyl ethyl ether (MW 86u) did not form adduct product ions from the  $\text{NO}^+$  reactions, of the form  $\text{NO}^+\text{M}$  (see Table 5). Of the seven remaining compounds, only the three carboxylic acids (one with MW 86u, two with MW 88u) also form hydrated adduct ions of the form  $\text{NO}^+\text{M}(\text{H}_2\text{O})$ , whereas the hydroxyketone, ester (both 88u), two ketones and ether (86u) compounds do not form hydrates under the SIFT-MS conditions. This trend is mirrored by the hydration of the  $\text{MH}^+$  product ions formed from reactions with  $\text{H}_3\text{O}^+$ , as shown in Table 6. These characteristics can assist in the analyses of isobaric compounds, as is shown in this case by the appearance of at least one unique product ion, or in some cases a hydrated product ion, for each of the four isobaric compounds of mass 86u or 88u (underlined in Table 5). These principles were similarly

employed in the previously mentioned SIFT-MS experiments which allow acetic acid, methyl formate and propanol to be distinguished, despite each having the same nominal MW of 60u (see section 3.1.) [134].

#### 3.3.2.4. Kinetics database entries

Entries for the SIFT-MS kinetics library can be produced from the kinetics data given in Table 4, and the  $m/z$  values of the primary and hydrated product ions shown in Table 5, appropriate to the conditions prevailing in the *Profile 3* SIFT-MS instrument. The kinetics library entries for diacetyl and acetoin are shown in Table 7. The entries include each of the coefficients which are required for quantitative SIFT-MS analyses of trace compounds present in humid air, according to the equations given in Španěl *et al.*, 2006 [75]. The precursors section of each entry contains the  $m/z$  value of each precursor ion, followed by the calculated or experimentally-derived rate coefficient (k-value), and finally a corrective coefficient, known in the literature as  $f_i$ , which is multiplied by the count rate of the assigned precursor ion. The products section requires only the  $m/z$  values of each of the product ions and a similar multiplication coefficient ( $f_p$ ). In the examples shown in Table 7, each of the f-factors has a value of 1.0, meaning that the count rates of the precursor and product ions directly contribute to the quantification of diacetyl and acetoin.

**Table 7. SIFT-MS kinetics library entries presented in the format required in order to the SIFT-MS software to perform on-line calculations of the concentrations of diacetyl and acetoin using the  $H_3O^+$  or  $NO^+$  precursor ions.**

Diacetyl( $H_3O^+$ )	Acetoin( $H_3O^+$ )
4 precursors	4 precursors
19 1.7e-9 1.0	19 3.7e-9 1.0
37 1.3e-9 1.0	37 3.0e-9 1.0
55 1.0e-9 1.0	55 2.4e-9 1.0
73 0.6e-9 1.0	73 1.5e-9 1.0
3 products	3 products
87 1.0	89 1.0
105 1.0	107 1.0
123 1.0	125 1.0
Diacetyl( $NO^+$ )	Acetoin ( $NO^+$ )
3 precursors	3 precursors
30 1.4e-9 1.0	30 3.0e-9 1.0
48 1.1e-9 1.0	48 2.6e-9 1.0
66 0.8e-9 1.0	66 2.2e-9 1.0
2 product	4 products
86 1.0	45 1.0
116 1.0	63 1.0
	81 1.0
	118 1.0

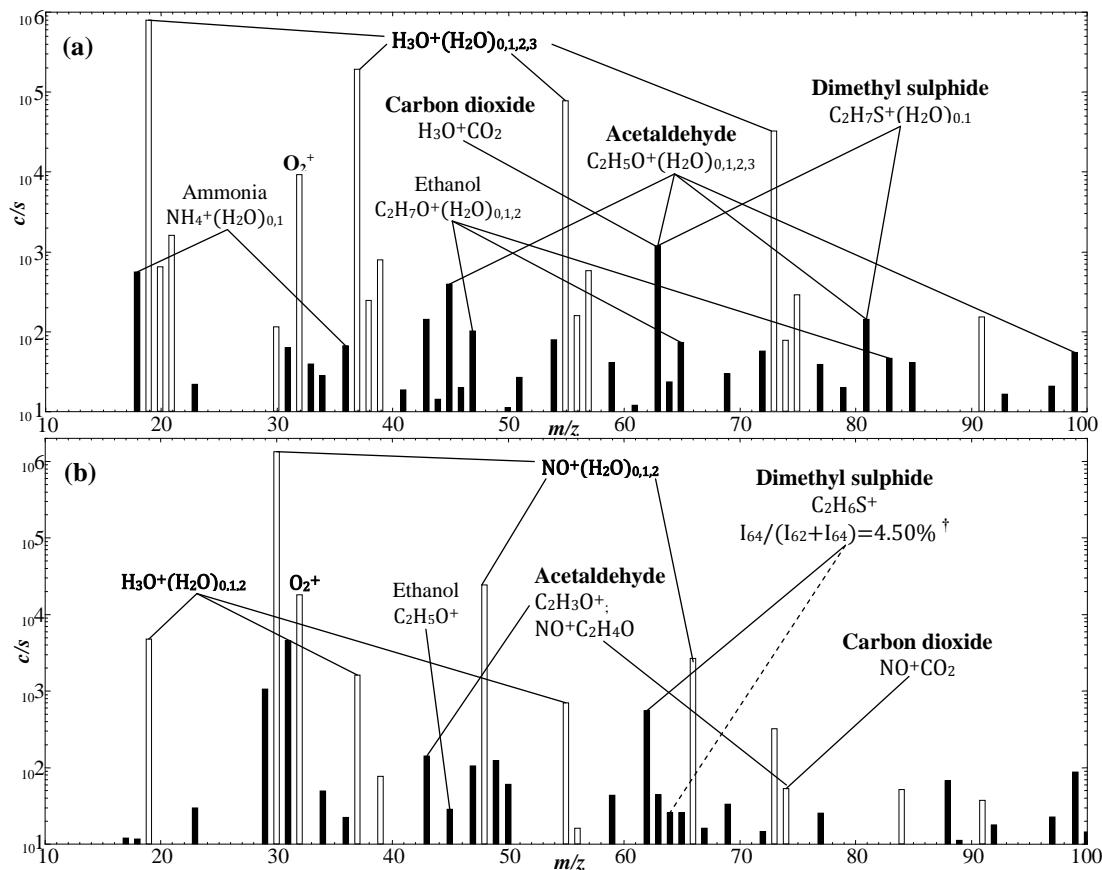
It is not possible to construct a kinetics database which can reliably quantify each of the MW 86u and 88u compounds analysed in this study when more than one isobaric compound is present in a sample, because the degree of overlap in the dominant product ions ( $m/z$  87 and 116, or  $m/z$  89 and 118) is too great (see section 3.3.3. for a case where such analyses are possible despite the generation of overlapping product ions). Thus, as

an example, the  $\text{H}_3\text{O}^+$  kinetics library entry for acetoin (Table 4) will result in the calculation of the combined concentrations of acetoin, n-butyric acid, ethyl acetate and pyruvic acid if more than one of these compounds is present in a sample. It is, however, possible to identify each of the MW 86u and 88u compounds using a combination of the  $\text{H}_3\text{O}^+$ ,  $\text{NO}^+$  and  $\text{O}_2^{+\bullet}$  mass spectra, in some cases by observing the presence of minor product ions or hydrates (see Table 5). The branching ratio for the primary product ions and any hydrates formed in the reaction of the chosen precursor ion with the particular compound can be experimentally determined under identical conditions of sample humidity to those used in the actual analysis.

### **3.4. Concurrent analyses of $\text{CO}_2$ , AA and DMS: results and discussion**

The standard methods for analysing carbon dioxide, AA and DMS individually have been summarised in the section 3.1.3., with reference to previously reported studies [80, 144-146]. The following sections relate to the refinement of these analytical methodologies to allow for the analysis of each of these compounds when all three are present; this being complicated by the presence of isobaric product ions, as discussed earlier. Figure 7 shows SIFT-MS mass spectra derived from the analyses of all three compounds, and this will be referred to in the sections that follow.

**Figure 7.** SIFT-MS ‘composite’ mass spectra (ion counts-per-second, *c/s*, against mass-to-charge ratio, *m/z*), obtained using (a)  $\text{H}_3\text{O}^+$ ; and (b)  $\text{NO}^+$  precursor ions, showing the combined analyses of samples of  $\text{CO}_2$ , AA and DMS in humid air.



† The count rates (*I*) of the DMS charge transfer product ion and its  $^{64}\text{S}$  isotopologue at *m/z* 62 and 64 respectively provide a useful check on the presence of DMS in the sample. The sulphur-34 isotope accounts for around 4.2% of the total sulphur atoms.

### 3.4.1. Analysis of AA in the presence of $\text{CO}_2$ and DMS

Due to the aforementioned overlap between the characteristic product ions at *m/z* 63, *viz.* hydrated protonated AA and the  $\text{H}_3\text{O}^+\text{CO}_2$  adduct ion, this *m/z* value is excluded from AA analysis with the  $\text{H}_3\text{O}^+$  precursor ion, so analysis of AA is based only on the product ions at *m/z* 45 and 81 (see section 3.1.3. and Table 3). Due to the additional presence of DMS, hydrated protonated DMS product ions,  $\text{C}_2\text{H}_7\text{S}^+(\text{H}_2\text{O})$ , will also be formed at *m/z* 81 (see Figure 7a), and so this *m/z* value must also be excluded from the analysis of AA. Consequently AA analysis must be accomplished using only *m/z* 45 product ions, whilst ensuring that the impurity ions formed from reactions between  $\text{O}_2^+\bullet$  and ethanol are accounted for (see section 3.1.3.) [146]. As the fraction of the *m/z* 45 product ions changes with humidity, the concentration of AA must be calculated from the ratio of *m/z* 45 to the sum of the precursor ions and their hydrates, multiplied by factors obtained from fitting experimental data [75, 146]. The kinetics library entry for this analysis is given in the left column of Table 8, with the ethanol

concentration in the sample derived from the count rate of the  $m/z$  83 dihydrate of protonated ethanol. The injected impurity  $O_2^{+\bullet}$  ions typically account for <1% of the total precursor ion signal (see Figure 7a), and so the correction for this impurity is very small. The correction was tested experimentally by monitoring the levels of AA in the presence of ethanol and the apparent AA concentration did not increase significantly above that obtained at near zero ethanol concentration, even at ethanol concentrations of several parts-per-million by volume (*ppmv*), when calculated using the library entry given in the left column of Table 8, headed as “Acetaldehyde45( $H_3O^+$ )”.

**Table 8. SIFT-MS kinetics library entries for the determination of the concentrations of acetaldehyde (AA) and dimethyl sulphide (DMS) in humid samples using  $H_3O^+$  and  $NO^+$  reagent ions. Further explanation in text.**

Acetaldehyde45( $H_3O^+$ )	AcetaldehydeC88( $NO^+$ )	DMS( $NO^+$ )
5 precursors	3 precursors	3 precursors
19 3.7e-9 1.0	30 3.4e-9 1.0	30 2.2e-9 1.0
37 3.0e-9 -1.0	48 3.0e-9 -1.0	48 2.0e-9 -1.0
55 2.7e-9 0.0	64 2.7e-9 0.0	64 1.9e-9 0.0
73 2.6e-9 0.0	32 3.7e-9 1.0 <sup>†</sup>	1 products
32 3.7e-9 1.0 <sup>†</sup>	2 products	62 1.04
2 products	43 1.33	
45 1.1	88 -100.9 <sup>†</sup>	
83 -100.5 <sup>†</sup>		
	AcetaldehydeC58( $NO^+$ )	
	3 precursors	
	30 3.4e-9 1.0	
	48 3.0e-9 -1.0	
	64 2.7e-9 0.0	
	2 products	
	43 1.33	
	58 -0.67 <sup>‡</sup>	

<sup>†</sup> For a product ion such as  $m/z$  83, an  $f_p$ -factor more negative than -100 acts as a trigger for the analytical software to carry out the subtraction of overlapping product ion formed by an “impurity ion” listed as the last item in the precursors section of the entry, in this case  $m/z$  32, according to the equation given in [146]. The portion of the  $f$ -factor in excess of -100 is used as a correction coefficient ( $f_m$ ). For example, where  $f_m = 0.5$  in the “Acetaldehyde45( $H_3O^+$ )” entry, the correction is  $-0.5[83][32]/[19]$ , where the numbers in square brackets indicate the count rates at the three  $m/z$  values.

AA can now also be analysed accurately using  $NO^+$  precursor ions. The characteristic product ions formed from this method of analysis occur at  $m/z$  43 and 74; the former being the major product ion formed at 75%, as shown earlier in reaction (3) (see section 3.1.3.). This ion is  $CH_3CO^+$ , which does not hydrate and therefore is not influenced by the humidity of the sample. Unfortunately, this is also a 40% product ion formed from the reactions of  $O_2^{+\bullet}$  with acetone [112], a VOC which is often present in biological samples, so this must be accounted for in order for accurate quantification of AA to be achieved using the  $NO^+$  precursor ion. Again, this potential problem is however limited due to the precursor ion filter, which ensures the impurity  $O_2^{+\bullet}$  present in the flow tube represents <1% of the injected  $NO^+$  ions (see Figure 7b), so the affect on AA quantification is only significant when acetone is present at a concentration more than 100 times greater than that of AA. Nonetheless, the presence of acetone and impurity  $O_2^{+\bullet}$  is accounted for by using a kinetics library entry for AA analysis using  $NO^+$  precursor ions that uses only the  $m/z$  43 ion and excludes, but accounts for, the  $m/z$  74 ion.

Two suitable entries are given in the centre column of Table 8. The entry “AcetaldehydeC88(NO+)” relates the ion counts of  $m/z$  88, the single product ion formed from the reaction between  $\text{NO}^+$  and acetone [112], to the count rate of  $\text{O}_2^{+\bullet}$ , thereby gaining a measure of the contribution of the  $\text{O}_2^{+\bullet}$ /acetone reaction to the count rate of  $m/z$  43. The second entry, “AcetaldehydeC58(NO+)” instead measures the count rate of the major product ion formed from  $\text{O}_2^{+\bullet}$ /acetone reactions at  $m/z$  58 to gain a measure of the contribution to the count rate of  $m/z$  43. In each case, the contribution of  $\text{O}_2^{+\bullet}$ /acetone reactions is subtracted in order to derive an accurate measure of the AA concentration. The efficacy of these library entries for AA quantification using  $\text{NO}^+$  precursor ions have also been checked experimentally, where it was observed that acetone concentrations of several *ppmv* increase the derived the apparent AA concentrations by less than a few *ppbv*, as calculated using both library entries.

### 3.4.2. Analysis of **DMS** in the presence of $\text{CO}_2$ and AA

Accurate analysis of DMS under these conditions is not feasible using  $\text{H}_3\text{O}^+$  due to the overlap of the protonated DMS product ions with the first hydrates of protonated ions AA and the  $\text{H}_3\text{O}^+\text{CO}_2$  adduct ions at  $m/z$  63 (see section 3.1.3.). Analysis using the hydrate of protonated DMS,  $\text{C}_2\text{H}_7\text{S}^+(\text{H}_2\text{O})$ , at  $m/z$  81 is not possible either due to the overlap with the second hydrate of protonated AA (see Figure 7a). The  $^{34}\text{S}$ -containing DMS isotopologue ions of the form  $\text{C}_2\text{H}_7^{34}\text{S}^+$ , that occur at  $m/z$  65, could be used to analyse DMS in principle, but this overlaps with the first hydrate of protonated ethanol ions and ethanol is a very common constituent of biological samples. This leaves  $\text{NO}^+$  as the only option for quantitative DMS analyses, in which a single product ion is formed, *viz.* the parent cation  $\text{C}_2\text{H}_6\text{S}^+$ , at  $m/z$  62. This product ion does not hydrate significantly, and so is not influenced greatly by the humidity of the sample. The kinetics library entry for the analysis of DMS using  $\text{NO}^+$  precursor ions, is therefore relatively simple (using a coefficient 1.04 to account for the isotopic abundance of the  $^{34}\text{S}$  isotope), shown in the right column of Table 8 as “DMS( $\text{NO}^+$ )”.

### 3.4.3. Analysis of $\text{CO}_2$ in the presence of AA and DMS

The analysis of  $\text{CO}_2$  in the presence of AA only using  $\text{H}_3\text{O}^+$  precursor ions has been addressed in section 3.4.1., above. It is straightforward when the  $\text{CO}_2$  levels are between 1% and 5%, which are typical in biological samples, provided that the AA concentrations are not excessive (<100 *ppbv*). However,  $\text{CO}_2$  analysis using  $\text{H}_3\text{O}^+$  reagent ions is challenging if the DMS concentration exceeds about 100 *ppbv*, and the quantification becomes increasingly uncertain as the DMS concentration increases further. The Henry’s Law coefficient of DMS is some 25 times lower than that of AA [151], and so only a relatively small quantity of DMS need be present in a liquid

source for excessive concentrations to be observed in the headspace/gas phase, increasing the likelihood of this analytical problem occurring in biological samples. Under these conditions, the CO<sub>2</sub> concentration can only be approximated; this being possible because the ratios of the characteristic product ion signals at  $m/z$  81 to  $m/z$  63 are different for the reactions of H<sub>3</sub>O<sup>+</sup> with AA and with DMS. It is then mathematically feasible to calculate the individual concentrations of AA, DMS and CO<sub>2</sub> from the three signal levels at  $m/z$  45, 63 and 81. This principle is implemented in the library entry in the left column of Table 9 where it is accepted that the ion count ratio for the characteristic primary and hydrated product ions of DMS, *i.e.* [81]/[63], is equal to 1/6 at 5% absolute humidity and a sample flow rate of 27 mL/min at standard temperature and pressure (STP). Since this ratio is sample flow rate and humidity dependent, it needs to be precisely determined in a separate experiment under the actual conditions of a particular study. Similarly, the coefficient for the  $m/z$  45 product ion must be adjusted according to the actual ratios of the primary and hydrated product ion count rates, *i.e.* [45]:[63]:[81], obtained for the H<sub>3</sub>O<sup>+</sup> reaction with AA at varying humidity and sample flow rate [146]. It should be noted that this approach can result in only approximate analyses.

**Table 9. SIFT-MS kinetics library entries for the determination of the concentrations of CO<sub>2</sub> in the presence of AA and DMS in humid samples using H<sub>3</sub>O<sup>+</sup> and NO<sup>+</sup> reagent ions.**

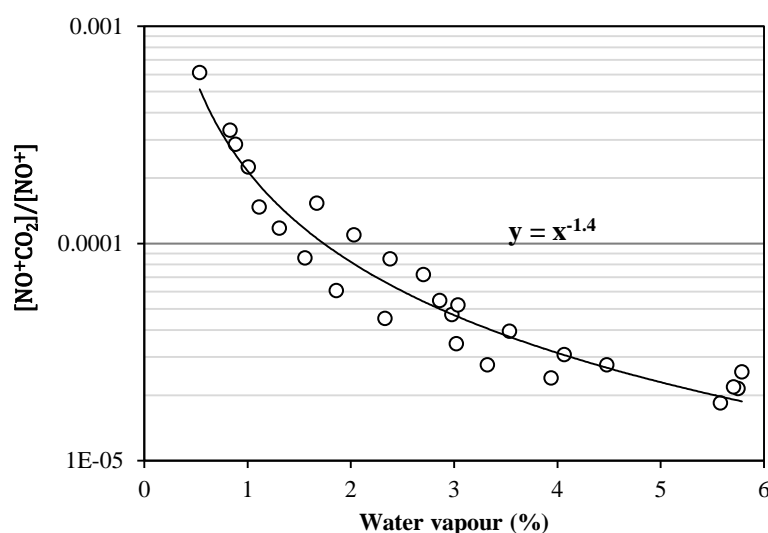
CO <sub>2</sub> _corrDMS_AA(H <sub>3</sub> O <sup>+</sup> ) <sup>†</sup>	CO <sub>2</sub> (NO <sup>+</sup> ) <sup>†</sup>
4 precursors	3 precursors
19 3e-15 1.0	30 1.5e-15 1.0
37 3e-15 1.0	48 1.5e-15 1.0
55 3e-15 1.0	66 1.5e-15 1.0
73 3e-15 1.0	3 products
3 products	74 1.0
63 1.0	73 -0.0029
45 1.5	43 -0.33
81 -6	

<sup>†</sup> Note that the order of the library entries is important to trigger the inclusion of the power law calculation in the Profile 3 SIFT-MS software and must be as given in this table.

The NO<sup>+</sup>/CO<sub>2</sub> reactions proceed by slow association, as mentioned earlier, and the resulting NO<sup>+</sup>CO<sub>2</sub> adduct ions at  $m/z$  74 (see section 3.1.3. and Figure 2) undergo ligand switching reactions with H<sub>2</sub>O molecules, forming NO<sup>+</sup>H<sub>2</sub>O ions at  $m/z$  48 (reaction (16)). The latter ion is also formed by direct association between NO<sup>+</sup> ions and H<sub>2</sub>O molecules and is consequently always present in SIFT-MS spectra when NO<sup>+</sup> is the reagent ion used to analyse humid samples. Both the  $m/z$  48 and 74 ions can be seen in the spectrum in Figure 2b, as are also the hydrates of H<sub>3</sub>O<sup>+</sup>. So, in order for quantitative analyses to be performed using the NO<sup>+</sup> precursor ion, the <sup>2</sup>H and <sup>17</sup>O isotopologues of H<sub>3</sub>O<sup>+</sup>(H<sub>2</sub>O)<sub>3</sub> at  $m/z$  74 and the switching reaction of NO<sup>+</sup>CO<sub>2</sub> with the H<sub>2</sub>O molecules injected with the sample must be accounted for. To this end, a simple experiment was carried out in order to study the rate of loss of the NO<sup>+</sup>CO<sub>2</sub> adduct ion with H<sub>2</sub>O molecules under SIFT-MS conditions, the

results of which are in Figure 3. The adduct ions were clearly depleted as the humidity increased, with the signal level of the  $\text{NO}^+\text{CO}_2$  ions decreasing by about a factor of 100 as the humidity increases from near zero to 6% of water vapour by volume. The data effectively describe the formation rate of the analytical adduct ion as obtained from the known rate coefficient for the association reaction and its loss by the aforementioned switching reaction. As mentioned, the overlap at  $m/z$  74 caused by the isotopologues of  $\text{H}_3\text{O}^+(\text{H}_2\text{O})_3$ , as well as the overlap with the  $\text{NO}^+\text{AA}$  product of the AA reaction (using the known  $[74]/[43]$  ratio for these products given in reaction (3)) must also be accounted for. Thus, a kinetics library entry is given in the right column of Table 9. The power law derived from Figure 3 has been implemented into the SIFT-MS software (Trans Spectra Ltd., UK) in order to account for the loss of product ions in a fashion similar to that implemented for  $\text{CO}_2$  quantification by  $\text{H}_3\text{O}^+$  [144].

**Figure 8.** Change of the relative count rate of  $\text{NO}^+\text{CO}_2$  with the humidity of the sample due to the ligand-switching reactions that occur with  $\text{H}_2\text{O}$ . The power law indicated can be used to account for this change and is implemented in the latest versions of *Profile 3* SIFT-MS software (Trans Spectra Limited, UK) using library entries presented in Table 9.



In order to test the efficacy of this new kinetics library entries for the analysis of  $\text{CO}_2$  with  $\text{NO}^+$  precursor ions, shown in Table 9, air samples containing  $\text{CO}_2$  at levels that are commonly observed in breath and biological samples (3-4.%) were analysed using both  $\text{H}_3\text{O}^+$  and  $\text{NO}^+$  precursor ions at varying humidity. The resulting scatter plot is shown in the published article (see Appendix A4). Despite some scatter, which was most likely due to by the low count rates upon which the analyses are based, due to the slow speed of the  $\text{NO}^+\text{-CO}_2$  association reaction, and the tendency for ligand switching, a reasonable agreement between the analyses by the two precursor ions is shown. This is sufficient for the analysis of most biological samples, especially when it is considered that the  $\text{CO}_2$  measurements are carried out simultaneously with other VOCs that are often present at the *ppbv* concentrations.



### 3.5. Summary remarks

Contained within the two kinetics studies presented in this chapter are several fundamental ion chemistry challenges relating to the SIFT-MS analyses of isobaric volatile compounds or volatile compounds that react to produce isobaric product ions.

The first study, presented in Appendix A3, will allow SIFT-MS users to detect and quantify three compounds that had not been characterised for SIFT-MS analyses previously (*viz.* cyclopropane carboxylic acid, pyruvic acid, and acetoin), all of which have some biological relevance. The other five compounds that were analysed (*viz.* diacetyl,  $\gamma$ -butyrolactone (GBL), allyl ethyl ether, n-butyric acid and ethyl acetate) had previously been characterised for analysis with older SIFT-MS instruments, and so it was useful to check the kinetics data and branching ratios of the formed product ions on a modern *Profile 3* SIFT-MS instrument. The agreement with the previous SIFT/SIFT-MS data was found to be excellent, with the single exception being the ethyl acetate reaction with  $O_2^{+\bullet}$ , for which a previously reported product ion with an  $m/z$  of 31 was found not to occur. In addition, the VOCs were analysed under humid conditions, with 3-body rate coefficients derived to account for the ligand switching reactions that occur with  $H_2O$  molecules when analysing humid samples.

The second study, presented in Appendix A4, was concerned with the concurrent analyses of acetaldehyde (AA), dimethyl sulphide (DMS) and carbon dioxide. New correction factors ( $f$ ) were derived to allow the analysis of AA using both  $H_3O^+$  and  $NO^+$  as precursor ions when DMS and  $CO_2$  are present in the same sample vapour mixture; with  $H_3O^+$  using only the protonated AA ion with an  $m/z$  of 45, and with  $NO^+$ , using only the hydride ion transfer product ion at  $m/z$  43. The analysis of DMS was found to be unrealistic using  $H_3O^+$  precursor ion when AA and  $CO_2$  were also present, but DMS could be analysed easily using  $NO^+$  under these conditions, by exploiting the product parent cation, which has an  $m/z$  of 62, as shown in previous work [80]. Finally new kinetics database entries were constructed to provide approximate measurements of  $CO_2$  concentrations using both  $H_3O^+$  and  $NO^+$  precursor ions. The  $H_3O^+$  entry built upon the database entry derived previously [144] to correct for the presence of AA and DMS, while the  $NO^+$  entry devised a completely new method of  $CO_2$  analysis based on slow three-body association reactions, forming  $NO^+CO_2$  product ions with an  $m/z$  of 74.

In both of the studies, the headspace of bacterial cultures has been analysed using SIFT-MS in order to provide a simple demonstration of the value of this fundamental work. In the paper presented in Appendix A3, probiotic yoghurt was incubated for around 2 weeks inside a sealed bottle before headspace analyses revealed the presence of two of the analysed VOCs, one of mass 86u (diacetyl) and one of mass 88u (acetoin), as well as

several other volatile compounds. The concentrations derived using  $\text{H}_3\text{O}^+$  and  $\text{NO}^+$  showed good agreement for these newly characterised VOCs, with the concentrations both being measured at approximately 500 *ppbv* using both precursor ions. The paper shown in Appendix A4 includes  $\text{H}_3\text{O}^+$  and  $\text{NO}^+$  mass spectra of the headspace of a bacterial culture following overnight incubation in Dulbecco's modified Eagle's medium (DMEM) supplemented with 10% *v/v* foetal bovine serum (FBS), 2mM L-glutamine and, crucially, 0.001% *v/v* dimethyl sulphoxide (DMSO). AA,  $\text{CO}_2$  and DMS were simultaneously detected in the headspace of this culture, with DMS formed from the reduction of the added DMSO by cellular action. This cell-driven DMSO-reduction reaction is exploited in experiments presented in Chapter 5, and similar analyses of bacterial culture headspace are present in Chapters 6 and 7. This highlights the usefulness of the newly derived analytical methodologies, as only DMS could have been accurately analysed (by exploiting the DMS cation formed from  $\text{NO}^+$  reactions) in this complex mixture of gases/vapours prior to this study.

The data that were obtained in these studies have contributed to the advancement of SIFT-MS as an analytical technique for the rapid quantification of trace gas compounds. Some of the newly-derived kinetics database entries are of importance in the work presented in the following chapters of this thesis, and all of the database entries relate to the analysis of biologically-relevant volatile compounds, and could therefore find application in the future.

## 4. Headspace analyses of human cell cultures

Presented in this chapter are various SIFT-MS studies of the headspace above various human cell cultures following overnight incubation in glass bottles or while attached to microcarriers contained inside spinner flasks.

The key aspects of this work have been introduced earlier in Chapter 1.

### 4.1. Materials and methods

#### 4.1.1. Cell culture in tissue culture flasks

Six different adherent human cell types were analysed during the course of this study. These are summarised in Table 10, along with the media used for their culture. The Dulbecco's modified Eagle's medium (**DMEM**), antibiotic-antimycotic and L-glutamine were purchased from Biosera (UK), and the RPMI 1640, DMEM/Ham's F12, foetal bovine serum (**FBS**) and penicillin-streptomycin (pen-strep) were purchased from Lonza, (UK).

**Table 10. Summary of the human cell types used in the study, including the base media and supplements. Substance abbreviations are listed below the table.**

Cell type			Base medium	Glucose (g/L)	Supplementary substances
hMSCs	Mesenchymal stem cells	Primary	DMEM (BioSera, UK)	1.0	10% v/v FBS 1% v/v antibiotic-antimycotic 1% v/v (2mM) L-glutamine
hepG2	Hepatocellular carcinoma cells	Cell line			
Huh-7	Hepatocellular carcinoma cells				
HEK 293	Embryonic kidney cells				
NCI-H292	Lung, mucoepidermoid carcinoma cells				
T84	Colonic adenocarcinoma cells				
			RPMI 1640 (Lonza, UK)	2.0	10% v/v FBS 1% v/v pen-strep 1% v/v (2mM) L-glutamine
		DMEM/ Ham's F12 (Lonza, UK)	3.2	10% v/v FBS 1% v/v pen-strep 1% v/v (2mM) L-glutamine	

**Abbreviations: DMEM: Dulbecco's modified Eagle's medium; RPMI: Roswell Park Memorial Institute (medium); FBS: foetal bovine serum; pen-strep: penicillin-streptomycin.**

The primary human mesenchymal stem cell, hMSC, samples were isolated from bone marrow aspirate samples (purchased from Lonza, USA) by allowing them to attach to fibronectin-coated surfaces inside tissue culture flasks, with the non-adherent cell types, largely blood/haematopoietic cells, simply removed during routine media exchanges [152]. Cells isolated from bone marrow aspirates that were obtained from three different donors were used during this project. These cells were never cultured beyond passage number 5 (P5), in order to ensure that their multipotency was maintained.

The hepG2, huh-7, HEK 293, NCI-H292 and T84 cells are all established, immortal cell lines which have been derived elsewhere and were purchased or donated from various sources. All cell culture operations were performed under sterile conditions inside a laminar flow hood, and, in all cases, the cells were cultured in tissue culture flasks, submerged in their respective media, as indicated in Table 10. The vessels were incubated

at 37°C in a humid air environment with the carbon dioxide adjusted and maintained constantly at 5%. The medium was routinely completely removed and exchanged every 2 or 3 days in all cases.

In addition to the cell types presented in Table 10, a primary, so-called embryonic chick femur cell type (ECFC) was cultured for headspace analysis. These highly proliferative cells were obtained by first incubating chicken eggs to induce foetal development. Femurs were then removed from the foetuses and placed in tissue culture-treated flasks and submerged in a high glucose (4.5 g/L) variant of the DMEM medium indicated in Table 10. The cells that subsequently attached and grew on the surface of the vessel (ECFCs) consisted of a mixture of cells of the mesenchymal lineage, as supported by their fibroblast-like morphology. The work to derive these cells was performed by Dr. J. Henstock (Keele University).

#### 4.1.2. *Cell culture in spinner flasks using microcarriers*

Spinner flask culture was attempted as an alternative method of hMSC and hepG2 cell culture in some experiments. Both hMSCs and hepG2 cells are adherent cell types and so it was necessary to add microcarrier beads to the spinner flask cultures, in order to provide a surface area for the cells to attach, thereby ensuring that the cells would be able to grow/divide. Cytodex-1 surface microcarriers (Sigma, UK) were used for this purpose. It was necessary to hydrate/swell the microcarriers using phosphate-buffered saline (PBS), sterilise by autoclaving, and wash them several times using PBS, according to the respective manufacturers' instructions.

The Techne® spinner flasks used throughout this study were operated using a magnetic stirrer system, typically set at 20 *rpm*. During routine culture, the spinner flasks were kept open to allow gas exchange between the cells and the incubator environment which consisted of humid air with 5% carbon dioxide, maintained at a temperature of 37°C. Every 2-3 days, the spinner flasks were transferred to a laminar flow hood, the microcarriers were allowed to settle to the bottom of the vessel, and 50% of the medium was removed and replaced with fresh media. Cell numbers were monitored by removing a 1mL sample and applying a Cellstain double staining kit (Sigma, UK), according to the manufacturers' instructions. The stained samples were then examined using fluorescence microscopy and the visible live cells were counted. The total number was then doubled to account for hidden live cells.

#### 4.1.3. *Sample preparation*

In order to prepare samples of each of the cell types shown in Table 1 for headspace analysis, following expansion in standard tissue culture flasks to near-confluence, the cells were first removed from the vessels using

trypsin enzyme. The corresponding serum-containing medium was then added to deactivate the enzyme, and the cell suspension pelleted using a centrifuge, set to 4000 g for 5 minutes. The cell pellet was then suspended again in the relevant fresh medium, now additionally containing HEPES (4-(2-hydroxyethyl)-1-piperazineethanesulfonic acid) buffer at a concentration of 0.01M, so as to maintain the pH of the culture. The cells could then be counted under a microscope against the haemocytometer grid, with the viability assessed using the trypan blue exclusion method. The cell suspensions containing the required number of cells were then transferred to clean, sterile 150mL glass bottles, and topped up to the required medium volume. The headspaces of the bottles were then purged with dry, sterile air (nitrogen and oxygen mixture; BOC, UK), before they were finally sealed and then incubated at 37°C overnight (around 16 hours). This method for analysing the headspace of cells suspended in a liquid medium inside a sealed container was developed previously at Keele University [40, 41].

In order to facilitate headspace analysis of spinner flask-cell cultures, a hole was drilled into the caps of one of the two side-arms of each vessel with a silicone septum added (Fisher Scientific, UK). This could then be penetrated with a hypodermic needle coupled to the sampling arm of the SIFT-MS instrument, allowing direct headspace sampling into the flow tube. Preparation for the headspace analysis of spinner flask cultures involved simply exchanging 75% of the media (100% cannot be exchanged without losing the microcarriers), prior to purging the headspace with dry air, sealing the vessel, and incubating overnight at 37°C.

#### 4.1.4. *Headspace analysis*

The temperatures of the samples were maintained at 37°C during analysis using a water bath or incubator. Direct sampling of the headspace of each vessel was achieved by puncturing a septum, located on the caps of the glass bottles or a side-arm cap of the spinner flask. SIFT-MS analysis was then conducted in order to generate FS mass spectra or MIM mode time profiles, from which the concentrations of gaseous compounds could be derived. The pressure inside the bottles reduced by about 10-20% (depending on the sample flow rate) as the headspace was sampled, and so dry air was used to return the pressure to 1 bar between analyses. Further details of the analytical technique can be found in Chapter 2, and in some recently-published review articles [35, 36].

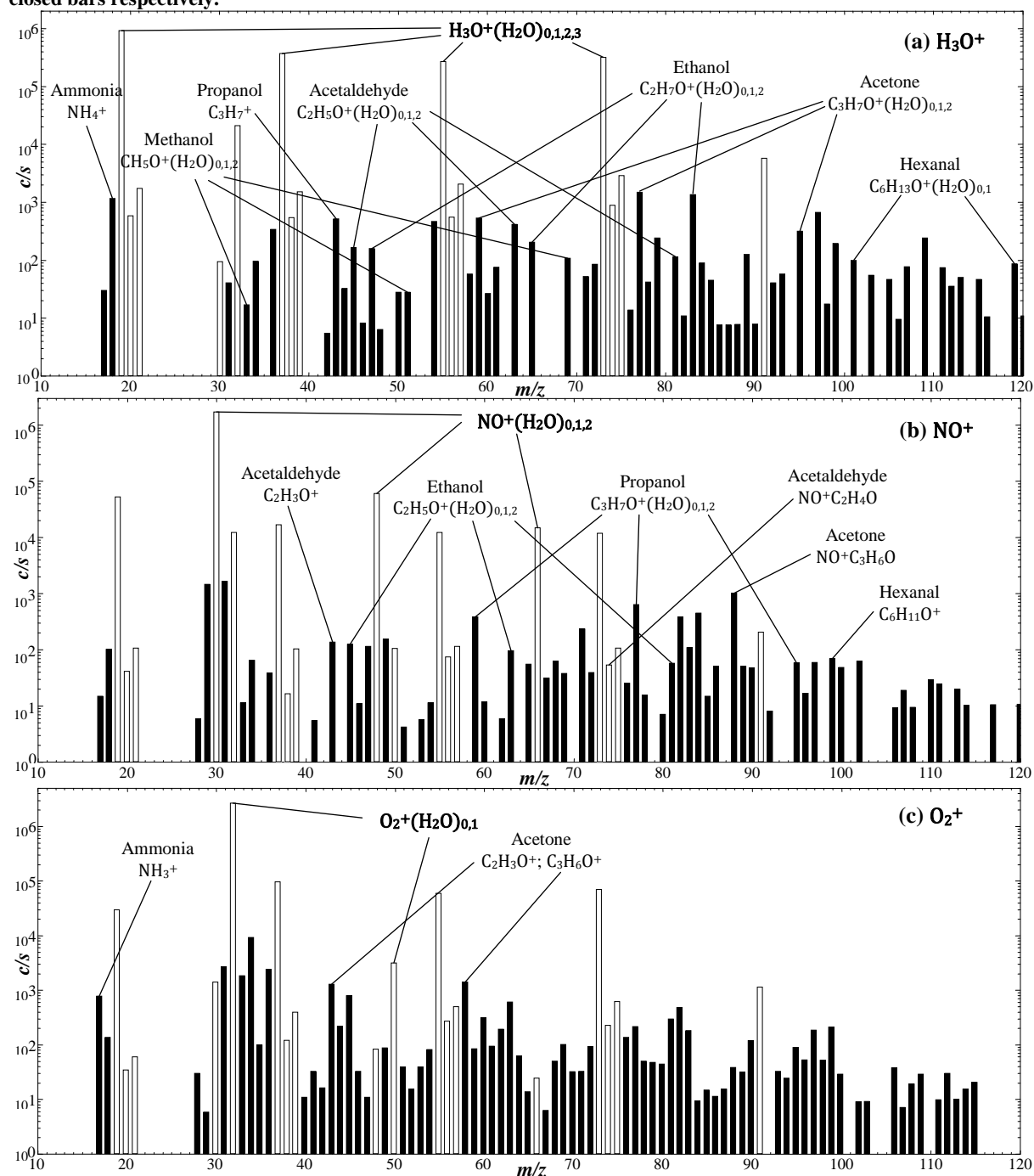
## 4.2. Results and discussion

### 4.2.1. Analysis of the headspace of cell culture media and supplements

In order to determine which volatile compounds were emitted or consumed by each of the cultured cell types, it was first necessary to determine which compounds were present in the headspace of their respective culture media (see Table 10). Thus, for each medium type, mass spectra were obtained by operating SIFT-MS in the Full Scan (FS) mode. Example spectra showing the analysis of the DMEM medium used to culture four of the analysed cell types are shown in Figure 9. Evidently, numerous compounds are present in the headspace of this medium, some of which are not immediately identifiable. Nonetheless, ammonia, acetone, acetaldehyde (AA) and the three simplest alcohols can be identified with confidence, as these are commonly observed in human breath [81, 86, 153]. Hexanal is also labelled in the  $\text{H}_3\text{O}^+$  and  $\text{NO}^+$  spectra (Figure 9a and 9b respectively), as this was shown to be present in the headspace of DMEM media in solid-phase microextraction gas chromatography mass spectrometry (SPME-GC-MS) experiments, which were performed by the Mass Spectrometry Group during a visit to the J. Heyrovský Institute in the Czech Republic. The product ions formed from the reactions of hexanal with  $\text{H}_3\text{O}^+$  and  $\text{NO}^+$ , as well as the kinetics data necessary to perform quantitative analyses were derived previously [112]. Notably, fewer compounds have been labelled in the  $\text{O}_2^{+\bullet}$  spectrum, despite the fact that a greater number of product ions are present. These  $\text{O}_2^{+\bullet}$  reactions more often proceed *via* dissociative charge transfer [35], and therefore more often result in the formation of overlapping product ions in complex mixtures of gases/vapours, which are difficult to identify with certainty and are therefore of limited value in analysis.

Ammonia quantification is most reliable when performed with  $\text{O}_2^{+\bullet}$ , however, because the primary product ion appears at  $m/z$  17, which is separated from the peak at  $m/z$  19 which is always relatively large in  $\text{H}_3\text{O}^+$  spectra [35, 36]. The ammonia concentration in the headspace is measured as 200 *ppbv* in to the  $\text{O}_2^{+\bullet}$  spectrum. This equates to  $\sim 7\mu\text{M}$  in the liquid phase, assuming a dynamic equilibrium consistent with Henry's Law ( $K_{\text{H}}(37^\circ\text{C}) = 34 \text{ mol kg}^{-1} \text{ bar}^{-1}$  [151]). Given that between pH 7.4 and 8.0, then around 97% of the ammonia is present in its ionised form, ammonium ( $\text{NH}_4^+$ ), according to the acid dissociation constant ( $\text{p}K_{\text{a}}=4.74$ ), and so the total ammonia and ammonium present in the liquid phase is approximately  $230\mu\text{M}$ .

**Figure 9.** SIFT-MS FS mode spectra (ion counts-per-second, *c/s*, against mass-to-charge ratio, *m/z*) of the headspaces of 50mL of DMEM supplemented with FBS (10%), antibiotic-antimycotic (1%) and L-glutamine (2mM), obtained using (a)  $\text{H}_3\text{O}^+$ ; (b)  $\text{NO}^+$ ; and (c)  $\text{O}_2^+$  precursor ions. The precursor and product ions are indicated with open and closed bars respectively.



The source of several of these compounds has previously been tied to the presence of foetal bovine serum (FBS) in the culture media by a previous SIFT-MS study [41] and, as indicated in Table 10, each of the media types used cultured each of the cell types during this study contained 10% (v/v) FBS. Thus further analyses of the compounds present in the headspace of the FBS and neat DMEM were conducted, the results of which are presented in Table 11.

**Table 11.** The headspace concentrations, given in parts-per-billion by volume (*ppbv*) of various volatile compounds present in samples of neat DMEM (0%), DMEM with 10% v/v FBS, and neat FBS (100%), following a sealed incubation period of around 16 hours at 37°C. The analyses were performed using SIFT-MS operated in MIM mode using H<sub>3</sub>O<sup>+</sup>.

FBS concentration in DMEM (v/v)	Headspace concentration ( <i>ppbv</i> )				
	Methanol	AA	Ethanol	Propanol	Acetone
0%	280	131	124	5	21
10%	255	172	358	43	453
100%	90	467	2051	341	4144

The data indicate that ethanol and acetone largely originate from the FBS, given that their concentrations in the 100% FBS are measured to be approximately 10 times greater than those in the 10% samples. However, the acetaldehyde (AA) concentration is increased by only about 3 times in the 100% FBS, relative to the 10%, indicating that the serum is not the sole source, but does contribute to the acetaldehyde concentration of the complete DMEM medium. These results are consistent with the data published in 2009 [41]. The data additionally indicate that propanol also originates from the FBS, and that methanol is actually present in higher concentrations in DMEM and is diluted by the addition of FBS. FS mode analyses of the headspaces of the other supplementary cell culture media components, L-glutamine and antibiotic-antimycotic, also revealed elevated levels of ethanol: approximately 2000 *ppbv* in both cases. However, considering that these components constituted only 1% of the complete media volumes, the contributions to the headspace ethanol concentrations were only around 20 *ppbv*, which is 5% of the ethanol level when FBS is present at the usual 10% v/v level.

An additional experiment was performed in order to further understand the origins of these common volatile compounds, particularly the AA, which did not clearly originate from the DMEM or FBS. In this case, samples of distilled water, glucose solution, neat DMEM (0%), DMEM with 10% v/v FBS, and neat FBS (100%), were incubated at 37°C or 70°C for the 16-hour period. The samples were all then returned to 37°C immediately prior to the SIFT-MS headspace analyses, which were performed using the MIM mode, with H<sub>3</sub>O<sup>+</sup> employed as the precursor ions. The results of these analyses are presented in Table 12.

**Table 12.** The headspace concentrations, given in parts-per-billion by volume (*ppbv*) of various volatile compounds present in samples of distilled water (dH<sub>2</sub>O), a 1 g/L glucose solution in water, neat DMEM (0%), DMEM with 10% v/v FBS, and neat FBS (100%), following a sealed incubation period of around 16 hours. Separate samples were incubated at either 37°C or 70°C, as indicated, but all were held at 37°C during headspace analyses, which were performed using SIFT-MS operated in MIM mode using H<sub>3</sub>O<sup>+</sup> precursor ions. The DMEM and FBS samples analysed in these experiments originate from batches different from those that were analysed in [41].

Sample	Headspace concentration ( <i>ppbv</i> )							
	Methanol		AA		Ethanol		Acetone	
	37°C	70°C	37°C	70°C	37°C	70°C	37°C	70°C
dH <sub>2</sub> O	41	50	11	19	40	50	31	23
Glucose (1g/L)	50	49	10	60	60	48	19	32
DMEM	261	268	70	1081	126	167	14	31
DMEM, 10% FBS	227	266	95	415	219	222	162	80
FBS	100	170	167	643	807	904	1670	1853



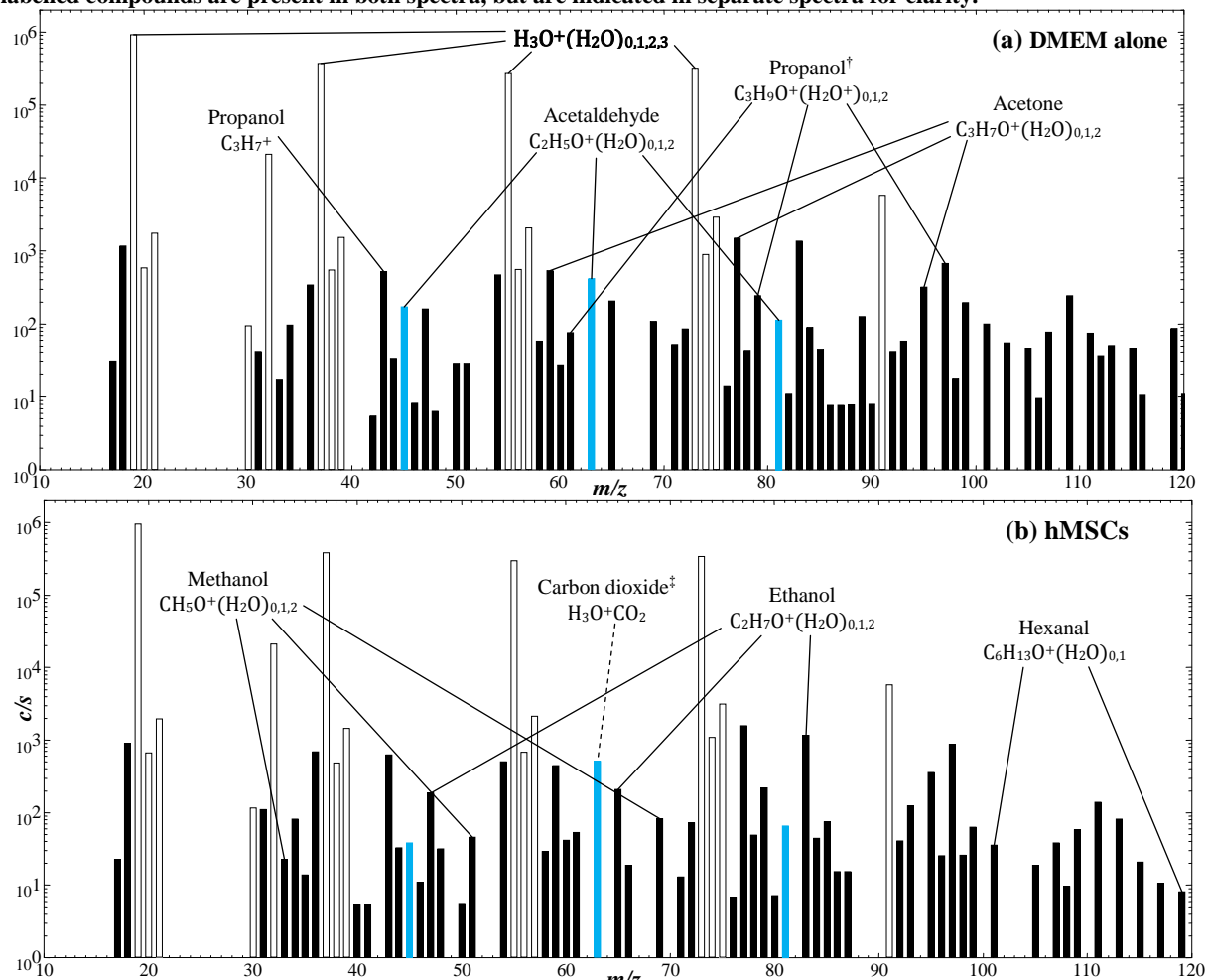
The lower concentrations of AA, ethanol and acetone measured in the FBS samples that were incubated for 37°C for the 16-hour period prior to analysis, compared to those presented in Table 11, are surely due to biological variability between the different batches of FBS, which originate from different animals. However, the key findings that these compounds originate largely from the FBS, and that the methanol originates largely from the DMEM, were substantiated.

Incubating at 70°C had little effect on the concentrations of methanol, ethanol and acetone in any of the samples, indicating that these compounds are not formed from the breakdown of glucose nor other compounds present in the DMEM or FBS. Evidently, these compounds are either present due to contamination from air at some point during their processing, or are naturally present in the FBS when it is extracted. The major finding from this brief study was that AA was clearly increased by more than ten times in the DMEM and five times in the FBS headspace following overnight incubation at 70°C. The DMEM contained glucose at a concentration of 1g/L, and yet a similar increase was not observed in the glucose-water solution, which suggests that simple breakdown of glucose was not responsible for the increased concentrations of acetaldehyde. The AA formation must therefore be caused by breakdown of other compounds present in the DMEM and FBS, or by their interaction with glucose. In any case, the results of these two experiments suggest that low levels of AA, as well as ethanol, acetone and propanol will always be present in the headspace of cell cultures when FBS is present in the media.

#### 4.2.2. *Interpretation of SIFT-MS mass spectra derived from the headspace of static cells cultures*

In all of the experiments described in this section, the cells were initially cultured in tissue culture flasks, suspended in 50mL of their respective media and transferred to 150mL glass bottles, prior to their analysis using SIFT-MS (see the Materials and Methods section). Example FS mass spectra showing the analysis of the medium alone and medium containing  $1(10^8)$  hMSCs are given in Figure 10.

**Figure 10.** SIFT-MS mass spectra (ion counts-per-second, *c/s*, against mass-to-charge ratio, *m/z*) obtained using the  $\text{H}_3\text{O}^+$  precursor ion showing the headspace of glass bottles containing (a) DMEM medium (10% FBS, 1% antibiotic-antimycotic, 2mM L-glutamine) alone (repeated from Figure 9a for comparison); and (b) the same medium containing  $1(10^8)$  human mesenchymal stem cells (hMSCs) following 16-hours incubation at  $37^\circ\text{C}$ . Each of the labelled compounds are present in both spectra, but are indicated in separate spectra for clarity.



<sup>†</sup> The listed ions and labelled peaks are known to be formed from propanol, but quantitative analysis is usually achieved using only the ion at *m/z* 43, due to the potential for overlaps with the isobaric product ions formed from other volatile compounds, such as acetic acid or methyl formate [134]

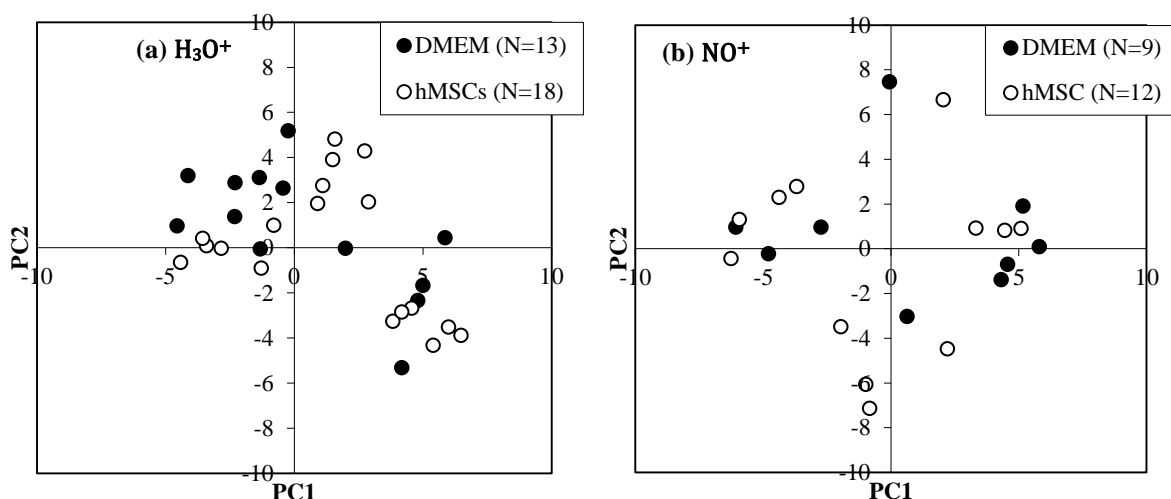
<sup>‡</sup> the contribution of  $\text{CO}_2$  to the peak shown at *m/z* 63 is only a small fraction of the total peak height due to the presence of AA in the sample, and the fact that the  $\text{H}_3\text{O}^+\text{CO}_2$  ion is formed *via* slow 3-body association reactions (see Chapter 3 and [108, 144])

As mentioned above, various compounds are easily identifiable in the medium headspace (see previous section). However, the concentrations of the majority of these compounds are seemingly unchanged in the headspace following incubation with  $1(10^8)$  hMSCs (see Figure 10b). The two most notable exceptions, however, are carbon dioxide, which is produced by the cells, as one might expect, and AA, which is depleted from the culture headspace. The causes of this AA-depletion are explored further in the next chapter. The product ions formed from  $\text{CO}_2$  and AA are highlighted in red in the spectra presented in Figure 10 and, as is shown, they form product ions which overlap at *m/z* 63 ( $\text{H}_3\text{O}^+\text{CO}_2$  and  $\text{C}_2\text{H}_5\text{O}^+\text{H}_2\text{O}$ ). Clearly, this could create a problem in the quantification of both compounds, but the results of previous experiments have made it possible

to perform such analyses such as those in Chapter 3 and [108, 144]. Another major point to be derived from the mass spectra is that there are clearly numerous product ion signals which cannot readily be assigned to an analyte compound without further investigation. Indeed, as mentioned in the previous section, the presence of hexanal in the DMEM headspace could only be ascertained by SPME-GC-MS analyses which were performed by the Mass Spectrometry Group at the J. Heyrovský Institute (Prague, Czech Republic). SIFT-MS can also be used to measure the concentration of hexanal in culture headspaces [112] was also found to be depleted due to the additional presence of hMSCs, and this is somewhat consistent with the concentrations measured in the headspaces of the samples analysed in Figure 10. These were around 40 *ppbv* of hexanal in the DMEM headspace and 20 *ppbv* in the hMSC sample headspace.

Ultimately, however, it has to be said that the spectra derived from the analyses of the DMEM alone and the DMEM containing hMSCs are only clearly distinguishable due to the loss of AA. This unfortunate finding was consistently the case for the analyses of samples of DMEM with and without hMSCs. Further evidence for this is provided by principal component analysis (PCA), which was performed using software that is specific for SIFT-MS datasets, developed by Dryahina & Španěl [154]. Example PCA plots are shown in Figure 3.

**Figure 11. Principal component analysis (PCA) plot (principal component 1 against principal component 2) showing the analysis of the data obtained from SIFT-MS mass spectra, derived from the headspace analyses of samples of DMEM alone, and DMEM containing hMSCs. The PCA analysis is based on the peak heights contained in spectra that were obtained using (a)  $\text{H}_3\text{O}^+$  and (b)  $\text{NO}^+$  precursor ions, over the  $m/z$  range of 10-120.**



The PCA data presented in Figure 11 is based on the peak heights (count rates) of each of the peaks present in SIFT-MS mass spectra ( $m/z$  range: 10-120) derived from analyses of the headspace of sealed vessels containing DMEM medium alone or the medium with hMSCs. No clear separation between the two populations is observed in either  $\text{H}_3\text{O}^+$  or  $\text{NO}^+$  spectra, but it should be noted that the sample numbers (N) were low.

Performing simple T-tests on the same data revealed that the count rates were significantly different ( $p < 0.05$ ) between the medium and hMSCs samples at eight  $m/z$  values, of which the three most significant are known to be associated with AA and/or  $\text{CO}_2$  ( $m/z$  45, 63 and 81; see Chapter 3 and [108, 144]), and one has an  $m/z$  value of 99, which indicates the compound could be the third hydrate of protonated AA. The remaining four  $m/z$  values may relate to product ions formed from other volatile compounds that are either produced or consumed by the cells, but the mean ion count rates ( $c/s$ ) for most are approaching 1  $c/s$ . This is considered to be equivalent to 0.1  $ppbv$  for compounds that react with  $\text{H}_3\text{O}^+$  at the typical rate ( $k$ ) of  $3(10^{-9}) \text{ cm}^3 \text{ s}^{-1}$  [36], which is below the limit of detection for most VOCs when analysed by SIFT-MS.

#### 4.2.3. *Quantification of VOCs present in the headspace of static cell cultures*

While it is possible to measure the concentrations of volatile compounds using the count rates present in SIFT-MS FS mode mass spectra such as in Figure 10, the use of the MIM mode for this process is more accurate due to the extra dwell time of the downstream mass spectrometer on the product ions [35, 36]. In order to progress the work presented in the previous section, the increased accuracy of the MIM mode was exploited in order to accurately quantify the concentrations of methanol, AA, carbon dioxide, ethanol and acetone in the headspaces of the seven different cell types shown in Table 10 (section 4.1.1.) when cultured inside sealed glass bottles. The results of these analyses are shown in Table 13.

As shown in the mass spectra in Figure 10, the headspace concentrations of methanol, ethanol and acetone are not obviously affected by the presence of any of the cell types, with the possible exception of the NCI-H292 lung epithelial cells, for which the headspace ethanol concentrations appear to increase proportionally with cell number. This ethanol increase could simply be due to contamination during sample preparation, as the original cell suspension is diluted in fresh media in order to produce the correct cell numbers for each sample, but given that the possibility of ethanol production by human cells has been hypothesised [155], and that this trend is not so apparent in the other human cell types and so may be worthy of further investigation. The carbon dioxide concentrations were seen to increase with cell number in all cell types, albeit by varying amounts. The extent of the  $\text{CO}_2$  increase could be related to the proliferative state of the cells, which may vary by cell type or the condition of the cells (cell cycle) immediately before they were transferred to the glass bottles.

**Table 13.** Single SIFT-MS measurements of the concentrations of methanol, acetaldehyde (AA), carbon dioxide, ethanol and acetone, given in parts-per-billion by volume (*ppbv*), in the headspaces of varying numbers of six different human cell types and one embryonic chick femur cell, ECFC, type. All analyses were performed by operating SIFT-MS in MIM mode, employing  $\text{H}_3\text{O}^+$  as precursor ions. Details of these cells can be found in Table 10. All samples contained typical liquid and headspace volumes of 50mL and 100mL respectively, and measurements were performed following an overnight (16 hours) incubation period. The water vapour levels were between 3.5 and 4.5% in all experiments.

Cell type	Cell number ( $\times 10^6$ )	Headspace concentration ( <i>ppbv</i> )				
		Methanol	AA	$\text{CO}_2$ ( $\times 10^7$ )	Ethanol	Acetone
hMSC	0	Not measured	143	0.0	324	578
	5		37	0.5	311	558
	10		14	1.5	350	551
	13		22	1.8	361	595
	0	228	191	0.1	440	217
	30	280	20	0.8	565	260
	0	47	122	0.0	409	496
hepG2	100	46	27	1.2	373	431
	0	541	239	0.0	544	508
	38	577	10	0.6	599	624
huh-7	0	257	76	0.1	761	416
	50	229	1	0.9	922	401
	80	284	1	1.2	794	472
	100	317	0	1.5	921	557
HEK 293	0	56	78	0.1	368	312
	20	53	17	1.3	402	339
	40	56	17	1.4	383	348
	60	64	18	1.8	409	334
NCI-H292	0	71	87	0.0	289	323
	10	90	15	2.2	444	341
	20	99	16	3.3	602	338
T84	0	168	64	0.4	361	350
	5	146	21	1.9	478	312
ECFC (chick)	0	324	204	0.0	434	638
	60	320	9	4.4	565	701

The AA concentrations were depleted in the headspaces of each of the seven mammalian cell types, four of which are cancer cell types (hepG2, huh-7, NCI-H292 and T84; see Table 10) to an apparent baseline concentration, which in the case of the huh-7 cells was at sub-*ppbv* concentrations. This contrasts with the previously mentioned SIFT-MS studies of the gas/vapour phase above cultured lung cancer cell lines SK-MES and CALU-1, and the non-tumourigenic lung epithelial cell line NL20 [40, 41], all of which produced AA in proportion to their cell number under essentially the same experimental conditions. On the other hand a telomerase-positive lung fibroblast cell line, 35FL121 Tel+, was found to consume AA similarly to the cell types listed in Table 13, consuming AA to an apparent minimum headspace concentration of 50 *ppbv* [41]. The minimum level that is reached over the 16 hour incubation period is likely to be cell type-, number- and culture condition-dependent. The cause of this AA depletion from the headspace of cell cultures is explored in Chapter 5.

An experiment was also performed to explore the influence of prolonged culture of the cells inside the sealed glass bottles on the concentrations of compounds present in the culture headspace. In this case, 25 million hMSCs were first suspended in 50mL of DMEM media inside a glass bottle and the headspace was analysed by

SIFT-MS in the usual way, as detailed in section 4.1. Following the analysis, the bottle was returned to the incubator and held for another 24 hours, before the headspace was analysed again, and then one more time after another 24 hours. The results are given in Table 14

**Table 14. Concentrations of several volatile compounds (given in parts-per-billion by volume, *ppbv*) measured in the headspace of samples containing 50mL of complete DMEM medium alone (see Table 10), and medium containing approximately 25 million human mesenchymal stem cells, hMSCs. The analyses first took place following the usual overnight (~16 hours) incubation period, and then following a further 24 and 48 hours, as indicated.**

Incubation period (h)	Headspace concentration ( <i>ppbv</i> )							
	Acetaldehyde		Carbon dioxide ( $\times 10^7$ )		Ethanol		Acetone	
	DMEM	hMSCs	DMEM	hMSCs	DMEM	hMSCs	DMEM	hMSCs
16	168	18	0.45	0.76	392	495	196	235
40	192	16	0.56	2.07	381	422	208	226
64	199	16	0.58	2.30	437	521	196	277

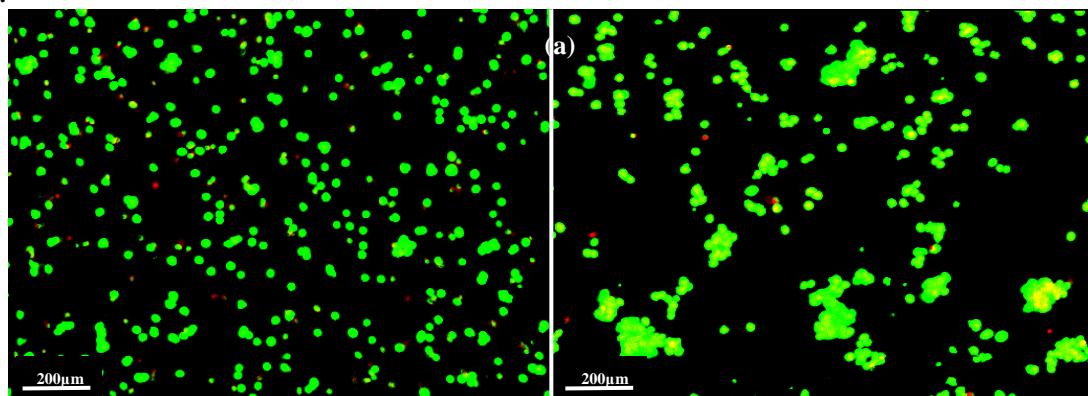
The headspace concentrations derived in the analysis after the initial 16 hour incubation period generally agree with the results presented in Table 13, in that ethanol and acetone concentrations in the headspace of samples of DMEM alone and cells with media remained essentially equal, while the concentrations of CO<sub>2</sub> increased and AA decreased. The concentrations of ethanol and acetone remained constant in the headspace over the two days that followed (40 and 64 hours total incubation), as did the concentration of AA, indicating that the aldehyde was consumed to a minimum level within the first 16 hours. This apparent minimum level in the headspace, ~20 *ppbv*, is approximately equivalent to 140nM by Henry's Law ( $K_H(37^\circ\text{C}) = 7 \text{ mol kg}^{-1} \text{ bar}^{-1}$  [151, 156]). The decline in the concentration of AA is likely due to the activities of intracellular aldehyde dehydrogenase (ALDH) enzymes, which are responsible for the metabolism of aldehydes. The decline and apparent stagnation at a minimum concentration can be partially explained by Michaelis-Menton enzyme kinetics, which indicate that the activities of the ALDH enzymes will decline when the substrate concentration is low [139]. This is explored further in Chapter 5. Also shown by the analyses in Table 14 is that the CO<sub>2</sub> concentration continues to increase when the bottles are incubated for 48 further hours, indicating that the cells remain viable in the glass bottles. This trend is confirmed in the next section with a different cell type.

#### 4.2.4. *Effects of overnight incubation on cell viability*

Prior to the 16-hour incubation period, the viability of the cultured cells was routinely checked using the Trypan blue exclusion method, and measured at typically 80-90% viability in all experiments. The cell viability was also checked following SIFT-MS analyses in many cases, with no significant decline observed. This is further illustrated by an additional experiment in which the Cellstain double stain (Sigma, UK) was applied to samples of hepG2 cells following their removal from a tissue culture flask. The cells were then examined using confocal microscopy, with the live cells stained green and the nuclei of dead cells stained red. Images were

obtained from this sample; an example of this is given in Figure 12a, in which  $1.5(10^7)$  of the remaining cells that were removed from the flask were suspended in a 150mL glass bottle and suspended in 15mL of medium (see Table 10), following the standard sample preparation method for the analysis of cell culture headspace by SIFT-MS (see section 4.1.3. and [40, 41]). Following the 16 hour period, the Cellstain double stain was applied to samples of the hepG2 cells and fluorescence microscopy was again applied in order to obtain new images for comparison, an example of which is shown in Figure 12b. This method of viability assessment is qualitative, but the images do show that the viability of the hepG2 cells was maintained at a similar level following the overnight incubation period.

**Figure 12. Microscopy images (10x) showing hepG2 hepatocellular carcinoma cells following application of the Cellstain double stain, with live cells stained green and the nuclei of dead cells stained red. The samples were analysed (a) prior to and (b) following overnight incubation at 37°C inside sealed glass bottles. The images are adapted from [157].**



#### 4.2.5. Spinner flask cell cultures

A potential problem with the headspace analysis methods described in the previous section, with the cells contained inside sealed bottles, is that the cells are transferred from the tissue culture flasks to the glass bottles 16 hours before the analysis, disturbing their growth. As a result, the proliferation rate of the cells is likely much lower than when attached to the surface of the flask, which would surely affect their enzyme expression levels [158] and may thereby impact the concentrations of the volatile compounds present in the headspace. Given that the main goal of the project was to develop methods of analysing larger scale bioreactor cultures, it was decided that the cells should be cultured in small scale spinner flask bioreactors. In order to culture these adherent cell types in spinner flasks, it was also necessary to attach them to microcarrier beads. Cytodex-1 surface microcarriers were utilised for the culture of the cells (see Materials and Methods section for further details).

In order to ensure that the microcarrier beads would not contaminate the cell-containing samples, the volatile compounds were analysed in the headspace of the microcarrier beads contained in PBS (2 g/L

concentration) inside sealed glass bottles, following the hydration step (see section 4.1.2.). In one experiment, the headspace was analysed following this step, while in another, the beads were washed three times with fresh PBS prior to the analysis, as is the normal protocol for microcarrier preparation. The results are shown in the Table 15.

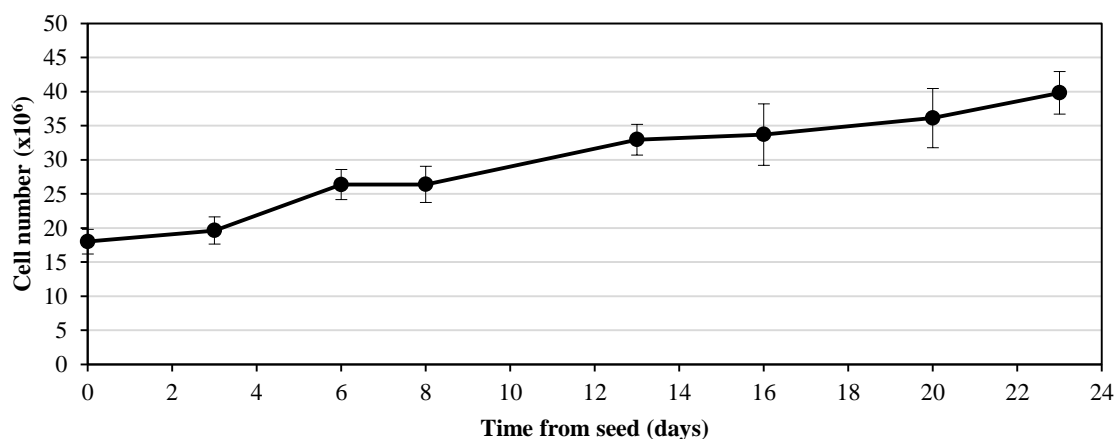
**Table 15. Concentrations of methanol, acetaldehyde (AA), ethanol and acetone measured in the headspace of Cytodex-1 microcarriers contained in 15mL of PBS at a concentration of 2 g/L.**

		Headspace concentration ( <i>ppbv</i> )			
		Methanol	AA	Ethanol	Acetone
PBS		76	15	200	24
Cytodex-1	unwashed	76	11	241	54,497
	washed	64	12	171	147

As is shown in Table 15, the only serious contaminant that could be identified was acetone, which was emitted by the Cytodex-1 microcarriers. The concentration measured in the unwashed microcarriers is extremely high, but the washing steps largely removed this contaminant. Cell cultures containing Cytodex-1 microcarrier beads could be expected to contain a falsely high acetone concentration, but only by around 60 *ppbv* for every g/L of microcarriers, which is acceptable, considering that the FBS alone can contribute as much as 700*ppbv* in cultures where microcarriers are not present (see Table 13). The concentrations of other compounds present in the headspace of washed and unwashed microcarriers were not elevated above the levels in the PBS alone, and therefore pose no complication to the analyses of the vapours emitted by microcarrier-cell cultures.

During spinner flask culture, the cell numbers were measured every few days, as described in section 4.1.2.. An example plot of the cell counts for hMSCs cultured in a spinner flask containing 100mL of DMEM medium and a microcarrier concentration of 7 g/L is plotted in Figure 13.

**Figure 13. The cell numbers measured over the course of a 24-day spinner flask culture (100mL working volume) of hMSCs attached to Cytodex-1 surface microcarriers (7 g/L).**



It is seen that the cell numbers increased gradually from a starting cell number of  $1.8(10^7)$  to a maximum of approximately  $3.9(10^7)$  cells, amounting to a 2.2-fold increase over the 24 days, with a mean



doubling time of around 20 days. Headspace analyses were performed on day 13, when approximately  $3.3(10^7)$  cells were present, and gave consistent results with those reported in section 4.2.3., where the cells were cultured in glass bottles, with concentrations of methanol (270 *ppbv*), ethanol (750 *ppbv*) and acetone (800 *ppbv*) consistent between the headspace of samples with hMSCs present and the control sample which did not contain cells. The carbon dioxide concentrations were elevated from 0.9% by volume in the control to 1.8% in the hMSC-containing spinner flask, and AA was again depleted from 172 *ppbv* in the control to only 2 *ppbv* in the cell-sample.

Given that the medium was exchanged immediately before sealing the vessel, 16 hours before the headspace analysis, as usual, one might speculate that the particularly low AA concentration measured in the cell-containing sample, which is approaching the limit of detection of the SIFT-MS instrument, could be due to a heightened proliferative state of the cells, given that they were analysed mid-culture, as opposed to in the previously described methods, where their culture is disturbed by their transfer to the glass bottles. Clearly this would require further analysis. This point aside, however, the culture of hMSCs on microcarriers induced no clear difference to the compounds, or the product ions present in the mass spectra (data not shown), obtained from the analysis of the headspace by SIFT-MS.

### 4.3. Summary remarks

The studies presented in this chapter concern the analysis of the headspace of cell cultures by SIFT-MS. As was highlighted in the earlier work [41], it is prudent to first analyse the compounds present in the culture media alone. The present work confirmed the previous findings that foetal bovine serum (FBS), commonly a 10% v/v supplement in DMEM medium, is the major source of the VOCs acetone and ethanol, and does contribute to the observed acetaldehyde (AA) concentration observed in media headspace. In addition, it was observed that FBS is also the major source of propanol, while larger concentrations of methanol are present in the headspace of the DMEM alone, and are diluted by the addition of FBS. The presence of acetaldehyde in the headspace of the DMEM alone and FBS samples was explored further, and it was found that heat-treating the samples overnight at 70°C before returning them to 37°C caused the concentrations of AA to increase several times in the headspace of both samples. This increase could not be attributed directly to the presence of glucose, however, as similar changes were not observed in the headspace of a glucose-water solution. Hence the work presented in this chapter has furthered the media studies initiated in the aforementioned previous report [41].

The compounds present in the headspace of human cell cultures have been analysed by SIFT-MS in this chapter using methods that were also pioneered previously [40, 41], in which the culture headspace was sampled from glass bottles containing the cells in liquid medium. SIFT-MS mass spectra obtained from the analyses of the headspace of cultured cells were compared to those obtained from the medium alone. The clearest difference in signal levels occurred at  $m/z$  45 and 81, which relate largely to AA. This was shown to be removed from the medium headspace due to the presence of each of the seven cell types analysed *via* mass spectra analyses and by quantitative MIM mode analyses, and is most likely due to the actions of intracellular aldehyde dehydrogenase enzymes (ALDH); the activities of which are explored in Chapter 5. This result was also related to the previously mentioned study [41], in which the headspace of three lung cell cultures were analysed by SIFT-MS. In this case one of the cell types (a non-cancerous telomerase-positive lung fibroblast) was found to remove AA from the medium, while two others, one cancerous the other not, were shown to emit AA in proportion with the cell number.

The product ion at  $m/z$  63, which relates to both AA and carbon dioxide (see Chapter 3), was also found to be significantly different in cell culture headspace compared to the medium alone, and indeed CO<sub>2</sub> was shown to be produced by the cells by quantitative MIM mode analyses. Despite this, the application of principal component analysis (PCA) to all of the available mass spectral data relating to the most studied cell type (hMSCs) could not distinguish between the data derived from the headspace analyses of the media alone and the media with cells. Similar results were also obtained from the analyses of the headspace of spinner flask cultures, in which the headspace was analysed non-invasively and without significantly disturbing the cells growth. These results are indicative of a lack of available biomarkers in the headspace of the human cell cultures analysed in the present study. However, the fact that SIFT-MS mass spectra derived from these headspace samples do not show large concentrations of compounds could facilitate the identification of microbial infections. This premise is explored later in Chapters 6 and 7.

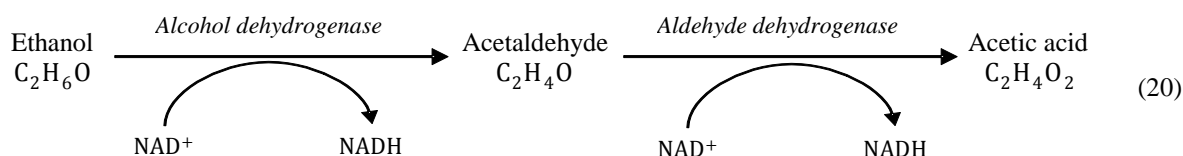
## 5. Acetaldehyde and dimethyl sulphoxide metabolism by cultured human cells

### 5.1. Introduction.

It was reported in the previous chapter that the concentrations of the toxic volatile organic compound (VOC) acetaldehyde (AA) were lowered in the headspace of cultures of six different human cell types, compared to those in their respective media, following 16 hours of incubation at 37°C. In addition, it has been determined as part of this work that some cultured cell types will act on the common cryopreservant and solvent dimethyl sulphoxide (DMSO), reducing it to the highly volatile dimethyl sulphide (DMS). These findings are examined in the present Chapter. Much of the work presented here has been accepted for publication under the title: “*A study of enzymatic activity in cell cultures via the analysis of volatile biomarkers*” [157]. A copy of this article can be found in Appendix A6.

#### 5.1.1. Aldehyde dehydrogenase (ALDH) and the detoxification of acetaldehyde (AA) by human cells

In mammals, AA is known to be an intermediate in the ethanol metabolism pathway [139], which is summarised in equation (20):



As is depicted, AA is formed from the oxidation of ethanol *via* the enzyme alcohol dehydrogenase (ADH) and removed (detoxified) by a second oxidation reaction mediated by aldehyde dehydrogenase (ALDH) enzymes to produce acetic acid, which exists largely in the form of acetate ions in pH-neutral solutions. The coenzyme nicotinamide adenine dinucleotide ( $\text{NAD}^+$ ) also participates in both reactions. It should be noted that both ADH and ALDH describe families of enzymes that are active for a variety of alcohol and aldehyde substrates respectively. ALDH1B1 and ALDH2 isozymes have the greatest affinity for AA in human cells [159, 160], and these are most abundant in the cells of the liver [159, 161], with the formed acetate ions further metabolised in peripheral tissues [162].

Deficiencies in ALDH activity have been linked to the development of diseases such as Sjögren–Larsson syndrome [163], pyridoxine-dependent epilepsy [163] and Parkinson’s disease [164]. Some such diseases have also been linked more specifically to the formation of AA including alcoholic liver disease [165, 166], ethanol-induced cancers [163], ischaemic tissue diseases [167] and Alzheimer’s disease [168]. In spite of

this, disulfiram (DSF; trade-name Antabuse), an ALDH inhibitor, has been utilised in the treatment of alcoholism, causing an extended “hangover” effect, and has been proposed for the treatment of cocaine addiction [169]. On the other hand, breast [170] and pancreatic [171] cancer stem cells have been characterised by their heightened ALDH expression *in vitro*, which may play a role in drug resistance [172, 173]. Furthermore, the aforementioned ALDH inhibitor, DSF, may contribute to future cancer therapies, according to *in vitro* [174], and *in vivo* [175], studies.

Analysis of ALDH activity is commonly performed in solutions containing the enzyme, a suitable aldehyde substrate and  $\text{NAD}^+$  by using a spectrophotometer to measure the change in absorbance at 340nm, caused by the formation of NADH, as the reaction progresses [159, 160]. This technique has been widely used for the study of the activities of individual enzymes obtained from cell lysates, but cannot be used for the study of the metabolism of live cells and cannot provide direct information on the substrate. More recently a flow cytometry-based assay, ALDEFLUOR® (STEMCELL Technologies Inc.), has been developed for isolating so-called ALDH-bright ( $\text{ALDH}^{\text{br}}$ ) cells from a mixed population. This technique also utilises an ALDH inhibitor, diethylaminobenzaldehyde (DEAB), for control experiments. The system has been used to isolate haematopoietic stem cells from bone marrow and peripheral blood based on their high ALDH expression [176]. In addition, the technique has been used to identify differences in the ALDH expression levels between several lung cancer cell lines, which may be due to the stem cell-like properties of some cancer cells [177]. ALDEFLUOR has found utility in the identification and isolation of cell types based on their ALDH expression, but it is not designed for the *in vitro* analysis of ALDH-mediated metabolism or enzyme kinetics.

As discussed in Chapter 4, the consumption of AA by six human cell types was detected by headspace analysis experiments. In addition, changes in vapour phase AA concentrations have previously been reported for at least twelve other cell types. A summary of their findings with respect to AA is given in Table 16, where it can be seen that six of these cell types were found to consume AA from the media, similarly to the cell types considered in Chapter 4, while six were conversely found to emit AA into the medium, with the effects being observed in the gas phase. The causes of these findings are surely related to the reactions that are illustrated by equation (20), and some evidence for this is provided by the consistency of the results of one the headspace analysis studies in Table 16, in which the BEAS2B cells produced AA and A549 cells consumed AA from their respective media [42], with the aforementioned ALDEFLUOR study which showed that the same cell types contained very low (0.3%) and very high (94%) ALDH expression levels respectively [177]. The results of these

two studies indicate the possibility that the production or consumption of AA by a cell type could be a predictor of their ALDH expression levels. This relationship is explored further in the present study using SIFT-MS.

*5.1.2. Methionine sulfoxide reductase A (MsrA) and the reduction of dimethyl sulfoxide (DMSO) in human cells*

Methionine sulfoxide enzymes are believed to be involved in repairing the damage caused by oxidative damage, and are found in both prokaryotes and eukaryotes [178]. The sub-type methionine sulfoxide A (MsrA) has been shown to act on DMSO, reducing it to DMS in yeast [179, 180] and mammalian [180, 181] cell types. Diminished MsrA activities have also been reported in the brains of Alzheimer's disease patients [182], and there is evidence to suggest that the enzyme protects dopaminergic cells from Parkinson's disease-related damage [183].

**Table 16.** List of cell types whose emitted vapour compounds have previously been analysed using the gas phase analysis techniques SIFT-MS, PTR-MS and GC-MS. The effects of these cells on the AA level measured in the headspace relative to their respective medium controls are indicated.

Cell type		Tumourigenicity	Cell characteristics		AA	Method	Base medium	Reference
hMSC	Primary	Non-tumorigenic	Bone marrow	Connective tissue stem cells	Decrease relative to medium level	SIFT-MS	DMEM	Data presented in Chapter 4
hepG2	Cell line	Carcinoma	Liver carcinoma	Epithelium			DMEM	
Huh-7	Cell line	Carcinoma	Liver carcinoma	Epithelium			DMEM	
HEK 293	Cell line	Non-tumorigenic	Kidney, embryo	Epithelium			DMEM	
NCI-H292	Cell line	Carcinoma	Lung, mucoepidermoid carcinoma cells	Epithelium			RPMI 1640	
T84	Cell line	Carcinoma	Colonic adenocarcinoma cells	Epithelium			DMEM: Ham's F12	
35FL121 Tel+	Cell line	Non-tumorigenic	Lung fibroblast	Connective tissue		PTR-MS	DMEM	[41]
A-549	Cell line	Adenocarcinoma	Lung alveolar	Epithelium			DMEM	[42]
EPLC	Cell line	Carcinoma	Lung	Epithelium			RPMI	
NCI-H2087	Cell line	Adenocarcinoma	Lung	Epithelium		GC-MS	RPMI	[44]
CALU-1 †	Cell line	Carcinoma	Lung epidermoid	Epithelium			DMEM	[184]
hFBs	Primary	Non-tumorigenic	Fibroblasts	Connective tissue			DMEM	[185]
HBEpC	Primary	Non-tumorigenic	Bronchus	Epithelium			PromoCell GmbH	
CALU-1 †	Cell line	Carcinoma	Lung epidermoid	Epithelium	Increase relative to medium level	SIFT-MS	DMEM	[40, 41]
SK-MES	Cell line	Carcinoma	Lung squamous	Epithelium			DMEM	[40]
NL20	Cell line	Non-tumorigenic	Bronchus	Epithelium			Hams' F12	[41]
BEAS2B	Cell line	Non-tumorigenic	Bronchus	Epithelium		PTR-MS	RPMI	[42]
hTERT-RPE1	Cell line	Non-tumorigenic	Retina	Epithelium			DMEM/F12	
HL60	Cell line	Leukemic	Neutrophilic promyelocyte	Blood		GC-MS	RPMI	[186]

† Note contradicting results.

## 5.2. Experimental procedures

### 5.2.1. Theoretical model of AA metabolism

As mentioned in section 5.1.1., AA is known to be formed from the oxidation of ethanol *via* the enzyme ADH, according to the ethanol metabolism pathway, and removed *via* ALDH [139]. A theoretical model of this process was derived assuming that it follows Michaelis-Menton enzyme kinetics, as described by the following formula [139]:

$$v = \frac{V_{\max} \cdot [S]}{K_M + [S]} \quad (21)$$

Here  $v$  is the rate of the enzyme reaction and  $[S]$  is the substrate concentration. The coefficients  $K_M$  and  $V_{\max}$  are the Michaelis-Menton constant and the maximum reaction velocity respectively, which are constant for a specific enzyme-mediated reaction.  $K_M$  is defined as the substrate concentration at  $0.5V_{\max}$  and is a measure of the specificity of an enzyme for a substrate. Values for these coefficients were obtained from the literature and are given in Table 17.

**Table 17. Michaelis-Menton constants ( $K_M$ ) and maximum reaction velocities ( $V_{\max}$ ) for alcohol dehydrogenase- and aldehyde dehydrogenase- (ALDH-) mediated oxidation reactions of ethanol and acetaldehyde respectively.  $K_M$  values are a given as liquid concentrations (M), as presented in the literature, and then converted to gas phase concentrations (*ppbv*), assuming the system is sealed and that Henry's Law applies.**

Enzyme		$K_M$		$V_{\max}$	Reference
		(M)	( <i>ppbv</i> )	( $\text{mol mg}^{-1} \text{min}^{-1}$ )	
ADH	1B1	$2.3 \times 10^{-5}$	260	$1.1 \times 10^{-7}$	[187]
	1C1	$1.2 \times 10^{-4}$	1400	$6.5 \times 10^{-7}$	
	1C2	$1.6 \times 10^{-4}$	1800	$3.8 \times 10^{-7}$	
ALDH	1B1	$5.5 \times 10^{-5}$	7857	$6.7 \times 10^{-7}$	[159]
	2	$5.9 \times 10^{-7}$	84	$4.5 \times 10^{-7}$	[160]

A number of other factors must also be considered in order describe the metabolism of AA by cultured cells, and to convert the concentration of AA in the liquid phase to a vapour phase concentration. A list of the variables that have been used to model the metabolism of AA by a hepatocellular carcinoma cell line (hepG2; see section 4.1.1.) and a non-small lung cancer cell line (CALU-1) is given in Table 18.

**Table 18.** List of the variables and starting conditions used to formulate the theoretical model of acetaldehyde (AA) consumption/production by hepG2 and CALU-1 cell culture headspaces *via* the ethanol metabolism pathway. The starting gas phase concentration AA for the CALU-1 experiments was obtained from [41] and that for the hepG2 cells were derived from averaging the experimental data derived in this study. The starting ethanol concentrations Henry's law coefficients ( $K_H$ ) for ethanol and AA at, obtained from [151, 156], were used to derive the apparent liquid phase concentrations at 37°C.

		hepG2	CALU-1
Liquid volume (L)		0.015	0.050
Headspace volume (L)		0.135	0.100
$K_H(37^{\circ}\text{C})$ (mol kg <sup>-1</sup> bar <sup>-1</sup> )	Ethanol	88	
	AA	7	
Initial ethanol concentrations	Headspace (ppbv)	500	700
	Liquid (μM)	44	62
Initial AA concentrations	Headspace (ppbv)	120	255
	Liquid (μM)	0.84	1.79
Enzyme molecular weight (Da)	ADH	80,000	
	ALDH	216,000	

The starting AA and ethanol concentrations are given as the mean of several SIFT-MS analyses of the media headspace. For the hepG2 cells, these measurements were conducted as part of the present study, and for the CALU-1 cell line the mean concentration was derived from the six media headspace measurements presented in [41]. The kinetics data for the enzyme reactions in Table 17 were combined with the other variables given in Table 18 in order to derive a theoretical model of the ethanol metabolism pathway, assuming that only the enzymes present in Table 17 participate in the reactions.

### 5.2.2. Cell culture and application of ALDH inhibitors

The hepG2 hepatocellular carcinoma cell line was used for the majority of the experiments in this study, but some experiments were also conducted with human bone marrow-derived mesenchymal stem cells (hMSCs). The routine culture of these cell types was performed as described previously in Chapter 4 (section 4.1.1.), with a culture medium of low glucose (1.0 g/L) DMEM (10% foetal bovine serum (FBS), 1% antibiotic-antimycotic and 2mM L-glutamine) used for both cell types.

The ALDH inhibitors diethylaminobenzaldehyde (DEAB; Sigma, UK) and disulfiram (DSF; Sigma, UK) were each dissolved in dimethyl sulphoxide (DMSO) prior to the experiments. DMSO was selected to be the common solvent because it has a relatively low vapour pressure (1.8 mbar at 37°C), and was therefore not expected to interfere significantly with the SIFT-MS analysis. The inhibitor/DMSO solutions were added to the DMEM-based culture medium so that the final DMSO concentration in each of the samples was always 0.1% v/v (~14,500 μM). It should be noted that the maximum solubility of DSF in DMSO is 20mM, which imposed a limit on the maximum concentration of DSF in the cell cultures of 20 μM. The concentration of DSF could have been increased by using ethanol as the solvent instead of DMSO, but a concentration of 0.1% v/v ethanol would equate to around 200 ppmv in the vapour phase, according to Henry's Law [151], and this would have seriously



interfered with the SIFT-MS experiments, because the ethanol molecules would have completely depleted the precursor ions, on which SIFT-MS analyses depend (see Chapter 2 and [188]). Dramatically increasing the ethanol concentration would not be desirable in any case due to additional formation of AA, according to the ethanol metabolism pathway, as discussed in section 5.1.1.. Solubility restrictions did not impact significantly on the DEAB experiments, and concentrations up to 500  $\mu\text{M}$  were used in the cell cultures.

In the majority of experiments the cells were removed from their tissue culture flasks using the enzyme trypsin about 16 hours before the headspace analysis experiment. The cells were counted using the trypan blue exclusion method, and suspended in a known volume of medium containing the DEAB or DSF solutions, contained inside 150mL glass bottles. In the hMSC experiments, the cells were pre-treated with the ALDH inhibitors for 24 hours prior to their removal and transfer to the glass bottles. In all cases, the headspace was purged from the bottles using dry cylinder air before they were finally sealed using metal caps with rubber septa, and incubated at 37°C for around 16 hours.

#### 5.2.4. *Headspace analysis*

The headspace analyses experiments were performed using SIFT-MS as described in section 4.1.4., with the samples held at 37°C throughout in a water bath. It is worth mentioning that it was necessary to employ the newly-derived kinetics database entries for the quantification of AA in the presence of the heightened DMS concentrations that were emitted by the cultures, due to the presence of DMSO in the liquid media. These AA measurements were performed using  $\text{H}_3\text{O}^+$  precursor ions and a single product ion with a mass-to-charge ratio ( $m/z$ ) of 45, as described in Chapter 3 and [108]. The analysis of DMS was achieved using  $\text{NO}^+$  precursor ions and the product ion at  $m/z$  62 [108, 117].

#### 5.2.5. *Viability assay*

The affects of the sealed incubation period on the viability of hepG2 cells was assessed in a similar manner to that described in section 4.2.4.. Here, cells were cultured to near-confluence using the untreated medium described earlier, stained with the Cellstain double stain (Sigma, UK) and observed using confocal microscopy.  $1.5(10^7)$  unstained cells were then suspended in 15mL of DMEM medium containing 200 $\mu\text{M}$  DEAB or 20 $\mu\text{M}$  DSF, prepared as described previously, or 0.1% v/v DMSO, as well as an untreated sample with no inhibitors or DMSO present. The cell-suspensions were then sealed inside 150mL glass bottles and incubated at 37°C for 16 hours. The suspensions were then removed from the bottles and assessed by the same Cellstain double stain.

The affects of the ALDH inhibitors on cell viability were also tested. In this case, hepG2 cells and hMSCs were cultured to near-confluence in 96-well plates, and treated with ALDH inhibitors for 16 hours. The concentrations ATP were then quantified by the resulting luminescence levels using the ATPLite assay (Perkin-Elmer, UK) and a Synergy 2 spectrophotometer (BioTek, UK).

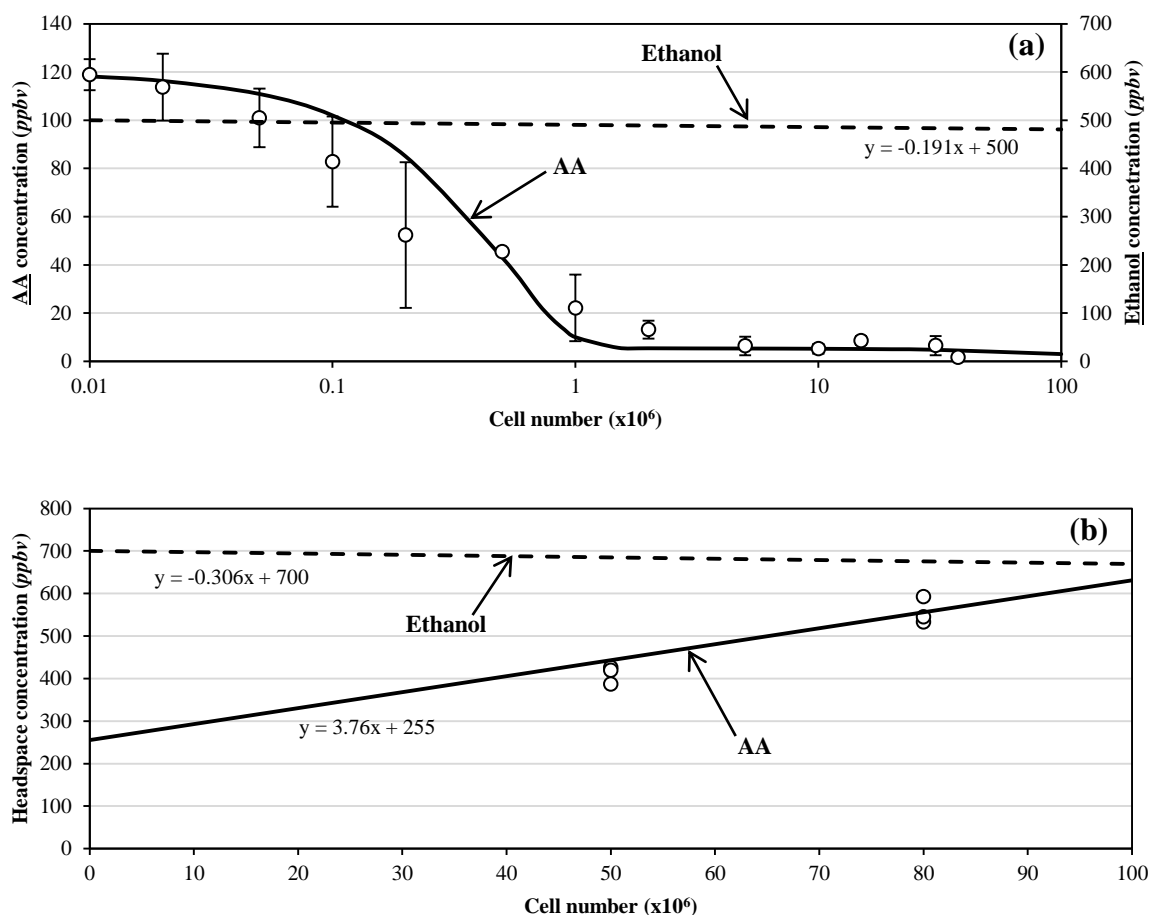
### 5.3. Results

#### 5.3.1. AA metabolism by hepG2 cells: theoretical and experimental results

The effects of varying numbers of hepG2 cells, from  $1(10^4)$  to  $4(10^7)$ , on the concentrations of AA present in the headspace of the culture media were measured using the previously described methods, following 16 hours incubation at  $37^\circ\text{C}$ , without treatment with ALDH inhibitor compounds. The results of these experiments are presented in Figure 14a, along with the results of the theoretical model of the AA metabolism (solid line) by hepG2 cells according to the ethanol metabolism pathway and conditions described in section 5.2.1.. Over the range of cell numbers analysed, the AA concentration reduces rapidly from the starting concentration of around 120 *ppbv*, before levelling off at 10 *ppbv* for around  $1(10^6)$  cells and asymptotically approaching zero *ppbv*. It is seen that the theoretical line follows the data points closely when the cells each contain 5000 ADH molecules and 6000 ALDH molecules. The effects on the metabolism of ethanol are also modelled in Figure 14a, where it is predicted that the concentration of ethanol in the headspace falls very slightly from 500 *ppbv* to around 490 *ppbv* even when  $1(10^8)$  cells are present in the culture. This predicted 10 *ppbv* decline is well within the 10% instrumental error of the SIFT-MS technique [36] and therefore cannot be measured.

Shown in Figure 14b are the concentrations of AA present in the headspace of CALU-1 cell cultures following 16 hours incubation at  $37^\circ\text{C}$ , as measured by SIFT-MS in the study published in 2009 [41]. It is shown that the production of AA by these cells can be modelled using the same formulae as in Figure 14a, by changing the numbers of ADH and ALDH molecules per cell to 1500 and 0 respectively. In addition, the concentration of ethanol in the headspace is seen to decline very slightly from around 700 *ppbv* (as measured in the headspace of the media controls in this study [41]) to around 680 *ppbv*.

**Figure 14.** Plot showing the concentrations of AA, in parts-per-billion by volume (*ppbv*) measured in the headspace of (a) varying numbers of hepG2 cells in 15mL DMEM media and (b) CALU-1 cultures in 50mL of media in a study published prior to the start of the present project [41], following 16 hours incubation at 37°C. In both cases, the open circles indicate AA concentrations derived from SIFT-MS analyses while the solid lines represent the concentrations of AA predicted by a model based on Michaelis-Menton enzyme kinetics. In addition, the predicted concentrations of ethanol in the vapour phase are plotted using dashed lines (plotted on a different y-axis in (a)). The model assumes that the hepG2 cells each contain 6000 molecules of ALDH and 5000 molecules of ADH, and the CALU-1 cells each contain no ALDH and 1500 molecules of ADH. Note the logarithmic scale on the x-axis. Other assumptions and important values are listed in Table 2 and Table 3.



The ability to model both the consumption and production of AA in the headspace of these cultures using simple Michaelis-Menton enzyme kinetics supports the hypothesis that the ethanol metabolism pathway is the primary cause of these effects, which have been observed previously in at least eight headspace analysis studies to date (see Table 16). The results of the theoretical model also explain why changes in the concentrations of headspace ethanol have not been reported. The small decline in headspace ethanol, compared to the AA, is due in part to the different  $K_M$  values of the relevant enzymes (ALDH2 being effective at substrate concentrations 3 times lower than that of ADH1B1 according to their  $K_M$  values; see Table 17) as well as the differences in Henry's Law coefficients, which indicate that the AA will be lost from the headspace >12 times faster than ethanol.

### 5.3.2. Neat AA added to hepG2 cell cultures

An experiment was conducted in order to test the effects of the starting AA concentration on the rate of consumption of AA by hepG2 cells. Here, three different volumes of neat AA were added three 50mL media samples to be used as controls, and three which were used to suspend  $2(10^7)$  cells in the 150mL glass bottles. The headspace of the media alone and the cell cultures were then analysed using SIFT-MS following the standard 16 hour incubation period. The cells were then returned to the incubator, and analysed again following another 24 hours. The AA measurements derived from these analyses are shown in Table 19.

**Table 19. The concentrations of AA, given in *ppbv*, measured in the headspace of hepG2 cells which initially contained varying quantities of AA. The initial AA concentrations are the values measured above the media alone, following the same incubation period as the cells, and the final concentrations are those measured when  $2(10^7)$  cells were additionally present. The decline in AA concentration measured in the headspace was then used to calculate the rate of AA consumption per cell by applying the Henry's Law coefficient at 37°C [151].**

Initial AA concentration ( <i>ppbv</i> )	Final AA concentration ( <i>ppbv</i> )		Rate of consumption ( $\times 10^5$ molecules cell <sup>-1</sup> s <sup>-1</sup> )		$\frac{\text{Rate}_{16h}}{\text{Rate}_{40h}}$
	16 hours	40 hours	16 hours	40 hours	
73	12	10	7	3	2.3
538	147	24	44	23	1.9
1366	181	27	132	60	2.2

At the lowest starting AA concentration (with no neat AA added to the media), the final concentration was depleted to around 10 *ppbv*, which is in agreement with the data presented in Figure 14a. When further AA is added to the culture, however, the cells were unable to remove the VOC to the same degree. In fact, following an additional 24 hours of incubation, the AA was still not depleted to this expected 10 *ppbv* level. The data given in Table 19 also indicate that the AA consumption rate is dependent on the starting concentration of AA, as in each case the rate of consumption during the first 16 hours of incubation is approximately double that of the following 24 hours. It is also worthy of note that the calculated rates of AA consumption were approximately equivalent to the AA production rates measured in the previously mentioned study of the lung cancer cell line CALU-1 [41].

### 5.3.3. Analysis of the culture medium headspace

Before commencing the ALDH inhibition experiments with cell cultures, it was first necessary to analyse the headspace of the culture media alone in order to establish the background concentrations of the common volatile compounds. Ethanol and acetone were previously found to originate largely from FBS in culture media in a previous study [41], while methanol was found to originate largely from the base DMEM; these compounds were routinely monitored as reference controls. AA, which also originates largely from FBS [41], and DMS were

also monitored as these are the primary focus of the study. The results of these media analyses are presented in Table 20.

**Table 20. Single measurements of the concentrations of several common volatile compounds measured in the headspace of samples of non-treated (NT) DMEM medium, as well as medium containing 0.1% v/v DMSO (~14,000  $\mu$ M) alone and with dissolved DEAB (200  $\mu$ M) and DSF (20  $\mu$ M). The mean and coefficient of variation (CV) are indicated for each compound.**

	Compound concentration (M)	Headspace concentrations ( <i>ppbv</i> )				
		Acetone	Methanol	Ethanol	AA	DMS
<b>NT</b>	-	190	248	483	104	13
<b>DMSO</b>	$1.4 \times 10^{-2}$	181	242	554	109	33
<b>DEAB</b>	$2.0 \times 10^{-4}$	203	259	421	106	12
<b>DSF</b>	$2.0 \times 10^{-5}$	173	263	478	104	18
<b>Mean</b>	-	187	253	484	106	29
<b>CV</b>	-	0.07	0.04	0.11	0.02	0.62

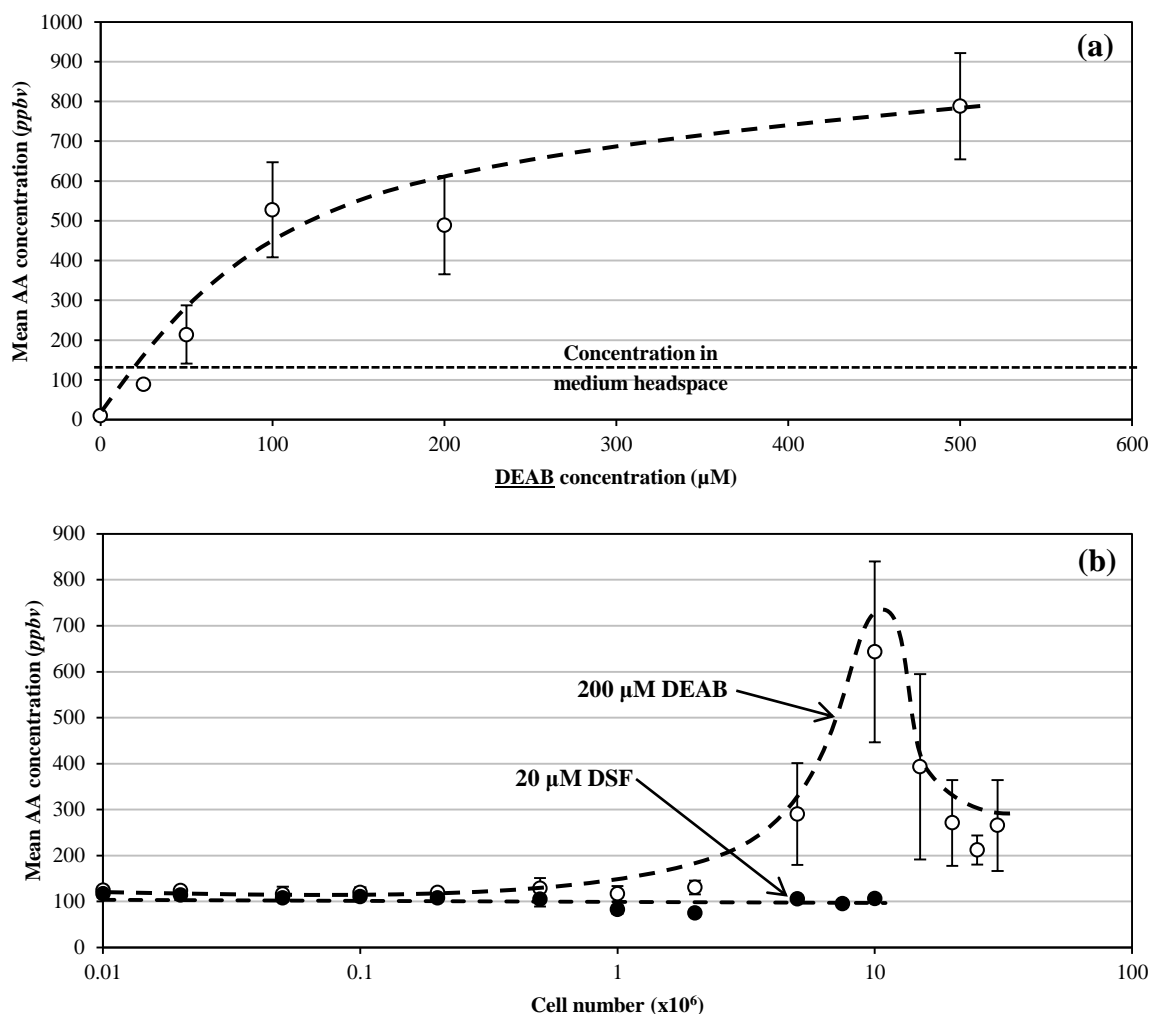
The results presented in Table 20 indicate that acetone, methanol, ethanol, and importantly, AA and DMS are essentially invariant with the addition of DMSO and ALDH inhibitors DEAB and DSF. The CV value for the DMS measurements is relatively large, but this is due to the low concentrations of DMS in the headspace, which are approaching the limit of detection of the SIFT-MS instrument.

#### 5.3.4. *Inhibition of AA metabolism using DEAB and DSF*

In order to investigate the metabolism of AA, different concentrations of the ALDH inhibitor DEAB were applied to the cells the evening prior to the morning of the experiment. Following the standard 16 hour incubation period, the headspaces of the cultures were analysed using SIFT-MS, and the results are given in the plot in Figure 15a. Here it is seen that when no DEAB is present, the cells consume AA to a few *ppbv* in the headspace, well below the medium concentration (~120 *ppbv*) as before (see Figure 14a and Table 19), but as the DEAB concentration is increased, a general increase in AA is observed in the headspace. However, the rate of AA increase slows down at the higher DEAB concentrations, however.

Headspace AA concentrations were also measured for fixed concentrations of ALDH inhibitors DEAB and DSF with varying cell numbers. A mid-range DEAB concentration of 200 was selected to perform the DEAB-inhibition experiments, in consideration of the results presented in Figure 15a, and 20  $\mu$ M DSF was used for the DSF experiments. The results of these analyses are shown in the plot in Figure 15b.

**Figure 15.** Plots showing the mean AA concentrations ( $N=2$ ), given in parts-per-billion by volume ( $ppbv$ ), measured in the headspace of cell cultures against (a) the DEAB concentration in the culture media; and (b) the cell number. In (a), each of the samples contained  $1.5(10^7)$  hepG2 cells, and all of the liquid samples were 15mL in volume. The short-dashed line in (a) indicates the concentration of AA that was measured in the liquid headspace. In (b) 20  $\mu\text{M}$  DSF (closed circles) is used as an inhibitor of ALDH, as well as 200  $\mu\text{M}$  DEAB. In both plots, the long-dashed lines are “eye ball” variations, following the experimental points.



It is shown that the DEAB-treated cells did not consume AA in the usual way, as can be seen in Figure 14a; rather the AA concentration remained relatively constant in the range of  $1(10^4)$  to  $2(10^6)$  cells, indicating that the AA consumption was prevented due to the inhibition of the ALDH enzymes. At high cell numbers, the AA concentrations then began to increase to a maximum of around 650  $ppbv$  when  $1(10^7)$  cells were present. As the cell numbers are increased further to  $3(10^7)$ , the AA concentration declined back to around 350  $ppbv$ . The increase in AA could be explained by the blocking of ALDH active sites with the DEAB molecules, accompanied by the increasing numbers of ADH enzyme molecules that are present due to the increasing cell numbers. Therefore, at the peak AA concentration, seen at  $1(10^7)$  cells, it could be considered that the ratio of ADH molecules to active ALDH molecules ( $\text{ADH}:\text{ALDH}_{\text{active}}$ ) has reached a maximum. However, as the cell

numbers are increased further, the DEAB concentration is no longer able to inhibit the increased numbers of ALDH molecules, so the ADH:ALDH<sub>active</sub> ratio declines, thereby causing the AA concentration to fall.

On the other hand, in the DSF-inhibition experiments, no increase in the AA concentration was observed rather the AA decreased very slightly with increasing cell numbers, over the range of  $1(10^4)$  to  $1(10^7)$  cells. This may be explained by the decreased inhibitor concentration (20  $\mu\text{M}$ ) compared to that used in the DEAB experiments (200  $\mu\text{M}$ ).

### 5.3.5. Detection of DMSO reduction by human cells

The formation of the highly volatile sulphur-compound DMS from cellular action on the common cryopreservant and solvent DMSO was observed earlier in the work relating to this thesis (data not shown). An example of this is given in Table 21. The data are derived from an experiment in which the vapours released by hepG2 cells were analysed after being thawed from liquid nitrogen cryostorage, during which, they are kept in a “freeze-medium” consisting of 80% FBS and 20% DMSO, with approximately  $2(10^6)$  cells-per-vial. In this experiment, immediately after thawing, the cells were washed between 0 and 3 times with 15mL of phosphate-buffered saline (PBS) and transferred to 25mL of DMEM medium in glass bottles. The headspace of each bottle was then purged with dry, cylinder air and incubated overnight at 37°C as usual.

**Table 21.** The concentrations of AA, acetone and DMS, in parts-per billion by volume (*ppbv*), measured in the headspace above samples containing  $\sim 2(10^6)$  hepG2 cells in 25mL of DMEM medium, following resuscitation from liquid nitrogen and varying numbers of post-thaw PBS-washes. The concentrations of these compounds in the medium headspace when no cells are present are given in *italics*.

Post-thaw washes	AA ( <i>ppbv</i> )	Acetone ( <i>ppbv</i> )	DMS ( <i>ppbv</i> )
0	8	278	106
1	7	240	5
2	9	231	5
3	5	215	6
<i>Medium alone</i>	<i>50</i>	<i>245</i>	<i>5</i>

As shown in Table 21, the concentration of AA was seen to decline from around 50 *ppbv* in the liquid phase to <10 *ppbv* in all cell-containing samples, indicating that the cells survived the thawing process, and were acting as expected (see Figure 14a). A general decrease in acetone concentration is also evident, which is likely due to the gradual dilution of FBS, which is known to be the major source of acetone in these cell cultures [41] and constitutes 80% of the freeze medium but only 10 % of the normal DMEM medium. When the hepG2 cells were not washed post-thaw, the concentration of DMS was seen to increase to around 100 *ppbv*, due to the reduction of DMSO, which is known to be mediated by the enzyme MsrA [180, 181] (see section 5.1.2.). However a single wash with PBS prior to transferring the cells to the bottles seemingly removed enough of the DMSO to prevent DMS emissions into the vapour phase.

### 5.3.6. *Inhibition of DMSO metabolism using ALDH inhibitors*

As DMSO was used as the solvent for the ALDH inhibitors DEAB and DSF, it was expected that DMS would be produced by the hepG2 cells, following the overnight incubation, as indicated by section 5.3.5.. Therefore, the concentrations of DMS were also routinely measured during the AA analyses presented in section 5.3.4., the results of which are given in Figure 16.

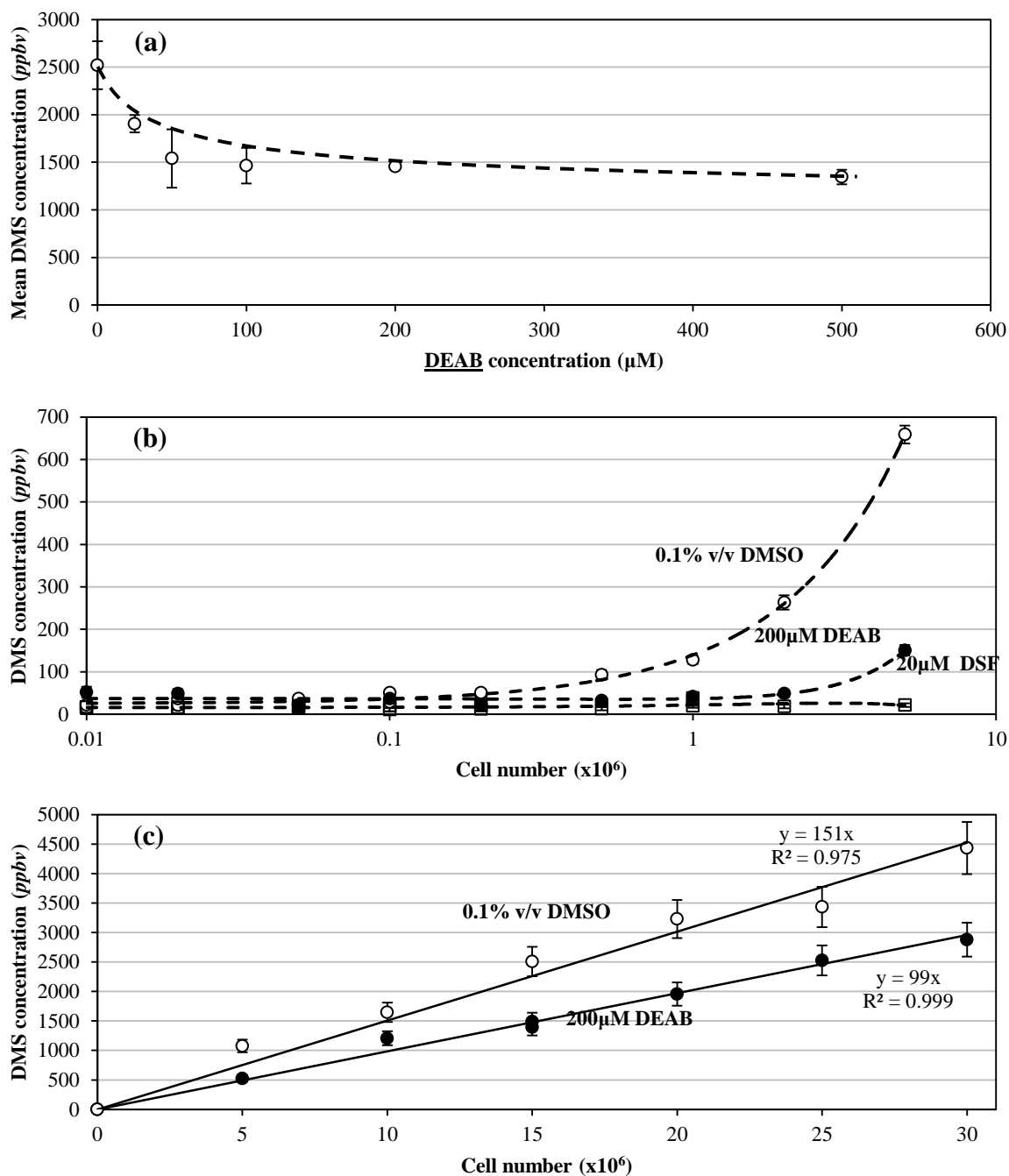
The results presented in Figure 16a were obtained from the same experiment as those presented in Figure 15a, earlier. Briefly, each of the samples contained 15mL of medium with  $1.5(10^7)$  hepG2 cells, with the DEAB concentration varied but always dissolved in DMSO to a final concentration of 0.1% v/v. In this case, the DMS concentrations were highest when no inhibitor is present (still with 0.1% v/v DMSO), with a maximum value of around 2500 *ppbv*, but dropped by 30% when 25mM DEAB is also present. However, little decline in DMS was observed as the DEAB concentration is increased further.

In Figure 16b, the cell number was varied from 0 to  $5(10^6)$  cells, while the ALDH inhibitor concentrations were maintained at 200  $\mu$ M DEAB or 20  $\mu$ M DSF. In addition the concentrations of DMS measured when 0.1% v/v DMSO was added to the media but no inhibitors were present. In this case, there is little evidence of DMS production at the lower cell numbers, from  $1(10^4)$  to  $2(10^5)$ , but then a general increase was seen to occur as the cell numbers increased towards  $5(10^6)$ . When 200  $\mu$ M DEAB was additionally present, no clear increase in DMS was observed below  $2(10^6)$ , but the level was elevated from around 20 *ppbv* to 200 *ppbv* in the  $5(10^6)$  cells sample. Samples containing cell numbers from  $5(10^6)$  to  $3(10^7)$ , treated with 0.1% v/v DMSO and 200  $\mu$ M DEAB were additionally analysed, with the results shown in Figure 16c. At these higher cell numbers, the DMS concentrations actually increased with cell number in a linear fashion in both cases. However, the slope of the line appears to decrease by around 30% when DEAB is present, compared to the DMSO alone samples.

The addition of 20  $\mu$ M DSF to the cultures seemingly prevented any production of DMS in cultures containing between  $1(10^4)$  and  $5(10^6)$  hepG2 cells, as shown in Figure 16b.



**Figure 16.** Plots showing the mean DMS concentrations ( $N=2$ ), given in parts-per-billion by volume ( $ppbv$ ), measured in the headspace of hepG2 cell cultures against (a) the DEAB concentration in the culture media; and (b) & (c) the cell number. Note the changes in scales on the x-axes.



### 5.3.7. Headspace analysis of hMSC cultures treated with ALDH inhibitor compounds.

Similar experiments to those performed with the hepG2 cell line, presented in the previous sections, were also performed with hMSC cultures. In this case, however, the cells were pre-treated by applying the inhibitor compounds (DEAB and DSF) for 24 hours during routine culture in tissue culture flasks, prior to their transfer to the 150mL glass bottles. These samples each contained typically  $5(10^6)$  cells. The media used to suspend the

cells in the bottles contained the same inhibitor compounds as in the pre-treatment. The results of the subsequent SIFT-MS headspace analysis experiments, performed following a total of 40 hours of inhibitor treatment, are presented in Table 22.

**Table 22. Concentrations of AA and DMS, given in parts-per-billion by volume (*ppbv*), measured in the headspace above typically  $5(10^6)$  hMSCs in 10mL of medium containing the ALDH inhibitor compounds DEAB and DSF. In this case the cells were pre-treated with the inhibitors for 24 prior to their transfer to the glass bottles which were incubated for a further 16 hours whilst sealed. Also shown are the concentrations of AA and DMS measured in the headspace of samples of non-treated (NT) cells and samples containing 0.1 v/v ( $\sim 14,000$   $\mu\text{M}$ ) DMSO solvent, without inhibitor compounds. The concentrations of AA and DMS measured in the medium alone, without cells were  $89\pm 37$  and  $6\pm 4$  *ppbv* respectively.**

Sample	Compound concentration ( $\mu\text{M}$ )	AA ( <i>ppbv</i> )		DMS ( <i>ppbv</i> )	
NT	-	1	9	11	3
DMSO	14,000	6	12	3016	963
DEAB	100	83	171	2269	1756
	200	76	162	2050	1524
	500	120	205	585	934
DSF	10	44	7	29	1067
	20	10	4	878	927

In these experiments, the non-treated (NT) and DMSO-containing samples behaved as expected, with both consuming AA (see Figure 14a) and DMS produced in the DMSO sample. However, only DEAB effectively inhibited the consumption of AA by these cells under these conditions, while DMS production also appeared to be inhibited, particularly at the higher DEAB concentration of  $500\mu\text{M}$ . DSF, on the other hand, had little or no effect on the consumption of AA, but did appear to inhibit the DMS production from DMSO. Again, the unavoidably lower concentration of DSF, relative to the DEAB experiments, may have contributed to the decreased inhibitory effects.

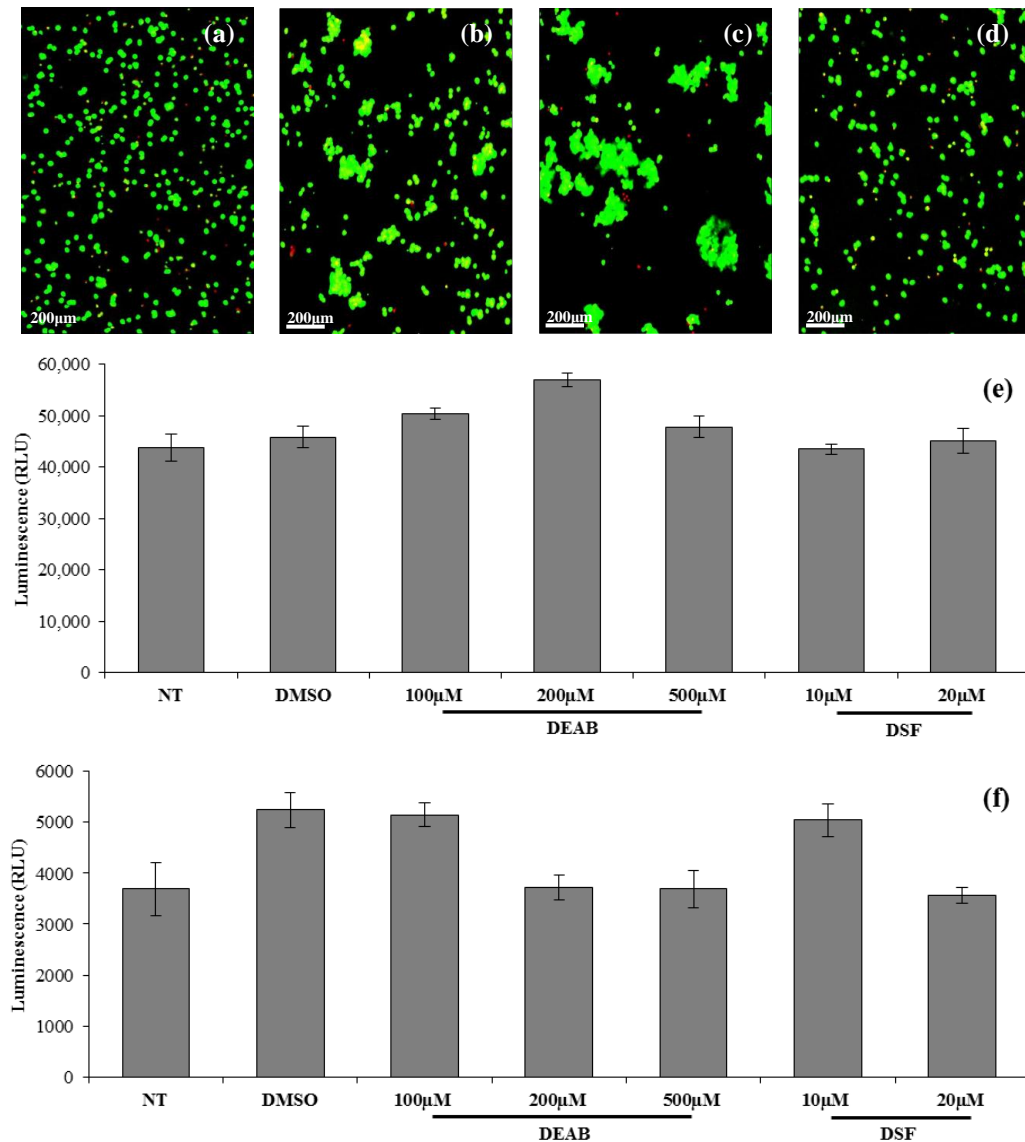
### 5.3.8. Assessment of cell viability in hepG2 and hMSC cultures

The potential effects of the overnight incubation in the sealed bottle on the viability of the hepG2 were observed using Cellstain double staining. The resulting images are shown in Figure 17a-d. The images indicate that the method of incubating the cells, whilst sealed for a period of 16 hours, with and without the presence of DEAB or DSF, caused little or no decline in the viability of the hepG2 cells cultured.

The effects of treating the cells with the ALDH inhibitors on the viabilities of hepG2 and hMSC cells were also assessed under more standard conditions, with the cells attached to 6-well plates, by their production of ATP, using the ATPLite assay. The resulting luminescence measurements, shown in Figure 17e-f, also indicate that the inhibitors had no clear affect on the viability of either cell type. It should be noted, however, that we have not thoroughly investigated the affects of this protocol of analysis on the condition of the cells, and it is surely true that these adherent cell types will initially proliferate at a decreased rate on transfer to suspension

culture conditions and will tend to form aggregates, which could affect cell behaviour. The essential point is that the cells were all exposed to ostensibly identical conditions, and the inhibitory effects of DEAB and DSF were clear.

**Figure 17.** Confocal microscopy images of hepG2 cells, following application of the Cellstain double stain, obtained (a) prior to and (b-d) following overnight incubation inside sealed glass bottles. The live cells are stained green while the nuclei of dead cells are stained red. The cells in (a) and (b) were not treated with ALDH inhibitors, whereas in (c) and (d) 200 $\mu$ M DEAB and 20 $\mu$ M DSF were added to the contained medium respectively. The results of ATPLite assays conducted on hepG2 (e); and hMSC (f), are also shown. The results were obtained following culture under normal conditions (non-treated; NT) or following 16 hours of treatment with 0.1% v/v DMSO, or with ALDH inhibitors: DEAB or DSF. The inhibitor concentrations are indicated on the x-axis where appropriate. The data is presented as the mean  $\pm$  standard error (N=8).



## 5.4. Discussion

The studies presented in this chapter progressed the work described and discussed in Chapter 4, and provide further examples of how SIFT-MS can be used to non-invasively identify and accurately quantify volatile compounds present in the vapour phase above immortalised cell lines and primary cell cultures. Here we have additionally described a method for studying specific metabolic processes occurring *in vitro*.

Under the standard conditions for SIFT-MS headspace analyses of cell cultures, as described in [41], the hepG2 cells, specifically the functional ALDH present within the cells, metabolised AA, which is present in DMEM and FBS (see Chapter 4), effectively removing it from the medium. This process was also modelled using simple Michaelis-Menton enzyme kinetics, indicating the importance of the ethanol metabolism pathway (see section 5.1.1.) in the removal of AA. However, when the ALDH enzyme inhibitor DEAB was also present in the cell cultures the consumption of AA, as measured in the headspace, was either limited or completely prevented, or the concentration of AA was seen to increase, depending on the concentration of DEAB used, or the number of hepG2 cells present in the sample. These effects are clearly caused by the inhibition of the ALDH enzyme. Also, alcohol dehydrogenase was not inhibited by the DEAB, and therefore continued to metabolise ethanol to AA, according to equation (20), and consequently the AA concentration increased in some cases. This explains why DEAB appeared to cause the accumulation of AA, as opposed to simply preventing the loss of the compound, as was the case for DSF.

It is shown in Figure 15b that at higher cell numbers, the increase in AA, caused by the presence of DEAB, began to decline. This is likely due to the increase in ALDH expression, which naturally accompanies the increase in cell numbers, becoming too great for the concentration of the DEAB inhibitor. In essence the AA concentration increases initially because the activity of the uninhibited ADH exceeds that of the ALDH, but when the cell numbers become too high, the levels of uninhibited ALDH increase, causing the metabolism of AA to speed up again, resulting in lower AA concentrations in the headspace. The spread in the AA levels measured in each experiment are presumably due to batch-to-batch variations in the cell status (cell cycle), which are likely linked to enzyme expression levels [158].

It is worth mentioning that acetic acid can be quantified by SIFT-MS [134], but because the pH of the cell culture media is typically 7.5, any acetic acid that is formed will exist largely as non-volatile acetate ions. However, several biogenic molecular species, including methanol, ethanol, acetone and AA were observed in the headspace of the DMEM medium used exclusively for these studies. AA, acetone and ethanol were previously reported to originate largely in the FBS in [41] and in Chapter 4.

Reduction of DMSO to DMS by the hepG2 cells was observed, a processes that is apparently also inhibited by the presence of DEAB and DSF in the hepG2 cell cultures. To the authors' knowledge this finding has not been reported previously. It has been reported that DMSO can be reduced by the actions of the enzyme methionine sulfoxide reductase A (MsrA) [178, 180, 181] (see section 5.1.2.). It is possible that DEAB and DSF directly inhibit the actions of the cellular MsrA, for example by interacting with the cysteine residues of the enzyme active site [189]. Alternatively, the inhibitors could have indirectly affected the activity of this enzyme by causing aldehyde concentrations to increase in the media, although no linear relation is evident from the plots in Figure 15b and 16b. However, to the authors' knowledge, the possibility of a link between ALDH/AA and MsrA function/activity levels has not been reported in the literature. This may have implications for the use of DSF (Antabuse) for the treatment of alcohol and cocaine addictions, mentioned previously in the Introduction [169]. Also, given that both MsrA and ALDH have been linked to the development of both Parkinson's [164] and Alzheimer's [168] diseases, these findings may be significant in the pathology of these diseases

The results presented in this chapter indicate that SIFT-MS headspace analyses of volatile compounds may be useful for the targeted analysis of metabolic processes in cultured cells. The scope of this technique is not limited to the study of AA metabolism by ALDH, as is demonstrated by the finding that the cell-types studied both reduced DMSO to DMS. Provided that the substrates and/or products of enzymatic reactions are volatile, these techniques could certainly be applied for the analysis of metabolic processes in hepG2 and other cells types, including microbial and animal cells.

## 6. Headspace analyses of *Escherichia coli* cell cultures

The work presented in this chapter relates largely to the published study of the compounds emitted by cultures of the bacterium *Escherichia coli*, strain JM109, entitled: “*Time-resolved selected ion flow tube mass spectrometric quantification of the volatile compounds generated by E. coli JM109 cultured in two different media*” [190]. A copy of the journal article is given in Appendix A7. A review of some earlier studies of vapours emitted by cultured bacterial cells is given in the Introduction (section 1.3.3.).

### 6.1. Experimental

#### 6.1.1. Culture of *E. coli* cells and preparation for SIFT-MS headspace analyses

*E. coli* strain JM109 cells are commonly used in genetic transformation experiments for the production of plasmid DNA or recombinant proteins [191, 192]. In the present study, the cells (purchased from Stratagene, now Agilent) were initially cultured for around 16 hours at 37°C in a lysogeny broth medium (**LB**; Sigma, UK), which contains no glucose, using a shaker flask system. The culture was open to the atmosphere during this period, to allow gas exchange. Following the culture period, the cells grew to a high density, the extent of which could be estimated by taking optical density measurements at a wavelength of 600nm. This was found to be approximately  $1.5\text{--}2.0(10^9)$  cells-per-mL.

In order to prepare cell cultures for SIFT-MS headspace analyses, a 1mL sample of the high density culture of *E. coli* in LB was added to 24mL of fresh media, either Dulbecco’s modified Eagle’s medium (**DMEM**) supplemented with 10% v/v foetal bovine serum (**FBS**) and 2mM L-glutamine or fresh LB, inside a 150mL glass bottle. The headspace of the bottle was then purged with dry cylinder air and the vessel was sealed by a rubber septum and incubated for a further 16 hours at 37°C. Following this incubation period, the increase in cell number could be checked visually by the change in opacity or by the colour change to yellow in the DMEM medium, due to the presence of phenol red indicator and the increased acidity of the sample.

LB is a commonly used medium for the culture of *E. coli* and other bacteria. There are several formulations of LB, which are generally composed of nitrogenous tryptone peptides formed from the digestion of casein by the enzyme trypsin, vitamins, trace elements and sodium chloride. On the other hand, DMEM is commonly used in mammalian cell cultures, including many of the human cell cultures examined in Chapters 4 and 5. The high glucose variant (4.5 g/L) was used in this study, and it also contains several inorganic salts,

amino acids and vitamins, while sodium pyruvate is also present as an additional energy source. The importance of the differing compositions of these two culture media will become clear in the Results section.

In previous SIFT-MS studies of cultured human cells, such as those presented in Chapters 4 and 5, and in those reported in the literature [40, 41, 157], the loss of oxygen from the sealed system was considered to be insufficient to cause the culture conditions to transition from aerobic to anaerobic, and this is evidenced by the subsequent viability assessments, which never showed any significant increases in cell death [40, 41, 157]. However, even the highly proliferative lung tumour cells of the SK-MES cell line (used in [40]) have doubling times of 20 hours [193], whereas bacterial cells, such as *E. coli*, can grow according to doubling times of around 20 minutes under optimal conditions [194]. The initial oxygen consumption rate of the  $1.5(10^9)$  *E. coli* cells that are added to the 25mL of media in the glass bottles is estimated to be of the order of 1  $\mu\text{mol}$  of  $\text{O}_2$  per hour (based on a value derived from [195]). Considering the rapid growth of these cells, it is highly possible that the oxygen present in the system (liquid phase and headspace) would be depleted in <10 hours, which would cause the cells to alter their metabolism in order to continue to survive in these hypoxic conditions. Consequently, it is highly likely that different volatile compounds would be emitted into the gas phase than in a situation in which the cells were open to the atmosphere.

#### 6.1.2. *Headspace analysis*

The headspace analyses of the sealed glass bottles were performed using SIFT-MS (see Chapter 2) in essentially the same manner as described in section 4.1.4. and in [40, 41], with a hypodermic needle used to pierce the septum of the bottle cap, allowing the sample to flow directly into the flow tube of the SIFT-MS instrument. The samples were held at 37°C throughout using a water bath or an incubator. In one experiment, the compounds emitted from a bottle with the culture open to the atmosphere were analysed by holding the hypodermic needle in place above the culture positioned inside the incubator.

In order to identify the compounds present in the vapour phase above the bacterial cell cultures the SIFT-MS instrument was operated in the FS mode to derive mass spectra using each of the precursor ions. Compounds could then be identified by the characteristic product ions. The instrument could then be operated in MIM mode, in which the appropriate primary precursor ion and its hydrates, and the characteristic primary product ions of particular volatile compounds, and their hydrates (given in Table 23), are selectively monitored, thereby providing a more accurate quantitative analyses than can be achieved by the FS mode of data acquisition (see Chapter 2, section 2.1.3.).

**Table 23.** List of the precursor ions and the primary product ions together with their mass-to-charge ratio ( $m/z$ ) and those of their hydrates, as used for the compound analyses reported in this chapter. The importance of the selection of the precursor for the analysis of each compound is highlighted by the two studies of isobaric compound and isobaric product ions, as given in Chapter 3. Noted in parentheses in the right column are the  $m/z$  values of the  $^{34}\text{S}$  isotopologue ions, which constitute about 4.2% of the total signal for a particular compound per sulphur atom.

Compound	Precursor ions [ $m/z$ ]	Primary product ion	$m/z$
Water vapour	$\text{H}_3\text{O}^+(\text{H}_2\text{O})_{0,1,2,3}$ [19, 37, 55, 73]	$\text{H}_3\text{O}^+(\text{H}_2\text{O})$	37, 55, 73
Ammonia		$\text{NH}_4^+$	18, 36, 54
Methanol		$\text{CH}_5\text{O}^+$	33, 51, 69
Hydrogen sulphide		$\text{H}_3\text{S}^+$	35
Acetaldehyde		$\text{C}_2\text{H}_5\text{O}^+$	45, 63, 81
Ethanol		$\text{C}_2\text{H}_7\text{O}^+$	47, 65, 83
Methanethiol		$\text{CH}_5\text{S}^+$	49, 67, 85
Acetone		$\text{C}_3\text{H}_7\text{O}^+$	59, 77, 95
Propanol		$\text{C}_3\text{H}_7^+$	43
Dimethyl disulphide		$\text{C}_2\text{H}_7\text{S}_2^+$	95 (97)
Acetone	$\text{NO}^+(\text{H}_2\text{O})_{0,1,2}$ [30, 48, 66]	$\text{NO}^+\text{C}_3\text{H}_6\text{O}$	88
Acetic acid		$\text{NO}^+\text{C}_2\text{H}_4\text{O}_2$	90, 108
Butanone		$\text{NO}^+\text{C}_4\text{H}_8\text{O}$	102
Dimethyl disulphide		$\text{C}_2\text{H}_6\text{S}_2^+$	94 (96)
Ammonia	$\text{O}_2^+$	$\text{NH}_3^+$	17, 35
Dimethyl disulphide	[32]	$\text{C}_2\text{H}_6\text{S}_2^+$	94 (96)

## 6.2. Results

### 6.2.1. *E. coli* cultured in lysogeny broth

In order to identify the compounds emitted by the *E. coli* cultures, it was first necessary to analyse the headspace of the medium under the same conditions (incubated at 37°C overnight), and this was done in each experiment. Thus, mass spectra were derived by running the SIFT-MS instrument in FS mode for three consecutive 20s scans. Following this, spectra were obtained for the media containing the *E. coli* cells for comparison. Example mass spectra obtained using  $\text{H}_3\text{O}^+$  primary precursor ions are given in Figure 18a and 18b for the LB medium and an *E. coli* culture respectively.

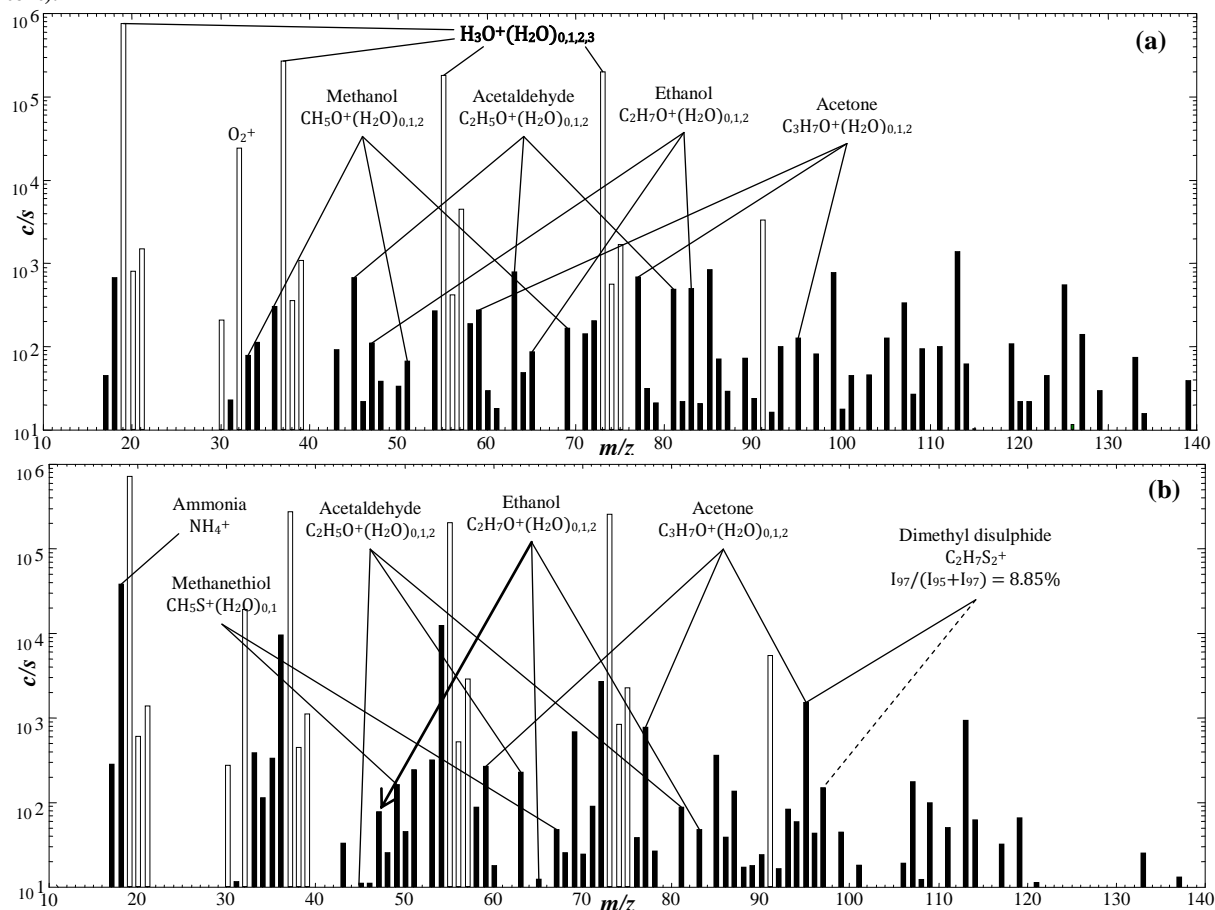
As is usually the case in  $\text{H}_3\text{O}^+$  spectra, the major peaks in those present in Figure 18 are the hydronium ion and its hydrates at the  $m/z$  values of 19, 37, 55, 73 and 91; the relative count rates of which provide a measure of the sample humidity [133], which is typically around 5% in each of the samples. The smaller peaks relate to the trace gas compounds in the sample headspace which, in the LB sample (Figure 18a) include (concentrations in parentheses) ammonia (400 ppbv), methanol (350 ppbv), acetaldehyde (600 ppbv), ethanol (300 ppbv) and acetone (340 ppbv). On the other hand, some relatively large peaks are present in the spectrum derived from the headspace of the *E. coli* culture (Figure 18b) at the  $m/z$  values 18, 36 and 54, which are due to the production of  $\text{NH}_4^+$  and its hydrates from ammonia (50,000 ppbv). Smaller peaks are also present at  $m/z$  49 and 67 (methanethiol), and 95 and 97 (due to  $^{32}\text{S}$  and  $^{34}\text{S}$  isotopologues of dimethyl disulphide,  $(\text{CH}_3)_2\text{S}_2$ ). The



relative abundances of the  $^{32}\text{S}$  and  $^{34}\text{S}$  isotopologue ions can serve as an aid in the identification of sulphur-containing compounds present in the mass spectra. Each  $^{34}\text{S}$ -containing ion should account for around 4.2% of the combined count rates of both ions, and the example analysis shown in Figure 18 shows this to be the case for the assigned dimethyl sulphide product ions at  $m/z$  95 and 97.

It is important to note that the detection of dimethyl disulphide using  $\text{H}_3\text{O}^+$  precursor ions, can be confused by the presence of acetone, because an overlap occurs with the second hydrate of protonated acetone ( $\text{CH}_3\text{COCH}_3\text{H}^+(\text{H}_2\text{O})_2$ ) that also appears at  $m/z$  95. Fortunately, this overlap can be avoided by using  $\text{NO}^+$  or  $\text{O}_2^+$  precursor ions to analyse dimethyl disulphide that produce characteristic product ions at  $m/z$  values of 94 and 96 (see Table 23).

**Figure 18.** SIFT-MS spectra (ion counts-per-second,  $c/s$ , against mass-to-charge ratio,  $m/z$ ) obtained using  $\text{H}_3\text{O}^+$  precursor ions for the analysis of the headspace of (a) 25mL of LB culture medium and (b) a highly concentrated suspension of *E. coli* in LB following overnight incubation at  $37^\circ\text{C}$ . Only the major compounds are indicated. Dimethyl disulphide is identified by the abundance ratio of its characteristic isotopologue ions at  $m/z$  95 and 97 (see text).



In a separate experiment, a sample of high density “stock” *E. coli* was diluted by adding different volumes of LB, with the final total volume maintained at 25mL in each case. In this way, the final “stock” *E. coli* concentrations varied from 0% (neat LB) through 20%, 40%, 60%, 80% and 100%. The samples were then

incubated whilst sealed in the 150mL glass bottles for 2 hours before the headspace was analysed with the SIFT-MS instrument operated in MIM mode. The results of these analyses are shown in Table 24.

**Table 24. Concentrations of various compounds (in parts-per-billion by volume, *ppbv*) as measured by SIFT-MS in the headspace above different concentrations of growing cultures of *E. coli* JM109 in LB. The bacteria were first cultured overnight in shaker flasks containing LB, resulting in a highly concentrated “stock” cell suspension. A volume of this suspension, indicated in the top row of the table, was then added to bottles containing fresh LB medium, so that the final volume was always 25mL.**

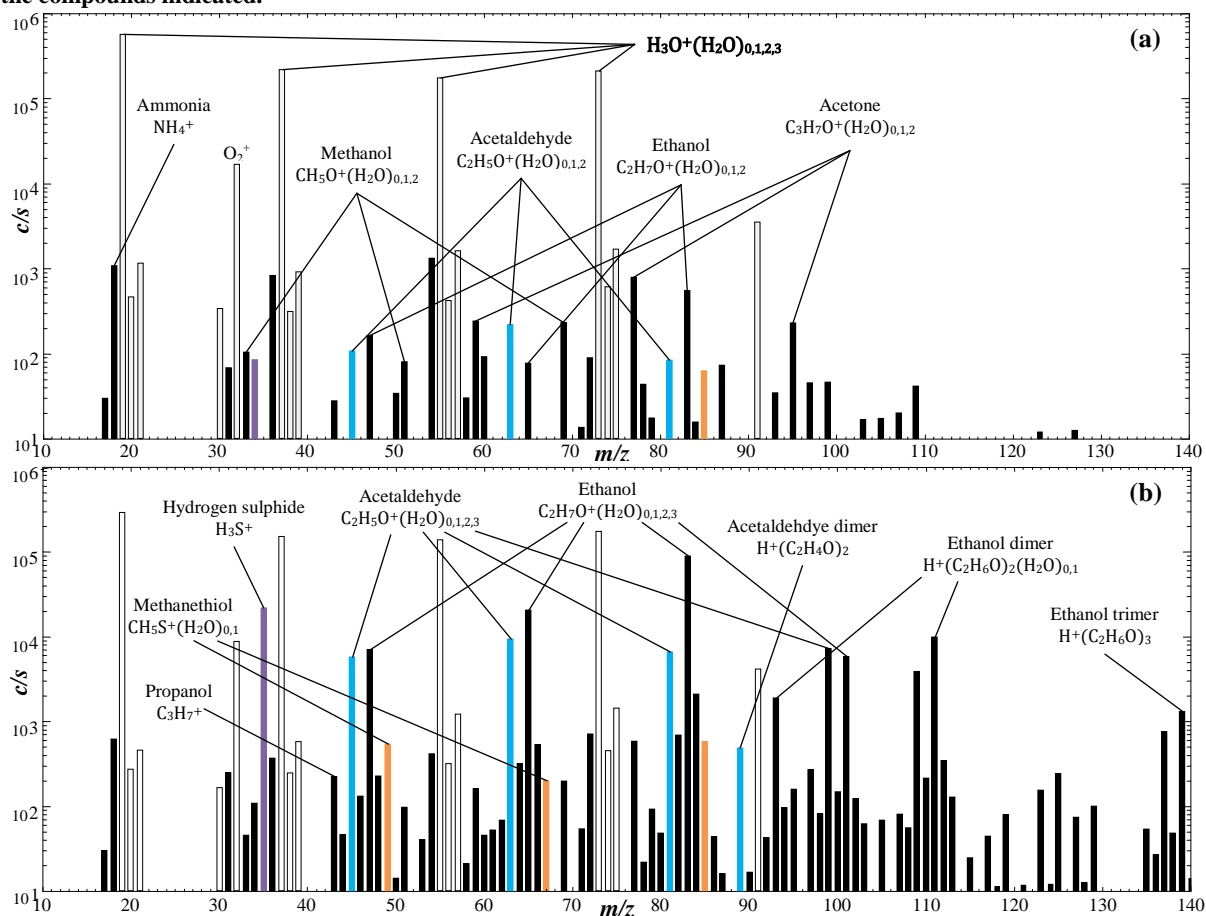
Compound	Primary precursor ion	“Stock” <i>E. coli</i> suspension added (mL)					
		0	5	10	15	20	25
Acetaldehyde	H <sub>3</sub> O <sup>+</sup>	600	170	320	360	110	20
Ethanol		200	3000	3100	2300	900	70
Acetone		340	390	400	450	430	400
Ammonia	O <sub>2</sub> <sup>+</sup>	1700	1400	1300	5200	19,000	50,000
Dimethyl disulphide		20	30	110	140	60	140

The concentration of ammonia in the headspace of the cultures was found to increase rapidly when >10mL of “stock” *E. coli* suspension (40%) was added; ranging from around 1 to 50 parts-per-million by volume (*ppmv*). The headspace concentrations of several other compounds are listed in Table 24. Ethanol was initially seen to increase at the lower “stock” *E. coli* concentrations (0 to 40%), and then decline with increasing “stock” concentration. Acetaldehyde was seen to follow a strange pattern, but similarly clearly falling overall with increasing “stock” *E. coli* concentrations. This could provide some insight into the metabolic state of the cells and the nutritional value of the remaining media, which was partially depleted in all cases where *E. coli* was present. Finally it is worthy of mention that the acetone concentration remained consistent between samples, indicating that acetone does not participate in the metabolism of the cells under these conditions.

#### 6.2.2. *E. coli* cultured in high glucose DMEM

As before, the compounds present in the headspace above the medium alone were first analysed. In this case, this medium consisted of high glucose DMEM supplemented with FBS and L-glutamine, as described in section 6.1.1.. A sample FS mass spectrum obtained from the analysis of this medium is given in Figure 19a. Here it is seen that, as before, the major peaks are detected at *m/z* 19, 37, 55, 73 and 91, due to the hydronium ion and its hydrates, while several smaller peaks are detected due to the presence of trace volatile compounds. These include (concentrations in parentheses) ammonia (700 *ppbv*), methanol (250 *ppbv*), acetaldehyde (150 *ppbv*), ethanol (500 *ppbv*) and acetone (500 *ppbv*). As mentioned in previous chapters, acetaldehyde, ethanol and acetone have been demonstrated to originate largely from the FBS, while the methanol is present largely in the DMEM alone, with no added supplements (see [41] and section 4.2.1.).

**Figure 19.** SIFT-MS mass spectra (ion counts-per-second, *c/s*, against mass-to-charge ratio, *m/z*) obtained using  $\text{H}_3\text{O}^+$  precursor ions for the analysis of the headspace of (a) 25mL of DMEM supplemented with 10% v/v FBS and 2mM L-glutamine; and (b) 24mL of the same medium with 1mL of highly concentrated *E. coli* cells in LB medium following overnight incubation at 37°C inside sealed 150mL glass bottles. Also identified are the characteristic product ions of the compounds indicated.



A second bottle containing 1mL of “stock” *E. coli* in LB and 24mL of DMEM was also analysed following overnight incubation at 37°C, with mass spectra derived by operating the SIFT-MS in FS mode. A sample mass spectrum for the analysis of this headspace sample is given in Figure 19b, above. In comparison to the mass spectrum obtained from the medium alone, (Figure 19a), several relatively intense product ion peaks can be easily identified at indicating the presence of ethanol (100 *ppmv*), as identified by the product ions at *m/z* 47, 65 and 83, and acetaldehyde (10 *ppmv*), present at *m/z* 45, 63 and 81, are clearly massively enhanced by the *E. coli* cells. The concentrations of these compounds are so high that the proton-bound dimer and, in the case of ethanol, proton-bound trimer ions can easily be identified in the mass spectrum [188]. Another major peak is present at *m/z* 35, which is known to be due to the presence of hydrogen sulphide ( $\text{H}_2\text{S}$ ; 50 *ppmv*) [127], and a second sulphur-compound, methanethiol ( $\text{CH}_4\text{S}$ ; 1 *ppmv*), is indicated by the product ions at *m/z* 49, 67 and 85 [80].

In a separate experiment, different volumes of a concentrated “stock” *E. coli* suspension (produced via the overnight culture of *E. coli* cells in LB using a spinner flask system) were added to DMEM so that the final volume was always 25mL. The refreshed cultures were incubated overnight (~16h) inside sealed 150mL glass bottles with septa. The following morning, quantitative MIM mode analyses were performed on the headspace of each sample, in order to measure the concentrations of the previously identified volatile metabolites (see Figure 19). The results of these analyses are presented in Table 25.

**Table 25. Concentrations of various compounds (in parts-per-billion by volume, *ppbv*) as measured by SIFT-MS in the headspace above *E. coli* cultures in DMEM medium. The volume of concentrated “stock” *E. coli* suspension (in LB) added to the DMEM (final volume 25mL), is indicated in the top row of the table (see text). These *E. coli*/DMEM suspensions were incubated at 37°C without agitation in sealed 150mL glass bottles for around 16 hours prior to the analysis.**

Compound	Primary precursor ion	“Stock” <i>E. coli</i> suspension added (mL)		
		0	1	5
Methanol	H <sub>3</sub> O <sup>+</sup>	270	280	300
Hydrogen sulphide		10	1000	37,000
Acetaldehyde		150	10,000	16,000
Ethanol		600	37,000	67,000
Methanethiol		10	350	1500
Propanol		50	160	150
Acetone	NO <sup>+</sup>	420	380	250
Dimethyl disulphide		10	500	1000
Ammonia	O <sub>2</sub> <sup>+</sup>	700	700	600

It is evident in Table 25 that the concentration of the volatile compounds is not simply related to the five-fold increase in starting cell numbers. Acetaldehyde and ethanol are likely formed from glucose metabolism, and the fact that the increase is much less than five-fold with the increase in starting cell number indicates that the glucose was used up depleted from the medium. The hydrogen sulphide concentration is much greater than five times larger in the 5mL “stock” sample, which might indicate that H<sub>2</sub>S is formed from an alternative energy source which is consumed as the glucose is used up. There is some evidence to suggest that propanol and dimethyl disulphide are produced, but the accuracy of the measurements of these lower-level compounds might be diminished by the extremely high concentrations of acetaldehyde and ethanol in the headspace.

### 6.2.3. Real-time monitoring of *E. coli* culture growth in DMEM medium

Having identified the major metabolites emitted into the gas phase by *E. coli* JM109 cell cultures in DMEM, a new experiment was devised to track these emissions in real time. This was performed by producing a culture of 10mL “stock” *E. coli* cell suspension added to 15mL of DMEM medium (with FBS and L-glutamine, as before) inside a 150mL glass bottle. In this case, the bottle was kept inside an incubator, set to 37°C, and open to the atmosphere. The opening to the vessel was positioned close to a small hole at the incubator wall, while the

hypodermic needle, which is directly coupled to the sampling arm of the SIFT-MS instrument, was held in place, a few centimetres inside the neck of the glass bottle. The SIFT-MS was operated in the MIM mode, continuously monitoring the concentrations of the previously-identified volatile compounds in real time for around four hours. The omission of a septum at the opening to the glass bottle prevented the loss of pressure which would have occurred in a sealed system (due to the headspace sampling), and consequently there was a free flow of air into the bottle and the emitted trace compounds were able to flow out of the bottle. The loss of emitted volatile compounds took place largely by diffusion since the vapour phase above the sample was not agitated. In this study, a total of 25 ions (including precursor and product ions) were monitored using the MIM mode, meaning that each compound under analysis was sampled every 5 seconds. This allowed the acquisition of about 2700 data points for each compound, in the approximately 14,000 seconds of observation. Plots resulting from this long, continuous scan of the vapour compounds emitted by the *E. coli* culture are shown in Figure 20.

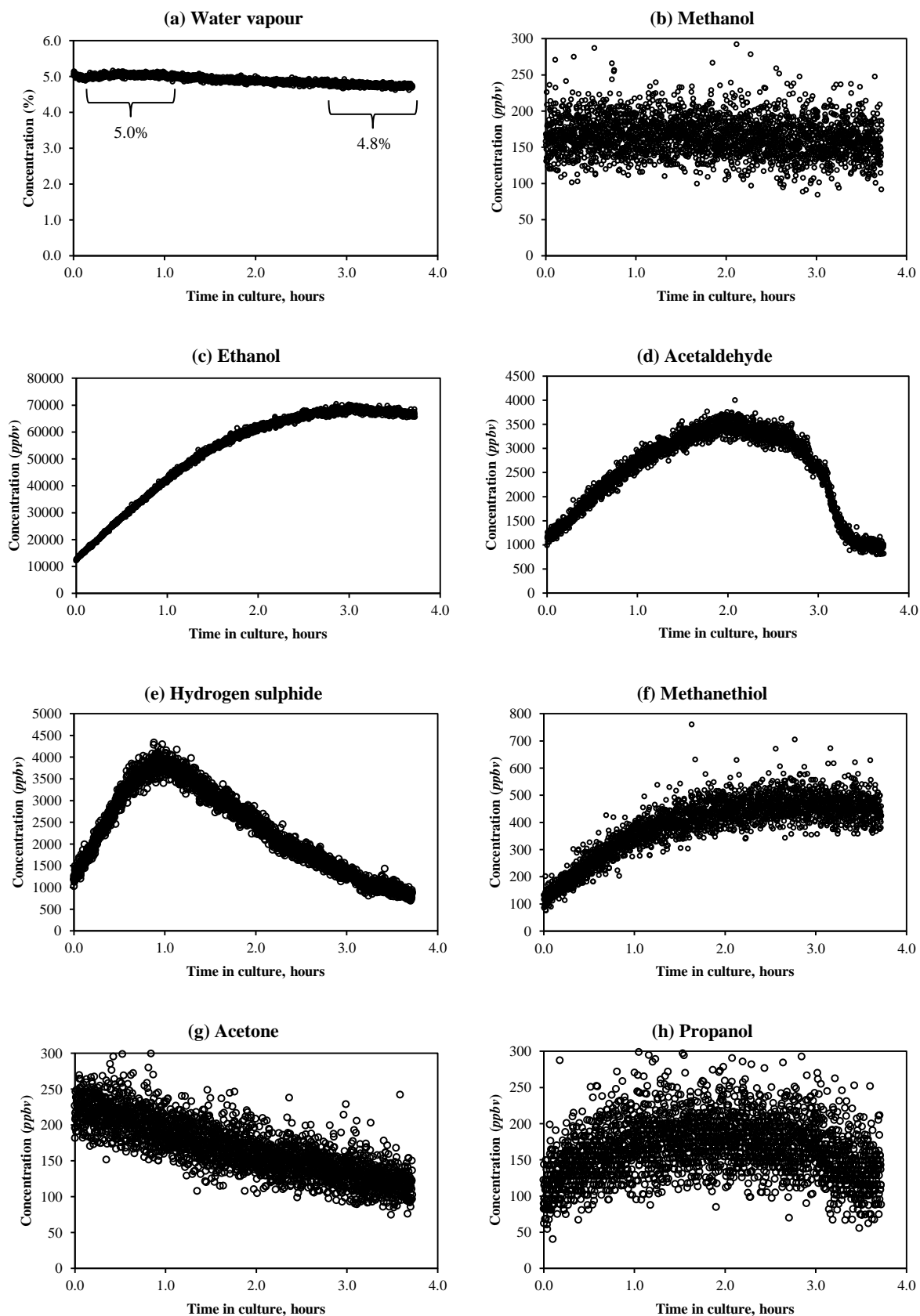
According to the plot shown in Figure 20a the water vapour pressure remained steady at about 5% over the course of the 4 hour monitoring period, this being equivalent to a temperature of about 35°C. Given that the incubator was set to 37°C and the bottle was kept open during the analysis, the water vapour measurements obtained attest to the instrument stability. Also, in Figure 20b, the methanol concentration is remains closely invariant over the 4 hour monitoring period at a concentration of 180 *ppbv* with a standard deviation of 52 *ppbv*. The origin of this alcohol is the neat DMEM medium as mentioned (see section 4.2.1.), and so *E. coli* JM109 cells do not produce methanol when cultured in this medium.

Interestingly, the volatile compounds that were emitted into the headspace of sealed *E. coli* cultures (see Table 25) were also emitted into the atmosphere under the open conditions of this monitoring experiment. As was the case in the sealed culture experiments, ethanol was found to be the most abundant compound present in the vapour phase above these open bottles. Its concentration increases initially, reaching a peak value of around 70 *ppmv* after 3 hours, when it then begins to fall, again presumably due to the depletion of the glucose in the medium (see Figure 20c). The acetaldehyde concentration also increases, reaching its peak value of around 4 *ppmv* after 2 hours. It is also noticeable that the reduction in the headspace acetaldehyde concentration is faster than for ethanol. This could be explained by the relatively high volatility of acetaldehyde, as is reflected by its Henry's Law coefficient, which is around thirteen times greater than that of ethanol [151, 156]. Notice also that the maximum acetaldehyde concentration of 3.5 *ppmv* is 3-4 times lower than the value that was observed in the analysis of the headspace of the sealed bottle culture (see Figure 20d and Table 25), which presumably is also a result of its high volatility.

Similarly, hydrogen sulphide reached a peak concentration of about 4 *ppmv*, which is around ten times lower than the headspace concentration derived in the previous experiment (see Table 25). This peak value was observed to occur earlier than the peaking of acetaldehyde and also declines more quickly (Figure 20e). The origin of the H<sub>2</sub>S could be the sulphur-containing amino acids, viz. L-cysteine (C<sub>3</sub>H<sub>7</sub>NO<sub>2</sub>S) and L-methionine (C<sub>5</sub>H<sub>11</sub>NO<sub>2</sub>S) that are present in neat DMEM, but it is also possible that some sulphur-containing proteins are present in the FBS. In any case, the results presented in Figure 20f indicate that the sulphur-compounds are relatively quickly consumed by the *E. coli* cells. The maximal concentration reached by the methanethiol is about 500 *ppbv*, which is several times lower than that in the headspace of the sealed bottle (see Figure 20f and Table 25).

The plot in Figure 20g that the emitted acetone concentration was depleted from the vapour phase above the *E. coli* culture. The cause of this depletion is likely evaporative loss from the medium, rather than consumption by the cells. This is supported by the fact that the Henry's law coefficient for acetone at 37°C is around 10 times lower than that of methanol, which was seen to be extremely stable over the 4 hour period (Figure 20b). In addition, the acetone concentration in the headspace of the sealed cultures was relatively consistent between samples (see Table 25). There is an indication that propanol is produced in the cell cultures (see Figure 20h and Table 25). The concentration of propanol was evaluated using the *m/z* 43 product ion only [146], avoiding the protonated propanol ion at *m/z* 61, because of the potential overlap with the protonated ions of the isobaric compounds methyl formate and acetic acid [134]. This was necessary particularly because of the presence of a small concentration of acetic acid (100 *ppbv*), as indicated by *m/z* 90 product ions when NO<sup>+</sup> was used to analyse the headspace [134].

**Figure 20.** Plots showing the concentrations of water vapour, methanol, ethanol, acetaldehyde, hydrogen sulphide, methanethiol, acetone and propanol as they were monitored *via* real time SIFT-MS analyses above an open *E. coli* JM109 culture in a medium consisting largely of DMEM. The analyses were performed simultaneously using  $\text{H}_3\text{O}^+$  precursor ions.



### 6.3. Summary and concluding remarks

Presented in this chapter are the results of a study of the volatile compounds released into the medium by *E. coli* JM109 cells by monitoring only the vapour phase by SIFT-MS. The vapours have been analysed following the culture of the cells in two different media types, viz. LB and DMEM. It was found that cells cultured in a DMEM-based medium inside sealed bottles emitted easily-measurable quantities of several volatile compounds, particularly ethanol, acetaldehyde, hydrogen sulphide and methanethiol. Consequently it was possible to monitor the levels of these compounds in the vapour phase above an open culture for a period of around 4 hours. In addition, the headspace of *E. coli* cells cultured in LB inside a sealed bottle was also analysed, with only the concentration of ammonia clearly elevated in the gas phase. There was also some evidence of the production and consumption of ethanol and acetaldehyde with increasing cell number densities, when cultures were intentionally seeded with varying quantities of cells (see Table 24). This could be due to the cells undergoing changing metabolism, which requires further investigation. Also the differences between the compounds emitted by the cells highlight the importance of the medium used to culture cells when considering the analysis of the volatile compounds. Clearly the cultured cells must metabolise the contents of the media in order to survive, and this will affect the metabolite compounds that are subsequently produced. This is an important consideration for the research into the detection of medically important microbes that invade the human body.

It should be noted that the headspace concentrations we have obtained for each volatile compound are clearly subject to variable parameters that we have not accounted for, particularly the concentration (numbers) of the cells in each medium/cell sample. Therefore, the derived concentrations of the volatile compounds are only intended to show that the emissions are high enough to be readily identified, quantified and monitored by SIFT-MS and that these several compounds can be used to monitor suspensions of growing cells. It is certain that these bacterial cells are emitting other VOCs that have not been seriously searched for in this preliminary study. An example of this was observed in solid-phase microextraction gas chromatography mass spectrometry (SPME-GC-MS) experiments, which were performed on *E. coli*/DMEM cell cultures by the Mass Spectrometry Group during a visit to the J. Heyrovský Institute in the Czech Republic. Several additional volatile product compounds were identified including indole, butanal, acetoin and diacetyl. These compounds have all been characterised for analysis by SIFT-MS (see Chapter 3 and [112, 143]), but these are not major headspace compounds, and could not be readily identified in the headspace in the present studies, possibly due to the excessive levels of ethanol and acetaldehyde which are present.



Comparing the results of the present chapter with the studies of the headspace compounds present above human cell cultures, given in Chapters 4 & 5, it is clear that *E. coli* cultures are far more active in producing volatile compounds. It should be noted, however that each of the *E. coli* cultures could contain as many as  $5(10^{10})$  cells, while the greatest human cell numbers analysed so far by SIFT-MS have contained around  $2(10^7)$  cells [40] with cell densities at least  $5(10^3)$  times lower. However, the fact that relatively few compounds are emitted by these human cell cultures means that deviations from the healthy culture environment could be more easily identified; hence this system might be used to non-invasively and rapidly detect infection by microbial cell types. Indeed the results of these studies are applied later in Chapter 7 for some studies of the intentional infection of human cell cultures. It may also be considered that these methods of analysis could be applied to non-invasively monitor the progression of *E. coli* and other microbial cell cultures; these being of great importance in various industries, such as biopharmaceuticals.

## 7. Identification of microbial contamination in mammalian cell cultures using headspace analysis techniques

### 7.1. Introduction

Loss of sterility in an industrial bioprocess is the most common cause of process failure [196]. Then, the entire batch of cells, or other biological product, will be unusable, and the cause of the contamination must be investigated, creating unwanted, costly down time [196]. Checks for microbial contamination of industrial bioreactors are usually performed once a day using time-consuming and invasive methods, requiring samples to be taken from the bioreactor [197]. In addition, the standard *in situ* sensor probes that monitor the levels of dissolved oxygen (DO) and pH will only indicate the presence of contaminating microbial cells at a late stage [197]. This can create costly setbacks; however rapid, online methods for the detection of bacterial infection are rarely implemented industrially [197]. As mentioned in Chapter 1 (section 1.3.3.), gas chromatography mass spectrometry (GC-MS) has been applied for the early identification of *Enterobacter cloacae* infections in cultures of *Leuconostoc mesenteroides* bacterium by analysing the produced volatile compounds [61]. Similarly, statistical techniques were applied to GC-MS data in order to rapidly identify the presence of *bacillus subtilis* and *pseudomonas aeruginosa* (PA) infections in microalgae cultures [62]. In addition, GC-MS has been used to detect the presence of several different microbial cells when added to an animal cell culture [63].

An alternative method has been to use gas sensor arrays, commonly known as electronic noses (EN), to identify the changes in the gas phase caused by the release of volatile compounds produced by infectious cell types [22, 197]. In one reported study, Chinese hamster ovarian (CHO) cells were infected with PA at a concentration of 100 colony-forming units per millilitre (CFU/mL), and MOSFET (metal oxide semiconductor field-effect transistor) sensors, which vary in their sensitivities for different compounds, were used to detect changes in the gas phase composition. A change in the signal level of one MOSFET sensor was observed about 1 hour after the PA had been added, which was some 12 hours before any change in DO was detected [197]. An attempt to detect the presence of the bacterium *bacillus subtilis*, which was introduced at a much higher concentration of 4000 CFU/mL, using similar methods was also reported. A small change in the signal level of a different MOSFET sensor is apparent immediately following the introduction of the bacteria, although this signal response was less clear [197]. In the work reported in this chapter SIFT-MS is used to perform similar experiments regarding the detection of volatile biomarkers of the infection of human cell cultures by microbial cells.

## 7.2. Experimental

### 7.2.1. Sample preparation for headspace analysis

Several tissue culture flasks, used for the culture of human cell types, were donated for exploratory headspace analysis experiments by colleagues, upon their discovery of the presence of microbial cells in the media. The volumes of infected media that could be sampled were typically 5-10mL, depending on the size of the flask used for the culture of the human cells. The medium was transferred to a 150mL glass bottle, the headspace was purged with dry cylinder air, and each sample was incubated at 37°C for around 16 hours prior to the headspace analysis experiments.

### 7.2.2. Bioreactor culture using the CELL-tainer bioreactor® system

The CELL-tainer® single-use bioreactor system (CELLution Biotech B. V., Netherlands) was obtained on loan, via the company CELLON S. A., in order to analyse the gas/vapour compounds emitted from relatively large-scale cell cultures. This included analyses after human cell cultures were infected with *E. coli* bacterial cells, the major emissions from which have been characterised by SIFT-MS (see Chapter 6 and [190]). The human cell types used were primary human mesenchymal stem cells (hMSCs) which were derived from bone marrow and initially cultured in tissue culture flasks, submerged in DMEM, supplemented with 10% v/v foetal bovine serum (FBS), 1% v/v antibiotic-antimycotic and 2mM L-glutamine, as described in Chapter 4 (section 4.1.1.). In order to commence the bioreactor run, around  $3(10^7)$  hMSCs were removed using the enzyme trypsin and transferred to a pre-sterilised disposable bioreactor bag, which also contained Cytodex-1 surface microcarriers at a concentration of 2 g/L (prepared and sterilised as described in section 4.1.2.) and 1L of the same DMEM medium. The total volume of the disposable bioreactor bags is 20L, but this was restricted to around 4L using plastic dividers, leaving a headspace of around 3L. The bags were also fitted with *in situ* dissolved oxygen (DO) and pH sensor probes, which were calibrated prior to adding the cells and were used to continuously monitored the culture. The culture was incubated at 37°C and agitated at a rate of 5 rpm. Dry cylinder air was regularly injected, via a 0.2µm filter, in order to maintain a DO concentration of 20% (~0.21mM) and carbon dioxide was injected intermittently to maintain a pH of 7.4, in conjunction with the sodium bicarbonate buffer, which is present in DMEM at a concentration of 3.7 g/L. The gas was able to flow out of the bioreactor bag through a second 0.2 µm filter to the external laboratory environment.

Every 2-3 days well-mixed 5mL samples of the DMEM media, containing microcarriers and attached hMSCs, were removed from the bioreactor for cell counting. This was performed using a WST-8 colourimetric viability test (NBS Biologicals, UK). In short a water soluble tetrazolium (WST) salt is added to the cell sample, which is acted upon by the intracellular enzymes that exist in viable cells, causing the release of a formazan dye, which is then quantified by the resulting absorbance levels using a Synergy 2 spectrophotometer (BioTek, UK). In addition, 50% of the media was exchanged by tilting the bag to allow the microcarrier beads to settle to the bottom and the liquid was removed by pumping *via* one of the ports indicated in Figure 21. Fresh media was introduced using a sterile syringe to inject the liquid through a second port.

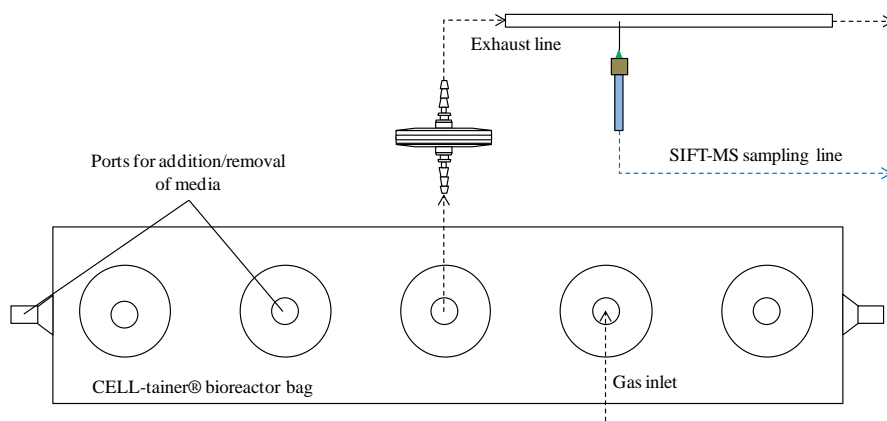
### 7.2.3. *Culture of E. coli (JM109) cells*

As before (see Chapter 6, section 6.1.1.), *E. coli* cells, strain JM109, were initially cultured for around 16 hours at 37°C in a lysogeny broth medium (**LB**; Sigma, UK) using a shaker flask system in order to produce a high density volume of *E. coli* cells. The actual cell density was found to be approximately  $1.5-2.0(10^9)$  cells-per-mL using optical density measurements at a wavelength of 600nm. In the present study, these bacteria were introduced into the bioreactor bag at the desired time point to check the ability of SIFT-MS to detect the culture infection could be tested. It is important to note that antibiotics were present in the culture medium, and this was previously found to impede the growth of the infecting *E. coli* cells (data not shown).

### 7.2.4. *Gas/vapour phase analysis by SIFT-MS*

Analyses of the headspace of sealed bottles containing samples of the infected culture media samples were performed, as before, by piercing the septa at the bottle cap with a hypodermic needle that is directly coupled to the SIFT-MS sampling arm. Thus the volatile compounds and the air that occupy the headspace simply flow into the flow tube of the SIFT-MS instrument for analysis.

**Figure 21. Schematic diagram of the CELL-tainer® bioreactor bag, displaying the gas inlet and exhaust lines and the sampling point for the hypodermic needle which was coupled directly to the SIFT-MS sampling line.**



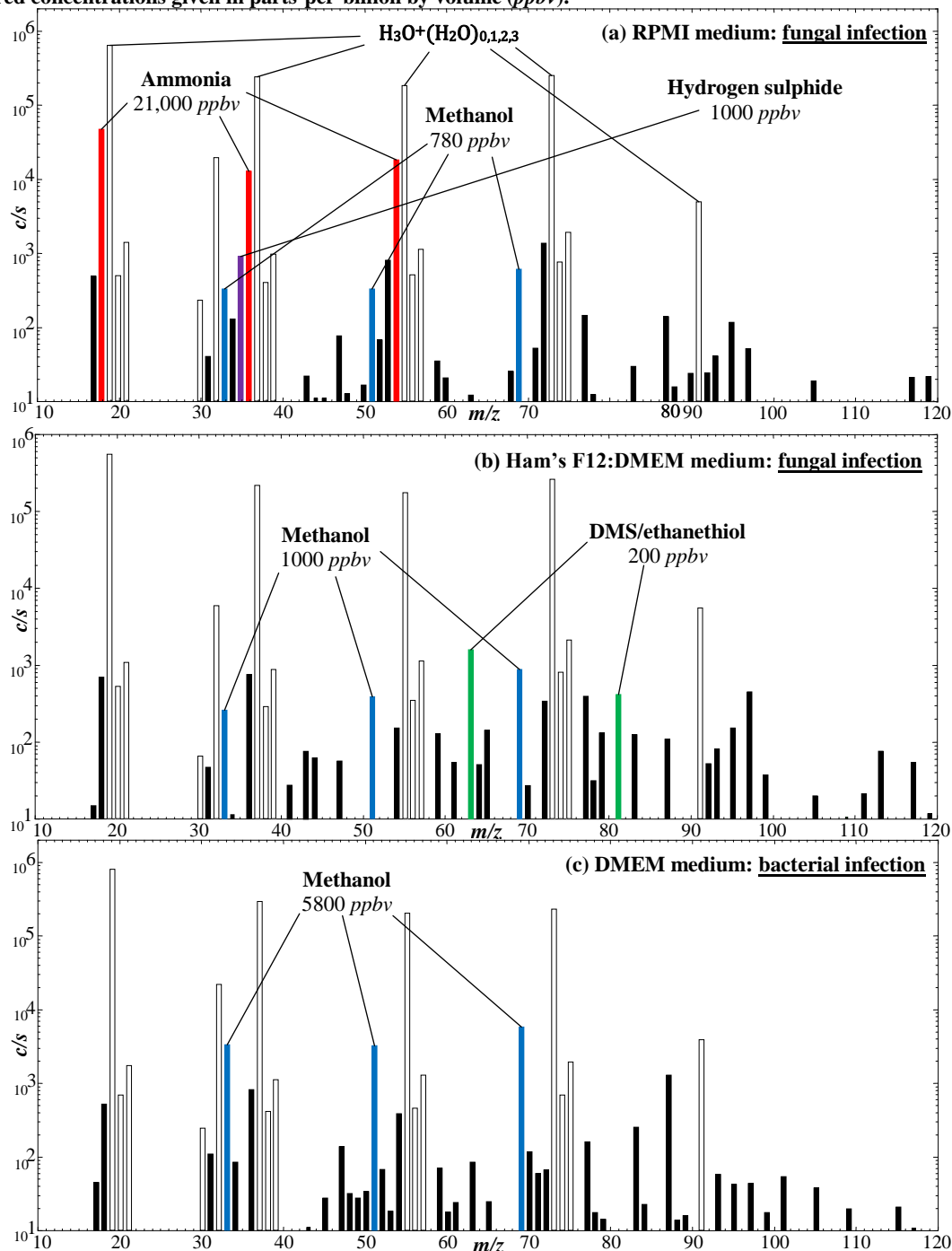
The flowing exhaust gases, which contained the compounds emitted from the culture present in the bioreactor bag, were sampled by piercing the soft tubing of the exhaust line, as is depicted in Figure 21. By sampling in this way, the door to the incubator could be kept closed, and this was necessary to ensure that the bioreactor continued to incubate the culture at 37°C, to agitate the vessel and to intermittently inject the cylinder gases (dry air and carbon dioxide) during the analysis by SIFT-MS, thereby ensuring that the culture could proceed undisturbed. The volatile compound emissions by *E. coli* cultured in DMEM media had been studied previously (see Chapter 6 and [190]), which had indicated that the concentrations of ethanol, acetaldehyde, hydrogen sulphide and methanethiol were large enough to be easily detected and quantified by SIFT-MS.

### 7.3. Results

#### 7.3.1. Bacterial and fungal infections in mammalian cell cultures

Several of the infected culture media samples were donated by other researchers and, as mentioned in section 7.1.1., these were contained in sealed glass bottles during headspace analysis experiments. Spectra derived from the analysis of the headspace above three of these infected culture media samples are shown in Figure 22. Although these microbial cells could not be fully identified, the samples that were analysed for Figure 22a and 22b were likely to be fungal cells, as shown by their filamentous morphology, and that in Figure 22c appeared to be a bacterial cell type. As can be seen in the spectra, each of these microbial cells emitted at least one volatile compound at a concentration clearly exceeding that expected from clean media or that containing only human cell types.

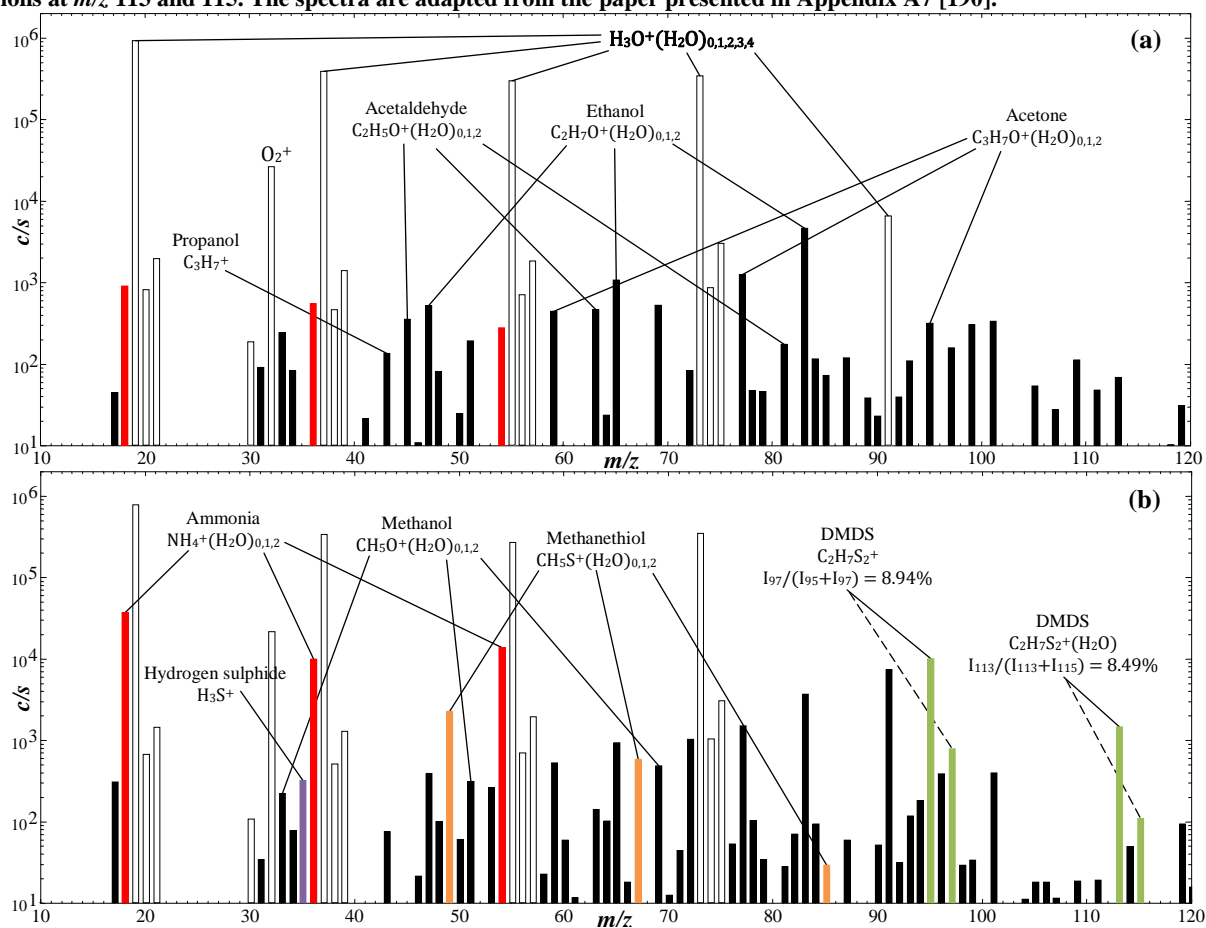
**Figure 22.** SIFT-MS mass spectra (ion counts-per-second, *c/s*, against mass-to-charge ratio, *m/z*) each obtained using  $\text{H}_3\text{O}^+$  precursor ions showing the analyses of the compounds present in the headspace above (a) RPMI media infected with fungal cells; (b) DMEM:Ham's F-12 media infected with fungal cells; and (c) DMEM media infected with bacteria. The major volatile compounds that are elevated above typical culture media levels are indicated, with the measured concentrations given in parts-per-billion by volume (*ppbv*).



The headspace of the fungal-infected RPMI (Roswell Park Memorial Institute) medium analysed in Figure 22a showed that ammonia was produced to a level of greater than 20 parts-per-million by volume (*ppmv*), which is around 40 times greater than the value measured above equivalent, clean RPMI medium. Hydrogen sulphide was also measured in the headspace at a concentration of 1000 *ppbv*, while methanol was measured to be 730 *ppbv*; in the clean media these compounds present at levels of 5 *ppbv* and 100 *ppbv* respectively (data not

shown). The headspace of the second fungal-infected medium, in this case composed of Dulbecco's modified Eagles medium/Nutrient F-12 Ham (DMEM:Ham's F-12), shown in Figure 22b, and was found to contain elevated concentrations of methanol (1000 *ppbv*) and dimethyl sulphide (DMS; 200 *ppbv*) compared to that of a sample of the medium alone that contained concentrations of around ten times lower for both compounds. The spectrum shown in Figure 22c, which was obtained from the analysis of the headspace of a DMEM medium sample infected with bacterial cells, displays a single biomarker, *viz.* methanol, at a concentration of 5800 *ppbv*, as opposed to the 100 *ppbv* which is typical in the headspace of media samples of this type (see Chapter 4).

**Figure 23.** SIFT-MS spectra (counts-per-second, *c/s*, against mass-to-charge ratio, *m/z*) obtained using  $\text{H}_3\text{O}^+$  precursor ions for the analysis of the headspace of (a) DMEM medium supplemented with 10% v/v FBS and 2mM L-glutamine; and (b) the same medium that had become infected with the bacterium *C. testosteroni*, contained inside sealed glass bottles. The major compounds and their product ions are indicated. Dimethyl disulphide (DMDS) is again identified by the abundance ratio of its characteristic isotopologue ions at *m/z* values of 95 and 97, and hydrated isotopologue ions at *m/z* 113 and 115. The spectra are adapted from the paper presented in Appendix A7 [190].



In addition, the headspace of one infected sample of DMEM medium (10% v/v FBS and 2mM L-glutamine) was analysed by SIFT-MS, resulting in the spectrum shown in Figure 23b, with a comparative sample of clean DMEM medium presented in Figure 23a. As can be seen, large quantities of ammonia and dimethyl disulphide (DMDS) were produced, with the identity of the latter checked by isotopologue analyses, as shown in the Figure 23b. Hydrogen sulphide and methanethiol were also produced by these bacteria in this

DMEM medium, similar to the *E. coli*, strain JM109, cells that were discussed in Chapter 6. The concentrations of the mentioned biomarkers of this bacterium, as well as some other common compounds, are given in Table 26. It is seen that each of the aforementioned volatile compounds was emitted into the headspace at easily measurable levels, while the concentrations of methanol, ethanol and acetone were very consistent between samples. There is also some evidence for the production of a small amount of butanone, this being easily identified in NO<sup>+</sup> spectra [113]. The infected culture media was also sent to a nearby pathology laboratory for assessment, where the infecting microbe was identified as a common gram negative soli bacterium *Comamonas testosteroni*.

**Table 26. The concentrations (in ppbv) of some selected volatile compounds measured in the headspace above clean DMEM medium (10% v/v FBS, 2mM L-glutamine) and DMEM infected with the bacterium *C. testosteroni*. The data are shown in the paper presented in Appendix A7 [190].**

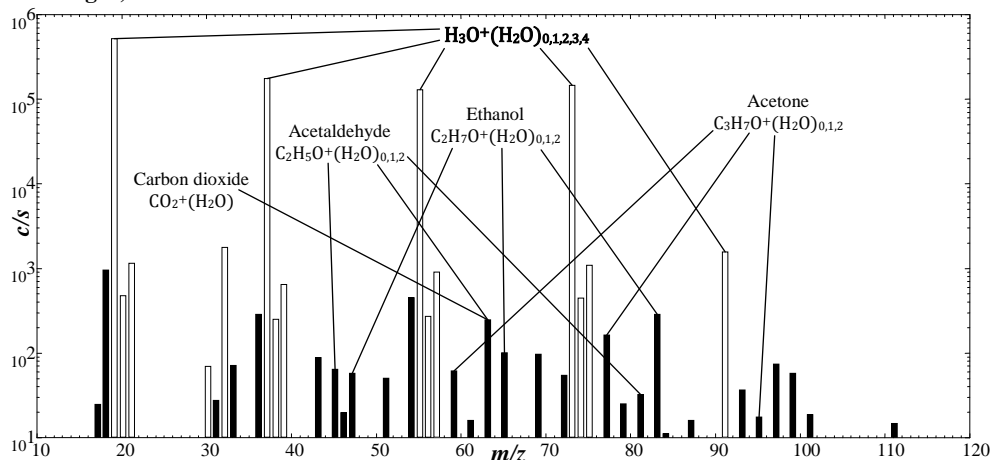
Compound	Primary precursor ions	DMEM control	DMEM infected with <i>C. testosteroni</i>
Ammonia	H <sub>3</sub> O <sup>+</sup>	300	13,200
Methanol		260	310
Hydrogen sulphide		0	200
Acetaldehyde		140	0
Ethanol		1400	1400
Methanethiol		10	760
Acetone	NO <sup>+</sup>	220	330
Butanone		0	40
Dimethyl disulphide		10	2500

### 7.3.2. Intentional *E. coli* infection of a bioreactor culture of human cells

As mentioned in section 7.1.2., the cells in this study were cultured on Cytodex-1 microcarrier beads inside a CELL-tainer<sup>®</sup> bioreactor system. The vapours released by the microcarrier beads have been analysed previously (see section 4.2.5), where it was shown that very large quantities acetone were present (around 50,000 ppbv for a 2 g/L sample) if the beads were not washed correctly, but only emitted a small quantity (60 ppbv-per-g/L of beads) when properly washed. It was additionally important to check for any volatile emissions by the bioreactor bag itself. Thus a mass spectrum is presented in Figure 24 which is derived from the analysis of the sealed bioreactor bag containing 500mL of DMEM (10% FBS, 1% antibiotic-antimycotic, 2mM L-glutamine). It is clear that clear signals are emitted due to neither the microcarriers nor the bioreactor bag. Some of the compounds present in the spectrum are as follows, with concentrations given in parentheses: water vapour (5.4%); methanol (200 ppbv); acetaldehyde (80 ppbv); CO<sub>2</sub> (2.3%); ethanol (280 ppbv); acetone (170 ppbv).

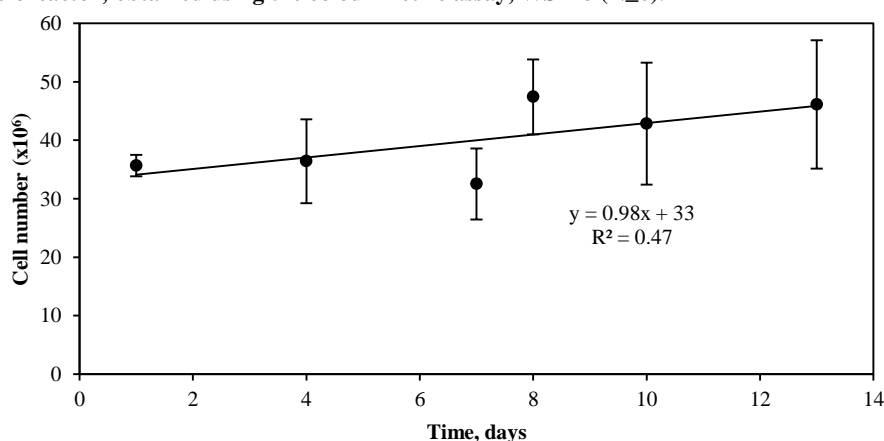


**Figure 24.** SIFT-MS spectra (counts-per-second,  $c/s$ , against mass-to-charge ratio,  $m/z$ ) obtained using  $H_3O^+$  precursor ions for the analysis of the sealed gas/vapour phase inside a sealed CELL-tainer<sup>®</sup> bioreactor bag containing 500mL of DMEM (10% FBS, 1% antibiotic-antimycotic, 2mM L-glutamine) and Cytodex-1 microcarrier beads at a concentration of 2 g/L, in the absence of human and microbial cells.



During the culture of the hMSCs in this bioreactor system, the cells were routinely counted using a colourimetric assay (WST-8). The results of these cell counts are given in Figure 25, where a gradual increase in the mean cell number of about  $1(10^6)$  cells/day is observed. The large error bars, which are derived from the range of measured values, are likely due to the sampling method from the bioreactor, which entails tilting the bag so that the cells/microcarriers/medium mixture can be drawn into a syringe *via* a narrow opening, which could hinder attempts to obtain a well-mixed, representative sample of the bioreactor contents. Further it was clear that the microcarrier beads would stick to the material of the bioreactor bag, and so the effective microcarrier concentration declined.

**Figure 25.** Cell counts of the hMSCs attached to the Cytodex-1 microcarrier beads present in the DMEM media of a CELL-tainer<sup>®</sup> bioreactor; obtained using the colourimetric assay, WST-8 ( $N \geq 6$ ).

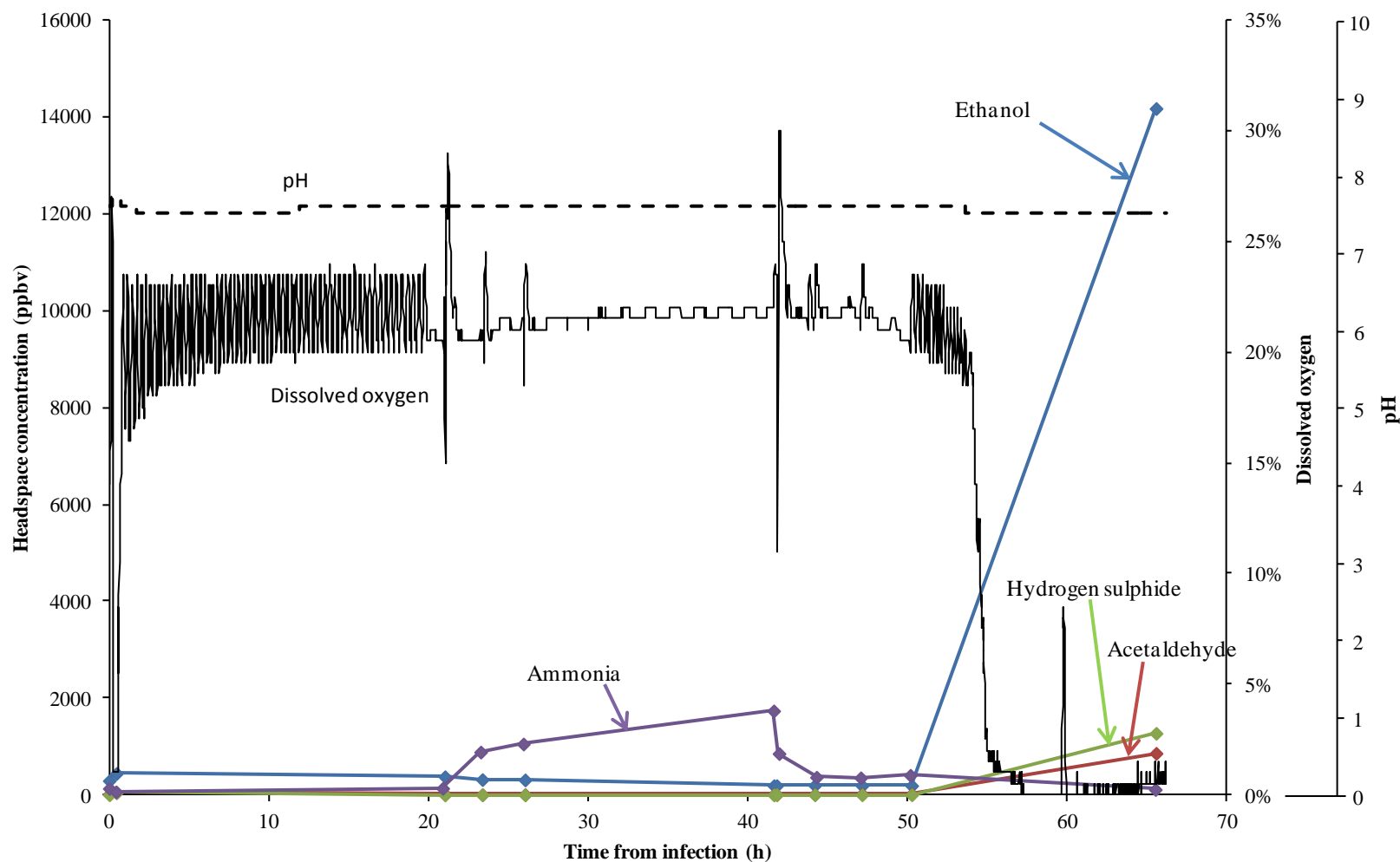


On the fourteenth day of culture, 40mL of the concentrated “stock” *E. coli* in LB (approximately  $5(10^{10})$  cells) was added to the bioreactor bag. The volume of DMEM in the bag was around 1L, so this was approximately equivalent to the situation for the headspace analysis experiments presented in Chapter 6 (see also Appendix A7 [190]), in which 1mL of “stock” *E. coli* was added to 24mL of DMEM medium. However in this

case the DMEM also contained 1% v/v of the antibiotic-antimycotic supplement, which slowed the progression of the infection. The DO concentration and pH were continuously monitored throughout the culture using the standard *in situ* probes of the CELL-tainer<sup>®</sup> bioreactor system, and the concentrations of the major compounds produced by *E. coli* when cultured in DMEM, *viz.* ethanol, acetaldehyde, hydrogen sulphide and methanethiol, as were characterised in Chapter 6 [190], were monitored in the exhaust gas (see Figure 21) several times on each subsequent day, using SIFT-MS. The results of these analyses are shown in the plot in Figure 26, where it is seen that it took around 50 hours for the *E. coli* to grow to sufficient numbers to overtake the culture, as is shown first by the decline in DO concentration. It is also seen that the concentrations of the major volatile compounds that are known to be produced by *E. coli* under similar conditions had also increased on the next SIFT-MS analysis, which occurred some 15 hours later. The methanethiol measurements are not shown, but an increase in the concentration of this compound in the headspace to around 100 ppbv was recorded at the final time-point. These results indicate that the DO concentration and SIFT-MS analyses of the exhaust gas were able to identify the presence of the bacterial infection to within several hours of each other. However, due to the timing of the *E. coli* growth, it was not possible to identify the earliest point when SIFT-MS would have identified the increased concentrations of ethanol, acetaldehyde and hydrogen sulphide. It is noteworthy, however, that the pH did not change significantly during the recorded time scale. This was only noticeable several hours after the experiment had ended because of the colour change which is caused by the presence of phenol red in the DMEM medium. So, under the conditions of the present experiment the pH did not change rapidly with the increased respiration rate of the culture, as indicated by the rapid decline in DO. This could have been caused by an increase in acid production as the conditions became less aerobic, or it could have been slowed by the sodium bicarbonate buffering system.

An interesting change in the ammonia concentration was detected by SIFT-MS after around 24 hours, almost 30 hours before any changes in DO of the major volatile metabolites was observed. The ammonia concentration increased from around 100 ppbv to over 1000 ppbv, then falling again to around 500 ppbv before production of the previously recognised metabolites (ethanol, acetaldehyde, hydrogen sulphide and methanethiol) became apparent. This analysis was performed using the  $O_2^{+\bullet}$  precursor ion, which is the preferred method of ammonia analysis [36]. This could be related to the metabolism of the *E. coli* cells, or to cell death which is likely to have occurred in the culture due to the presence of the antibiotics. In any case, this finding is worthy of further investigation.

Figure 26. Plot showing the online measurements of pH and the dissolved oxygen concentration inside a CELL-tainer® bioreactor bag containing hMSCs attached to Cytodex-1 microcarriers and *E. coli* JM109 in 1L of DMEM medium (10% FBS, 1% antibiotic-antimycotic, 2mM L-glutamine), and the headspace concentrations of ammonia, hydrogen sulphide, acetaldehyde and ethanol measured in the off-gas of the bioreactor culture at time intervals, without disturbing the culture, using SIFT-MS. Methanethiol was also detected and quantified, but the results are not shown for clarity (see text). On the x-axis is plotted the time, in hours, from which the 1L hMSC culture was intentionally infected with 40mL of stock *E. coli* JM109 bacteria ( $\sim 5(10^{10})$  cells).



#### 7.4. Summary and discussion

Reported in this chapter are the results of some exploratory studies of the volatile compounds emitted by human cell cultures that had become contaminated with microbial cell types. Four of the reported studies pertained to cell cultures that were inadvertently infected with microbial cells, of which three could only be identified as being fungal or bacterial, while the other was retrospectively identified as *C. testosteroni*. In each of these infected cultures, at least one microbial biomarker was identified at *ppmv* levels, which are easily detectable by SIFT-MS. It should be noted, however, that the types and quantities of the volatile compounds that are produced by a particular microbial cell are partly dependent on the composition of the culture medium that they occupy (See Chapter 6 and [190]). Therefore the biomarkers that were identified in the headspace of the DMEM media that became infected with *C. testosteroni* might not be produced in a different medium.

These preliminary investigations into the volatile compounds emitted into the gas phase by microbial cells upon infecting human cell cultures were conducted once the presence of infecting microbial cells was already obvious to the colleague who had donated them. The next step was to attempt to identify the infection earlier by purposefully adding a concentrated suspension of *E. coli* cells to a 1.0L bioreactor culture containing hMSCs attached to microcarriers in DMEM. The first clear indication of activity of the *E. coli* came in the form of a clear increase in the ammonia concentration, which was detected by SIFT-MS analysis of the exhaust gas around 20 hours after the bacteria were added to the culture. The expected decline in the DO content of the media, due to the respiring *E. coli* was detected by the *in situ* DO probe some 30 hours later, which was closely followed by the increased emission of the known volatile biomarkers of *E. coli* activity, *viz.* ethanol, acetaldehyde, hydrogen sulphide and methanethiol [190], which were detected by SIFT-MS analyses. The causes of this unexpected rise in ammonia are unclear: it may be due to the application of antibiotics, or it may be a more natural occurrence in *E. coli* cultures, which was not identified previously because experiments were conducted at strict time points. Some evidence of cell density-related changes are reported in Chapter 6 (Table 24, [190]), in which the concentration of ethanol first increased with starting cell density, when the *E. coli* cells were cultured in LB, but then dropped as the cell density was increased further. A similar emission pattern is seen in the ammonia concentrations measured in the exhaust gases released from the infected hMSC culture, but further investigation is required to determine whether this could be used as an early indicator of infection in human cell cultures.

## 8. Summary, concluding remarks and recommendations for further work

### 8.1. Summary

The work presented in this thesis was initiated in order to develop a non-invasive online technique for monitoring the progression of human cell cultures; specifically those of relevance to the field of regenerative medicine. The instrument of choice, upon which the present work is based, is selected ion flow tube mass spectrometry (**SIFT-MS**), which is capable of rapidly and accurately quantifying the concentrations of trace compounds in gas/vapour mixtures to parts-per-billion by volume (*ppbv*) levels. The potential value of this technique in the field of medicine, especially for breath analysis, been demonstrated by several studies as reported previously in a number of publications, now including two for which TWE Chippendale is co-author [88, 89].

The project work has included some fundamental selected ion flow tube (**SIFT**) experiments, in which specific ion-molecule reactions were studied under standard SIFT-MS conditions [107, 108]. The rate coefficients (*k*) and product ions formed from the reactions between the SIFT-MS precursor ions ( $\text{H}_3\text{O}^+$ ,  $\text{NO}^+$  and  $\text{O}_2^{+\bullet}$ ) were derived for two sets of four isobaric compounds with molecular weights of 86u (diacetyl,  $\gamma$ -butyrolactone, cyclopropane carboxylic acid and allyl ethyl ether) and 88u (acetoin, pyruvic acid, n-butyric acid and ethyl acetate). Each of the compounds analysed, with the exception of allyl ethyl ether, has some biological significance. In addition, methodologies were improved or newly developed for the analyses of acetaldehyde (**AA**), dimethyl sulphide (**DMS**) and carbon dioxide using SIFT-MS. As a result of this work, it is now possible to accurately quantify concentrations of AA in the presence of DMS (a capability that was vitally important in some of the headspace analyses of human cell cultures reported in Chapter 5 and ref. [157]). Carbon dioxide can now also be quantified using  $\text{NO}^+$  precursor ions by utilizing the  $\text{NO}^+\text{CO}_2$  adduct ions formed at  $m/z$  74, and accounting for the presence of AA that also forms the adduct  $\text{NO}^+\text{AA}$  ions also at  $m/z$  of 74.

SIFT-MS was also used for the analysis of the headspace of human cell cultures in experiments that were largely conducted using methods largely developed by the Keele Chemical Physics Group prior to the commencement of the present research project [40, 41]. The headspace above small scale bioreactor (spinner flask) cultures was analysed, with the cells attached to microcarrier beads during culture. Few differences were observed between the SIFT-MS mass spectra obtained from the headspace of cell cultures and the culture media alone and only carbon dioxide was found to be produced by the cells, as one might expect. However, the toxic volatile organic compound (**VOC**) AA was consistently depleted from the headspace of cultures of 6 different

human cell types, including cells of the **hepG2** hepatocellular carcinoma cells line, and primary human bone marrow-derived mesenchymal stem cells (**hMSCs**). The influence of the intracellular aldehyde dehydrogenase (**ALDH**) enzymes on this observed AA consumption was investigated in these two cell types (hepG2 and hMSCs) by adding ALDH inhibitor compounds diethylaminobenzaldehyde (**DEAB**) and disulfiram (**DSF**) to the culture medium and observing the changes in the concentrations of AA in the headspace. Indeed the application of the ALDH inhibitor compounds did prevent the oxidation of AA from the culture media, in some cases causing the AA concentration to increase in the headspace of the cell culture as a result of the alcohol dehydrogenase- (**ADH**-) mediated oxidation of ethanol to AA; a reaction which was not affected by the presence of DEAB and DSF. It was also observed that the solvent dimethyl sulphoxide (**DMSO**), which was used to dissolve the inhibitor compounds, was reduced to DMS due to cellular action, and that this reduction reaction was inhibited by the presence of DEAB and DSF [157].

The headspace of cultures of *Escherichia coli* (strain JM109) were also analysed by SIFT-MS in preparation for experiments into the identification of bacterial infection in human cell cultures. In this study, the bacteria were cultured in two different media prior to the headspace analyses, *viz.* lysogeny broth (**LB**) and Dulbecco's modified Eagle's medium (**DMEM**); the former commonly being used for the culture of *E. coli* and the latter for the culture of human cell types. The major compounds produced by the cells and emitted into the headspace differed greatly when cultured in LB or DMEM. The findings were then exploited for the purpose of monitoring the concentrations of the major compounds (biomarkers) emitted into the gas phase above an open culture of *E. coli* cells in DMEM. The culture was monitored for around 4 hours with the concentrations of each biomarker compound (*viz.* ethanol, AA, hydrogen sulphide and methanethiol) seen to rise and then decline at differing rates, which was attributed to the consumption of the sources of the volatile compounds in the media, while the water vapour and methanol levels remained constant for the duration of the experiment [190]. In addition to these experiments, the headspace above human cell cultures that had become infected by unidentified bacteria or fungi were also analysed by SIFT-MS in order to identify the major compounds that were emitted into the gas phase.

Subsequently, experiments were conducted in which hMSCs were cultured in a relatively large scale (1L) bioreactor. After 14 days of culture, the vessel (bag) was infected with 40mL of concentrated *E. coli* suspension (around  $5(10^{10})$  cells), and SIFT-MS was used to non-invasively monitor the levels of the known *E. coli* biomarker compounds in the exhaust gas of the culture, while the dissolved oxygen (DO) and pH of the culture was simultaneously monitored using *in situ* sensors. After 50 hours of culture, the DO concentration was

seen to decline and the concentrations of the aforementioned biomarkers (ethanol, AA, H<sub>2</sub>S and methanethiol) increased in the exhaust gas. An increase in the concentration of ammonia was also observed much earlier (around 30 hours), from around 100 *ppbv* to around 1000 *ppbv*, indicating that the SIFT-MS technique may be capable of detecting *E. coli* infections more rapidly than the *in situ* sensors. Given that this increase in ammonia was not observed in previous analyses of the headspace of smaller scale *E. coli* cultures, this result requires further investigation. In spite of this result, however, the ability of SIFT-MS to non-invasively monitor the progression of the infected culture in real time was successfully demonstrated.

## 8.2. Concluding remarks

The results of the fundamental SIFT kinetics experiments described above have contributed to the advancement of the SIFT-MS analytical technique and have provided a new method for the detection and quantification of several trace gas compounds. Also, the new ability to quantify AA in the presence of DMS is new and potentially extremely valuable, as was demonstrated in the ALDH-inhibition experiments, which resulted in the production of both compounds, and could well find utility in the detection of microbial infection of cell cultures.

The desirable situation for monitoring the progression of human cell cultures using a real time trace gas analysis technique such as SIFT-MS would be for a specific set of biomarkers to be emitted into the headspace that are indicative of healthy human cell growth. Ideally this would be specific for a single human cell type, particularly when considering the culture of stem or progenitor cells for a cell therapy product because these cells are able to differentiate into a number of more specialised cell types, which may not be desired for said cell-based product. That distinctive biomarkers were not detected in the headspace of any of the six human cell cultures that were investigated is most probably because such compounds are present at concentrations below the stated limit of detection of the current SIFT-MS instruments. It should be noted that sub-*ppbv* concentrations of some compounds can be measured using SIFT-MS by employing a longer integration time for deriving the count rates of the product ions [198]. Furthermore, analytical instruments are in constant development and should soon be capable of detecting volatile biomarkers present at the sub-*ppbv* concentrations more rapidly.

On the other hand, the absence of detectable compounds emitted into the gas phase by human cell cultures, can allow compounds that are emitted due to contamination to be detected more easily. This was demonstrated by the experiments described in Chapter 7, in which a 1L bioreactor culture was intentionally infected with *E. coli* and measurable quantities of ammonia, ethanol, AA, hydrogen sulphide and methanethiol were emitted by the bacteria, and analysed in the exhaust gas. The resulting data provided a proof-of-principle

that SIFT-MS can be used to non-invasively monitor bioreactor cultures and detect bacterial infection in human cell cultures.

The results given in Chapter 6 (and ref. [190]) indicate that the *E. coli* cells, when cultured in LB, began to emit ethanol when lower cell numbers were seeded, but then at higher cell numbers, the headspace ethanol concentration decreased. Also, as mentioned previously, when the *E. coli* were seeded to an hMSC-DMEM culture inside a bioreactor, the ammonia concentration was elevated in the exhaust gas following 20 hours of incubation, but then declined over the next 20 hours (see Chapter 7). Given that there was no change in the pH of the liquid during this period, it is possible that the ammonia was depleted either by being lost to the atmosphere, or by cellular action. With respect to the emission of volatile biomarkers by cultured cells, the results obtained from the *E. coli* experiments described in Chapters 6 and 7 indicate that there are at least three major factors that contribute to the production of volatile compounds: (1) the type of cells in culture; (2) the composition of the culture medium; and (3) the condition of the cultured cells. Clearly genetic differences between cell types cause them to metabolise substrates differently to produce different compounds, which explains factors (1) and (2). Factor (3), on the other hand, is less straightforward. The aforementioned observations could have been caused by their preferential consumption of a particular medium component, before then consuming other medium components. In any case, the key point is that *E. coli* cells appeared to emit different compounds at different stages of their culture, and this is an important consideration when attempting to identify volatile biomarkers for monitoring cell cultures.

Headspace analysis experiments were conducted using spinner flasks and a 1L (working volume) CELL-tainer<sup>®</sup> bioreactor, in which cells were cultured *via* attachment to microcarrier beads. Also experiments in which the cells of interest (lung cancer cell line CALU-1 and “normal” lung cell line NL20) were allowed to grow inside the usual 150mL glass bottles while attached to a hydrogel scaffold made of collagen-1. These cells were previously shown to produce AA when suspended in media without a collagen scaffold [41], but in this case produced excessive quantities of AA, which were measured in the gas phase. These results have been submitted to *Analyst* for publication [199]. These methodologies might be considered improvements over the method requiring the cells to be transferred to 150mL glass bottles prior to the analysis [40, 41], as was used frequently to conduct the experiments described in this thesis. The human cell types of interest in this particular study are typically expanded using adherent culture techniques in tissue culture flasks, and so their removal and transfer to a new environment is surely a disturbance to their growth; affecting the cells proliferation and enzyme expression levels [158]. Therefore, as indicated by factor (3) in the previous section, any potential biomarkers



that are detected in the headspace of the cells cultured and analysed under these conditions might not relate to “normal” cell growth, as was one of the major aims of this project. On the other hand, the aforementioned methods in which an attachment surface is provided to the cells should reduce disturbance to the culture prior to the headspace analysis experiments; thereby ensuring that the obtained results are a better indication of healthy cell growth.

The use of ALDH inhibitors DEAB and DSF to study the reactions of the intracellular ALDH enzymes present in hepG2 cells and hMSCs has provided compelling evidence that these enzymes are the cause of the depletion of AA from the culture headspace of the six human cell types, the results of which are presented and discussed in Chapter 4. Some possible implications of this finding are discussed below. It was also observed in the same study that DMSO was reduced to DMS by the cells, and this reaction is known to be catalysed by the enzyme methionine sulfoxide reductase A (**MsrA**) [180]. DMSO was used as a solvent in these experiments, but is also very commonly used as a cryopreservant in the long-term storage of cells in liquid nitrogen. This should be understood by researchers as DMS has been shown to induce apoptosis in two human leukaemia cell lines [200].

### **8.3. Suggestions for further work**

The search for volatile biomarkers of healthy human cell growth might be aided by a combination of different instruments. A new biomarker of *Pseudomonas aeruginosa* (PA) has recently been determined using solid phase microextraction- (SPME-) gas chromatography mass spectrometry (GC-MS), viz. methyl thiocyanate. The biomarker was subsequently quantified in the headspace of cultured PA and in the exhaled breath of cystic fibrosis patients using both GC-MS and SIFT-MS techniques [51]. Similar, exploratory GC-MS analyses of the headspace of hMSC cultures were conducted as a part of the present research project during a visit to the J. Heyrovský Institute (Prague, Czech Republic), where it was found that hexanal, as well as AA, is consumed by the cultured cells (see Chapter 4). Further combined GC-MS/SIFT-MS experiments of this type will surely be beneficial in the search for biomarkers in the headspace of human cell cultures.

Techniques for the early detection of microbial infection in mammalian cell cultures are not commonly employed in industry [196]. Therefore, the development of a non-invasive “early warning system” of infection, based on volatile biomarkers and the SIFT-MS technique is an attractive proposition. One potential difficulty in developing the technique for such purposes is that the types of microbial cells which could potentially infect a mammalian cell culture are not numerous, and it would not be feasible to “fingerprint” the emissions of every

type of bacterium or fungus for their detection. This is a challenging problem that can only be diminished by vision and carefully planned experiments using fit-for-purpose instrumentation, but the initial steps have been taken by the work described in this thesis.

It is also important to consider that microbial, plant and insect cells are cultured extensively industrially at large scale for a wide range of purposes, including for foods and pharmaceutical production. Given that SIFT-MS can easily identify and quantify the compounds that are emitted into the gas phase by *E. coli* and other bacterial and fungal cells, even from vessels that are open to the atmosphere [190], the possibility of applying this technique to the monitoring of large-scale bacterial/microbial cultures should be investigated.

ALDH enzyme expression is used as a biomarker of certain stem cell types and some cancer cells [163]. It has been demonstrated in animal models and in clinical studies that level of ALDH expression in haematopoietic cells is related to the clinical outcomes when implanted into patients as a treatment for cardiovascular disease [201]. The results of the experiments described in Chapter 5 and ref. [157] appear to give an indication of the activities and/or expression levels of the enzymes involved in the ethanol metabolism pathway, *viz.* ADH and ALDH. It should therefore be possible to derive methods for quantifying the expression levels of these enzymes based on SIFT-MS headspace analyses. Such methods could be used to assess the quality of a sample of cells, such as haematopoietic stem cells (HSCs) [176], prior to their use in cell therapies. Similar techniques could also be employed for different intracellular enzymes, such as ADH and MsrA, in other cultured cell types.

## 8.4 List of publications

The author contributed to the experimental work, including the experimental design and data analysis, and to the writing of each of the submitted or published works that are listed below.

### 8.4.1. Book chapter

- Chippendale TWE, El Haj AJ, Coopman K, Rafiq Q, Hewitt CJ: **5.10 - Isolation of Mesenchymal Stem Cells from Bone Marrow Aspirate**. In: *Comprehensive Biotechnology (Second Edition)*. Edited by Moo-Young M. USA: Academic Press; 2011: 115-123.

#### 8.4.2. *Published journal articles*

- Španěl P, Dryahina K, Rejšková A, Chippendale TWE, Smith D: **Breath acetone concentration; biological variability and the influence of diet.** *Physiol Meas* 2011, 32:N23.
- Španěl P, Shestivska V, Chippendale TWE, Smith D: **Determination of the deuterium abundances in water from 156 to 10,000 ppm by SIFT-MS.** *J Am Soc Mass Spectrom* 2011, 22:179-186.
- Smith D, Chippendale TWE, Španěl P: **Selected ion flow tube, SIFT, studies of the reactions of  $\text{H}_3\text{O}^+$ ,  $\text{NO}^+$  and  $\text{O}_2^+$  with some biologically active isobaric compounds in preparation for SIFT-MS analyses.** *Int J Mass Spectrom* 2011, 303:81-89.
- Chippendale TWE, Španěl P, Smith D: **Time-resolved selected ion flow tube mass spectrometric quantification of the volatile compounds generated by *E. coli* JM109 fcultured in two different media.** *Rapid Commun Mass Spectrom* 2011, 25:2163-2172.
- Chippendale TWE, Hu B, El Haj AJ, Smith D: **A study of enzymatic activity in cell cultures *via* the analysis of volatile biomarkers.** *Analyst* 2012, 137:4677-4685.

#### 8.4.3. *Articles in press*

- Smith D, Chippendale TWE, Španěl P: **Minimising the effects of isobaric product ions in SIFT-MS quantification of acetaldehyde, dimethyl sulphide and carbon dioxide.** *Curr Anal Chem* (in press).
- Smith D, Chippendale TWE, Dryahina K, Španěl P: **Nose-exhaled breath analysis by SIFT-MS; mouth contamination and the influence of exercise.** *Curr Anal Chem* (in press).
- Rutter AV, Chippendale TWE, Yang Y, Španěl P, Smith D, Sulé-Suso J: **Quantification by SIFT-MS of acetaldehyde released by lung cells in a 3D model.** *Analyst* (in press).

## 9. Bibliography

1. Bailey JE, Ollis DF: **Biochemical Engineering Fundamentals**, 2nd edn: McGraw-Hill Inc.; 1986.
2. Doran PM: **Bioprocess Engineering Principles**: Academic Press; 1995.
3. Kehoe DE, Jing D, Lock LT, Tzanakakis ES: **Scalable stirred-suspension bioreactor culture of human pluripotent stem cells**. *Tissue Eng A* 2010, **16**:405-421.
4. Krawetz R, Taiani JT, Liu SY, Meng GL, Li XY, Kallos MS, Rancourt DE: **Large-scale expansion of pluripotent human embryonic stem cells in stirred-suspension bioreactors**. *Tissue Eng C Meth* 2010, **16**:573-582.
5. Schop D, van Dijkhuizen-Radersma R, Borgart E, Janssen FW, Rozemuller H, Prins HJ, de Bruijn JD: **Expansion of human mesenchymal stromal cells on microcarriers: growth and metabolism**. *J Tissue Eng Regen Med* 2010, **4**:131-140.
6. Kowalczyk M, Waldron K, Kresnowati P, Danquah MK: **Process challenges relating to hematopoietic stem cell cultivation in bioreactors**. *J Ind Microbiol Biotechnol* 2011, **38**:761-767.
7. Rodrigues CAV, Fernandes TG, Diogo MM, da Silva CL, Cabral JMS: **Stem cell cultivation in bioreactors**. *Biotechnol Adv* 2011, **29**(6):815-829.
8. Martin I, Wendt D, Heberer M: **The role of bioreactors in tissue engineering**. *Trends Biotechnol* 2004, **22**:80-86.
9. Plunkett N, O'Brien FJ: **Bioreactors in tissue engineering**. *Technol Health Care* 2011, **19**:55-69.
10. Couet F, Meghezi S, Mantovani D: **Fetal development, mechanobiology and optimal control processes can improve vascular tissue regeneration in bioreactors: an integrative review**. *Med Eng Phys* 2012, **34**:269-278.
11. Derfus GE, Abramzon D, Tung M, Chang D, Kiss R, Amanullah A: **Cell culture monitoring via an auto-sampler and an integrated multi-functional off-line analyzer**. *Biotechnol Progr* 2010, **26**:284-292.
12. Teixeira AP, Oliveira R, Alves PM, Carrondo MJT: **Advances in on-line monitoring and control of mammalian cell cultures: supporting the PAT initiative**. *Biotechnol Adv* 2009, **27**:726-732.
13. Harthun S, Matischak K, Friedl P: **Simultaneous prediction of human Antithrombin III and main metabolites in animal cell culture processes by near-infrared spectroscopy**. *Biotechnol Tech* 1998, **12**:393-398.
14. Arnold SA, Crowley J, Woods N, Harvey LM, McNeil B: **In-situ near infrared spectroscopy to monitor key analytes in mammalian cell cultivation**. *Biotechnol Bioeng* 2003, **84**:13-19.
15. Card C, Hunsaker B, Smith T, Hirsch J: **Near-infrared spectroscopy for rapid, simultaneous monitoring of multiple components in mammalian cell culture**. *Bioproc Int* 2008, **6**:58-67.
16. Rhie M, Ducommun P, Bolzonella I, Marison I, von Stockar U: **Real-time *in situ* monitoring of freely suspended and immobilized cell cultures based on mid-infrared spectroscopic measurements**. *Biotechnol Bioeng* 2002, **77**:174-185.
17. Hisiger S, Jolicoeur M: **A multiwavelength fluorescence probe: is one probe capable for on-line monitoring of recombinant protein production and biomass activity?** *J Biotechnol* 2005, **117**:325-336.
18. Teixeira AP, Portugal CAM, Carinhas N, Dias JML, Crespo JP, Alves PM, Carrondo MJT, Oliveira R: ***In situ* 2D fluorometry and chemometric monitoring of mammalian cell cultures**. *Biotechnol Bioeng* 2009, **102**:1098-1106.
19. Cannizzaro C, Güçerli R, Marison I, von Stockar U: **On-line biomass monitoring of CHO perfusion culture with scanning dielectric spectroscopy**. *Biotechnol Bioeng* 2003, **84**:597-610.
20. Noll T, Biselli M: **Dielectric spectroscopy in the cultivation of suspended and immobilized hybridoma cells**. *J Biotechnol* 1998, **63**:187-198.
21. Abu-Absi NR, Kenty BM, Cuellar ME, Borys MC, Sakhamuri S, Strachan DJ, Hausladen MC, Li ZJ: **Real time monitoring of multiple parameters in mammalian cell culture bioreactors using an in-line Raman spectroscopy probe**. *Biotechnol Bioeng* 2011, **108**:1215-1221.
22. Bachinger T, Riese U, Eriksson R, Mandenius CF: **Monitoring cellular state transitions in a production-scale CHO-cell process using an electronic nose**. *J Biotechnol* 2000, **76**:61-71.
23. Sommerfeld S, Strube J: **Challenges in biotechnology production - generic processes and process optimization for monoclonal antibodies**. *Chem Eng Proc Process Intens* 2005, **44**:1123-1137.
24. **OPS Process Analytical Technology (PAT) Initiative**  
[[www.fda.gov/AboutFDA/CentersOffices/OfficeofMedicalProductsandTobacco/CDER/ucm088828.htm](http://www.fda.gov/AboutFDA/CentersOffices/OfficeofMedicalProductsandTobacco/CDER/ucm088828.htm)]

25. Park HE, Kim D, Koh HS, Cho S, Sung JS, Kim JY: **Real-Time monitoring of neural differentiation of human mesenchymal stem cells by electric cell-substrate impedance sensing.** *J Biomed Biotechnol* 2011, **2011**.
26. Justice C, Brix A, Freimark D, Kraume M, Pfromm P, Eichenmueller B, Czermak P: **Process control in cell culture technology using dielectric spectroscopy.** *Biotechnol Adv* 2011, **29**:391-401.
27. Pijanka JK, Kumar D, Dale T, Yousef I, Parkes G, Untereiner V, Yang Y, Dumas P, Collins D, Manfait M *et al*: **Vibrational spectroscopy differentiates between multipotent and pluripotent stem cells.** *Analyst* 2010, **135**:3126-3132.
28. Yue X, Drakakis EM, Lim M, Radomska A, Ye H, Mantalaris A, Panoskaltsis N, Cass A: **A real-time multi-channel monitoring system for sem cell culture process.** *IEEE Trans Biomed Circ Syst* 2008, **2**:66-77.
29. Jeffries RE, Macdonald JM: **New advances in MR-compatible bioartificial liver.** *NMR Biomed* 2012, **25**:427-442.
30. Prince BJ, Milligan DB, McEwan MJ: **Application of selected ion flow tube mass spectrometry to real-time atmospheric monitoring.** *Rapid Commun Mass Spectrom* 2010, **24**:1763-1769.
31. de Gouw J, Warneke C: **Measurements of volatile organic compounds in the earth's atmosphere using proton-transfer-reaction mass spectrometry.** *Mass Spectrom Rev* 2007, **26**:223-257.
32. Krausa M, Reznov (Eds) AA: **Vapour And Trace Detection Of Explosives For Anti-terrorism Purposes: Proceedings of the NATO Advanced Research Workshop on Vapour and Trace Detection of Explosives for Anti-Terrorism Purposes, Moscow, Russia: Kluwer Academic Publishers; 2003.**
33. Olivares A, Dryahina K, Španěl P, Flores M: **Rapid detection of lipid oxidation in beef muscle packed under modified atmosphere by measuring volatile organic compounds using SIFT-MS.** *Food Chem* 2012, **135**:1801-1808.
34. Amann A, Smith D: **Breath Analysis for Clinical Diagnosis and Therapeutic Monitoring:** World Scientific Publishing Co. Pte. Ltd.; 2005.
35. Smith D, Španěl P: **Selected ion flow tube mass spectrometry (SIFT-MS) for on-line trace gas analysis.** *Mass Spectrom Rev* 2005, **24**:661-700.
36. Smith D, Španěl P: **Ambient analysis of trace compounds in gaseous media by SIFT-MS.** *Analyst* 2011, **136**:2009-2032.
37. Blake RS, Monks PS, Ellis AM: **Proton-Transfer Reaction Mass Spectrometry.** *Chem Rev* 2009, **109**:861-896.
38. Jordan A, Haidacher S, Hanel G, Hartungen E, Herbig J, Mark L, Schottkowsky R, Seehauser H, Sulzer P, Mark TD: **An online ultra-high sensitivity Proton-transfer-reaction mass-spectrometer combined with switchable reagent ion capability (PTR+SRI-MS).** *Int J Mass Spectrom* 2009, **286**:32-38.
39. Watson JT, Sparkman O: **Introduction to Mass Spectrometry: Instrumentation, Applications, and Strategies for Data Interpretation, 4th Edition.** In.: Wiley; 2007: 571-600.
40. Smith D, Wang T, Sulé-Suso J, Španěl P, El Haj AJ: **Quantification of acetaldehyde released by lung cancer cells *in vitro* using selected ion flow tube mass spectrometry.** *Rapid Commun Mass Spectrom* 2003, **17**:845-850.
41. Sulé-Suso J, Pysanenko A, Španěl P, Smith D: **Quantification of acetaldehyde and carbon dioxide in the headspace of malignant and non-malignant lung cells *in vitro* by SIFT-MS.** *Analyst* 2009, **134**:2419-2425.
42. Brunner C, Szymczak W, Hollriegl V, Mortl S, Oelmez H, Bergner A, Huber RM, Hoeschen C, Oeh U: **Discrimination of cancerous and non-cancerous cell lines by headspace-analysis with PTR-MS.** *Anal Bioanal Chem* 2010, **397**:2315-2324.
43. Filipiak W, Sponring A, Mikoviny T, Ager C, Schubert J, Miekisch W, Amann A, Troppmair J: **Release of volatile organic compounds (VOCs) from the lung cancer cell line CALU-1 *in vitro*.** *Canc Cell Int* 2008, **8**:17.
44. Sponring A, Filipiak W, Mikoviny T, Ager C, Schubert J, Miekisch W, Amann A, Troppmair J: **Release of volatile organic compounds from the lung cancer cell line NCI-H2087 *in vitro*.** *Anticancer Res* 2009, **29**:419-426.
45. Shin HW, Umber B, Meinardi S, Leu SY, Zaldivar F, Blake D, Cooper D: **Acetaldehyde and hexanaldehyde from cultured white cells.** *J Transl Med* 2009, **7**:31.
46. Sponring A, Filipiak W, Ager C, Schubert J, Miekisch W, Amann A, Troppmair J: **Analysis of volatile organic compounds (VOCs) in the headspace of NCI-H1666 lung cancer cells.** *Cancer Biomark* 2010, **7**:153-161.
- 47.

- Filipiak W, Sponring A, Filipiak A, Ager C, Schubert J, Miekisch W, Amann A, Troppmair J: **TD-GC-MS analysis of volatile metabolites of human lung cancer and normal cells *in vitro***. *Canc Epidemiol Biomarkers Prev* 2010, **19**:182-195.
48. Aehle M, Kuprijanov A, Schaepe S, Simutis R, Lübbert A: **Simplified off-gas analyses in animal cell cultures for process monitoring and control purposes**. *Biotechnol Lett* 2011, **33**:2103-2110.
49. Carroll W, Lenney W, Wang T, Španěl P, Alcock A, Smith D: **Detection of volatile compounds emitted by *Pseudomonas aeruginosa* using selected ion flow tube mass spectrometry**. *Pediatr Pulmonol* 2005, **39**:452-456.
50. Gilchrist FJ, Alcock A, Belcher J, Brady M, Jones A, Smith D, Španěl P, Webb K, Lenney W: **Variation in hydrogen cyanide production between different strains of *Pseudomonas aeruginosa***. *Eur Respir J* 2011, **38**:409-414.
51. Shestivska V, Nemec A, Dřevínek P, Sovová K, Dryahina K, Španěl P: **Quantification of methyl thiocyanate in the headspace of *Pseudomonas aeruginosa* cultures and in the breath of cystic fibrosis patients by selected ion flow tube mass spectrometry**. *Rapid Commun Mass Spectrom* 2011, **25**:2459-2467.
52. Scotter JM, Langford VS, Wilson PF, McEwan MJ, Chambers ST: **Real-time detection of common microbial volatile organic compounds from medically important fungi by Selected Ion Flow Tube-Mass Spectrometry (SIFT-MS)**. *J Microbiol Meth* 2005, **63**:127-134.
53. Allardyce RA, Langford VS, Hill AL, Murdoch DR: **Detection of volatile metabolites produced by bacterial growth in blood culture media by selected ion flow tube mass spectrometry (SIFT-MS)**. *J Microbiol Meth* 2006, **65**:361-365.
54. Scotter JM, Allardyce RA, Langford VS, Hill A, Murdoch DR: **The rapid evaluation of bacterial growth in blood cultures by selected ion flow tube-mass spectrometry (SIFT-MS) and comparison with the BacT/ALERT automated blood culture system**. *J Microbiol Meth* 2006, **65**:628-631.
55. Storer MK, Hibbard-Melles K, Davis B, Scotter J: **Detection of volatile compounds produced by microbial growth in urine by selected ion flow tube mass spectrometry (SIFT-MS)**. *J Microbiol Meth* 2011, **87**:111-113.
56. Critchley A, Elliott TS, Harrison G, Mayhew CA, Thompson JM, Worthington T: **The proton transfer reaction mass spectrometer and its use in medical science: applications to drug assays and the monitoring of bacteria**. *Int J Mass Spectrom* 2004, **239**:235-241.
57. Bunge M, Araghipour N, Mikoviny T, Dunkl J, Schnitzhofer R, Hansel A, Schinner F, Wisthaler A, Margesin R, Märk TD: **On-Line monitoring of microbial volatile metabolites by proton transfer reaction-mass spectrometry**. *Appl Environ Microbiol* 2008, **74**:2179-2186.
58. Custer TG, Wagner WP, Kato S, Bierbaum VM, Fall R: **Potential of On-Line CIMS for Bioprocess Monitoring**. *Biotechnol Progr* 2003, **19**:1355-1364.
59. Mashgo M, Rumbold K, De Mey M, Vandamme E, Soetaert W, Heijnen J: **Microbial metabolomics: past, present and future methodologies**. *Biotechnol Lett* 2007, **29**:1-16.
60. Dettmer K, Aronov PA, Hammock BD: **Mass spectrometry-based metabolomics**. *Mass Spectrom Rev* 2007, **26**:51-78.
61. Elmroth I, Valeur A, Odham G, Larsson L: **Detection of microbial-contamination in fermentation processes - mass spectrometric determination of gram-negative bacterial in leuconostoc-mesenteroides cultures**. *Biotechnol Bioeng* 1990, **35**:787-792.
62. Sue T, Obolonkin V, Griffiths H, Villas-Boas SG: **An exometabolomics approach to monitoring microbial contamination in microalgal fermentation processes by using metabolic footprint analysis**. *Appl Environ Microbiol* 2011, **77**:7605-7610.
63. Elmroth I, Fox A, Holst O, Larsson L: **Detection of bacterial-contamination in cultures of eukaryotic cells by gas-chromatography mass-spectrometry**. *Biotechnol Bioeng* 1993, **42**:421-429.
64. Smith D, Španěl P: **Ions in the terrestrial atmosphere and in interstellar clouds**. *Mass Spectrom Rev* 1995, **14**:255-278.
65. Smith D, Adams NG: **The selected ion flow tube (Sift): studies of ion-neutral reactions**. *Adv Atom Mol Phys* 1988, **24**:1-49.
66. Smith D, Španěl P: **Selected ion flow tube mass spectrometry (SIFT-MS) for on-line trace gas analysis**. *Mass Spectrometry Reviews* 2005, **24**(5):661-700.
67. Španěl P, Rolfe P, Rajan B, Smith D: **The selected ion flow tube (SIFT) - a novel technique for biological monitoring**. *Ann Occup Hyg* 1996, **40**(6):615-626.
68. Španěl P, Smith D: **Quantitative selected ion flow tube mass spectrometry: The influence of ionic diffusion and mass discrimination**. *J Am Soc Mass Spectrom* 2001, **12**:863-872.
69. Ferguson EE, Fehsenfeld FC, Schmeltekopf AL: **Flowing afterglow measurements of ion-neutral reactions**. In: *Adv Atom Mol Phys*. Edited by Bates DR, Estermann I, vol. 5: Academic Press; 1969: 1-56.

70. Španěl P, Smith D: **Reactions of hydrated hydronium ions and hydrated hydroxide ions with some hydrocarbons and oxygen-bearing organic molecules.** *J Phys Chem* 1995, **99**:15551-15556.
71. Španěl P, Pavlik M, Smith D: **Reactions of  $\text{H}_3\text{O}^+$  and  $\text{OH}^-$  ions with some organic molecules; applications to trace gas analysis in air.** *Int J Mass Spectrom Ion Process* 1995, **145**:177-186.
72. Španěl P, Smith D: **A selected ion flow tube study of the reactions of  $\text{NO}^+$  and  $\text{O}_2^+$  ions with some organic molecules: the potential for trace gas analysis of air.** *J Chem Phys* 1996, **104**:1893-1899.
73. Bouchoux G, Salpin JY, Leblanc D: **A relationship between the kinetics and thermochemistry of proton transfer reactions in the gas phase.** *Int J Mass Spectrom Ion Process* 1996, **153**:37-48.
74. Su T, Chesnavich WJ: **Parametrization of the ion-polar molecule collision rate constant by trajectory calculations.** *J Chem Phys* 1982, **76**:5183-5185.
75. Španěl P, Dryahina K, Smith D: **A general method for the calculation of absolute trace gas concentrations in air and breath from selected ion flow tube mass spectrometry data.** *Int J Mass Spectrom* 2006, **249-250**:230-239.
76. Smith D, Pysanenko A, Španěl P: **Ionic diffusion and mass discrimination effects in the new generation of short flow tube SIFT-MS instruments.** *Int J Mass Spectrom* 2009, **281**:15-23.
77. Španěl P, Smith D: **Influence of water vapour on selected ion flow tube mass spectrometric analyses of trace gases in humid air and breath.** *Rapid Commun Mass Spectrom* 2000, **14**:1898-1906.
78. Boshier PR, Cushnir JR, Mistry V, Knaggs A, Španěl P, Smith D, Hanna GB: **On-line, real time monitoring of exhaled trace gases by SIFT-MS in the perioperative setting: a feasibility study.** *Analyst* 2011, **136**:3233-3237.
79. Smith D, Wang T, Pysanenko A, Španěl P: **A selected ion flow tube mass spectrometry study of ammonia in mouth- and nose-exhaled breath and in the oral cavity.** *Rapid Commun Mass Spectrom* 2008, **22**:783-789.
80. Pysanenko A, Španěl P, Smith D: **A study of sulfur-containing compounds in mouth- and nose-exhaled breath and in the oral cavity using selected ion flow tube mass spectrometry.** *J Breath Res* 2008, **2**.
81. Turner C, Španěl P, Smith D: **A longitudinal study of ammonia, acetone and propanol in the exhaled breath of 30 subjects using selected ion flow tube mass spectrometry, SIFT-MS.** *Physiol Meas* 2006, **27**:321-337.
82. Smith D, Turner C, Španěl P: **Volatile metabolites in the exhaled breath of healthy volunteers: their levels and distributions.** *J Breath Res* 2007, **1**:014004.
83. Enderby B, Lenney W, Brady M, Emmett C, Španěl P, Smith D: **Concentrations of some metabolites in the breath of healthy children aged 7-18 years measured using selected ion flow tube mass spectrometry (SIFT-MS).** *J Breath Res* 2009, **3**:036001.
84. Penault C, Španěl P, Smith D: **Detection of *H. Pylori* infection by breath ammonia following urea ingestion.** In: *Breath Analysis for Clinical Diagnosis and Therapeutic Monitoring*. Edited by Amann A, Smith D. Singapore: World Scientific; 2005: 393-399.
85. Smith D, Engel B, Diskin AM, Španěl P, Davies SJ: **Comparative measurements of total body water in healthy volunteers by online breath deuterium measurement and other near-subject methods.** *Am J Clin Nutr* 2002, **76**:1295-1301.
86. Španěl P, Wang T, Smith D: **Coordinated FA-MS and SIFT-MS analyses of breath following ingestion of D<sub>2</sub>O and ethanol: total body water, dispersal kinetics and ethanol metabolism.** *Physiol Meas* 2005, **26**:447-457.
87. Chan C, Smith D, Španěl P, McIntyre CW, Davies SJ: **A non-invasive, on-line deuterium dilution technique for the measurement of total body water in haemodialysis patients.** *Nephrol Dial Transplant* 2008, **23**:2064-2070.
88. Španěl P, Dryahina K, Rejšková A, Chippendale TWE, Smith D: **Breath acetone concentration; biological variability and the influence of diet.** *Physiol Meas* 2011, **32**:N23.
89. Španěl P, Shestivska V, Chippendale TWE, Smith D: **Determination of the deuterium abundances in water from 156 to 10,000 ppm by SIFT-MS.** *J Am Soc Mass Spectrom* 2011, **22**:179-186.
90. Kalapos MP: **On the mammalian acetone metabolism: from chemistry to clinical implications.** *Biochim Biophys Acta Gen Subj* 2003, **1621**:122-139.
91. Laffel L: **Ketone bodies: a review of physiology, pathophysiology and application of monitoring to diabetes.** *Diabetes Metab Res Rev* 1999, **15**:412-426.
92. O'Hara ME, O'Hehir S, Green S, Mayhew CA: **Development of a protocol to measure volatile organic compounds in human breath: a comparison of rebreathing and on-line single exhalations using proton transfer reaction mass spectrometry.** *Physiol Meas* 2008, **29**:309.

93. King J, Mochalski P, Kupferthaler A, Unterkofler K, Koc H, Filipiak W, Teschl S, Hinterhuber H, Amann A: **Dynamic profiles of volatile organic compounds in exhaled breath as determined by a coupled PTR-MS/GC-MS study.** *Physiol Meas* 2010, **31**:1169-1184.
94. Henderson MJ, Karger BA, Wren Shall GA: **Acetone in the breath; a study of acetone exhalation in diabetic and nondiabetic human subjects.** *Diabetes* 1952, **1**:188-193.
95. Tassopoulos CN, Barnett D, Fraser TR: **Breath-acetone and blood-sugar measurements in diabetes.** *Lancet* 1969, **1**:1282-1286.
96. Crofford OB, Mallard RE, Winton RE, Rogers NL, Jackson JC, Keller U: **Acetone in breath and blood.** *Trans Am Clin Climatol Assoc* 1977, **88**:128-139.
97. Smith D, Španěl P, Fryer AA, Hanna F, Ferns GAA: **Can volatile compounds in exhaled breath be used to monitor control in diabetes mellitus?** *J Breath Res* 2011, **5**:022001.
98. Deng CH, Zhang J, Yu XF, Zhang W, Zhang XM: **Determination of acetone in human breath by gas chromatography-mass spectrometry and solid-phase microextraction with on-fiber derivatization.** *J Chromatogr B* 2004, **810**:269-275.
99. Deng CH, Zhang W, Zhang J, Zhang XM: **Rapid determination of acetone in human plasma by gas chromatography-mass spectrometry and solid-phase microextraction with on-fiber derivatization.** *J Chromatogr B* 2004, **805**:235-240.
100. Musa-Veloso K, Likhodii SS, Cunnane SC: **Breath acetone is a reliable indicator of ketosis in adults consuming ketogenic meals.** *Am J Clin Nutr* 2002, **76**:65-70.
101. Turner C: **Potential of breath and skin analysis for monitoring blood glucose concentration in diabetes.** *Expert Rev Mol Diagn* 2011, **11**:497-503.
102. Španěl P, Smith D: **Progress in SIFT-MS: Breath analysis and other applications.** *Mass Spectrom Rev* 2011, **30**:236-267.
103. Španěl P, Smith D: **Selected ion flow tube mass spectrometry analyses of stable isotopes in water: isotopic composition of  $\text{H}_3\text{O}^+$  and  $\text{H}_3\text{O}^+(\text{H}_2\text{O})_3$  ions in exchange reactions with water vapor.** *J Am Soc Mass Spectrom* 2000, **11**:866-875.
104. Smith D, Španěl P: **On-line determination of the deuterium abundance in breath water vapour by flowing afterglow mass spectrometry with applications to measurements of total body water.** *Rapid Commun Mass Spectrom* 2001, **15**:25-32.
105. Španěl P, Smith D: **Accuracy and precision of flowing afterglow mass spectrometry for the determination of the deuterium abundance in the headspace of aqueous liquids and exhaled breath.** *Rapid Commun Mass Spectrom* 2001, **15**:867-872.
106. Davies S, Španěl P, Smith D: **Rapid measurement of deuterium content of breath following oral ingestion to determine body water.** *Physiol Meas* 2001, **22**:651-659.
107. Smith D, Chippendale TWE, Španěl P: **Selected ion flow tube, SIFT, studies of the reactions of  $\text{H}_3\text{O}^+$ ,  $\text{NO}^+$  and  $\text{O}_2^+$  with some biologically active isobaric compounds in preparation for SIFT-MS analyses.** *Int J Mass Spectrom* 2011, **303**:81-89.
108. Smith D, Chippendale TWE, Španěl P: **Minimising the effects of isobaric product ions in SIFT-MS quantification of acetaldehyde, dimethyl sulphide and carbon dioxide.** *Curr Anal Chem* (In press).
109. Hunter EP, Lias SG: **Proton Affinity Evaluation.** In: *NIST Chemistry WebBook, NIST Standard Reference Database Number 69.* Edited by Linstrom PJ, Mallard WG. Gaithersburg MD, 20899, US: National Institute of Standards and Technology.
110. Španěl P, Smith D: **SIFT studies of the reactions of  $\text{H}_3\text{O}^+$ ,  $\text{NO}^+$  and  $\text{O}_2^+$  with a series of alcohols.** *Int J Mass Spectrom Ion Process* 1997, **167-168**:375-388.
111. Španěl P, Wang T, Smith D: **A selected ion flow tube, SIFT, study of the reactions of  $\text{H}_3\text{O}^+$ ,  $\text{NO}^+$  and  $\text{O}_2^+$  ions with a series of diols.** *Int J Mass Spectrom* 2002, **218**:227-236.
112. Španěl P, Ji Y, Smith D: **SIFT studies of the reactions of  $\text{H}_3\text{O}^+$ ,  $\text{NO}^+$  and  $\text{O}_2^+$  with a series of aldehydes and ketones.** *Int J Mass Spectrom Ion Process* 1997, **165-166**:25-37.
113. Smith D, Wang T, Španěl P: **Analysis of ketones by selected ion flow tube mass spectrometry.** *Rapid Commun Mass Spectrom* 2003, **17**:2655-2660.
114. Španěl P, Van Doren JM, Smith D: **A selected ion flow tube study of the reactions of  $\text{H}_3\text{O}^+$ ,  $\text{NO}^+$ , and  $\text{O}_2^+$  with saturated and unsaturated aldehydes and subsequent hydration of the product ions.** *Int J Mass Spectrom* 2002, **213**:163-176.
115. Španěl P, Smith D: **SIFT studies of the reactions of  $\text{H}_3\text{O}^+$ ,  $\text{NO}^+$  and  $\text{O}_2^+$  with a series of volatile carboxylic acids and esters.** *Int J Mass Spectrom* 1998, **172**:137-147.
116. Španěl P, Smith D: **SIFT studies of the reactions of  $\text{H}_3\text{O}^+$ ,  $\text{NO}^+$  and  $\text{O}_2^+$  with several ethers.** *Int J Mass Spectrom* 1998, **172**:239-247.
117. Španěl P, Smith D: **Selected ion flow tube studies of the reactions of  $\text{H}_3\text{O}^+$ ,  $\text{NO}^+$ , and  $\text{O}_2^+$  with some organosulphur molecules.** *Int J Mass Spectrom* 1998, **176**:167-176.



118. Španěl P, Smith D: **Selected ion flow tube studies of the reactions of  $\text{H}_3\text{O}^+$ ,  $\text{NO}^+$ , and  $\text{O}_2^+$  with several amines and some other nitrogen-containing molecules.** *Int J Mass Spectrom* 1998, **176**:203-211.
119. Španěl P, Smith D: **Selected ion flow tube studies of the reactions of  $\text{H}_3\text{O}^+$ ,  $\text{NO}^+$ , and  $\text{O}_2^+$  with eleven amine structural isomers of  $\text{C}_5\text{H}_{13}\text{N}$ .** *Int J Mass Spectrom* 1999, **185–187**:139-147.
120. Španěl P, Smith D: **Selected ion flow tube studies of the reactions of  $\text{H}_3\text{O}^+$ ,  $\text{NO}^+$ , and  $\text{O}_2^+$  with several aromatic and aliphatic hydrocarbons.** *Int J Mass Spectrom* 1998, **181**:1-10.
121. Diskin AM, Wang T, Smith D, Španěl P: **A selected ion flow tube (SIFT), study of the reactions of  $\text{H}_3\text{O}^+$ ,  $\text{NO}^+$  and  $\text{O}_2^+$  ions with a series of alkenes; in support of SIFT-MS.** *Int J Mass Spectrom* 2002, **218**:87-101.
122. Wang T, Španěl P, Smith D: **Selected ion flow tube, SIFT, studies of the reactions of  $\text{H}_3\text{O}^+$ ,  $\text{NO}^+$  and  $\text{O}_2^+$  with eleven  $\text{C}_{10}\text{H}_{16}$  monoterpenes.** *Int J Mass Spectrom* 2003, **228**:117-126.
123. Schoon N, Amelynck C, Vereecken L, Arijs E: **A selected ion flow tube study of the reactions of  $\text{H}_3\text{O}^+$ ,  $\text{NO}^+$  and  $\text{O}_2^+$  with a series of monoterpenes.** *Int J Mass Spectrom* 2003, **229**:231-240.
124. Španěl P, Smith D: **Selected ion flow tube studies of the reactions of  $\text{H}_3\text{O}^+$ ,  $\text{NO}^+$ , and  $\text{O}_2^+$  with some chloroalkanes and chloroalkenes.** *Int J Mass Spectrom* 1999, **184**:175-181.
125. Španěl P, Smith D: **Selected ion flow tube studies of the reactions of  $\text{H}_3\text{O}^+$ ,  $\text{NO}^+$ , and  $\text{O}_2^+$  with several aromatic and aliphatic monosubstituted halocarbons.** *Int J Mass Spectrom* 1999, **189**:213-223.
126. Wang T, Španěl P, Smith D: **A selected ion flow tube study of the reactions of  $\text{H}_3\text{O}^+$ ,  $\text{NO}^+$  and  $\text{O}_2^+$  with some phenols, phenyl alcohols and cyclic carbonyl compounds in support of SIFT-MS and PTR-MS.** *Int J Mass Spectrom* 2004, **239**:139-146.
127. Španěl P, Smith D: **Quantification of hydrogen sulphide in humid air by selected ion flow tube mass spectrometry.** *Rapid Commun Mass Spectrom* 2000, **14**:1136-1140.
128. Španěl P, Wang T, Smith D: **Quantification of hydrogen cyanide in humid air by selected ion flow tube mass spectrometry.** *Rapid Commun Mass Spectrom* 2004, **18**:1869-1873.
129. Španěl P, Davies S, Smith D: **Quantification of ammonia in human breath by the selected ion flow tube analytical method using  $\text{H}_3\text{O}^+$  and  $\text{O}_2^+$  precursor ions.** *Rapid Commun Mass Spectrom* 1998, **12**:763-766.
130. Fairley DA, Milligan DB, Freeman CG, McEwan MJ, Španěl P, Smith D: **Competitive association and charge transfer in the reactions of  $\text{NO}^+$  with some ketones: a selected ion flow drift tube study.** *Int J Mass Spectrom* 1999, **193**:35-43.
131. Lias SG: **Ionization energy evaluation.** In: *NIST Chemistry WebBook, NIST Standard Reference Database Number 69*. Gaithersburg MD, 20899: National Institute of Standards and Technology.
132. Dryahina K, Smith D, Španěl P: **Quantification of methane in humid air and exhaled breath using selected ion flow tube mass spectrometry.** *Rapid Commun Mass Spectrom* 2010, **24**:1296-1304.
133. Španěl P, Smith D: **On-line measurement of the absolute humidity of air, breath and liquid headspace samples by selected ion flow tube mass spectrometry.** *Rapid Commun Mass Spectrom* 2001, **15**:563-569.
134. Pysanenko A, Španěl P, Smith D: **Analysis of the isobaric compounds propanol, acetic acid and methyl formate in humid air and breath by selected ion flow tube mass spectrometry, SIFT-MS.** *Int J Mass Spectrom* 2009, **285**:42-48.
135. Macciola V, Candela G, De Leonardis A: **Rapid gas-chromatographic method for the determination of diacetyl in milk, fermented milk and butter.** *Food Contr* 2008, **19**:873-878.
136. Visai C, Vanoli M: **Volatile compound production during growth and ripening of peaches and nectarines.** *Scientia Horticulturae* 1997, **70**:15-24.
137. Du X, Plotto A, Baldwin E, Rouseff R: **Evaluation of volatiles from two subtropical strawberry cultivars using GC-olfactometry, GC-MS odor activity values, and sensory analysis.** *J Agr Food Chem* 2011, **59**:12569-12577.
138. Ulrich D, Komes D, Olbricht K, Hoberg E: **Diversity of aroma patterns in wild and cultivated *Fragaria* accessions.** *Genet Resour Crop Evol* 2007, **54**:1185-1196.
139. Berg JT, JL; Stryer, L: **Biochemistry**, 5 edn: W. H. Freeman and Company; 2002.
140. Vose J, Tighe T, Schwartz M, Buel E: **Detection of gamma-butyrolactone (GBL) as a natural component in wine.** *J Forensic Sci* 2001, **46**:1164-1167.
141. Gallimberti L, Spella MR, Soncini CA, Gessa GL: **Gamma-hydroxybutyric acid in the treatment of alcohol and heroin dependence.** *Alcohol* 2000, **20**:257-262.
142. Galloway GP, Frederick-Osborne SL, Seymour R, Contini SE, Smith DE: **Abuse and therapeutic potential of gamma-hydroxybutyric acid.** *Alcohol* 2000, **20**:263-269.

143. Wang T, Španěl P, Smith D: **A selected ion flow tube, SIFT, study of the reactions of  $\text{H}_3\text{O}^+$ ,  $\text{NO}^+$  and  $\text{O}_2^+$  ions with several N- and O-containing heterocyclic compounds in support of SIFT-MS.** *Int J Mass Spectrom* 2004, **237**:167-174.
144. Smith D, Pysanenko A, Španěl P: **The quantification of carbon dioxide in humid air and exhaled breath by selected ion flow tube mass spectrometry.** *Rapid Commun Mass Spectrom* 2009, **23**:1419-1425.
145. Španěl P, Smith D: **Influence of weakly bound adduct ions on breath trace gas analysis by selected ion flow tube mass spectrometry (SIFT-MS).** *Int J Mass Spectrom* 2009, **280**:128-135.
146. Španěl P, Smith D: **Quantification of trace levels of the potential cancer biomarkers formaldehyde, acetaldehyde and propanol in breath by SIFT-MS.** *J Breath Res* 2008, **2**.
147. Lide DR: **Handbook of Chemistry and Physics, 71st Edition (1990-1991):** CRC Press; 1990.
148. Battin-Leclerc F, Herbinet O, Glaude PA, Fournet R, Zhou Z, Deng L, Guo H, Xie M, Qi F: **New experimental evidences about the formation and consumption of ketohydroperoxides.** *Proc Combust Inst* 2011, **33**:325-331.
149. Mölder U, Pikver R, Koppel I, Burk P, Koppel IA: **Photoelectron spectra of molecules. Part 12. Vinyl, allyl, and phenyl ethers and sulphides.** *J Mol Struct (Theochem)* 2002, **579**:205-220.
150. Sovová K, Dryahina K, Španěl P: **Selected ion flow tube (SIFT) studies of the reactions of  $\text{H}_3\text{O}^+$ ,  $\text{NO}^+$  and  $\text{O}_2^+$  with six volatile phytogetic esters.** *Int J Mass Spectrom* 2011, **300**:31-38.
151. Sander R: **Henry's Law constants.** In: *NIST Chemistry WebBook, NIST Standard Reference Database Number 69.* Gaithersburg MD, 20899: National Institute of Standards and Technology.
152. Chippendale TWE, El Haj AJ, Coopman K, Rafiq Q, Hewitt CJ: **5.10 - Isolation of Mesenchymal Stem Cells from Bone Marrow Aspirate.** In: *Comprehensive Biotechnology (Second Edition).* Edited by Moo-Young M. USA: Academic Press; 2011: 115-123.
153. Turner C, Španěl P, Smith D: **A longitudinal study of methanol in the exhaled breath of 30 healthy volunteers using selected ion flow tube mass spectrometry, SIFT-MS.** *Physiol Meas* 2006, **27**:637.
154. Dryahina K, Španěl P: **Principal component analysis for SIFT-MS.** In: J. Heyrovský Institute, Academy of Sciences of the Czech Republic; 2009: Software tool for the analysis of data obtained using selected ion flow tube mass spectrometry.
155. Antoshechkin AG: **On intracellular formation of ethanol and its possible role in energy metabolism.** *Alcohol Alcohol* 2001, **36**:608.
156. Španěl P, Diskin AM, Abbott SM, Wang T, Smith D: **Quantification of volatile compounds in the headspace of aqueous liquids using selected ion flow tube mass spectrometry.** *Rapid Commun Mass Spectrom* 2002, **16**:2148-2153.
157. Chippendale TWE, Hu B, El Haj AJ, Smith D: **A study of enzymatic activity in cell cultures via the analysis of volatile biomarkers.** *Analyst* 2012, **137**:4677-4685.
158. Córdoba-Pedregosa MDC, Villalba JM, González-Aragón D, Bello RI, Alcaín FJ: **Cellular density and cell type are the key factors in growth inhibition induced by 2,5bis [1-aziridinyl]-1,4 benzoquinone (DZQ).** *Anticancer Res* 2006, **26**:3535-3540.
159. Stagos D, Chen Y, Brocker C, Donald E, Jackson BC, Orlicky DJ, Thompson DC, Vasiliou V: **Aldehyde dehydrogenase 1B1: molecular cloning and characterization of a novel mitochondrial acetaldehyde-metabolizing enzyme.** *Drug Metabol Dispos* 2010, **38**:1679-1687.
160. Wang MF, Han CL, Yin SJ: **Substrate specificity of human and yeast aldehyde dehydrogenases.** *Chem Biol Interact* 2009, **178**:36-39.
161. Lundquist F, Tygstrup N, Winkler K, Mellempgaard K, Munck-Petersen S: **Ethanol metabolism and production of free acetate in the human liver.** *J Clin Invest* 1962, **41**:955-961.
162. Yamashita H, Kaneyuki T, Tagawa K: **Production of acetate in the liver and its utilization in peripheral tissues.** *Biochim Biophys Acta Mol Cell Biol Lipids* 2001, **1532**:79-87.
163. Moreb JS: **Aldehyde dehydrogenase as a marker for stem cells.** *Curr Stem Cell Res Ther* 2008, **3**:237-246.
164. Galter D, Buervenich S, Carmine A, Anvret M, Olson L: **ALDH1 mRNA: presence in human dopamine neurons and decreases in substantia nigra in Parkinson's disease and in the ventral tegmental area in schizophrenia.** *Neurobiol Dis* 2003, **14**:637-647.
165. Eriksson CJ: **The role of acetaldehyde in the actions of alcohol (update 2000).** *Alcohol Clin Exp Res* 2001, **25**:15S-32S.
166. Mello T, Ceni E, Surrenti C, Galli A: **Alcohol induced hepatic fibrosis: role of acetaldehyde.** *Mol Aspect Med* 2008, **29**:17-21.
167. White HS, Smith L, Gentry T, Balber AE: **Mechanisms of action of human aldehyde dehydrogenase bright cells in therapy of cardiovascular diseases: expression analysis of angiogenic factors and aldehyde dehydrogenase isozymes.** *J Stem Cell Res Ther* 2011, **S1**.

168. Ohta S, Ohsawa I, Kamino K, Ando F, Shimokata H: **Mitochondrial ALDH2 deficiency as an oxidative stress.** *Ann New York Acad Sci* 2004, **1011**:36-44.
169. Carroll KM, Fenton LR, Ball SA, Nich C, Frankforter TL, Shi J, Rounsaville BJ: **Efficacy of disulfiram and cognitive behavior therapy in cocaine-dependent.** *Arch Gen Psychiatr* 2004 **61**:264-272.
170. Marcato P, Dean CA, Pan D, Araslanova R, Gillis M, Joshi M, Helyer L, Pan L, Leidal A, Gujar S *et al*: **Aldehyde dehydrogenase activity of breast cancer stem cells is primarily due to isoform ALDH1A3 and its expression is predictive of metastasis.** *Stem Cell* 2011, **29**:32-45.
171. Kim MP, Fleming JB, Wang H, Abbruzzese JL, Choi W, Kopetz S, McConkey DJ, Evans DB, Gallick GE: **ALDH activity selectively defines an enhanced tumor-initiating cell population relative to CD133 expression in human pancreatic adenocarcinoma.** *Plos One* 2011, **6**.
172. Moreb JS, Mohuczy D, Ostmark B, Zucali JR: **RNAi-mediated knockdown of aldehyde dehydrogenase class-1A1 and class-3A1 is specific and reveals that each contributes equally to the resistance against 4-hydroperoxycyclophosphamide.** *Cancer Chemother Pharmacol* 2007, **59**:127-136.
173. Moreb JS, Ucar D, Han S, Amory JK, Goldstein AS, Ostmark B, Chang LJ: **The enzymatic activity of human aldehyde dehydrogenases 1A2 and 2 (ALDH1A2 and ALDH2) is detected by Aldefluor, inhibited by diethylaminobenzaldehyde and has significant effects on cell proliferation and drug resistance.** *Chem Biol Interact* 2012, **195**:52-60.
174. Cen D, Brayton D, Shahandeh B, Meyskens FL, Farmer PJ: **Disulfiram facilitates intracellular Cu uptake and induces apoptosis in human melanoma cells.** *J Med Chem* 2004, **47**:6914-6920.
175. Brar SS, Grigg C, Wilson KS, Holder WDJ, Dreau D, Austin C, Foster M, Ghio AJ, Whorton AR, Stowell GW *et al*: **Disulfiram inhibits activating transcription factor/cyclic AMP-responsive element.** *Mol Cancer Ther* 2004, **3**:1049-1060.
176. Lioznov MV, Freiburger P, Kroger N, Zander AR, Fehse B: **Aldehyde dehydrogenase activity as a marker for the quality of hematopoietic stem cell transplants.** *Bone Marrow Transplant* 2005, **35**:909-914.
177. Moreb JS, Zucali JR, Ostmark B, Benson NA: **Heterogeneity of aldehyde dehydrogenase expression in lung cancer cell lines is revealed by Aldefluor flow cytometry-based assay.** *Cytometry B Clin Cytometry* 2007, **72B**:281-289.
178. Weissbach H, Resnick L, Brot N: **Methionine sulfoxide reductases: history and cellular role in protecting against oxidative damage.** *Biochim Biophys Acta Protein Proteomics* 2005, **1703**:203-212.
179. Hansen J: **Inactivation of MXR1 abolishes formation of dimethyl sulfide from dimethyl sulfoxide in *Saccharomyces cerevisiae*.** *Appl Environ Microbiol* 1999, **65**:3915-3919.
180. Kwak GH, Choi SH, Kim JR, Kim HY: **Inhibition of methionine sulfoxide reduction by dimethyl sulfoxide.** *BMB Rep* 2009, **42**:580-585.
181. Moskovitz J, Weissbach H, Brot N: **Cloning the expression of a mammalian gene involved in the reduction of methionine sulfoxide residues in proteins.** *Proc Natl Acad Sci USA* 1996, **93**:2095-2099.
182. Gabbita SP, Aksenov MY, Lovell MA, Markesbery WR: **Decrease in peptide methionine sulfoxide reductase in Alzheimer's Disease brain.** *J Neurochem* 1999, **73**:1660-1666.
183. Liu F, Hindupur J, Nguyen JL, Ruf KJ, Zhu J, Schieler JL, Bonham CC, Wood KV, Davisson VJ, Rochet JC: **Methionine sulfoxide reductase A protects dopaminergic cells from Parkinson's disease-related insults.** *Free Radic Biol Med* 2008, **45**:242-255.
184. Filipiak W, Sponring A, Mikoviny T, Ager C, Schubert J, Miekisch W, Amann A, Troppmair J: **Release of volatile organic compounds (VOCs) from the lung cancer cell line CALU-1 in vitro.** *Cancer Cell International* 2008, **8**(1):17.
185. Filipiak W, Sponring A, Filipiak A, Ager C, Schubert J, Miekisch W, Amann A, Troppmair J: **TD-GC-MS analysis of volatile metabolites of human lung cancer and normal cells in vitro.** *Cancer Epidemiology Biomarkers & Prevention* 2010, **19**(1):182-195.
186. Shin H-W, Ueber B, Meinardi S, Leu S-Y, Zaldivar F, Blake D, Cooper D: **Acetaldehyde and hexanaldehyde from cultured white cells.** *Journal of Translational Medicine* 2009, **7**(1):31.
187. Lee SL, Shih HT, Chi YC, Li YP, Yin SJ: **Oxidation of methanol, ethylene glycol, and isopropanol with human alcohol dehydrogenases and the inhibition by ethanol and 4-methylpyrazole.** *Chem Biol Interact* 2011, **191**:26-31.
188. Dryahina K, Pehal F, Smith D, Španěl P: **Quantification of methylamine in the headspace of ethanol of agricultural origin by selected ion flow tube mass spectrometry.** *Int J Mass Spectrom* 2009, **286**:1-6.

189. Lowther WT, Brot N, Weissbach H, Honek JF, Matthews BW: **Thiol-disulfide exchange is involved in the catalytic mechanism of peptide methionine sulfoxide reductase.** *Proc Natl Acad Sci Unit States Am* 2000, **97**:6463-6468.
190. Chippendale TWE, Španěl P, Smith D: **Time-resolved selected ion flow tube mass spectrometric quantification of the volatile compounds generated by *E. coli* JM109 cultured in two different media.** *Rapid Commun Mass Spectrom* 2011, **25**:2163-2172.
191. Shima S, Kato J, Igarashi Y, Kodama T: **Cloning and expression of a *Clostridium cellobioparum* cellulase gene and its excretion from *Escherichia coli* JM109.** *J Ferment Bioeng* 1989, **68**:75-78.
192. Shiloach J, Kaufman J, Guillard AS, Fass R: **Effect of glucose supply strategy on acetate accumulation, growth, and recombinant protein production by *Escherichia coli* BL21 (lambda DE3) and *Escherichia coli* JM109.** *Biotechnol Bioeng* 1996, **49**:421-428.
193. La Monica S, Galetti M, Alfieri RR, Cavazzoni A, Ardizzoni A, Tiseo M, Capelletti M, Goldoni M, Tagliaferri S, Mutti A *et al*: **Everolimus restores gefitinib sensitivity in resistant non-small cell lung cancer cell lines.** *Biochem Pharmacol* 2009, **78**:460-468.
194. Maloy SR, Cronan JE, Fereifelder D: **Bacteria.** In: *Microbial Genetics*. 2nd edn: Jones & Bartlett Publishers Inc.; 1994: 67-80.
195. Lin HY, Mathiszik B, Xu B, Enfors SO, Neubauer P: **Determination of the maximum specific uptake capacities for glucose and oxygen in glucose-limited fed-batch cultivations of *Escherichia coli*.** *Biotechnol Bioeng* 2001, **73**:347-357.
196. Junker B, Lester M, Leporati J, Schmitt J, Kovatch M, Borysewicz S, Maciejak W, Seeley A, Hesse M, Connors N *et al*: **Sustainable reduction of bioreactor contamination in an industrial fermentation pilot plant.** *J Biosci Bioeng* 2006, **102**:251-268.
197. Bachinger T, Riese U, Eriksson RK, Mandenius CF: **Gas sensor arrays for early detection of infection in mammalian cell culture.** *Biosens Bioelectron* 2002, **17**:395-403.
198. Ross B: **Sub-parts per billion detection of trace volatile chemicals in human breath using Selected Ion Flow Tube Mass Spectrometry.** *BMC Res Notes* 2008, **1**:41.
199. Rutter AV, Chippendale TWE, Yang Y, Španěl P, Smith D, Sulé-Suso J: **Quantification by SIFT-MS of acetaldehyde released by lung cells in a 3D model.** *Analyst* (submitted).
200. Zhang GL, Wu HT, Zhu BW, Shimoishi Y, Nakamura Y, Murata Y: **Effect of dimethyl sulfides on the induction of apoptosis in human leukemia Jurkat cells and HL-60 cells.** *Biosci Biotechnol Biochem* 2008, **72**:2966-2972.
201. Balber AE: **Concise Review: Aldehyde Dehydrogenase Bright Stem and Progenitor Cell Populations from Normal Tissues: Characteristics, Activities, and Emerging Uses in Regenerative Medicine.** *Stem Cell* 2011, **29**:570-575.
202. Španěl P, Dryahina K, Smith D: **Microwave plasma ion sources for selected ion flow tube mass spectrometry: optimizing their performance and detection limits for trace gas analysis.** *Int J Mass Spectrom* 2007, **267**:117-124.

## **Appendix A. Publications**

### **A1. Breath acetone concentration; biological variability and the influence of diet**

Španěl P, Dryahina K, Rejšková A, Chippendale TWE, Smith D. *Physiol Meas* 2011, 32:N23.

## NOTE

## Breath acetone concentration; biological variability and the influence of diet

Patrik Španěl<sup>1,2</sup>, Kseniya Dryahina<sup>1</sup>, Alžběta Rejšková<sup>1</sup>,  
Thomas W E Chippendale<sup>2</sup> and David Smith<sup>2</sup>

<sup>1</sup>J Heyrovský Institute of Physical Chemistry, Academy of Sciences of the Czech Republic, Dolejškova 3, 182 23, Prague 8, Czech Republic

<sup>2</sup>Institute for Science and Technology in Medicine, School of Medicine, Keele University, Thornburrow Drive, Hartshill, Stoke-on-Trent ST4 7QB, UK

Received 5 April 2011, accepted for publication 3 June 2011

Published 1 July 2011

Online at [stacks.iop.org/PM/32/N23](http://stacks.iop.org/PM/32/N23)

### Abstract

Previous measurements of acetone concentrations in the exhaled breath of healthy individuals and the small amount of comparable data for individuals suffering from diabetes are briefly reviewed as a prelude to the presentation of new data on the sporadic and wide variations of breath acetone that occur in ostensibly healthy individuals. Data are also presented which show that following a ketogenic diet taken by eight healthy individuals their breath acetone concentrations increased up to five times over the subsequent 6 h. Similarly, the breath acetone increased six and nine times when a low carbohydrate diet was taken by two volunteers and remained high for the several days for which the diet was continued. These new data, together with the previous data, clearly indicate that diet and natural intra-individual biological and diurnal variability result in wide variations in breath acetone concentration. This places an uncertainty in the use of breath acetone alone to monitor blood glucose and glycaemic control, except and unless the individual acts as their own control and is cognizant of the need for dietary control.

Keywords: acetone, breath, ketogenic diet, glycaemic control, SIFT-MS

### 1. Introduction

The simple ketone, acetone, is present in the breath of all human beings and most mammals (Kalapos 2003). It is the most abundant of the so-called ketone bodies, the others being beta-hydroxybutyric acid and acetoacetic acid, these generally being considered as products of lipolysis (Laffel 1999). Acetone is very volatile and is readily released into the gas phase from blood and urine, whereas the other two ketone bodies are less volatile and largely exist in

the blood stream as ions. However, beta-hydroxybutyric acid has been detected above urine, but acetoacetic acid is unstable against dissociation in the gas phase (Wang *et al* 2008b).

Because of its relatively high concentration in the blood stream and its volatility, acetone is readily detected in exhaled breath and numerous measurements of it have been made using a variety of techniques, as previously reported in *Physiol. Meas.* (Turner *et al* 2006, O'Hara *et al* 2008, King *et al* 2010) and reviewed in other journals (Dummer *et al* 2010, Miekisch *et al* 2004, Bajtarevic *et al* 2009). Blood acetone, and hence breath acetone concentrations, may be elevated in patients with diabetes, but this depends on many other factors, including duration of fasting, dextrose concentrations, degree of insulin resistance and the extent of activation of lipolysis, and so it is now well understood that high acetone concentrations alone cannot be taken as indicative of diabetes (Henderson *et al* 1952, Crofford *et al* 1977, Tassopou *et al* 1969, Smith *et al* 2011). A very recent discourse on the relevance of breath acetone to diabetes monitoring has been published (Turner 2011). However, as a result of a misunderstanding of the true clinical implications, it is often assumed in the current literature in the field of sensor development for breath analysis that the detection of elevated breath acetone can be used to diagnose type-1 or even type-2 diabetes (Deng *et al* 2004a, 2004b), but there is little evidence to support this. Yet this notion persists and is being propagated in the literature thus stimulating considerable technological efforts to produce a simple (hand-held) sensor for breath acetone measurements (see, for example, Righettoni *et al* 2010a, 2010b). The objective of this note is to present further experimental evidence that there are a number of confounding factors that considerably influence the concentration of breath acetone even in the healthy population.

### 1.1. Summary of the previous SIFT-MS measurements of acetone in exhaled breath

The influence of fasting/feeding on breath concentrations of acetone was the subject of an early selected ion flow tube mass spectrometry (SIFT-MS) pilot study in which the exhaled breath of six healthy volunteers was analysed for several trace metabolites, including acetone, in the morning following overnight fasting after which each volunteer ingested a protein- or a carbohydrate-based meal. This early pilot study showed that the initial relatively high levels of breath acetone in all six volunteers decreased postprandial reaching their nadir after about 5 h (Smith *et al* 1999, Smith and Španěl 2005). In a subsequent SIFT-MS study, the volatile compounds in the exhaled breath of 30 volunteers (19 males, 11 females) were analysed over a 6 month period. The inter-individual breath acetone concentration distribution was seen to be close to log normal, the geometric mean acetone concentration was 477 ppb (with a geometrical standard deviation, GSD, of 1.58), the mean values ranging from 148 to 2744 ppb for this cohort of healthy individuals (Turner *et al* 2006). The influence of calorie intake was also studied by feeding some of the volunteers with *Lucozade*, when the measured blood sugar increased and the breath acetone concentrations decreased. These collected studies leave little doubt that fasting/feeding does result in variations in breath acetone concentrations. More recently, intra-individual distributions for the acetone breath concentrations of several healthy individuals have been published that show log normal distributions with similar median concentrations and with intra-individual GSD values ranging from 1.2 (a narrow distribution) to 1.7 (a wider distribution) (Wang *et al* 2008a). We demonstrate later, with some new data, that such differences are not unusual. In this same study (Wang *et al* 2008a) it was shown that breath acetone is almost entirely systemic in origin, unlike some other breath compounds such as ammonia and ethanol that are most efficiently generated in the oral cavity by bacterial/enzymatic action. Two SIFT-MS studies have been carried out that explore the dependence of breath acetone with age (Španěl *et al* 2007a, 2007b). It was found that the

distributions are still log normal for the different age cohorts, but there is a significant increase in the mean breath acetone in the young (4 to 18 years) as compared to those in adults (20–60 years). These results were later confirmed and extended by an independent proton transfer reaction mass spectrometry (PTR-MS) study using a larger population of 243 adult volunteers and 44 children aged 5–11 years (Bajtarevic *et al* 2009).

### 1.2. Breath acetone in diabetes

Investigations of the concentrations of acetone in the breath of patients with diabetes compared to the breath of healthy controls have been inconclusive. An early study showed that the acetone levels in the breath of a cohort of children with type-1 diabetes in the age range 8–19 years were somewhat higher than those in the breath of a cohort of age-matched healthy controls (Nelson *et al* 1998), although the ranges clearly overlapped. Somewhat surprisingly, a subsequent study apparently showed that all patients included in a group of patients with type-2 diabetes had breath acetone concentrations greater than 1760 ppb, whereas the healthy controls all had breath acetone concentrations lower than 800 ppb (Deng *et al* 2004a). The latter results are in major conflict with the observation in the subsequent SIFT-MS study (Španěl *et al* 2007a) where no significant increase was observed in any of the type-2 diabetes volunteers included in the study.

Clearly, it cannot be said with confidence at the current state of experimental knowledge that breath acetone alone can be used as an indicator of glycaemic status (Smith *et al* 2011). The results of a recent study, in which breath acetone in eight patients with type-1 diabetes was studied using the glucose clamp technique (Turner *et al* 2009), are surprising. A positive correlation between breath acetone and blood glucose was reported and the range of breath acetone varied widely between patients. Similarly, in another study, the breath of 34 patients with type-1 diabetes was analysed for acetone and the data obtained suggested linear relationships between blood glucose, haemoglobin A1C and breath acetone (Wang *et al* 2010). These trends are contrary to expectation born of studies of the blood glucose/breath acetone of healthy individuals, emphasizing again the complexity of the diabetic condition. Clearly, there is a need for more research before breath acetone detectors can be promoted as diagnostic tools for diabetes.

## 2. Methods

SIFT-MS (Smith and Španěl 2005, Španěl and Smith 2011) was used to directly analyse exhaled breath on-line without any sample collection and storage. Two SIFT-MS instruments were used (in Prague a *Profile 3* manufactured by Instrument Science Limited, Crewe, UK and at Keele a SIFT-MS instrument manufactured by Trans Spectra Limited, Newcastle-under-Lyme, UK). In both instruments the flow rate of sampled air was configured such that the flow tube pressure in the absence of helium carrier gas was 0.1 Torr and then the analyses were carried out at a total flow tube pressure (sample gas plus carrier gas) of about 1 Torr. The accuracy of the absolute measurement of acetone concentrations calculated from the SIFT-MS data (Španěl *et al* 2006) was validated previously using standard mixtures (Smith *et al* 2009). All volunteers were informed about the purpose of the study and provided informed consent. Each breath acetone measurement was taken as the mean value from three consecutive exhalations and the concentration of water vapour in exhaled air was used as an indicator of the sample quality (Španěl and Smith 2011, Španěl *et al* 2006).



### 3. Results and discussion

#### 3.1. An example of marked differences in intra-individual variations of breath acetone

In order to demonstrate that there can be significant differences between individuals with respect to the biological variability of breath acetone concentrations, we have analysed the exhaled breath of two healthy volunteers in our Keele laboratory over a period of several weeks during the post-breakfast morning period. The very different distributions for two male individuals are shown in figures 1(a) and (b). Note the narrow distribution for volunteer A (male, age 70 years; body mass index (BMI) 25) and the much wider and erratic distribution for volunteer B (male, age 25 years; BMI 23). Given that neither individual had no reason to believe that their diet might have caused dramatic fluctuations in their levels of blood glucose, the results leave little confidence that breath acetone alone can be used as an indicator of blood glucose concentration, although it must be said that blood glucose was not measured in this limited study. Data are presented below that indicate the powerful influence of diet and the change from carbohydrate metabolism to lipid (fat) metabolism. These data have been scrutinized for any diurnal variations. As can be seen in figure 1(c), for volunteer A, there is a slow but steady increase in the breath acetone with time over several hours from the earliest measurements at 8:00 am. This is due to a change in metabolism from predominantly utilizing the readily available carbohydrates consumed for breakfast into that utilizing energy stored in the lipids. However, the data for volunteer B is so highly variable that any systematic trend in the acetone is indiscernible. It might be tempting to deduce that these data for volunteer B are symptomatic of an underlying metabolic disorder, perhaps latent diabetes but, obviously, to substantiate this requires much more clinical evidence and any diagnosis on the basis of a breath test alone would clearly be unjustified.

#### 3.2. Variability in individual changes in breath acetone due to a 6 h ketogenic diet

A more dramatic example of the influence of food on breath acetone is revealed by the experiment described below involving the ingestion of a ketogenic diet by several healthy subjects in the Prague laboratory. The background to this study is the work of Musa-Veloso *et al* (2002) who investigated the efficacy of breath acetone as an indicator of ketosis in adults consuming ketogenic meals (often used therapeutically to treat intractable seizures). They found that plasma acetoacetate and beta-hydroxybutyrate (see the introduction) were strongly correlated with breath acetone ( $R^2 = 0.7$ ,  $P < 0.0001$  and  $R^2 = 0.54$ ,  $P = 0.004$ ) and concluded that breath acetone is just as good a predictor of ketosis as are the urinary ketone bodies. Thus, it was concluded that breath acetone analysis can be used as an indicator of ketosis in epilepsy patients consuming a ketogenic diet, and may be useful for understanding the mechanistic aspects of the diet, elucidating the importance of ketosis in seizure protection, and ultimately, enhancing the efficacy of the diet by improving patient monitoring.

Following this precedence, a simple SIFT-MS experiment was carried out in our Prague laboratory to study the kinetics of acetone production induced by a simple ketogenic diet and its variation with the body composition. Thus, eight healthy volunteers (C to J) were recruited, three males and four females, ranging in age from 18 to 42 years and BMI values ranging from 24 to 32. The baseline values of breath acetone concentrations were measured in the afternoon/early evening before the main experiment using SIFT-MS. After an overnight fast (no breakfast) the breath acetone concentrations were measured again for each volunteer. Then a ketogenic diet was started (using a similar protocol as used in (Musa-Veloso *et al* 2002)) involving consumption every 3 h of a dose of 125 g of whipping cream, calculated on the basis of the typical dietary energy requirement. Simple dairy whipping cream was

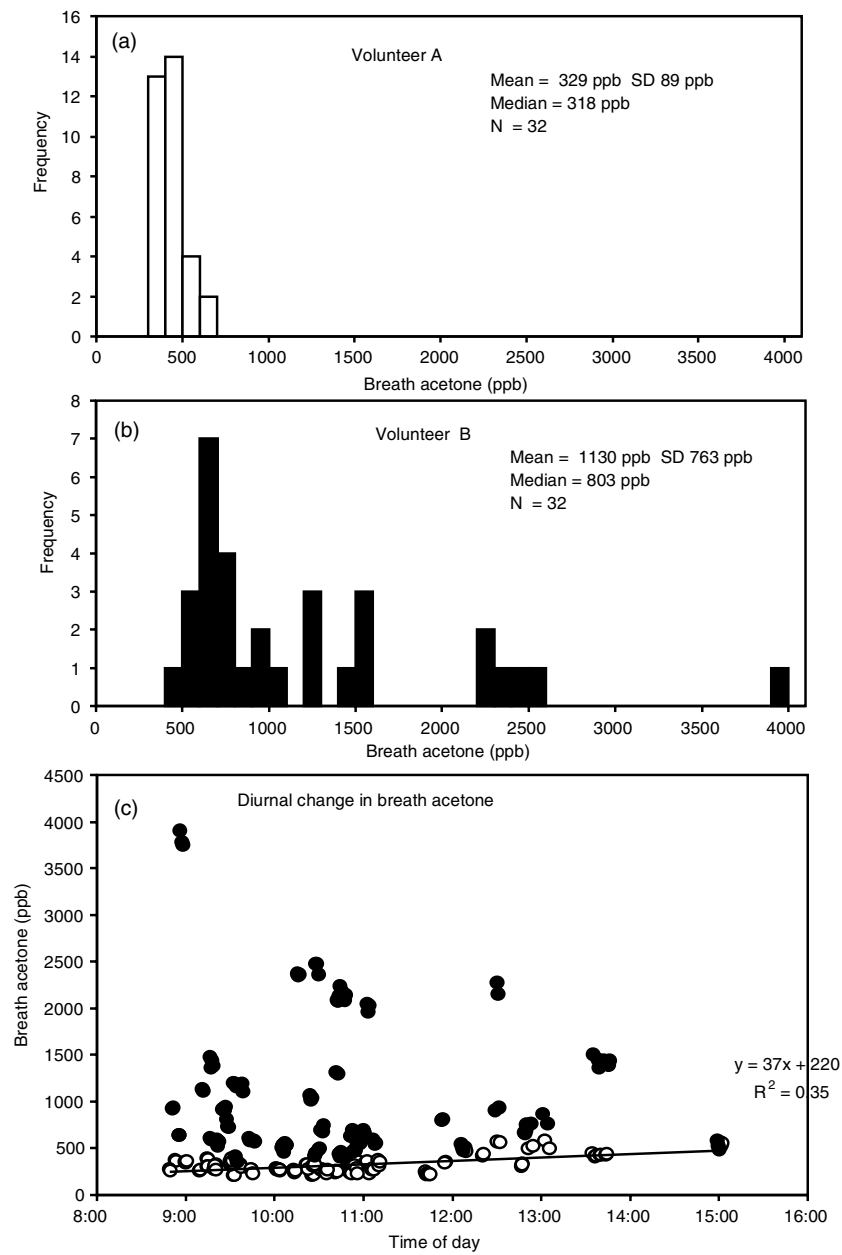


**Figure 1.** The histograms in (a) and (b) are the intra-individual distributions of exhaled breath acetone as measured by SIFT-MS (given in parts-per-billion, ppb) for volunteers A and B over a period of several weeks during the post-breakfast morning periods. (c) Dependence of the exhaled breath acetone concentrations on the time of day at which the breath was analysed, for the same volunteers (A, open symbols; B, filled symbols). The mean values and their standard deviations, SD, and the median values are given in ppb.

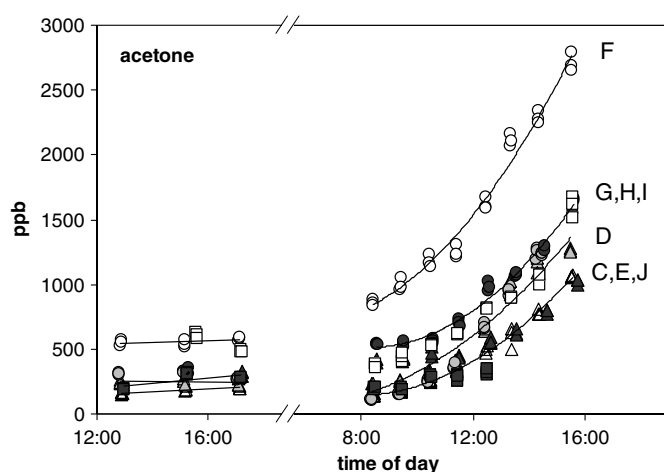


**Figure 2.** The concentrations of acetone (in parts-per-billion, ppb) in the exhaled breath of eight healthy volunteers plotted against the time of day, firstly for several hours during the day before the ketogenic meal investigation, and then the following day during the course of the ketogenic diet (initiated at 8:00 am).

used (produced by the Kunin dairy, Prague, 33% fat) without protein supplement. Then the breath of each volunteer was analysed regularly by direct exhalation at the entry port of the SIFT-MS instrument, a simple procedure made possible due to the high sample throughput of the instrument. The average of three exhalations was taken at each sampling time and the time of day was recorded automatically. The order of sampling of the individuals remained the same throughout the total sampling period of about 7 h, sampling each individual every hour.

The results of this study are plotted in figure 2 as the concentration of acetone in the breath of all eight volunteers against the real time of day. The fractional increase of breath acetone with time for all eight individuals is remarkable, being about a factor of 3 in all cases. Note that the curves essentially track each other with no overlaps and the higher the starting level of acetone the greater is the absolute increase. The actual concentrations range from about 200 ppb to about 2700 ppb, which nevertheless still remain within the wide range for healthy people on normal diets (Turner *et al* 2006), as noted in section 1.1. Within this limited amount of data there is no obvious relation between the fasting acetone level and its increase and the BMI.

### 3.3. Response of breath acetone to the initial 2 week period of a low carbohydrate ketogenic diet

The low carbohydrate ketogenic diet described and investigated in (McClernon *et al* 2007) is commonly known as the Atkins diet. In order to assess what effects might be observed in healthy subjects if they follow this diet or a similar low carbohydrate nutritional approach, a preliminary experiment was carried out using SIFT-MS to measure breath acetone. Two female volunteers (C: age 28 years, BMI 26. D: age 30 years; BMI 24) followed the requirements of a low carbohydrate ketogenic diet for 12 days. In essence, this consists in limiting carbohydrate intake to  $20 \text{ g day}^{-1}$ . In order to keep within that limit only meat, fish, suitable types of cheese and a limited amount of vegetables (salad greens, broccoli, spinach, cucumber,

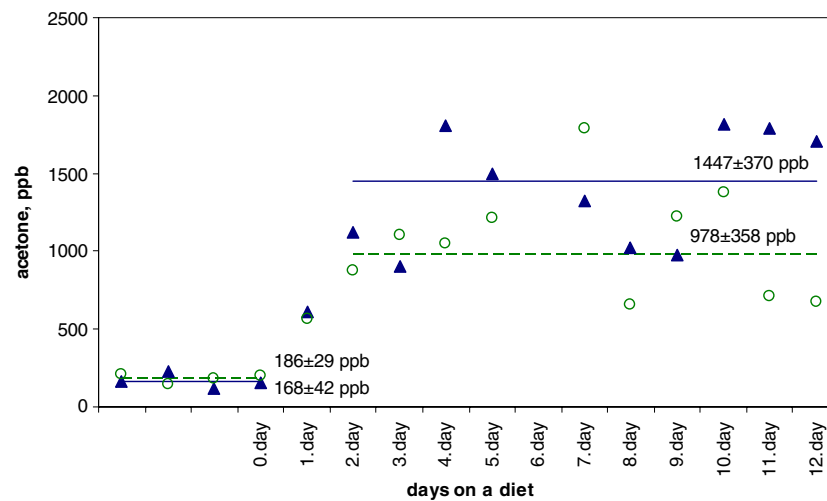


**Figure 3.** Breath concentrations of acetone (in parts-per-billion, ppb) measured during the 4 days prior to the start of a low carbohydrate ketogenic diet, and during the 12 days of the diet for volunteers C (open symbols) and D (filled symbols) and also indicated are the mean values and the standard deviations during these two periods.

(This figure is in colour only in the electronic version)

mushrooms, and soured cabbage) were consumed avoiding any high carbohydrate foods. Breath concentrations of acetone were monitored daily in these two volunteers, 4 days prior to the start of the course and then 12 days during the course of the diet.

The measured breath acetone concentrations obtained are shown in figure 3. Note the consistent breath acetone values a few days before commencing the low carbohydrate diet and then the relatively large increase for both subjects during the first two days of the diet. This is followed by a period during which the breath acetone values fluctuate to a greater extent than do the pre-diet values, but on average remain elevated by about six to nine times above the pre-diet values. Following the re-establishment of the normal diet, their breath acetone concentrations returned to their normal levels. These limited data indicate that dietary variation and control can apparently induce significant changes in metabolism as indicated by breath acetone monitoring.

#### 4. Concluding remarks

The results of this short study support the general sense of the previous work. Hence, it must be concluded that several factors influence the level of acetone in exhaled breath which must receive close attention if breath acetone can seriously be considered as a potential monitor of blood glucose and glycaemic control.

- The inter-individual variation of breath acetone can be very wide, commonly varying by a factor of 2 over a normal day on a normal diet.
- Nutritional status and the nature of diet: fasting elevates breath acetone as does fat ingestion and, equivalently, the restriction of carbohydrate intake.
- A slight increase in breath acetone occurs with increasing age, especially in children and young adults.

- The apparent increase of breath acetone in diabetes, as indicated by a limited amount of data, is not greater than the diurnal increase that occurs in healthy people and by varying the diet.

Notwithstanding these essential points that largely relate to healthy individuals, it should not immediately be dismissed that variations in breath acetone both in healthy individuals and in patients with diabetes, who can act as their own controls, might be used to monitor control of their blood glucose. However, for screening for diabetes to be feasible, individuals would have to pay careful attention to their diet by stabilizing their nutritional input before breath analysis. Nevertheless, before the hypothesis that breath acetone can be used to diagnose and monitor diabetes can be totally abandoned, more studies on breath acetone in patients with both type-1 and type-2 diabetes are essential (Turner 2011). Such studies are in train when other breath metabolites (biomarkers) will be searched for, which, in combination with each other and acetone, might be more definite indicators of glycaemia (Smith *et al* 2011).

Finally, the following points are worthy of note. In the light of the major relative changes and variations in breath acetone reported in this note, attempts to improve the accuracy of such measurement by procedures such as re-breathing (O'Hara *et al* 2008) or well-defined single-exhalation breathing manoeuvres (Dummer *et al* 2010), which are surely of some fundamental value for modelling of gas exchange (King *et al* 2010), are not critical with respect to the clinical relevance of breath acetone since they generally only address 10–20% effects. But, as demonstrated by the few case studies presented in this note, natural biological intra-individual variability and changes induced by diet can produce changes in breath acetone levels by as much as a factor of 5 or more.

## Acknowledgments

We thank all the volunteers for participating in this study and Kvetoslava Stejskalova for managing the study stay of AR. We gratefully acknowledge the partial funding for this study by the Grant Agency of Czech Republic project no 203/09/P172 and by the Ministry of Education of Czech Republic CZ.1.07/2.3.00/09.0034.

## References

- Bajtarevic A *et al* 2009 Noninvasive detection of lung cancer by analysis of exhaled breath *BMC Cancer* **9** 348
- Crofford O B, Mallard R E, Winton R E, Rogers N L, Jackson J C and Keller U 1977 Acetone in breath and blood *Trans. Am. Clin. Climatol. Assoc.* **88** 128–39
- Deng C H, Zhang J, Yu X F, Zhang W and Zhang X M 2004a Determination of acetone in human breath by gas chromatography-mass spectrometry and solid-phase microextraction with on-fiber derivatization *J. Chromatogr. B* **810** 269–75
- Deng C H, Zhang W, Zhang J and Zhang X M 2004b Rapid determination of acetone in human plasma by gas chromatography-mass spectrometry and solid-phase microextraction with on-fiber derivatization *J. Chromatogr. B* **805** 235–40
- Dummer J F, Storer M K, Hu W P, Swanney M P, Milne G J, Frampton C M, Scotter J M, Prisk G K and Epton M J 2010 Accurate, reproducible measurement of acetone concentration in breath using selected ion flow tube-mass spectrometry *J. Breath Res.* **4** 046001
- Henderson M J, Karger B A and Wrenshall G A 1952 Acetone in the breath; a study of acetone exhalation in diabetic and nondiabetic human subjects *Diabetes* **1** 188–93
- Kalapos M P 2003 On the mammalian acetone metabolism: from chemistry to clinical implications *Biochim. Biophys. Acta* **1621** 122–39
- King J, Mochalski P, Kupferthaler A, Unterkofler K, Koc H, Filipiak W, Teschl S, Hinterhuber H and Amann A 2010 Dynamic profiles of volatile organic compounds in exhaled breath as determined by a coupled PTR-MS/GC-MS study *Physiol. Meas.* **31** 1169–84

- Laffel L 1999 Ketone bodies: a review of physiology, pathophysiology and application of monitoring to diabetes *Diabetes Metab. Res. Rev.* **15** 412–26
- McClernon F J, Yancy W S, Eberstein J A, Atkins R C and Westman E C 2007 The effects of a low-carbohydrate ketogenic diet and a low-fat diet on mood, hunger, and other self-reported symptoms *Obesity* **15** 182–7
- Miekisch W, Schubert J K and Noeldge-Schomburg G F E 2004 Diagnostic potential of breath analysis—focus on volatile organic compounds *Clin. Chim. Acta* **347** 25–39
- Musa-Veloso K, Likhodii S S and Cunnane S C 2002 Breath acetone is a reliable indicator of ketosis in adults consuming ketogenic meals *Am. J. Clin. Nutr.* **76** 65–70
- Nelson N, Lagesson V, Nosratabadi A R, Ludvigsson J and Tagesson C 1998 Exhaled isoprene and acetone in newborn infants and in children with diabetes mellitus *Pediatr. Res.* **44** 363–7
- O'Hara M E, O'Hehir S, Green S and Mayhew C A 2008 Development of a protocol to measure volatile organic compounds in human breath: a comparison of rebreathing and on-line single exhalations using proton transfer reaction mass spectrometry *Physiol. Meas.* **29** 309–30
- Righettoni M, Tricoli A and Pratsinis S E 2010a Si:WO<sub>3</sub> sensors for highly selective detection of acetone for easy diagnosis of diabetes by breath analysis *Anal. Chem.* **82** 3581–7
- Righettoni M, Tricoli A and Pratsinis S E 2010b Thermally stable, silica-doped epsilon-WO<sub>3</sub> for sensing of acetone in the human breath *Chem. Mater.* **22** 3152–7
- Smith D, Pysanenko A and Španěl P 2009 Ionic diffusion and mass discrimination effects in the new generation of short flow tube SIFT-MS instruments *Int. J. Mass Spectrom.* **281** 15–23
- Smith D and Španěl P 2005 Selected ion flow tube mass spectrometry (SIFT-MS) for on-line trace gas analysis *Mass Spectrom. Rev.* **24** 661–700
- Smith D, Španěl P and Davies S 1999 Trace gases in breath of healthy volunteers when fasting and after a protein-calorie meal: a preliminary study *J. Appl. Physiol.* **87** 1584–8
- Smith D, Španěl P, Fryer A A, Hanna F and Ferns G A A 2011 Can volatile compounds in exhaled breath be used to monitor glycaemic control in diabetes mellitus? *J. Breath Res.* **5** 022001
- Španěl P, Dryahina K and Smith D 2006 A general method for the calculation of absolute trace gas concentrations in air and breath from selected ion flow tube mass spectrometry data *Int. J. Mass Spectrom.* **249** 230–9
- Španěl P, Dryahina K and Smith D 2007a Acetone, ammonia and hydrogen cyanide in exhaled breath of several volunteers aged 4–83 years *J. Breath Res.* **1** 011001
- Španěl P, Dryahina K and Smith D 2007b The concentration distributions of some metabolites in the exhaled breath of young adults *J. Breath Res.* **1** 026001
- Španěl P and Smith D 2011 Progress in SIFT-MS; breath analysis and other applications *Mass Spectrom. Rev.* **30** 236–67
- Tassopou C N, Barnett D and Fraser T R 1969 Breath-acetone and blood-sugar measurements in diabetes *Lancet* **1** 1282–6
- Turner C 2011 Potential of breath and skin analysis for monitoring blood glucose concentration in diabetes *Expert Rev. Mol. Diagn.* **11** 497–503
- Turner C, Španěl P and Smith D 2006 A longitudinal study of ammonia, acetone and propanol in the exhaled breath of 30 subjects using selected ion flow tube mass spectrometry, SIFT-MS *Physiol. Meas.* **27** 321–37
- Turner C, Walton C, Hoashi S and Evans M 2009 Breath acetone concentration decreases with blood glucose concentration in type I diabetes mellitus patients during hypoglycaemic clamps *J. Breath Res.* **3** 046004
- Wang C J, Mbi A and Shepherd M 2010 A study on breath acetone in diabetic patients using a cavity ringdown breath analyzer: exploring correlations of breath acetone with blood glucose and glycohemoglobin A1C *IEEE Sensors J.* **10** 54–63
- Wang T, Pysanenko A, Dryahina K, Španěl P and Smith D 2008a Analysis of breath, exhaled via the mouth and nose, and the air in the oral cavity *J. Breath Res.* **2** 037013
- Wang T, Španěl P and Smith D 2008b Selected ion flow tube mass spectrometry of 3-hydroxybutyric acid, acetone and other ketones in the headspace of aqueous solution and urine *Int. J. Mass Spectrom.* **272** 78–85

**A2. Determination of the deuterium abundances in water from 156 to 10,000 ppm by SIFT-MS**

Španěl P, Shestivska V, Chippendale TWE, Smith D. *J Am Soc Mass Spectrom* 2011, 22:179-186.



## RESEARCH ARTICLE

# Determination of the Deuterium Abundances in Water from 156 to 10,000 ppm by SIFT-MS

Patrik Španěl,<sup>1,2</sup> Violetta Shestivska,<sup>1</sup> Thomas W.E. Chippendale,<sup>2</sup> David Smith<sup>2</sup>

<sup>1</sup>J. Heyrovský Institute of Physical Chemistry, Academy of Sciences of the Czech Republic, Dolejškova 3, 182 23, Prague 8, Czech Republic

<sup>2</sup>Institute for Science and Technology in Medicine, School of Medicine, Keele University, Thornburrow Drive, Hartshill, Stoke-on-Trent, ST4 7QB, UK

## Abstract

In response to a need for the measurement of the deuterium (D) abundance in water and aqueous liquids exceeding those previously recommended when using flowing afterglow mass spectrometry (FA-MS) and selected ion flow tube mass spectrometry (SIFT-MS) (i.e. 1000 parts per million, ppm), we have developed the theory of equilibrium isotopic composition of the product ions on which these analytical methods are based to encompass much higher abundances of D in water up to 10,000 ppm (equivalent to 1%). This has involved an understanding of the number density distributions of the H, D, <sup>16</sup>O, <sup>17</sup>O and <sup>18</sup>O isotopes in the isotopologues of H<sub>3</sub>O<sup>+</sup>(H<sub>2</sub>O)<sub>3</sub> hydrated ions (i.e. H<sub>9</sub>O<sub>4</sub><sup>+</sup> cluster ions) at mass-to-charge ratios (*m/z*) of 73, 74 and 75, the relative ion number densities of which represent the basis of FA-MS and SIFT-MS analyses of D abundance. Specifically, an extended theory has been developed that accounts for the inclusion of D atoms in the *m/z* 75 ions, which increasingly occurs as D abundance in the water is increased, and which is used as a reference signal for the *m/z* 74 ions in the measurement of D abundance. In order to investigate the efficacy of this theory, experimental measurements of deuterium abundance in standard mixtures were made by the SIFT-MS technique using two similar instruments and the results compared with the theory. It is demonstrated that the parameterization of experimental data can be used to formulate a simple calculation algorithm for real-time SIFT-MS measurements of D abundance to an accuracy of 1% below 1000 ppm and degrades to about 2% at 10,000 ppm.

**Key words:** Deuterium abundance, Total body water, Selected ion flow tube mass spectrometry, SIFT-MS, Stable isotopes

## Introduction

Some 10 years ago we developed selected ion flow tube mass spectrometry (SIFT-MS) [1] and flowing afterglow mass spectrometry (FA-MS) [2], methods with the specific objective to determine in real time the abundance of deuterium (D) in water vapour containing H<sub>2</sub>O, HDO and D<sub>2</sub>O molecules (i.e. the ratio of the number of D atoms to the total number of atoms of all hydrogen isotopes), from

which the D abundance in the associated liquid water phase can be derived [2–4]. Research has focused on the measurement of total body water (TBW) by analysing exhaled breath for HDO following the ingestion of an accurate amount of pure D<sub>2</sub>O, exploiting the principle of isotope dilution [4, 5]. Thus, the ingested D<sub>2</sub>O rapidly becomes HDO via fast isotopic exchange with the abundant body water molecules and after some time, typically 100 min, the HDO is equilibrated throughout the body water, which is reflected in its level in the exhaled water vapour. Thus, in a series of longitudinal studies in close collaboration with our nephrology colleagues led by S.J. Davies, we have successfully exploited FA-MS to determine the TBW in significant

Correspondence to: Patrik Španěl; e-mail: spanel@jh-inst.cas.cz

Received: 2 September 2010  
Revised: 4 October 2010  
Accepted: 14 October 2010  
Published Online: 21 January 2011



cohorts of healthy volunteers and in patients suffering from renal disease who are being treated by haemodialysis and peritoneal dialysis [6, 7]. This non-invasive, painless and rapid approach to the measurement of TBW is proving to be most valuable in nephrology.

The basic principle of FA-MS deuterium analysis is simple, but there are details that need to be understood to promote this method towards accurate analyses of D abundance and these important details are given in a later section. For the moment, the method is based on the creation of a swarm of water cluster ions,  $\text{H}_3\text{O}^+(\text{H}_2\text{O})_3$  (i.e.  $\text{H}_9\text{O}_4^+$ ), held in an inert support gas, usually helium, in the presence of water molecules at a constant, known temperature, for time periods sufficient to allow the D,  $^{17}\text{O}$  and  $^{18}\text{O}$  isotopologues of these cluster ions to reach their thermal equilibrium distribution. The abundance of D in the water vapour introduced into the support gas is then obtained by measuring the relative number densities of these isotopologues using quantitative mass spectrometry, as explained later. These isotopologue ions have mass-to-charge ratios ( $m/z$ ) of 73 ( $\text{H}_9^{16}\text{O}_4^+$ ), 74 ( $\text{H}_8\text{D}^{16}\text{O}_4^+$  and  $\text{H}_9^{16}\text{O}_3^{17}\text{O}^+$ ) and 75 ( $\text{H}_9^{16}\text{O}_3^{18}\text{O}^+$ ). More combinations are possible at  $m/z$  75, including  $\text{H}_8\text{D}^{16}\text{O}_3^{17}\text{O}^+$  and  $\text{H}_7\text{D}_2^{16}\text{O}_4^+$ , but their expected contributions are negligible ( $\ll 1\%$ ) at the natural abundances of the minor isotopes D and  $^{17}\text{O}$  and for small D enrichments. However, contributions of the last two ions can become important if the number density of the HDO molecules in the analyte vapour is high enough; even isotopologue ions at  $m/z$  76 can become significant at high HDO levels. These enrichment phenomena are the major focus of this paper in which we show how they can be accounted for and how SIFT-MS in addition to FA-MS can be used to accurately measure D abundances up to ten thousands of parts per million in water vapour and hence in liquid water using the appropriate vapour phase/liquid phase partition coefficients.

### *SIFT-MS and FA-MS for Measurements of D Abundance in Water Vapour*

These analytical methods evolved from the well-known selected ion flow tube and flowing afterglow, both fast flow tube/quantitative mass spectrometric techniques that have been used by us and others to study the kinetics of ion/molecule reactions [8, 9] and recombination reactions [10]. Subsequently, these methods were adapted as the gas-phase analytical mass spectrometric techniques SIFT-MS and FA-MS. SIFT-MS has been used to measure trace gas concentrations in air samples down to the parts per billion (ppb) level and below [11, 12] and is proving to be especially valuable for on-line, real-time analyses of exhaled breath. Our first exploratory studies on the measurement of the deuterium abundance in water vapour were carried out using an early SIFT-MS instrument of low sensitivity [1]. This involved the selective injection of  $\text{H}_3\text{O}^+$  ions (formed in an external microwave discharge) via an upstream quadrupole

mass filter into helium carrier gas and the introduction into the carrier gas/ion swarm of water vapour (having an abundance of D atoms, later described by  $R_1$ ) evolving from the liquid water for which the deuterium abundance was to be determined (later described as  $R_{\text{liq}}$ ). Thus, the  $\text{H}_3\text{O}^+$  ions are converted to their hydrated isotopologues referred to above (i.e. water cluster ions at  $m/z$  values 73, 74 and 75). It is then a matter of measuring accurately the relative count rates of these ions and including them in the theoretical analysis described below, whence the abundance of D in the water vapour and then in the liquid water is determined. These initial SIFT-MS studies confirmed the soundness of this unique approach to D abundance measurements. Thus, by using standard  $\text{D}_2\text{O}/\text{H}_2\text{O}$  mixtures the accuracy of measurement was confirmed [1], but the precision was found to be inadequate unless long integration times were used, because of the low ion count rates (counts per second) of the analytical  $m/z$  73, 74 and 75 ions (typically  $2 \times 10^4$  c/s for  $m/z$  73 ions and about 100 times lower for the  $m/z$  75 ions) that could be created at the time of these initial studies in the old SIFT-MS instrument. It was then necessary to re-think the approach and this gave rise to our FA-MS method [2–4].

In FA-MS the upstream mass filter that is standard in SIFT-MS is absent and the precursor  $\text{H}_3\text{O}^+$  ions are formed by a weak microwave discharge through the helium carrier gas into which the water vapour to be analysed is introduced [13]. This results in much larger count rates of typically  $2 \times 10^6$  c/s for  $m/z$  73 ions and typically  $10^4$  c/s for  $m/z$  74 and 75 ions with a subsequent increase in the precision of the D abundance measurements reaching the desired 1% and better [3, 14]. This allowed the TBW in human subjects to be determined to a comparable precision and accuracy (but see the important proviso and development described in the next paragraph). Much work in the measurement of TBW has been accomplished in collaboration with our clinical colleagues using FA-MS [5–7, 15–17]. However, this method does have a weakness in that by avoiding the upstream mass filter and directly discharging the helium carrier gas/water vapour mixture (which inevitably contains traces of air), ions like  $\text{NO}^+$  and  $\text{O}_2^+$  are formed in addition to  $\text{H}_3\text{O}^+$  and its hydrates. These  $\text{NO}^+$  and  $\text{O}_2^+$  ions can undergo reactions with trace gases in the air/water vapour sample to be analysed, especially when the analyte is exhaled breath that contains carbon dioxide and many trace organic metabolite molecules, and these ill-defined ternary association reactions can produce “rogue ions” at the same  $m/z$  value as the analytical  $m/z$  73, 74 and 75 ions that can diminish the accuracy of the determination of abundance of D. Whilst the influence of this interference can be minimized by software corrections, it is obviously undesirable. Fortunately, as we see below, the new generations of SIFT-MS instruments have much higher sensitivities implying that much greater count rates of injected  $\text{H}_3\text{O}^+$  ions can be produced and so it is now possible to revert back to SIFT-MS and achieve the required precision and accuracy of

measurements of D abundance, as is demonstrated by the results of the calibration experiments presented later.

Now an important technical aspect of SIFT-MS and FA-MS measurements must be explained. The count rate of the ions at  $m/z$  73 typically approaches  $10^6$  c/s, which is more than 100 times larger than those at  $m/z$  74 and 75. Clearly, for a measurement of the D/H ratio to an accuracy of 1% or better, the ion detectors (usually electron multipliers with single or multiple channels or with discrete dynodes) should be capable of measuring—to a similar accuracy—ions count rates at  $m/z$  73 of  $10^6$  c/s and also those of the  $m/z$  74 and 75 at count rates of typically  $(4\text{--}10) \times 10^3$  c/s. The statistical uncertainty in determining the lower count rates of the  $m/z$  74 and 75 ions can be decreased, and hence the precision of the measurements can be increased, by counting these ions for increasing time periods; single breath exhalations can be sustained for several seconds which is sufficient to realize good precision. However, the response of most detectors is not sufficiently fast that the high counts per second at  $m/z$  73 can be measured to the required accuracy. The solution to this problem is to avoid measurement of  $m/z$  73 and to measure accurately the count rate of the isotopologue at  $m/z$  75 as a reference signal, assuming this to be independent of the deuterium abundance in the sample water vapour. Then the deuterium abundance can be obtained from simultaneous accurate measurements of the relative count rates of the  $m/z$  74 and 75 ions. Details of this approach are given in previous papers [2–4] and briefly summarized below.

The count rates at  $m/z$  74 and 75 currently attainable by SIFT-MS are ideal for the available multipliers to handle and so measurement precision can be achieved. However, this

approach does require that a correct value of the isotopic abundance of  $^{18}\text{O}$  be adopted and it is also assumed that the  $m/z$  75 ion consists only of  $\text{H}_9^{16}\text{O}_3^{18}\text{O}^+$  ions (i.e. they contain just one  $^{18}\text{O}$  atom and an insignificant fraction of D atoms). We have shown that these requirements are met when the deuterium abundance in the water vapour to be analysed is less than 1000 ppm and using FA-MS in this regime we have made many measurements on TBW in healthy controls and dialysis patients that demonstrate its validity [5–7]. But above about 1000 ppm an increasing fraction of the  $m/z$  75 ions become populated with a single D atom in combination with a single  $^{17}\text{O}$  atom and/or two D atoms (see Figure 1 later), and this added complication must then be taken into account in order to obtain accurate deuterium abundances. In some applications of isotopic dilution, restricted volumes of water are involved and this results in a need for measurements of deuterium abundance in water at several thousand parts per million. Thus, it has become necessary to consider the extension of the theoretical analysis underlying the analytical methods. This has also demanded an experimental check on the efficacy of the extended theory using standard solutions of deuterated water. The comparison of this new theory and experiment is reported below and the approach to accurate measurements of deuterium abundance in water vapour at levels from 1000 ppm up to 10,000 ppm is indicated. So, in summary, the goal of this work is to find an empirical expression for the vapour phase D abundance ( $R_1$ ) in terms of the known oxygen isotopic abundances and the ratio of the measured  $m/z$  74 and 75 peak heights in the mass spectrum.

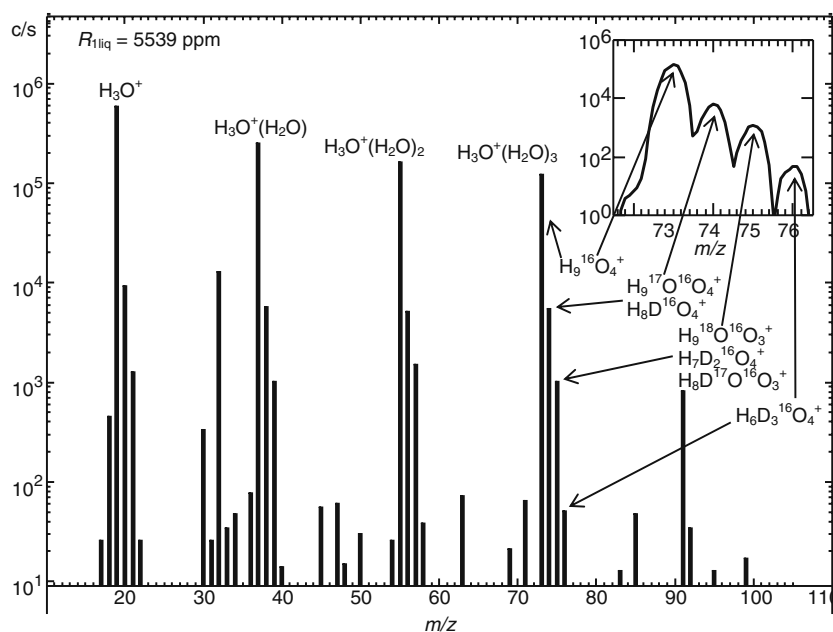
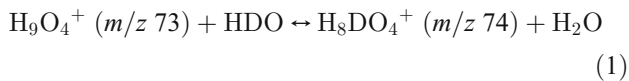


**Figure 1.** The SIFT-MS mass spectrum (counts per second, c/s against ion mass-to-charge ratio,  $m/z$ ) obtained for a standard mixture enriched to an  $R_{1\text{liq}}$  of 5539 ppm. The observed isotopologues of the trihydrate of  $\text{H}_3\text{O}^+$  are indicated in the inset

## Theoretical Considerations

The SIFT-MS and FA-MS methods for the determination of deuterium abundance in water vapour are based on the fact that deuterium/hydrogen isotope exchange is facile between the trihydrate hydronium ion  $\text{H}_3\text{O}^+(\text{H}_2\text{O})_3$  (i.e.  $\text{H}_9\text{O}_4^+$ ) and HDO in the gas phase, because there are no significant energy barriers and the enthalpy change is very small [18] in the isotope-exchange reactions:



As indicated, the reaction can proceed in both directions and dynamic equilibrium amongst the reacting ions is rapidly established at room temperature in the helium support gas of SIFT-MS. Then the distribution of the reacting ions is totally determined by the statistics of the isotope-exchange reactions and it is on this premise that the analysis below is based. Further details are given in previous papers [1, 2]. A typical mass spectrum obtained by using SIFT-MS when the vapour above natural water enriched in HDO by the addition of  $\text{D}_2\text{O}$  is introduced into an  $\text{H}_3\text{O}^+$  ion swarm is shown in Figure 1. Note the obvious presence of the isotopologues of the  $\text{H}_3\text{O}^+(\text{H}_2\text{O})_{0-3}$  cluster ions and the expansion of the spectrum around  $m/z\ 73$  to 76 indicating the nature of these important isotopologue ions around which much of the discussion below revolves. Thus, the ions at  $m/z\ 75$  are predominantly  $\text{H}_9^{16}\text{O}_3^{18}\text{O}^+$ , but at high HDO concentrations  $\text{H}_8\text{D}^{16}\text{O}_3^{17}\text{O}^+$  and  $\text{H}_7\text{D}_2^{16}\text{O}_4^+$  become significant contributors. Given the known abundances [19, 20] of the  $^{17}\text{O}$  ( $R_2=0.00387$ ) and  $^{18}\text{O}$  ( $R_3=0.0198$ ) in natural water, the contributions of these various isotopologues can be predicted statistically for varying abundance of D ( $=R_1$ ) in the water vapour. Note that  $R_1$  is proportional to the D abundance in the liquid water from which the vapour is derived and they are related by the known, temperature-dependent, partition coefficient of HDO between the liquid and vapour phases [21].

The equilibrium fractions ( $I$ ) of each isotopologue ion at  $m/z\ 75$  ( $\text{H}_9^{16}\text{O}_3^{18}\text{O}^+$ ,  $\text{H}_8\text{D}^{16}\text{O}_3^{17}\text{O}^+$  and  $\text{H}_7\text{D}_2^{16}\text{O}_4^+$ ) within the total of all possible  $\text{H}_9\text{O}_4^+$  isotopologues can be expressed as:

$$I[\text{H}_9^{16}\text{O}_3^{18}\text{O}^+] = 4(1 - R_1)^9(1 - R_2 - R_3)^3 R_3 \quad (2)$$

$$I[\text{H}_8\text{D}^{16}\text{O}_3^{17}\text{O}^+] = 36(1 - R_1)^8 R_1(1 - R_2 - R_3)^3 R_2 \quad (3)$$

$$I[\text{H}_7\text{D}_2^{16}\text{O}_4^+] = 36(1 - R_1)^7 R_1^2(1 - R_2 - R_3)^4 \quad (4)$$

Here, the  $(1 - R_1)$  factors correspond to the abundance of the major  $^1\text{H}$  isotopes amongst all hydrogen atoms and

the  $(1 - R_2 - R_3)$  factors correspond to the abundance of  $^{16}\text{O}$  amongst all O atoms. Four and 36 are the numbers of different combinations of atomic positions contributing to the specific isotopologues. The exponents directly correspond to the number of atoms of the given isotope in the molecular ion. To repeat, these equations are derived by assuming there are insignificant enthalpy changes in all these isotope-exchange reactions and that the equations only describe truly statistical mixing of isotopes in the ions. A graphical representation of the equilibrium fractions calculated from Equations (2) to (4) are shown in Figure 2a.

The insets in this figure indicate the variations in the equilibrium fractions of the  $\text{H}_9^{16}\text{O}_3^{18}\text{O}^+$  and  $\text{H}_7\text{D}_2^{16}\text{O}_4^+$  isotopologues at deuterium abundances below 1000 ppm for which previous work has shown that  $m/z\ 75$  is a reliable reference level for measurements of D abundance [3]. Whilst there clearly is a diminution of the  $\text{H}_9^{16}\text{O}_3^{18}\text{O}^+$  fraction with increasing  $R_1$ , it is less than 0.5% of the initial (zero D/H) fraction, as indicated previously. Similarly, the increase in the fraction of the doubly deuterated ion  $\text{H}_7\text{D}_2^{16}\text{O}_4^+$  is commensurately small and so the total signal of  $m/z\ 75$  can be considered to be devoid of the  $\text{H}_7\text{D}_2^{16}\text{O}_4^+$  ions at these low  $R_1$  values. However, major changes of the nature of the  $m/z\ 75$  isotopologues occur with increasing  $R_1$ , the  $\text{H}_7\text{D}_2^{16}\text{O}_4^+$  becoming an increasing fraction and the  $\text{H}_9^{16}\text{O}_3^{18}\text{O}^+$  becoming a decreasing fraction, and the total ion signal at  $m/z\ 75$  (also indicated in Figure 1a) significantly increases. Obviously, this needs to be accounted for if  $m/z\ 75$  is to be used as a reference for measurements of  $R_1$  in the range from 1000 to 11,000 ppm, as described below.

A similar analysis, again taken relative to the total ion signal intensity of all  $\text{H}_9\text{O}_4^+$  ions, can be made for the two isotopologues contributing to  $m/z\ 74$  (see Figure 1) as:

$$I[\text{H}_9^{16}\text{O}_3^{17}\text{O}^+] = 4(1 - R_1)^9(1 - R_2 - R_3)^3 R_2 \quad (5)$$

$$I[\text{H}_8\text{D}^{16}\text{O}_4^+] = 9(1 - R_1)^8 R_1(1 - R_2 - R_3)^4 \quad (6)$$

The results of this analysis are graphically represented in Figure 2b. The inset shows the variation of the  $\text{H}_9^{16}\text{O}_3^{17}\text{O}^+$  fraction as calculated from Equation (5), which is about 0.15% and decreases only slightly even at much higher  $R_1$ . Obviously, the fraction of  $\text{H}_8\text{D}^{16}\text{O}_4^+$  will proportionately increase with increasing  $R_1$  (this is the principle on which the measurement of  $R_1$  depends!) reaching close to 10% at the highest  $R_1$  considered, as calculated from Equation (6) and shown in Figure 2b. The total ion counts at  $m/z\ 74$  are also shown, as obtained by simply summing the contributions of the two isotopologues, indicating the diminishing but still significant contribution of  $\text{H}_9^{16}\text{O}_3^{17}\text{O}^+$  at high  $R_1$ .

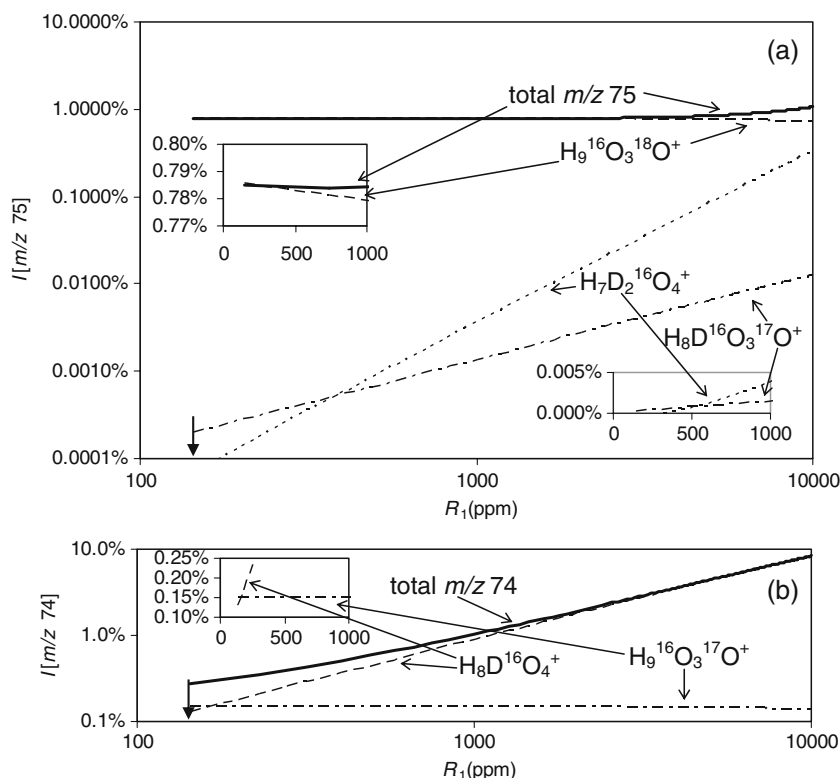


**Figure 2.** The percentages ( $I$ ) of the minor isotopologues of  $\text{H}_9\text{O}_4^+$  ions from the total concentration of all possible isotopologues calculated as a function of  $R_1$ , the equilibrium abundance of D in the water vapour in the helium carrier gas, as calculated by using Eqs. (2) to (6). **(a)** Contributions to the total count rate at  $m/z$  75. The contributions of the  $\text{D}_2$  and  $\text{D}^{17}\text{O}$  isotopologues increase with  $R_1$  increases but both are insignificant below 1000 ppm. **(b)** Contributions to the total count rate at  $m/z$  74. The  $^{17}\text{O}$  isotopologue is important below  $R_1$  of 1000 ppm but decreases at higher abundances of D. Vertical arrows indicate the value  $R_1 = 144$  ppm corresponding to natural abundance of D in water  $R_{1\text{liq}} = 156$  ppm

Now it is possible to write a rigorous equation relating the observed ratio of equilibrium ion densities at  $m/z$  74 to  $m/z$  75, which we designate  $Q = [74]/[75]$  (see [2, 3]) as:

$$Q = \frac{9R_1(1 - R_1)(1 - R_2 - R_3) + 4(1 - R_1)^2 R_2}{4(1 - R_1)^2 R_3 + 36R_1(1 - R_1)R_2 + 36R_1^2(1 - R_2 - R_3)} \quad (7)$$

This rigorous equation can be compared with the approximate equation used previously in routine FA-MS analyses [2, 3]:

$$Q = (9R_1 + 4R_2)/4R_3 \quad (8)$$

In the range of  $R_1$  up to 0.001 (i.e. D abundance of 1000 ppm) the difference in  $Q$  derived from Equations (7) and (8) is less than 0.5%, but for higher  $R_1$  the discrepancy becomes very significant. Note that the linear relation between  $Q$  and  $R_1$  given by Equation (8) can easily be implemented for the analysis of  $R_1$ , and it is this that has been adopted for all our previous on-line, real-time measurements of  $R_1$  in the water vapour above aqueous liquids and

in exhaled breath [2, 3, 13]. However, the use of the exact Equation (7) involves the solution of a complex quadratic equation, which is feasible analytically, but more complicated to implement. Thus, it is desirable to formulate and parameterize a practical expression or algorithm for deriving  $R_1$  from the measured  $Q$  obtained for  $R_1$  values above 1000 ppm where Equation (8) would lead to significant errors. Such an expression will be presented later (as Equation 9) after discussing the experimental results.

So Equation 7, together with experimental measurement of  $Q$ , can be used to determine  $R_1$  above 1000 ppm. But clearly it is essential to check experimentally the efficacy of this theoretical analysis by using prepared standard mixtures of deuterated water with known  $R_1$ . The results obtained from such experiments are reported in the next section.

## Experimental Work and Comparison with Theory

### Materials and Methods

These experiments were conducted by using two SIFT-MS instruments of the latest generation in Prague (*Profile 3* manufactured by Instrument Science Limited, Crewe, UK)



and at Keele (SIFT-MS instrument manufactured by Trans Spectra Limited, Newcastle-under-Lyme, UK) that realize close to  $10^6$  c/s of the  $m/z$  73  $\text{H}_3\text{O}_4^+$  ions [12, 22, 23]. The flow rate of sampled air was configured such that the flow tube pressure in the absence of He carrier gas was about 0.15 Torr and then the experiments were carried out with total flow tube pressure of sample and carrier gas of about 1 Torr. Two separate approaches were carried out to experimentally determine the dependence of  $Q$  on the deuterium enrichment of tap water. In one approach (Prague) a number of standard mixtures were prepared volumetrically, either by adding constant amounts of  $\text{D}_2\text{O}$  (99.9% purity, Isotech Inc., USA) to a known volume of tap water or by sequential factoring of two dilutions of a known “mother solution” (10,000 ppm). The equilibration time for each sample was at least 60 min at room temperature (22 °C) to allow for the  $\text{D}_2\text{O}/\text{H}_2\text{O}$  isotope-exchange reaction (equilibration) times [24]. Our preliminary experiments have shown that an approach to equilibrium mixing can be observed during the first 10 min following the addition of pure  $\text{D}_2\text{O}$  to tap water. In a second approach (Keele) the gravimetric method was used in which accurately weighed amounts of  $\text{D}_2\text{O}$  were added to accurately weighed amounts of tap water.

The prepared samples were placed in bottles sealed by septa and the liquid water/water vapour headspace (in atmospheric air) was allowed to equilibrate at a constant temperature of 20 °C for a few minutes. The septa were then pierced by a needle connected to the sample inlet line of the SIFT-MS instrument when the headspace air/water vapour mixture flowed into the helium carrier gas into which  $\text{H}_3\text{O}^+$  ions had been selectively injected. Thus, hydration of the  $\text{H}_3\text{O}^+$  rapidly occurred and the isotope-exchange reactions indicated in Equation (1) proceeded to equilibrium. Hence, the count rates of the  $m/z$  74 and 75 ions were accurately measured (each at four different positions on the peak produced by quadrupole mass spectrometer, see [2]), whence the  $Q$  values were calculated as the count rate ratio  $[74]/[75]$ . At the onset it is essential to understand that it is tacitly assumed that ion number densities of the various ions in the helium carrier gas of the SIFT-MS (to which the analytical equations above relate) are directly related to their count rates as detected by the analytical mass spectrometer. This is only true if there is no discrimination in the mass spectrometer sampling/detection system between the analytical ions at  $m/z$  74 and 75. We consider this to be a valid assumption and this is discussed further in [23].

## Results

The results are shown in Figure 3a as the dependence of the experimentally determined  $Q$  on the known  $R_{\text{liq}}$  in the standard samples. The data points from the two independent experiments in Prague and Keele are shown and the continuous solid line is a result of theory using Equation (7) after converting  $R_{\text{liq}}$  to  $R_1$  using the known partition

coefficient  $K_1=0.92$  between liquid and vapour concentrations of HDO at 20 °C [21], while the dashed line represents the previously used linear relation (Equation 8). The inset is the plot of the experimental points obtained below  $R_{\text{liq}}=1400$  ppm, which is closely linear and shows agreement between experiment and the theory to within 1%, as we have previously shown for both FA-MS data [3] and the very early SIFT-MS data [1]. However, the departure from linearity at the highest  $R_{\text{liq}}$  values is stark, the difference between the experimental values of  $Q$  and those predicted by the simple theory reaching 2% at 2000 ppm, 10% at 5000 ppm and 30% at 10,000 ppm. But the theoretical curve for  $Q$  against  $R_{\text{liq}}$  derived by using the precise Equation (7) closely matches the experimental results in both form and magnitude. So the theory properly accounts for the changing composition of the  $m/z$  74 and especially of the major changes that occur in the composition of  $m/z$  75 with increasing  $R_1$ . At the largest D abundances investigated (about 10,000 ppm) there is about 3% difference between the experimental and theoretical values of the ratio  $Q$ , and both differ from the result of the simple Equation (8) by about 30%.

On the basis of these experimental results it is now possible to parameterize a correction that must be applied to the results calculated by using Equation (8) in order to obtain accurate values of  $R_1$  from experimentally measured  $Q$  values, as

$$R_1 = \frac{4(R_3 Q - R_2)/9}{1 - 0.0061(Q - 0.19)^2} \quad (9)$$

The numerator in Equation (9) represents the solution to Equation (8) with respect to  $R_1$  and the denominator is a parameterized correction factor obtained by a least-squares fit through the experimental data points. It is important to note here that the unknown  $R_1$  value itself cannot be used as a variable in the parameterization if a straightforward (not iterative) calculation algorithm is to be proposed.

Figure 3b shows a plot of the expected values of  $R_{\text{liq}}$  (standard mixtures) and those derived by using Equation (9) together with the known partition coefficient  $K_1=0.92$  [21]. Note that using this simple correction in Equation (9), one achieves excellent linearity and near perfect agreement between the measured and expected  $R_{\text{liq}}$  and also that the correction does not greatly influence the values within the low D abundance range up to 1300 ppm (actually the correction at 1000 ppm amounts to only 0.7%). Because Equation (9) is based on the fit through the experimental data and not the theoretical predictions, it negates the 3% difference between theory and experiment mentioned above. Note also that for increasing  $R_{\text{liq}}$  the measurements become less precise, because a given error in the experimental  $Q$  is projected as an increasingly larger error in the derived  $R_{\text{liq}}$ . An error analysis of Equation (9) shows that a 1% error in the measured  $Q$  corresponds at 1000 ppm to a 1.1% error in  $R_{\text{liq}}$ , but at 10,000 ppm this error is 2%. At even higher

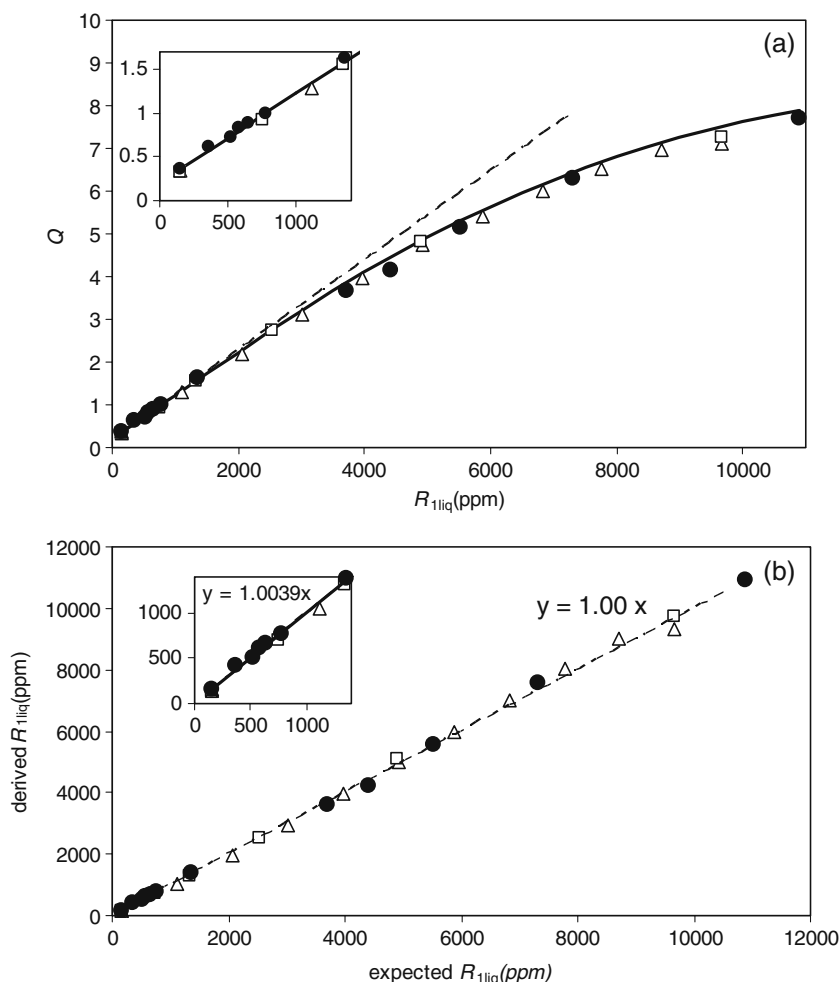


**Figure 3.** (a) Experimentally determined  $Q=[74]/[75]$  as a function of the known  $R_{1liq}$  in standard mixtures. The solid circles are the results of measurements of gravimetrically prepared mixtures (Keele instrument), the open triangles are results from volumetrically prepared mixtures obtained by using incremental additions and the open squares are results from volumetric mixtures obtained by sequential dilutions (Prague instrument). The solid line is the value of  $Q$  predicted by the theoretical Eq. (7) and the dashed line corresponds to the previously used approximate Eq. (8). (b)  $R_{1liq}$  values derived from measured  $Q$  values using the new empirical Eq. (9) with a correction factor  $1/[1-0.0061(Q-0.19)^2]$  obtained by fitting the data from (a), which shows the good agreement with the expected standard mixture values

deuterium concentrations the variation of  $Q$  with  $R_{1liq}$  is more gradual and so the present method of measurement of  $R_1$  cannot be used reliably, because information on  $m/z$  76 ions (see Figure 1) or even higher  $m/z$  ions would have to be included, which would seriously complicate the analysis with the consequent reduction in precision and accuracy.

## Discussion and Concluding Remarks

The critical message to be taken from these results is that the experiments show that the theory described by Equations (2) through (7) closely models the statistics of the isotope-exchange reactions and so within the stated uncertainty it can be used in association with experimental  $Q$  measurements obtained by SIFT-MS to accurately determine deuterium abundances up to levels up to 10,000 ppm, as was intended in this work. This is remarkable in view of the complexity of the ion chemistry and

the many isotope-exchange reactions involved. In fact, the situation in detail is even more complex than we have described. Inspection of the SIFT-MS spectrum shown in Figure 1 obtained for water vapour enriched to D abundance of about 5000 ppm reveals the presence of ions at  $m/z$  76, which we have not included in our analysis because it would add another degree of complexity. At this point, we conclude that the theory has been taken as far as is sensible and if it is to be used in association with  $Q$  measurements to determine D/H values around 10,000 ppm then an uncertainty of about 3% would have to be accepted. The small discrepancy between the statistical theory and the experimental results may be related to small enthalpy changes in reaction (1) or in its analogue involving incorporation of a second D atom into the product ions. However, a bona fide approach, which bypasses the need for even more complex theory, is to curve fit (parameterize) the experimental data obtained by using standard mixtures, as is shown in Figure 3b.

The statistical theory serves as a solid foundation and qualitatively explains the sources of non-linearity; the experimental calibration is used to enhance the accuracy of measurement beyond the limits imposed by the necessary and inherent assumptions. This approach allows  $R_1$  values above 1000 ppm and up to 10,000 ppm to be determined to better than 2% by using SIFT-MS.

## References

- Španěl, P., Smith, D.: Selected ion flow tube mass spectrometry analyses of stable isotopes in water: Isotopic composition of  $\text{H}_3\text{O}^+$  and  $\text{H}_3\text{O}^+(\text{H}_2\text{O})_3$  ions in exchange reactions with water vapor. *J. Am. Soc. Mass Spectrom.* **11**, 866–875 (2000)
- Smith, D., Španěl, P.: On-line determination of the deuterium abundance in breath water vapour by flowing afterglow mass spectrometry with applications to measurements of total body water. *Rapid Commun. Mass Spectrom.* **15**, 25–32 (2001)
- Španěl, P., Smith, D.: Accuracy and precision of flowing afterglow mass spectrometry for the determination of the deuterium abundance in the headspace of aqueous liquids and exhaled breath water. *Rapid Commun. Mass Spectrom.* **15**, 867–872 (2001)
- Davies, S., Španěl, P., Smith, D.: Rapid measurement of deuterium content of breath following oral ingestion to determine body water. *Physiol. Meas.* **22**, 651–659 (2001)
- Smith, D., Engel, B., Diskin, A.M., Španěl, P., Davies, S.J.: Comparative measurements of total body water in healthy volunteers by online breath deuterium measurement and other near-subject methods. *Am. J. Clin. Nutr.* **76**, 1295–1301 (2002)
- Chan, C., McIntyre, C., Smith, D., Španěl, P., Davies, S.J.: Combining near-subject absolute and relative measures of longitudinal hydration in hemodialysis. *Clin. J. Am. Soc. Nephrol.* **4**, 1791–1798 (2009)
- Chan, C., Smith, D., Španěl, P., McIntyre, C.W., Davies, S.J.: A non-invasive, on-line deuterium dilution technique for the measurement of total body water in haemodialysis patients. *Nephrol. Dial. Transplant.* **23**, 2064–2070 (2008)
- Ferguson, E., Fehsenfeld, F., Schmeltekopf, A.: Flowing afterglow measurements of ion-neutral reactions. *Adv. At. Mol. Phys.* **5**, 1–56 (1969)
- Adams, N.G., Smith, D.: Selected ion flow tube (SIFT) - technique for studying ion-neutral reactions. *Int. J. Mass Spectrom. Ion Process.* **21**, 349–359 (1976)
- Španěl, P., Dittrichová, L., Smith, D.: FALP studies of the dissociative recombination coefficients for  $\text{O}_2^+$  and  $\text{NO}^+$  within the electron temperature range 300 K to 2000 K. *Int. J. Mass Spectrom. Ion Proc.* **12**, 183–191 (1993)
- Smith, D., Španěl, P.: Selected ion flow tube mass spectrometry (SIFT-MS) for on-line trace gas analysis. *Mass Spectrom. Rev.* **24**, 661–700 (2005)
- Španěl, P., Smith, D.: Progress in SIFT-MS; breath analysis and other applications. *Mass Spectrom. Rev.* (2010), doi:10.1002/mas.20303.
- Španěl, P., Smith, D.: Selected ion flow tube mass spectrometry (SIFT-MS) and flowing afterglow mass spectrometry (FA-MS) for the determination of the deuterium abundance in water vapour. In: de Groot, P.A. (ed.) *Handbook of Stable Isotope Analytical Techniques*, pp. 88–102. Elsevier, Amsterdam (2004)
- Španěl, P.: Flowing afterglow mass spectrometry (FA-MS) for the determination of the deuterium abundance in breath water vapour and aqueous liquid headspace. In: Smith, D., Amann, A. (eds.) *Breath Analysis for Clinical Diagnosis and Therapeutic Monitoring*, pp. 439–455. World Scientific, Singapore (2005)
- John, B., Tan, B.K., Dainty, S., Španěl, P., Smith, D., Davies, S.J.: Plasma volume, albumin, and fluid status in peritoneal dialysis patients. *Clin. J. Am. Soc. Nephrol.* **5**, 1463–1470 (2010)
- Asghar, R.B., Diskin, A.M., Španěl, P., Smith, D., Davies, S.J.: Influence of convection on the diffusive transport and sieving of water and small solutes across the peritoneal membrane. *J. Am. Soc. Nephrol.* **16**, 437–443 (2005)
- Asghar, R.B., Diskin, A.M., Španěl, P., Smith, D., Davies, S.J.: Measuring transport of water across the peritoneal membrane. *Kidney Int.* **64**, 1911–1915 (2003)
- Henchman, M., Smith, D., Adams, N.: Proton motion within proton-bound dimers:  $\text{H}_3\text{O}^+ \cdot \text{H}_2\text{O} \leftrightarrow \text{H}_2\text{O} \cdot \text{H}_3\text{O}^+$ ,  $\text{NH}_4^+ \cdot \text{NH}_3 \leftrightarrow \text{NH}_3 \cdot \text{NH}_4^+$  and  $\text{CH}_5^+ \cdot \text{CH}_4 \leftrightarrow \text{CH}_4 \cdot \text{CH}_5^+$  - a kinetic-model for isotope-exchange reactions. *Int. J. Mass Spectrom. Ion Process.* **109**, 105–132 (1991)
- Assonov, S.S., Brenninkmeijer, C.A.M.: A redetermination of absolute values for 17RVPDB-CO<sub>2</sub> and 17RVSMOW. *Rapid Commun. Mass Spectrom.* **17**, 1017–1029 (2003)
- Begley, I., Scrimgeour, C.: High-precision <sup>2</sup>H and <sup>18</sup>O measurement for water and volatile organic compounds by continuous-flow pyrolysis isotope ratio mass spectrometry. *Anal. Chem.* **69**, 1530–1535 (1997)
- Japas, M.L., Fernandez-Prini, R., Horita, J., Wesolowski, D.J.: Fractionation of isotopic species between coexisting liquid and vapor water: complete temperature range, including the asymptotic critical behavior. *J. Phys. Chem.* **99**, 5171–5175 (1995)
- Ross, B.: Sub-parts per billion detection of trace volatile chemicals in human breath using selected ion flow tube mass spectrometry. *BMC Res. Notes* **1**, 41 (2008)
- Smith, D., Pysanenko, A., Španěl, P.: Ionic diffusion and mass discrimination effects in the new generation of short flow tube SIFT-MS instruments. *Int. J. Mass Spectrom.* **281**, 15–23 (2009)
- Katsir, Y., Shapira, Y., Mastai, Y., Dimova, R., Ben-Jacob, E.: Entropic effects and slow kinetics revealed in titrations of D<sub>2</sub>O-H<sub>2</sub>O solutions with different D/H ratios. *J. Phys. Chem. B* **114**, 5755–5763 (2010)

**A3. Selected ion flow tube, SIFT, studies of the reactions of  $\text{H}_3\text{O}^+$ ,  $\text{NO}^+$  and  $\text{O}_2^+$  with some biologically active isobaric compounds in preparation for SIFT-MS analyses**

Smith D, Chippendale TWE, Španěl P. *Int J Mass Spectrom* 2011, 303:81-89.





# Selected ion flow tube, SIFT, studies of the reactions of $\text{H}_3\text{O}^+$ , $\text{NO}^+$ and $\text{O}_2^+$ with some biologically active isobaric compounds in preparation for SIFT-MS analyses

David Smith<sup>a</sup>, Thomas W.E. Chippendale<sup>a</sup>, Patrik Španěl<sup>a,b,\*</sup>

<sup>a</sup> Institute for Science and Technology in Medicine, School of Medicine, Keele University, Thornburrow Drive, Hartshill, Stoke-on-Trent ST4 7QB, UK

<sup>b</sup> J. Heyrovský Institute of Physical Chemistry, Academy of Sciences of the Czech Republic, Dolejškova 3, 182 23, Prague 8, Czech Republic

## ARTICLE INFO

### Article history:

Received 16 December 2010

Received in revised form 5 January 2011

Accepted 6 January 2011

Available online 14 January 2011

### Keywords:

SIFT-MS

Ion–molecule reactions

Proton transfer

Charge transfer

Three-body association

Isobaric compounds

## ABSTRACT

A study of the reactions of  $\text{H}_3\text{O}^+$ ,  $\text{NO}^+$  and  $\text{O}_2^+$  ions with two groups of four isobaric, biologically active compounds with molecular weights, MW, of 86u and 88u has been carried out using the selected ion flow tube, SIFT, technique in preparation for the analyses of these compounds in the headspace of bacterial and cell cultures using SIFT-MS. These compounds are: MW 86u: 2,3 butanedione (diacetyl),  $\text{C}_4\text{H}_6\text{O}_2$ ; allyl ethyl ether,  $\text{C}_5\text{H}_{10}\text{O}$ ; cyclopropane carboxylic acid,  $\text{C}_4\text{H}_6\text{O}_2$ ;  $\gamma$ -butyrolactone,  $\text{C}_4\text{H}_6\text{O}_2$ . MW 88u: 3-hydroxybutanone (acetoin),  $\text{C}_4\text{H}_8\text{O}_2$ ; n-butyric acid,  $\text{C}_4\text{H}_8\text{O}_2$ ; ethyl acetate,  $\text{C}_4\text{H}_8\text{O}_2$ ; pyruvic acid,  $\text{C}_3\text{H}_4\text{O}_3$ . All 24 reactions proceed at the gas kinetic rate, the dominant primary product ions of the  $\text{H}_3\text{O}^+$  reactions being the protonated reactant molecules,  $\text{MH}^+$  with a common mass-to-charge ratio,  $m/z$ , in each group of isobaric compounds; those of the  $\text{NO}^+$  reactions being the adduct ions,  $\text{NO}^+\text{M}$ , also with a common  $m/z$  value; for the  $\text{O}_2^+$  ion reactions, fragmentation ions of the nascent parent ion  $\text{M}^+$  are produced. SIFT-MS analysis of each compound individually is straightforward, but when more than one isobaric compound is present, SIFT-MS analyses become more challenging. However, hydration of some, but not all, of the primary  $\text{MH}^+$  and  $\text{NO}^+\text{M}$  primary ions occurs, variously generating  $\text{MH}^+(\text{H}_2\text{O})_{1,2}$  and  $\text{NO}^+\text{MH}_2\text{O}$  ions, and the occurrence/non-occurrence of these hydrates can assist in distinguishing between some of the isobaric compounds. From the kinetic data obtained in this study, the required SIFT-MS kinetics library entries for each compound can be constructed that allow their quantification. As an example, SIFT-MS spectra are presented relating to the analysis of the headspace of incubated yoghurt, which show the presence of several volatile organic compounds, including acetoin and diacetyl.

© 2011 Elsevier B.V. All rights reserved.

## 1. Introduction

Since its inception, selected ion flow tube mass spectrometry, SIFT-MS, [1–3] has been applied to the analysis of many gas phase media, notably humid exhaled breath and urine headspace, aimed at clinical diagnosis and therapeutic monitoring [4], bacterial cultures in medicine [5] and food and foods flavours [6,7]. In essence, this often requires the detection and quantification of a wide range of volatile organic compounds, VOCs, present in humid air at concentrations down to parts-per-billion by volume, ppbv. A major objective in the development of SIFT-MS has been to facilitate real time analyses of VOCs present in exhaled breath and those emitted from aqueous solutions and moist samples such as food products, obviating sample collection and manipulation with subsequent analysis, procedures that can compromise the samples. The grow-

ing literature on SIFT-MS studies demonstrates its unique utility, especially for breath analysis, as summarised in our recent reviews [2,8,9].

An essential requirement for SIFT-MS is an extensive kinetics library of rate coefficients and product ions for the gas phase reactions of the available precursor ions  $\text{H}_3\text{O}^+$ ,  $\text{NO}^+$  and  $\text{O}_2^+$  with a wide variety of VOCs that are present in naturally occurring media, because it is on these reactions that the analytical technique depends, especially accurate quantification [10]. We and others (see [11,12] and references therein) have given a great deal of time and effort to building and continuously extending the SIFT-MS kinetics library, by supplementing it as gas analysis is extended to encompass different areas of research and the monitoring of, for example, food freshness via VOC emissions when an increasing number of compounds are detected that need to be quantified [13]. In general, the media of interest are humid, in the case of exhaled breath it is saturated with water vapour at about 6% absolute humidity. Because of the presence of water vapour in the samples to be analysed, the  $\text{H}_3\text{O}^+$ ,  $\text{NO}^+$  and  $\text{O}_2^+$  precursor ions used for the analysis are partially converted to their hydrates  $\text{H}_3\text{O}^+(\text{H}_2\text{O})_{1,2,3}$ ,  $\text{NO}^+(\text{H}_2\text{O})_{1,2}$  and  $\text{O}_2^+(\text{H}_2\text{O})_{1,2}$ , by sequences of three-body reactions

\* Corresponding author at: J. Heyrovský Institute of Physical Chemistry, Academy of Sciences of the Czech Republic, Dolejškova 3, 182 23, Prague 8, Czech Republic. Tel.: +420 266052112; fax: +420 286582307.

E-mail addresses: [patrik.spanel@jh-inst.cas.cz](mailto:patrik.spanel@jh-inst.cas.cz), [spanel@seznam.cz](mailto:spanel@seznam.cz) (P. Španěl).

[14,15] and if these hydrates are not accounted for then erroneous analyses will result. Equally important is that the reactions of these hydrated ions with the trace compounds, M, can produce hydrated ions like  $MH^+(H_2O)_{1,2,3}$  and  $NO^+MH_2O$  and these must be recognised and included in the total of characteristic product ions for accurate analyses [10,14]. Furthermore, the primary products of the analytical reactions, especially  $MH^+$  ions, can undergo direct three-body association with  $H_2O$  molecules again producing  $MH^+(H_2O)_{1,2,3}$  ions. Therefore, when studying these ion/molecule reactions with a view to establishing SIFT-MS library entries, it is essential in the presence of water molecules (humid samples) to record all the products of the reactions, obviously including the primary products of the precursor ion reactions with M and also the hydrated product ions that form from them.

In our laboratories at Keele and Prague, not least prompted by our collaborations with local clinicians and groups in other universities and research institutes, we have initiated studies of the VOC emissions from cell cultures [16], bacterial cultures and processed cultures such as yoghurt, fermented meat [7], alcoholic beverages [17], and compounds involved in other biochemistries both *in vitro* and *in vivo*. In these endeavours, we are constantly recognising VOCs that we need to analyse for which SIFT-MS library entries are not yet available. Thus, we have seen that, for us, there are new compounds being observed for which kinetics library entries are required if they are to be analysed by SIFT-MS. We are also seeing that some of these biochemically related compounds have the same nominal molecular weight, MW, (isobaric compounds) and then the challenge is to identify them via the characteristic product ions that are likely to form using the available precursor ions in SIFT-MS. The essential points to recognise are that there is no pre-separation of trace compounds prior to analysis in SIFT-MS (as there is in GC-MS) and that the resolution of the analytical mass spectrometers on current SIFT-MS instruments is not sufficiently high to obtain fractional mass-to-charge ratios,  $m/z$ . Thus, to progress this analytical method, it is necessary to carry out a detailed study of the product ions of the reactions of such isobaric compounds with the SIFT-MS precursor ions in order to explore this potentially confounding ion chemistry and to see if differing characteristic product ions are formed with the three precursor ion species that might allow the separate identification of these isobaric compounds.

### 1.1. Compounds of interest

The compounds of interest in this study together with their molecular weights, MW, and their molecular formulae are the following: (see Table 1)

MW 88u: 3-hydroxybutanone (acetoin),  $C_4H_8O_2$ ; n-butyric acid,  $C_4H_8O_2$ ; ethyl acetate,  $C_4H_8O_2$ ; pyruvic acid,  $C_3H_4O_3$

MW 86u: 2,3 butanedione (diacetyl),  $C_4H_6O_2$ ; allyl ethyl ether,  $C_5H_{10}O$ ; cyclopropane carboxylic acid,  $C_4H_6O_2$ ;  $\gamma$ -butyrolactone,  $C_4H_6O_2$

Note that three of the four isobaric compounds in each of the two groups have the same molecular formula. The structural formula of each compound is given below in Tables 2 and 3. The selected ion flow tube, SIFT, technique was used previously to provide the basic kinetic data for the reactions of five of these eight compounds in support of the earliest SIFT-MS work [18–21], but in those early measurements the hydrated ions referred to above were not reported; this is now considered essential for accurate SIFT-MS analyses of humid samples and we pay some attention to this in this study. In general, the primary product ions of the reactions seen in the present studies conform to the results obtained previously, as will be remarked upon later when discussing the results. The new compounds not studied previously are acetoin, pyruvic acid and cyclopropane carboxylic acid.

Acetoin is used as an external energy store by a number of fermenting bacteria [22]. Along with diacetyl [23], it is one of the compounds giving butter its characteristic flavour. Acetoin is present in many fruits and vegetables and is used as food flavouring. Both compounds are quite volatile, the vapour having a pleasant odour and should readily be detected using SIFT-MS. They are added to margarine to give it a buttery flavour. Their molecular structures are sufficiently different (see Tables 2 and 3) suggesting that their chemistry may be sufficiently different to provide a means to distinguish between them by SIFT-MS. The structural isomeric compounds acetoin, ethyl acetate and butyric acid are also emitted from natural products including ripe fruit [24]. When these compounds coexist it will be a challenge to distinguish between them; to explore this is an objective of the study described here.

Pyruvic acid (in solution, its anion usually referred to as pyruvate) is the simplest volatile  $\alpha$ -keto acid and there are three active centres (see Table 2). For this alone its ion chemistry is worthy of study. Pyruvate is an important chemical compound in biochemistry. It is the output of the metabolism of glucose, viz. glycolysis, which provides energy for an organism; the detailed chemistry is described by the Krebs cycle [25].  $\gamma$ -Butyrolactone (or GBL) is often used as an aroma compound. In humans it acts as a pro-drug for  $\gamma$ -hydroxybutyrate, GHB, a naturally occurring substance found in the central nervous system and in almost all animals in small amounts, and is a component of some wines, beef, and small citrus fruits. GBL is also categorized as an illegal drug in many countries and it is used as a recreational intoxicant. Both pyruvic acid and GBL are volatile and might be detectable in the gas phase above natural products using SIFT-MS. Hence, the reason for studying the ion chemistry of these and the other six compounds listed above and given in Tables 2 and 3.

## 2. Experimental

Selected ion flow tube mass spectrometry, SIFT-MS, has been developed principally for the rapid, real time analysis of trace gases in air and exhaled breath [1,16]. The need for kinetic data on the reactions of the available precursor ions,  $H_3O^+$ ,  $NO^+$  and  $O_2^+$ , with any compound to be analysed is explained in detail in our previous review papers [2,3] and the method of quantification of trace compounds in humid air, including the involvement of water vapour in the ion chemistry, is treated in detail in two recent papers [10,26]. The currently used, most highly developed SIFT-MS instrument is the Profile 3 [26,27]. This analytical instrument can equally well be used as a SIFT instrument for the study of ion/molecule reactions under the very conditions that pertain to SIFT-MS, and it is the Profile 3 instrument (Instrument Science Limited, Crewe, UK) that was used for the present study. The precursor ions are formed in a microwave discharge source and the  $H_3O^+$ ,  $NO^+$  and  $O_2^+$  ions can be individually selected and injected into flowing helium carrier gas where they are convected along the flow tube as a thermalised swarm. These three ion species can also be injected together into the helium carrier gas by drastically lowering the resolution of the upstream mass filter, as is needed to determine the rate coefficients for the ion/molecule reactions (see below).

In order to identify the products of the reaction of each precursor ion with those neutral compounds (purchased from Sigma–Aldrich) included in this study, it is only necessary to inject the precursor ions and then to offer up the vapour of the solid or liquid present in the small compound container to the sampling port of the instrument, ensuring only that the flow rate of the sample of laboratory air/compound vapour is low enough that the fractional loss of precursor ions does not exceed a few percent (as required for any SIFT-MS analysis [10]). Then the downstream analytical mass spectrometer is operated in the full scan (FS) mode over a range of mass-to-charge-ratio,  $m/z$ , to encompass all precursor and product

ions and their hydrates and for a sufficient number of full scans to ensure appreciable count rates of all ions in the spectrum. In practice, 3 scans of 20 s duration is all that was required to accumulate data that allowed accurate product branching ratios to be obtained from the signal intensities of each ion on the spectrum. By targeting the known product ions using the multi-ion monitoring (MIM) mode of the SIFT-MS instrument, more accurate product ion distributions are obtained if required [3]. In the current instrument, the product ion intensities are corrected for mass discrimination and differential diffusion effects [26], which if ignored can seriously distort product ion ratios, especially when their  $m/z$  values are widely different.

Additional to these compound vapour analyses, and cognisant that most of the compounds included in this study would be encountered in the liquid phase, we chose to dissolve these compounds in water to explore their stability in the dissolved state, by analysing the headspace of the air/water vapour/compound vapour that developed above 50 ml of the solution contained in a glass bottle of volume about 200 ml sealed with a septum at about 20 °C. The headspace was sampled by puncturing the septa with a hypodermic needle coupled directly to the input port of the instrument. The molar concentrations of the solutions were chosen empirically such that sufficient concentrations of the VOCs were established above the solution; these concentrations are given in Tables 2 and 3. These vary, principally due to the differing Henry's Law (partition) coefficients of these compounds in aqueous solution. This solution approach was further prompted because acetoin existed as a mixture of its monomer and dimer, both of which are partially volatile and so the evolving vapour consists of a mixture of monomer and dimer molecules; more is said about this when discussing the reactions of acetoin. Concerning the pyruvic acid measurements, we found it beneficial to acidify the aqueous solution with hydrochloric acid in order to enhance the partition of this weaker fatty acid into the vapour phase, but this approach had interesting consequences, as described and discussed later. An added benefit of these solution studies was that the headspace sample was more humid than that of the lab air/compound vapour sample and so the hydrates of the product ions were more clearly defined on the SIFT spectra ensuring their positive detection. From these data the three-body rate coefficients for the formation of the monohydrates of the primary product ions were determined, as described later. Finally, a note of caution; if either the supplied compounds contain volatile impurities or if partial hydrolysis occurs in solution to generate new volatile compounds, then these may be seen at relatively high levels in the headspace of the solutions should they be more readily be partitioned into the vapour phase than is the major compound of interest.

To determine the rate coefficients for the reactions of the precursor ions with each compound, the vapour above its liquid/solid was introduced into the helium at sufficiently high flow rates to reduce the precursor ion count rates at the downstream mass spectrometer by about an order-of-magnitude or more [28]. Then plots of

the decay rates of the three precursor ions were constructed, and assuming that the rate coefficient of the exothermic proton transfer reactions of  $\text{H}_3\text{O}^+$  ions with all the eight compounds are collisional, then the rate coefficients for the  $\text{NO}^+$  and  $\text{O}_2^+$  ions can be obtained from the relative decay rates of these ions. This procedure has been justified and explained in detail in previous publications [18–20]. In this way, the rate coefficients for the reactions of  $\text{H}_3\text{O}^+$ ,  $\text{NO}^+$  and  $\text{O}_2^+$  have been determined with many types of compounds and thus a large kinetics library has been built up in support of SIFT-MS analyses (see [2,3] and the references therein).

### 3. Results and discussion

The collected data obtained in this study are given in four tables. Table 1 gives the two-body (binary) rate coefficients and the effective two-body rate coefficients for the primary reactions of the  $\text{H}_3\text{O}^+$ ,  $\text{NO}^+$  and  $\text{O}_2^+$  ions with the 8 compounds, M, involved in this study. Tables 2 and 3 present the data on the primary product ion distributions for the primary ion/molecule reactions, also indicating which of these primary products form hydrates, and Table 4 gives the derived three-body (ternary) rate coefficients for the association reactions of the protonated compounds,  $\text{MH}^+$ , with  $\text{H}_2\text{O}$  molecules.

#### 3.1. Binary rate coefficients

The proton affinities of all eight compounds generously exceed that of the water molecule and so proton transfer between  $\text{H}_3\text{O}^+$  and all eight compounds, M, is exothermic. So, as noted previously, it can be assumed that the rate coefficients,  $k$ , for these exothermic proton transfer reactions proceed at the collisional rate described by the collisional rate coefficient  $k_c$  [29]. The latter can be calculated according to the formulation given previously [30] if both the permanent dipole moment and the electric polarisability of the reactant molecule are known or if these parameters can be estimated as was needed for both acetoin and pyruvic acid. Using these physical parameters, the  $k_c$  values for the  $\text{NO}^+$  and  $\text{O}_2^+$  reactions can also be calculated; these  $k_c$  values are given in parentheses in Table 1 for the total of 24 reactions. Also given are the experimentally derived  $k$  values for the  $\text{NO}^+$  and  $\text{O}_2^+$  by the approach outlined in the previous section, where it can be seen that all these  $k$  values are very close to their respective  $k_c$  values. Thus, there are no inefficient reactions in this group of 24, which means that they can all be useful, in principle, for SIFT-MS analysis of these 8 compounds. These  $k$  values are used to construct the kinetics library entries for these compounds, as indicated later in this paper. The  $k$  values obtained in this study are in excellent agreement with those determined in previous SIFT studies for *n*-butyric acid, ethyl acetate [19], diacetyl [18], allyl ethyl ether [20] and  $\gamma$ -butyrolactone [21], as are the observed products of these reactions.

**Table 1**

The collisional rate coefficients,  $k_c$ , given in square brackets, for the reactions of  $\text{H}_3\text{O}^+$ ,  $\text{NO}^+$  and  $\text{O}_2^+$  with four isobaric compounds of molecular mass ( $m$ ) 88u, and four of molecular mass 86u, as calculated using their polarisabilities,  $\alpha$ , and their permanent dipole moments,  $\mu$ , [39] in the formulation given by Su and Chesnavich [30] together with experimentally derived rate coefficients,  $k$ , for the  $\text{NO}^+$  and  $\text{O}_2^+$  reactions; see the text and [18] for further explanation.

Compound	$m$ (u)	$\alpha$ ( $10^{-24}$ cm <sup>3</sup> )	$\mu$ (D)	$[k_c]$ ( $\text{H}_3\text{O}^+$ )	$k$ [ $k_c$ ] ( $\text{NO}^+$ )	$k$ [ $k_c$ ] ( $\text{O}_2^+$ )
3-Hydroxybutanone	88	8.8*	2.6	[3.7]	3.0 [3.1]	3.4 [3.0]
<i>n</i> -Butyric acid		10	1.8	[3.0]	2.4 [2.5]	2.6 [2.4]
Ethyl acetate		9.7	1.8	[2.9]	2.3 [2.4]	2.5 [2.4]
Pyruvic acid		6.6 <sup>a</sup>	2.3	[3.2]	2.1 [2.7]	2.8 [2.6]
2,3-Butanedione	86	8.2	0	[1.7]	1.4 [1.4]	1.5 [1.4]
Allyl ethyl ether		10.7	1.2	[2.5]	2.2 [2.1]	2.1 [2.0]
Cyclopropane carboxylic acid		10	1.8	[3.0]	2.1 [2.5]	2.4 [2.4]
$\gamma$ -Butyrolactone		8.5	3	[4.1]	3.5 [3.4]	3.9 [3.3]

**Table 2**

The percentages, %, of the primary product ions (in bold) of the reactions of  $\text{H}_3\text{O}^+$ ,  $\text{NO}^+$  and  $\text{O}_2^+$  with the four isobaric molecules indicated that have a common molecular weight, MW, of 88u. Also included in parentheses are the observed hydrates of the primary ions when they occur, that must be accounted for in SIFT-MS analyses of these compounds. These experimental data were obtained for the analyses of these compounds in the headspace of aqueous solutions; see the text. The ionisation energies of each compound in electron volts [31] are also given in *italics*.

Compound	Physical state	$\text{H}_3\text{O}^+$	$m/z$	$\text{NO}^+$	$m/z$	$\text{O}_2^+$	$m/z$
3-hydroxybutanone (acetoin) $\text{C}_4\text{H}_8\text{O}_2$ 9.4 <sup>a</sup>	Solid	$\text{C}_4\text{H}_9\text{O}_2^+$	100% <b>89</b> (107, 125)	$\text{C}_4\text{H}_8\text{O}_2\text{NO}^+$	80% <b>118</b>	$\text{C}_2\text{H}_5\text{O}^+$	85% <b>45</b> (63, 81)
3-hydroxybutanone (acetoin) $\text{C}_4\text{H}_8\text{O}_2$ 9.4 <sup>a</sup>	MP 15 °C solution 0.2M			$\text{C}_2\text{H}_5\text{O}^+$	10% <b>45</b> (63, 81)	$\text{C}_2\text{H}_3\text{O}^+$	15% <b>43</b>
				$\text{C}_4\text{H}_8\text{O}_2^+$	≤5% <b>88</b>		
				$\text{C}_4\text{H}_7\text{O}_2^+$	≤5% <b>87</b> (105)		
n-butyric acid $\text{C}_4\text{H}_8\text{O}_2$ 10.2	Liquid	$\text{C}_4\text{H}_9\text{O}_2^+$	95% <b>89</b> (107, 125)	$\text{C}_4\text{H}_8\text{O}_2\text{NO}^+$	80% <b>118</b> (136)	$\text{C}_2\text{H}_4\text{O}_2^+$	85% <b>60</b> (78, 96)
n-butyric acid $\text{C}_4\text{H}_8\text{O}_2$ 10.2	BP 163 °C solution 0.02 M	$\text{C}_4\text{H}_7\text{O}^+$	5% <b>71</b>	$\text{C}_4\text{H}_7\text{O}^+$	20% <b>71</b>	$\text{C}_3\text{H}_5\text{O}_2^+$	5% <b>73</b>
						$\text{C}_4\text{H}_8\text{O}_2^+$	5% <b>88</b> (106)
						$\text{C}_2\text{H}_3\text{O}^+$	≤5% <b>43</b>
Ethyl acetate $\text{C}_4\text{H}_8\text{O}_2$ 10.0	Liquid	$\text{C}_4\text{H}_9\text{O}_2^+$	100% <b>89</b> (107)	$\text{C}_4\text{H}_8\text{O}_2\text{NO}^+$	100% <b>118</b>	$\text{C}_2\text{H}_5\text{O}^+$	40% <b>61</b> (79, 97)
Ethyl acetate $\text{C}_4\text{H}_8\text{O}_2$ 10.0	BP 79 °C solution 0.1 M					$\text{C}_2\text{H}_5\text{O}^+$	20% <b>45</b> (63, 81)
						$\text{C}_4\text{H}_8\text{O}_2^+$	20% <b>88</b> (106)
						$\text{C}_2\text{H}_3\text{O}^+$	20% <b>43</b>
Pyruvic acid $\text{C}_3\text{H}_4\text{O}_3$ 9.9–10.4	Liquid	$\text{C}_3\text{H}_5\text{O}_3^+$	80% <b>89</b> (107,125,143)	$\text{C}_3\text{H}_4\text{O}_3\text{NO}^+$	100% <b>118</b> (136)	$\text{C}_2\text{H}_3\text{O}^+$	100% <b>43</b>
Pyruvic acid $\text{C}_3\text{H}_4\text{O}_3$ 9.9–10.4	BP 165 °C solution 2M	$\text{C}_2\text{H}_3\text{O}^+$	20% <b>43</b>				

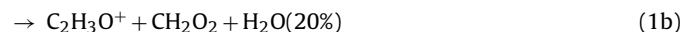
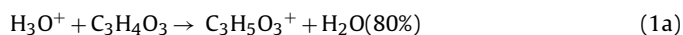
<sup>a</sup>Calculated ionisation energy [40].

### 3.2. Product ion distributions for the $\text{H}_3\text{O}^+$ , $\text{NO}^+$ and $\text{O}_2^+$ reactions

Insignificant differences are seen in the primary product ion distributions for all 24 reactions using the direct vapour on the one hand and the aqueous solution headspace on the other hand. Thus, in Tables 2 and 3 we list only the data obtained for the liquid headspace vapour analyses. Inspection of the data in these tables reveals that within each group of four isobaric compounds there is a high degree of commonality for the  $m/z$  values of the product ions (given in bold) for the  $\text{H}_3\text{O}^+$  and  $\text{NO}^+$  reactions, whilst there are clear differences in the products of the  $\text{O}_2^+$  reactions. Thus, the  $\text{O}_2^+$  reactions might be a route to the separate identification and analysis of the individual isobaric compounds when two or more are present in a sample, but this requires much further consideration. For some of these reactions there are minor product ions observed at the percentage level, but we omit these and place a lower limit of 5% of the reported primary product ions, as can be seen in the tables. Also indicated in parentheses in the tables are the  $m/z$  values of the observed hydrates of the primary product ions that should be included in the kinetics library entries to obtain accurate analyses of each compound. Included in the tables are the ionisation energies, IE, of the compounds, mostly known from experiments, but with two values derived theoretically as indicated. The IE for most compounds exceed that for the NO molecule, so charge exchange between ground state  $\text{NO}^+$  and these molecules is endothermic and cannot occur. For two of the compounds their IE is close to that of NO and these reactions are discussed below.

### 3.3. Isobaric compounds with MW 88u

The reaction of  $\text{H}_3\text{O}^+$  with all four compounds, M, proceed rapidly and the dominant primary product ion in all cases is the protonated parent molecule,  $\text{MH}^+$  (see Table 2). These primary product  $\text{MH}^+$  ions form hydrates, as is indicated in parentheses after each  $\text{MH}^+$  ion species, and the association reactions by which they form are discussed later in a separate section. In only the pyruvic acid reaction is a second significant primary product ion observed:



The neutral product in reaction channel (1b) is most probably a formic acid molecule,  $\text{HCOOH}$ . Noted in Table 2 is that a relatively high molar strength of pyruvic acid solution was required to generate a measurable headspace concentration. However, to enhance the headspace concentration the solution was acidified with the stronger hydrochloric acid. However, this acidification resulted in the production of methanol, which was readily measured in the headspace. After two days held at 37 °C the pyruvic acid in the acidified solution (headspace) had been largely removed and apparently totally converted to methanol. We cannot describe the complex solution phase chemistry that occurs, but occur it most surely does!

The other new data are for 3-hydroxybutanone, acetoin, which results in just one product ion. However, as stated earlier, the sample of acetoin consists of a mixture of its monomer (low melt-



**Table 3**

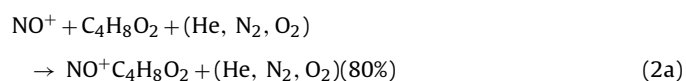
The percentages, %, of the primary product ions (in bold) of the reactions of  $\text{H}_3\text{O}^+$ ,  $\text{NO}^+$  and  $\text{O}_2^+$  with the four isobaric molecules indicated that have a common molecular weight, MW, of 86u. Also included in parentheses are the observed hydrates of the primary ions when they occur, that must be accounted for in SIFT-MS analyses of these compounds. These experimental data were obtained for the analyses of these compounds in the headspace of aqueous solutions; see the text. The ionisation energies of each compound in electron volts are also given in italics [31].

Compound	Physical state	$\text{H}_3\text{O}^+$	$m/z$	$\text{NO}^+$	$m/z$	$\text{O}_2^+$	$m/z$
2,3-butanedione (diacetyl) $\text{C}_4\text{H}_6\text{O}_2$ 9.3 2,3-butanedione (diacetyl) $\text{C}_4\text{H}_6\text{O}_2$ 9.3	Liquid BP 88 °C solution 0.05M	$\text{C}_4\text{H}_7\text{O}_2^+$ 100%	<b>87</b> (105, 123)	$\text{C}_4\text{H}_6\text{O}_2^+$ 75%	<b>86</b>	$\text{C}_2\text{H}_3\text{O}^+$ 65%	<b>43</b>
Allyl ethyl ether $\text{C}_5\text{H}_{10}\text{O}$ 9.6*	Liquid BP 66 °C solution 0.01M	$\text{C}_5\text{H}_{11}\text{O}^+$ 75%	<b>87</b> (105)	$\text{C}_4\text{H}_6\text{O}_2\text{NO}^+$ 25% $\text{C}_5\text{H}_9\text{O}^+$ 95%	<b>116</b> <b>85</b>	$\text{C}_4\text{H}_6\text{O}_2^+$ 35% $\text{C}_3\text{H}_6\text{O}^+$ 70%	<b>86</b> <b>58</b> (76, 94)
Allyl ethyl ether $\text{C}_5\text{H}_{10}\text{O}$ 9.6*		$\text{C}_3\text{H}_7\text{O}^+$ 15% $\text{C}_2\text{H}_5\text{O}^+$ 10%	<b>59</b> (77, 95) <b>45</b> (63, 81)			$\text{C}_5\text{H}_{10}\text{O}^+$ 15% $\text{C}_3\text{H}_5\text{O}^+$ 10% $\text{C}_3\text{H}_5^+$ ≤5%	<b>86</b> <b>57</b> (75) <b>41</b>
Cyclopropane carboxylic acid $\text{C}_4\text{H}_6\text{O}_2$ 10.6 Cyclopropane-carboxylic acid $\text{C}_4\text{H}_6\text{O}_2$ 10.6	Liquid BP 183 °C solution 0.5 M	$\text{C}_4\text{H}_7\text{O}_2^+$ 90%	<b>87</b> (105, 123)	$\text{C}_4\text{H}_6\text{O}_2\text{NO}^+$ 60%	<b>116</b> (134)	$\text{C}_4\text{H}_6\text{O}_2^+$ 35%	<b>86</b> (104)
$\gamma$ -butyrolactone $\text{C}_4\text{H}_6\text{O}_2$ 10.3 $\gamma$ -butyrolactone $\text{C}_4\text{H}_6\text{O}_2$ 10.3	Liquid BP 206 °C solution 0.5 M	$\text{C}_4\text{H}_7\text{O}_2^+$ 100%	<b>87</b> (105, 123)	$\text{C}_4\text{H}_6\text{O}_2\text{NO}^+$ 100%	<b>116</b>	$\text{C}_4\text{H}_5\text{O}_2^+$ 20% $\text{C}_4\text{H}_5\text{O}^+$ 20% $\text{C}_2\text{H}_2\text{O}_2^+$ 15% $\text{C}_3\text{H}_6^+$ 10% $\text{C}_2\text{H}_2\text{O}^+$ or $\text{C}_3\text{H}_3^+$ 80%	<b>85</b> (103) <b>69</b> (87) <b>58</b> (76) <b>42</b> <b>42</b> (60)
		$\text{C}_4\text{H}_5\text{O}^+$ 10%	<b>69</b>	$\text{C}_4\text{H}_5\text{O}^+$ 40%	<b>69</b>	$\text{C}_4\text{H}_6\text{O}_2^+$ 20%	<b>86</b>

<sup>a</sup>Calculated ionization energy from [41]

ing point, coloured yellow) and its dimer (higher melting point, white crystals) and a wide  $m/z$  scan using both  $\text{H}_3\text{O}^+$  and  $\text{NO}^+$  precursor ions clearly revealed the presence of the dimer in the headspace vapour, but at a much lower concentration than that of the monomer. On vacuum pumping above the composite material the volatile monomer was gradually removed by evaporation leaving only the white crystalline acetoin dimer. When the latter was dissolved in water the headspace vapour contained only monomer acetoin molecules indicating that this dimer had dissociated in aqueous solution. Hence, the data given in Table 2 were obtained for this solution headspace. The results for the n-butyric acid and ethyl acetate are in good agreement with previous SIFT data obtained several years ago [19].

In all the  $\text{NO}^+$  reactions the major primary product ion, or the only product ion, is the adduct  $\text{NO}^+\text{M}$ , which form very efficiently at the gas kinetic rate (see Table 1) mediated by the He carrier gas atoms and the major air molecules. The acetoin reaction is the most complex:



Reaction channel (2b) involves the abstraction of the  $\text{CH}_3\text{CO}$  group from the acetoin molecule (see the structure of acetoin in Table 2). The minor channels proceed via slightly endothermic charge transfer (2c), which is possible because of the proximity of the ionisation energies of the acetoin molecule (9.4 eV [31]) and the recombination energy of  $\text{NO}^+$  (9.26 eV [31]), and the well-known process of hydride ion ( $\text{H}^-$ ) transfer (2d). The minor channel observed in the  $\text{NO}^+$ /butyric acid reaction proceeds via hydroxyl ion

**Table 4**

Kinetic data for the formation of hydrates of the protonated compounds indicated, as formed by ligand switching and three-body association. See the text.

Compound	No. of functional groups	$A_{\text{eff}}^a$	$k_3$ ( $10^{-27} \text{ cm}^6 \text{ s}^{-1}$ ) <sup>b</sup>
3-Hydroxybutanone	1	$1.8 \pm 0.1$	$0.8 \pm 0.3$
n-Butyric acid	2	$10.1 \pm 4.4$	$5.8 \pm 2.6$
Ethyl acetate	1	$5.8 \pm 0.8$	$3.3 \pm 0.6$
Pyruvic acid	3	$13.5 \pm 0.8$	$7.8 \pm 0.6$
2,3-Butanedione	2	$7.2 \pm 0.1$	$4.1 \pm 0.1$
Allyl ethyl ether	1	$6.2 \pm 0.1$	$3.5 \pm 0.1$
Cyclopropane carboxylic acid	2	$8.5 \pm 0.3$	$4.9 \pm 0.3$
$\gamma$ -Butyrolactone	2	$4.9 \pm 0.3$	$2.7 \pm 0.3$

<sup>a</sup> Association efficiency calculated from the experimental data. The uncertainties correspond to the differences between the results from the experiment using the vapours from the neat compounds and those obtained using the headspace of aqueous solutions.

<sup>b</sup> Three-body association rate coefficients estimated from  $A_{\text{eff}}$  using the theoretical maximum contribution of ligand switching reactions [35] and an assumed value of  $k_{\text{H}_3\text{O}^+}$ ; see the text.

(OH<sup>-</sup>) transfer. These last two reaction processes commonly occur in many NO<sup>+</sup> reactions with organic compounds containing an –OH group [3,19].

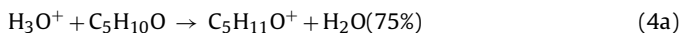
The O<sub>2</sub><sup>+</sup> reactions mostly proceed via dissociative charge transfer producing fragment ions, although the parent cation represents 20% of the total product ions in the ethyl acetate reaction. The pyruvic acid reaction apparently results in a single product ion:



Here, the centre C–C bond is cleaved producing the observed ion at *m/z* 43 and a formic acid molecule. The single product ion is surely CH<sub>3</sub>CO<sup>+</sup>, as indicated, and we know from numerous SIFT studies that this ion does not hydrate under SIFT and SIFT-MS conditions and none is seen to be formed as a secondary product. More will be said about hydration later in a separate section. It should also be reported here that in our much earlier paper [19] we reported that a product ion at an *m/z* value of 31 was seen in the O<sub>2</sub><sup>+</sup>/ethyl acetate reaction, yet we do not see this in the present study. Therefore, we accept that the previous report of this product ion, identified as CH<sub>3</sub>O<sup>+</sup>, is in error, and this is further evidenced by the fact that an ion at *m/z* 31 is not seen in the NIST library electron ionisation spectrum [32]. No further comment is necessary on these O<sub>2</sub><sup>+</sup> reactions.

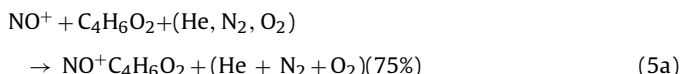
#### 3.4. Isobaric compounds with MW 86u

As for the previous four compounds, the reaction of H<sub>3</sub>O<sup>+</sup> of these four compounds, M, proceed rapidly and again the dominant primary product ion in all cases is the protonated parent molecule, MH<sup>+</sup> (see Table 3) that invariably form hydrates, as is indicated. The most complex of these reactions is that of allyl ethyl ether which, unusually for exothermic proton transfer, results in three product ions:



Note the release of the hydrocarbon molecules and the production of the RO<sup>+</sup> ions that readily hydrate (see Table 3). The protonated cyclopropane carboxylic acid partially releases an H<sub>2</sub>O molecule leaving an RC=O<sup>+</sup> ion which rarely hydrate. The two ketones remain intact after protonation, as is usually the case.

The NO<sup>+</sup> reactions with these four MW 86u isobaric compounds are more varied than the NO<sup>+</sup> reactions with the MW 88u compounds. In the γ-butyrolactone reaction the single product ion is the NO<sup>+</sup>M adduct formed by association in the corresponding way to reaction (2a). The single product ion in the allyl ethyl ether reaction is the result of hydride ion abstraction, a process commonly seen in the reactions of NO<sup>+</sup> with alkenes [33]. In both the 2,3-butanedione and the cyclopropane carboxylic acid reactions, adduct ion formation is the major channel, but in the former reaction charge transfer competes with adduct formation:



Charge transfer is energetically allowed because the IE of 2,3-butanedione at 9.3 eV [31] is only slightly greater than the recombination energy of NO<sup>+</sup>. In the cyclopropane carboxylic acid reaction, hydroxide ion transfer produces C<sub>4</sub>H<sub>5</sub>O<sup>+</sup> ions and nitrous acid, HNO<sub>2</sub> molecules. Note that the product ion RC=O<sup>+</sup> does not hydrate, as predicted.

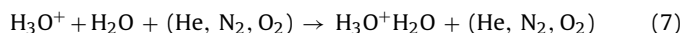
In all four O<sub>2</sub><sup>+</sup> reactions the parent cations are significant products and multiple fragmentation products are evident in most (see Table 3). An interesting point is that a product ion at *m/z* 42 is seen in both the cyclopropane carboxylic acid and the γ-butyrolactone reactions. In the former reactions this ion must be C<sub>3</sub>H<sub>6</sub><sup>+</sup>, but in the latter reaction it could be either C<sub>3</sub>H<sub>6</sub><sup>+</sup> or C<sub>2</sub>H<sub>2</sub>O<sup>+</sup>, but note that this product ion hydrates (Table 3) and so we favour the production of a C<sub>2</sub>H<sub>2</sub>O<sup>+</sup> ion and a C<sub>2</sub>H<sub>4</sub>O neutral molecule. The results for the product distributions for the 2,3-butanedione and γ-butyrolactone reactions are in good agreement with previous SIFT data obtained several years ago [18,21].

#### 3.5. Hydration of the primary product ions MH<sup>+</sup> and NO<sup>+</sup>M

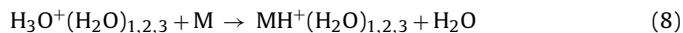
At several points in the presentation and discussion of the data obtained in this study we have referred to the hydration of the primary product ions and how this is dependent on the structure of the ion. Now we focus only on the protonated parent compounds, MH<sup>+</sup>, formed in the H<sub>3</sub>O<sup>+</sup> reactions and consider the efficiency of the first step of hydration via the three-body association reaction:



H<sub>3</sub>O<sup>+</sup> and its hydrates H<sub>3</sub>O<sup>+</sup>(H<sub>2</sub>O)<sub>1,2,3</sub> are always the dominant ions on the SIFT spectra and the distribution of these ions provides a measurement of the humidity of the sample being analysed [34]. In the present measurements using the laboratory air/compound vapour mixture the water vapour content was typically 1.5% whereas when analysing the aqueous solutions in the sealed bottles the water vapour content was typically 3%. The initial hydration reaction is:



The three-body rate coefficient for reaction (7) has been previously determined to be  $K_{\text{H}_3\text{O}^+} = 6 \times 10^{-28} \text{ cm}^6 \text{ s}^{-1}$  [34]. By a sequence of similar reactions the H<sub>3</sub>O<sup>+</sup>(H<sub>2</sub>O)<sub>2,3</sub> hydrates are formed. In addition to reaction (6), the MH<sup>+</sup>(H<sub>2</sub>O) ions can be formed via ligand switching reactions involving the H<sub>3</sub>O<sup>+</sup>(H<sub>2</sub>O)<sub>1,2,3</sub> cluster ions [35]:



So these hydrated protonated molecules MH<sup>+</sup>(H<sub>2</sub>O)<sub>1,2,3</sub> can be produced by two routes. Since reactions (6)–(8) occur in parallel, then measurements of the count rates of each of the ions involved in the ion chemistry contain the information required to calculate the three-body rate coefficients,  $k_{\text{MH}^+}$ , of the hydration reaction (6). Essentially, this involves comparison of the efficiencies of reactions (6) and (7) expressed by a dimensionless association efficiency coefficient,  $A_{\text{eff}}$ , [14] describing how efficiently the product ions form hydrates with respect to H<sub>3</sub>O<sup>+</sup>. The value of  $A_{\text{eff}}$  is obtained experimentally from the ratio of the count rates of MH<sup>+</sup> to the total count rate MH<sup>+</sup>(H<sub>2</sub>O)<sub>1,2,3</sub> taken relatively to a corresponding ratio for H<sub>3</sub>O<sup>+</sup> and its hydrates. Details of this calculation, including all equations and numerical examples, are given in a recent paper on ion chemistry of esters released by plants [36]. The value of  $A_{\text{eff}}$  should be invariant with the sample humidity for a given compound concentration (or its flow rate into the helium carrier gas) and this has been validated in the present experiments by calculating its value at two different humidities, as realized using the direct vapour measurements and the aqueous solutions of the compounds, as referred to in Section 2. The contribution of the switching reactions (8) to  $A_{\text{eff}}$  can be calculated theoretically, assuming collisional rate coefficients for reaction (8), and it has a typical value of  $S_{\text{eff}} = 0.4$  [14,36]. The  $k_{\text{MH}^+}$  values are then obtained as  $(A_{\text{eff}} - S_{\text{eff}})k_{\text{H}_3\text{O}^+}$  and the

results for the 8 compounds included in this study are given in Table 4.

Note that the hydration rates of these protonated compounds are more efficient than the hydration rate of  $\text{H}_3\text{O}^+$  ions, so production of  $\text{MH}^+$  hydrates is inevitable in SIFT-MS. If these hydrates are not accounted for in SIFT-MS analyses, erroneously low quantification of these compounds will result. Note in Tables 2 and 3 that dihydrates of the  $\text{MH}^+$  ions are usually formed and that the trihydrate of protonated pyruvic acid is seen; all these hydrates must be included in the analyses. The data in Table 4 reveals that the protonated compounds with the most active sites tend to hydrate most efficiently. Thus, protonated pyruvic acid most efficiently adds a water molecule, presumably because there are three active sites in this molecule, and the hydration of the two protonated fatty acids that have two active sites is also relatively efficient. Hydration of the protonated ester, ether and ketones is relatively less efficient. Whilst this is not the basis of a hard-and-fast rule, observation of hydration rates of a particular protonated molecule can give a clue to the nature of the molecule.

Concerning hydration of the adduct product ions of the  $\text{NO}^+$  reactions,  $\text{NO}^+\text{M}$ . A glance at Table 2 shows that the two acid molecule adducts do form hydrates  $\text{NO}^+\text{MH}_2\text{O}$ , whereas the  $\text{NO}^+$  adduct of the hydroxyketone and the ester do not form hydrates under the conditions of SIFT-MS. Similarly, it can be seen in Table 3 that, again, the acid molecule adducts form hydrates whereas the two ketones and the ether adducts do not. This has its parallel in the  $\text{MH}^+$  hydration, as can be seen in Table 4. Such features can assist analyses of isobaric compounds, and this has been carried out to great effect in distinguishing acetic acid from the isobaric methyl formate [37], which has allowed the definite detection and quantification of acetic acid in exhaled human breath [38].

### 3.6. Kinetics library entries for the MW 86u and MW 88u compounds

From the kinetics data given in Table 1 (rate coefficients) and the  $m/z$  values for primary product ions and their hydrates (Tables 2 and 3), SIFT-MS kinetics library entries can be constructed for these eight compounds, as appropriate to the Profile 3 instrument. The kinetic library entries for acetoin and for diacetyl are given in Table 5. These entries define the coefficients specific for each compound that should be used in the equations given in [10]

**Table 5**

SIFT-MS kinetics library entries in the format required by the SIFT-MS software for on-line calculations of the concentrations of acetoin and diacetyl using both  $\text{H}_3\text{O}^+$  and  $\text{NO}^+$  precursor ions.

Acetoin ( $\text{H}_3\text{O}^+$ )	Diacetyl ( $\text{H}_3\text{O}^+$ )
4 Precursors	4 Precursors
19 3.7e–91.0	19 1.7e–9 1.0
37 3.0e–91.0	37 1.3e–9 1.0
55 2.4e–91.0	55 1.0e–9 1.0
73 1.5e–91.0	73 0.6e–9 1.0
3 Products	3 Products
89 1.0	87 1.0
107 1.0	105 1.0
125 1.0	123 1.0
Acetoin ( $\text{NO}^+$ )	Diacetyl ( $\text{NO}^+$ )
3 Precursors	3 Precursors
30 3.0e–91.0	30 1.4e–91.0
48 2.6e–91.0	48 1.1e–91.0
66 2.2e–91.0	66 0.8e–91.0
4 Products	2 Products
45 1.0	861.0
63 1.0	1161.0
81 1.0	
118 1.0	

for the absolute quantification of the concentrations of trace compounds present in humid air. Each row in the precursors section gives the  $m/z$  of each precursor ion followed by the rate coefficient for its reaction with the given compound and terminated by a coefficient by which the ion count rate should be multiplied (normally 1.0, meaning that the total ion count obtained at that  $m/z$  value should be included). Rows in the products section again give the  $m/z$  values for each product ion followed by a similar multiplication coefficient. In this case the calculation simply involves the sum of the count rates of all product ions of the reactions together with their hydrates.

Note that in the case of these MW 86u and MW 88u compounds it is not possible to construct reliable kinetics library entries that would automatically and separately quantify their concentrations when two or more of them are simultaneously present in a sample. This is because the degree of overlap at the dominant product ions ( $m/z$  87,  $m/z$  89,  $m/z$  116 and  $m/z$  118) is too great. Thus, for example, the entry acetoin ( $\text{H}_3\text{O}^+$ ) from Table 5 will provide calculation of the total concentration of acetoin, all isomers of butyric and pyruvic acids and ethyl acetate, in principle giving an upper limit to the concentration of any of the individual compounds. However, careful examination of the SIFT-MS mass spectra obtained using all three precursor ions, with reference to the branching ratio data given in this paper and considering the relative count rates of the hydrated ions, can help the researchers to narrow down the list of the isobaric compounds that are present. It is strongly recommended that if only selected characteristic product ions are used to determine the concentration of a particular compound rather than all the characteristic ions and their hydrates, then the branching ratio for the primary product ions and any hydrates formed in the reaction of the chosen precursor ion with the particular compound should be experimentally determined under identical conditions of sample humidity to those used in the actual analysis.

## 4. A case study of VOCs present in the headspace of incubated yoghurt

This reaction kinetics study follows our well-established procedure by which the SIFT-MS the kinetics library is extended to encompass new compounds. The compounds included in the present study reflect the extension of our research work into the analysis of VOCs emitted from cell and bacterial cultures *in vitro*, and also the probing by breath analysis of lung cancer [38] and respiratory infection [5]. To demonstrate the utility of SIFT-MS and some of the new kinetic library entries given above, we show in Fig. 1 the SIFT-MS spectra obtained for the analysis of the headspace of supermarket probiotic yoghurt contained in a glass bottle that has been held at 37 °C for 2 weeks. Fig. 1a is the spectrum obtained using  $\text{H}_3\text{O}^+$  precursor ions and Fig. 1b is that obtained using  $\text{NO}^+$  ions; each spectrum is a composite of only 3 spectral scans of 20 s duration. The richness of these spectra is clear, some 8 compounds being immediately identified by their characteristic product ion  $m/z$  values. The headspace concentrations given in the figures have been obtained using existing library entries and the new entries for acetoin (3-hydroxybutanone) and diacetyl (2,3-butanedione), both compounds (known to be present in the headspace of fermented milk from previous GC–MS studies [22,23]) being seen on both the  $\text{H}_3\text{O}^+$  and  $\text{NO}^+$  spectra. These spectra are included as examples of how the VOC emissions from these bacterial cultures can simply and rapidly be investigated. The concentrations of the compounds in the headspace relate only to this particular yoghurt and its treatment. Note that the ammonia concentration is relatively low in the headspace, but this will be sensitively dependent of the pH of the yoghurt medium.

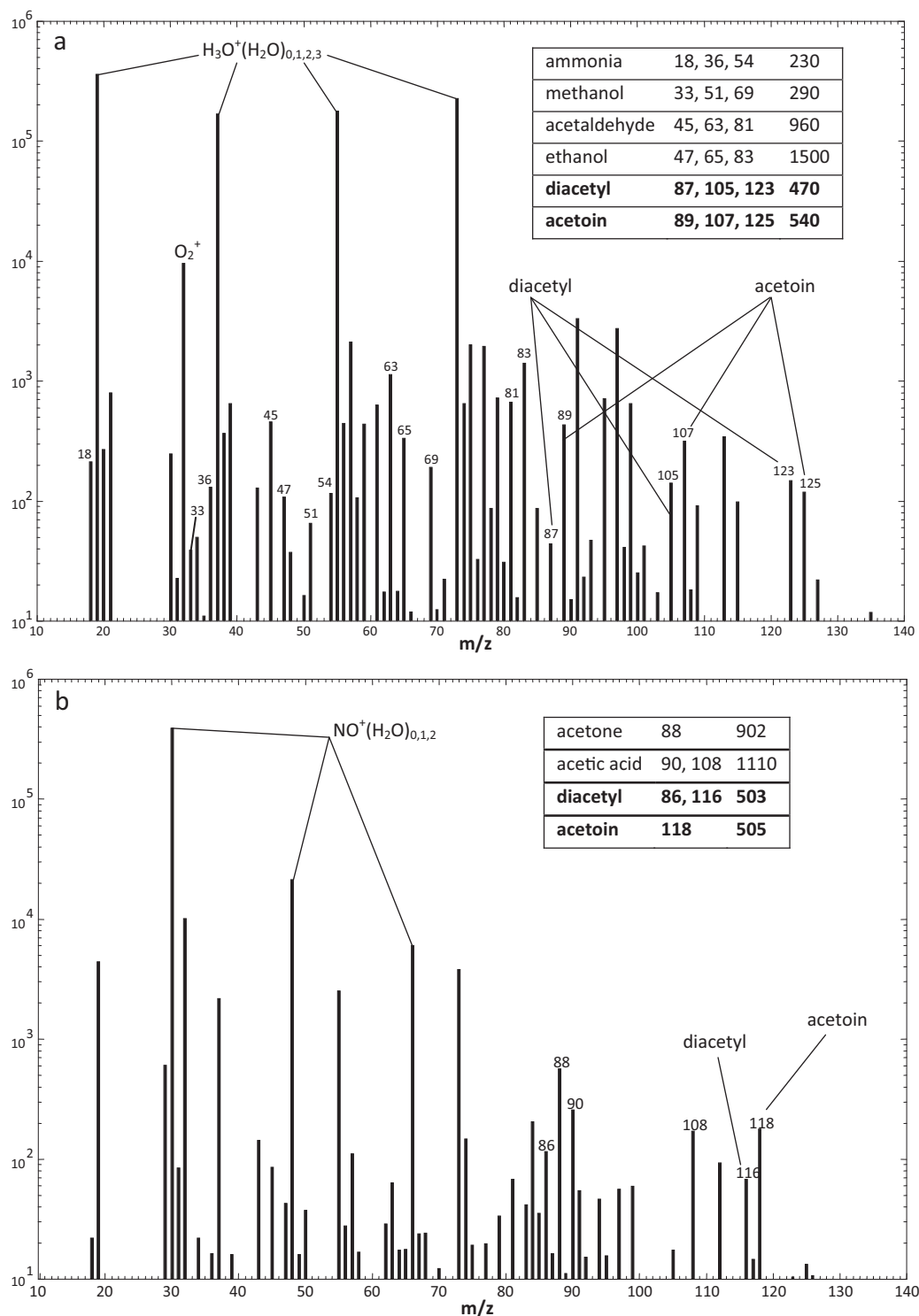


**Fig. 1.** Full scan (FS) SIFT-MS spectra (ion counts per second, c/s, against mass-charge-ratio,  $m/z$ ) obtained using (a)  $\text{H}_3\text{O}^+$  and (b)  $\text{NO}^+$  precursor ions for the analysis of the headspace above a commercially available probiotic yoghurt sample following incubation at  $37^\circ\text{C}$  for 2 weeks. Some of the readily identifiable compounds are indicated in the tables along with the  $m/z$  values of their characteristic product ions and their partial pressures in the headspace in parts-per-billion, ppb. Two of the compounds studied in detail in this paper, acetoin and diacetyl, are highlighted. Further explanation is given in the text.

## 5. Summary and concluding remarks

The choice of the isobaric compounds included in this study was predicated on those that are often met in biological media and fluids. The compounds present in each of the MW 86u and MW 88u groups can now readily be analysed by SIFT-MS when in isolation; then spectral  $m/z$  overlaps are not a problem. But when two or

more isobaric compounds are present in a sample, overlaps will inevitably occur, since when using  $\text{H}_3\text{O}^+$  precursor ions the major primary ion formed is  $\text{MH}^+$ , obviously having a common  $m/z$  value, and when using  $\text{NO}^+$  precursor ions the common primary product is the  $\text{NO}^+\text{M}$  adduct ion. However, all is not lost, because compound types can be distinguished by their degree of hydration, for example, protonated carboxylic acids are efficiently hydrated forming



their monohydrate and a dihydrate by the water vapour molecules that are inevitably present in real media, whereas protonated esters and ethers are more slowly hydrated producing only a monohydrate under SIFT-MS conditions. Perhaps the use of  $\text{NO}^+$  precursor ions holds more promise to distinguish between these isobaric compounds. For some specific compound types, the  $\text{NO}^+\text{M}$  common primary product ion of these reactions readily hydrate to form  $\text{NO}^+\text{MH}_2\text{O}$  ions, a process that is efficient when M is a carboxylic acid but does not occur when M is an ester, ether and a ketone. These tendencies are apparent in the data in Tables 2, 3 and 4, but it should be stressed that we do not have sufficient data to consider these trends to necessarily encompass all compounds. Hydration also occurs for some of the products of the  $\text{O}_2^+$  reactions with M, but these are not so readily utilized for analysis because multiple productions usually result from these reactions. Nevertheless, the analytical spectra obtained using  $\text{O}_2^+$  precursor ions can sometimes be useful as supplementary data to support compound identification.

Automated analyses of SIFT-MS data containing mixtures of isobaric compounds are clearly desirable. However, at the current state-of-the-art there is no substitute for careful examination of the full scan analytical mass spectra in the initial phases of any study using SIFT-MS. On the basis of such examinations, noting the important directions given in the last paragraph of Section 3.6, perhaps one or two characteristic product ions can be chosen from several (including hydrates) for inclusion in the kinetics database, in order to facilitate very efficient, high throughput quantification of the chosen compounds using the multiple ion monitoring mode of operation of SIFT-MS.

## Acknowledgements

Thomas Chippendale would like to acknowledge the financial support of the EPSRC and the Regenerative Medicine DTC programme. We also acknowledge partial financial support by the Grant Agency of the Czech Republic (projects number 202/09/0800 and 203/09/0256)

## References

- [1] P. Španěl, D. Smith, *Med. Biol. Eng. Comput.* 34 (1996) 409–419.
- [2] P. Španěl, D. Smith, *Mass Spectrom. Rev.*, in press.
- [3] D. Smith, P. Španěl, *Mass Spectrom. Rev.* 24 (2005) 661–700.
- [4] A. Amann, D. Smith, *Breath Analysis for Clinical Diagnosis and Therapeutic Monitoring*, World Scientific, Singapore, 2005, p. 536.
- [5] W. Carroll, W. Lenney, T.S. Wang, P. Španěl, A. Alcock, D. Smith, *Pediatr. Pulmonol.* 39 (2005) 452–456.
- [6] P. Španěl, D. Smith, *Rapid Commun. Mass Spectrom.* 13 (1999) 585–596.
- [7] A. Olivares, K. Dryahina, J.L. Navarro, M. Flores, D. Smith, P. Španěl, *Anal. Chem.* 82 (2010) 5819–5829.
- [8] D. Smith, C. Turner, P. Španěl, *J. Breath Res.* (2007) 014004.
- [9] D. Smith, P. Španěl, *Analyst* 132 (2007) 390–396.
- [10] P. Španěl, K. Dryahina, D. Smith, *Int. J. Mass Spectrom.* 249 (2006) 230–239.
- [11] F. Dhoghe, C. Amelynck, N. Schoon, E. Debie, P. Bultinck, F. Vanhaecke, *Int. J. Mass Spectrom.* 272 (2008) 137–148.
- [12] L. Iachetta, L. Malek, B. Ross, *Rapid Commun. Mass Spectrom.* 24 (2010) 815–822.
- [13] A. Onal, *Food Chem.* 103 (2007) 1475–1486.
- [14] P. Španěl, D. Smith, *Rapid Commun. Mass Spectrom.* 14 (2000) 1898–1906.
- [15] P. Španěl, D. Smith, *Int. J. Mass Spectrom.* 280 (2009) 128–135.
- [16] J. Sule-Suso, A. Pysanenko, P. Španěl, D. Smith, *Analyst* 134 (2009) 2419–2425.
- [17] K. Dryahina, F. Pehal, D. Smith, P. Španěl, *Int. J. Mass Spectrom.* 286 (2009) 1–6.
- [18] P. Španěl, Y.F. Ji, D. Smith, *Int. J. Mass Spectrom.* 165 (1997) 25–37.
- [19] P. Španěl, D. Smith, *Int. J. Mass Spectrom.* 172 (1998) 137–147.
- [20] P. Španěl, D. Smith, *Int. J. Mass Spectrom.* 172 (1998) 239–247.
- [21] T.S. Wang, P. Španěl, D. Smith, *Int. J. Mass Spectrom.* 237 (2004) 167–174.
- [22] D. Zareba, M. Ziarno, M. Obiedzinski, A. Bzducha, *ZYW. Nauk Technol. Jakosc.* 15 (2008) 60–73.
- [23] V. Macciola, G. Candela, A. De Leonardi, *Food Control* 19 (2008) 873–878.
- [24] C. Visai, M. Vanoli, *Sci. Hortic.* 70 (1997) 15–24.
- [25] D. Voet, J.G. Voet, C.W. Pratt, *Principles of Biochemistry: Life at the Molecular Level 3rd International Student Edition Ed.*, John Wiley & Sons, New York, 2005.
- [26] D. Smith, A. Pysanenko, P. Španěl, *Int. J. Mass Spectrom.* 281 (2009) 15–23.
- [27] [www.instrumentscience.com](http://www.instrumentscience.com), last accessed on December 2010.
- [28] D. Smith, N. Adams, *Adv. Atom. Mol. Phys.* 24 (1988) 1–49.
- [29] G. Bouchoux, J.Y. Salpin, D. Leblanc, *Int. J. Mass Spectrom. Ion Process.* 153 (1996) 37–48.
- [30] T. Su, W.J. Chesnavich, *J. Chem. Phys.* 76 (1982) 5183–5185.
- [31] S.G. Lias, Ionization energy evaluation, in: P.J. Linstrom, W.G. Mallard (Eds.), *NIST Chemistry WebBook, NIST Standard Reference Database Number 69*, National Institute of Standards and Technology, Gaithersburg, 2010.
- [32] S.E. Stein, Mass spectra, in: P.J. Linstrom, W.G. Mallard (Eds.), *NIST Chemistry WebBook, NIST Standard Reference Database Number 69*, National Institute of Standards and Technology, Gaithersburg, 2010.
- [33] A.M. Diskin, T.S. Wang, D. Smith, P. Španěl, *Int. J. Mass Spectrom.* 218 (2002) 87–101.
- [34] P. Španěl, D. Smith, *Rapid Commun. Mass Spectrom.* 15 (2001) 563–569.
- [35] P. Španěl, D. Smith, *J. Phys. Chem.* 99 (1995) 15551–15556.
- [36] K. Sovová, K. Dryahina, P. Španěl, *Int. J. Mass Spectrom.*, in press.
- [37] A. Pysanenko, P. Španěl, D. Smith, *Int. J. Mass Spectrom.* 285 (2009) 42–48.
- [38] D. Smith, P. Španěl, J. Sule-Suso, *Expert Rev. Mol. Diagn.* 10 (2010) 255–257.
- [39] <http://www.thegoodscentscompany.com/>, last accessed on October 2010.
- [40] F. Battin-Leclerc, O. Herbinet, P. Glaude, R. Fournet, Z. Zhou, L. Deng, H. Guo, M. Xie, F. Qi, *Proceedings of the Combustion Institute*, in press.
- [41] U. Mölder, R. Pikver, I.I. Koppel, P. Burk, I.A. Koppel, *J. Mol. Struct. Theochem.* 579 (2002) 205–220.

**A4. Minimising the effects of isobaric product ions in SIFT-MS quantification of acetaldehyde, dimethyl sulphide and carbon dioxide**

Smith D, Chippendale TWE, Španěl P. *Curr Anal Chem* (in press).

# Minimising the effects of isobaric product ions in SIFT-MS quantification of acetaldehyde, dimethyl sulphide and carbon dioxide

David Smith,<sup>1\*</sup> Thomas W. E. Chippendale<sup>1</sup> and Patrik Španěl<sup>2</sup>

<sup>1</sup> *Institute for Science and Technology in Medicine, School of Medicine, Keele University, Thornburrow Drive, Hartshill, Stoke-on-Trent ST4 7QB, UK.*

<sup>2</sup> *J. Heyrovský Institute of Physical Chemistry, Academy of Sciences of the Czech Republic, Dolejšková 3, 182 23, Prague 8, Czech Republic.*

**Abstract:** Analyses of the headspace of cell cultures using selected ion flow tube mass spectrometry, SIFT-MS, over the last few years have usually revealed the simultaneous presence of acetaldehyde, AA, and carbon dioxide, CO<sub>2</sub>. The characteristic primary product ions of reactions of the H<sub>3</sub>O<sup>+</sup> with these compounds are at  $m/z$  45, 63 and 81 for AA and  $m/z$  63 for CO<sub>2</sub>. Recently, the presence of dimethyl sulphide, DMS, reaction of which with H<sub>3</sub>O<sup>+</sup> ions also results in product ions at  $m/z$  63 and 81, has been also detected in mammalian cell and bacterial cell culture headspace. The challenge now is to facilitate quantification of AA, DMS and CO<sub>2</sub> when they coexist in humid air samples. Hence, an assessment has been made of the ion chemistry of H<sub>3</sub>O<sup>+</sup> and NO<sup>+</sup> with AA, DMS and CO<sub>2</sub> in order to seek the appropriate procedures for their analyses by SIFT-MS. Thus, appropriate analytical reactions have been identified and kinetics database entries have been constructed for the analyses of these three compounds. Separate analysis of AA and carbon dioxide can now be achieved when they coexist in a humid sample by using both H<sub>3</sub>O<sup>+</sup> and NO<sup>+</sup> reagent ions by SIFT-MS, and the present study has revealed that DMS can be separately identified in a humid mixture using NO<sup>+</sup> reagent ions. An additional experimental study has also shown how the CO<sub>2</sub> concentration can be approximated using NO<sup>+</sup> ions, which had not been considered in previous SIFT-MS analyses.

**Keywords:** Selected ion flow tube mass spectrometry, SIFT-MS, acetaldehyde, carbon dioxide, dimethyl sulphide

## 1. INTRODUCTION

Selected ion flow tube mass spectrometry, SIFT-MS, has developed into an accurate analytical instrument by which real time analyses of exhaled breath and the headspace of biogenic fluids such as urine and cell cultures can be accomplished, obviating sample collection into bag or onto traps if the instrument can be located in the appropriate setting. The details of the instrumentation and the wide applications of SIFT-MS have been discussed in detail previously [1-3] and need not be repeated here. What is important here is to recognize some very important and potentially frustrating features of this analytical technique, in particular, overlap of the characteristic analytical (product) ions. However, if such overlaps can be overcome, then the value of SIFT-MS for gas/vapour phase analysis can be further expanded. These comments also apply to most mass spectrometric analytical techniques, and so the general aspects of the problems highlighted and some of the solutions indicated in this paper are more widely applicable than simply to SIFT-MS analyses only.

At the heart of SIFT-MS is chemical ionisation of the trace gas analytes present in the (invariably humid) samples to be analysed by specific reagent (precursor) ions, which occurs in a fast flow tube in a well-defined time. The available reagent ions are H<sub>3</sub>O<sup>+</sup>, NO<sup>+</sup> and O<sub>2</sub><sup>+</sup>, the most appropriate one being selected according to the chemical reactivity of the neutral analytes, M, in the humid sample and the adjudged mass-to-charge ratios,  $m/z$ , of the characteristic product ions [3, 4]. Often, it is seen that there is a unique characteristic product ion for a specific neutral analyte

and then SIFT-MS analysis can be accomplished both unambiguously and accurately. However, it is often seen that overlaps of the  $m/z$  values of characteristic product ions occur when analysing complex mixtures such as exhaled breath and the headspace of cell [5] and bacterial cultures [6-10]. When the analyte ions are of the form MH<sup>+</sup>, which is often the result of the reactions of H<sub>3</sub>O<sup>+</sup> ions with M (almost always a volatile organic compound, VOC), then there is a great propensity for the formation of hydrates of MH<sup>+</sup> especially when analysing humid samples. These hydrates must be included in the total product ions originating from the neutral analyte if accurate quantification is to be achieved. With the appearance of MH<sup>+</sup>(H<sub>2</sub>O)<sub>n</sub> hydrate ions there is a greatly increased probability of  $m/z$  overlaps, which can be such that separate analyses of some trace compounds become inaccurate if not impossible.

But all is not lost, because switching between the reagent ions H<sub>3</sub>O<sup>+</sup> and NO<sup>+</sup>, invariably results in the formation of different characteristic ions at different  $m/z$  values in the reactions of these two reagent ions with M, and this can often result in positive identification of M and, equally importantly, allow its accurate unambiguous quantification. Further to this, quantification can sometimes be achieved by excluding from the analysis those characteristic hydrated ions that are isobaric with the primary characteristic product ion of a different compound, yet accounting for this exclusion by ion-chemical modelling. A case in point relates to the analysis of acetaldehyde (hereafter shortened to AA) and carbon dioxide (CO<sub>2</sub>) when they co-exist in a sample, as they do in exhaled breath. The only reagent ion that

\*Address correspondence to this author at the Institute for Science and Technology in Medicine, School of Medicine, Keele University, Thornburrow Drive, Hartshill, Stoke-on-Trent ST4 7QB, UK.  
Email d.smith@keele.ac.uk

has been used previously for CO<sub>2</sub> analysis in SIFT-MS is H<sub>3</sub>O<sup>+</sup>[11], since the reactions of both NO<sup>+</sup> and O<sub>2</sub><sup>+</sup> with CO<sub>2</sub> have, until now (see later), been judged to be too slow to be exploited for CO<sub>2</sub> analysis. Thus, the adduct ion H<sub>3</sub>O<sup>+</sup>CO<sub>2</sub> at an *m/z* value of 63 is exploited for CO<sub>2</sub> analysis, as detailed in a recent paper [12], but the problem is that the monohydrate of protonated AA, viz. AAH<sup>+</sup>.H<sub>2</sub>O, is isobaric with H<sub>3</sub>O<sup>+</sup>CO<sub>2</sub>, i.e. also occurs at an *m/z* value of 63. Fortunately, the AA concentration in exhaled breath is usually very low, typically at the 5 parts-per-billion by volume, *ppbv*, concentration and so CO<sub>2</sub>, which is typically at the 3-6 % level in exhaled breath, can be analysed to acceptable accuracy. This is achieved by subtracting the contribution of AA to *m/z* 63, as derived from the count rates of the product ions at *m/z* 45 and 81, a procedure which is described in detail in [12]. Similarly, AA analysis in exhaled breath must take into account the contribution of CO<sub>2</sub> to the *m/z* ion at 63. The characteristic product ions of the H<sub>3</sub>O<sup>+</sup> reaction with AA are AAH<sup>+</sup> at *m/z* 45 and its mono-, di- and trihydrates at *m/z* 63, 81 and 99, although the trihydrate ion at *m/z* 99 essentially can be ignored to avoid unnecessary complication, since even in humid mixtures it contributes < 5% to the total product ions in the SIFT-MS flow reactor. A practical approach that does not rely on knowledge of the actual CO<sub>2</sub> contribution to *m/z* 63 is to base the analysis of AA on *m/z* 45 and 81 only, accounting for their % age contribution at different humidity, as determined by separate experiments [13].

A further complication has recently arisen in that during the sampling of *in vitro* cell cultures [6], it is seen that dimethyl sulphide, DMS, appears in the headspace together with CO<sub>2</sub> and AA. The molecular mass of neutral DMS is 62, which when protonated by H<sub>3</sub>O<sup>+</sup> results in a characteristic ion, DMSH<sup>+</sup>, also at *m/z* 63. To further complicate this analytical situation, the DMSH<sup>+</sup> ion forms a monohydrate ion at *m/z* 81, that is, at the same *m/z* value as the dihydrate of AAH<sup>+</sup>. Thus, we now considered it worthwhile to investigate if NO<sup>+</sup> or O<sub>2</sub><sup>+</sup> reagent ions can be used to analyse CO<sub>2</sub> in these complex mixtures. From previous SIFT studies relating to atmospheric ion chemistry [14], it is known that NO<sup>+</sup> associates with CO<sub>2</sub> at 300K with a three-body rate coefficients of 4.5x10<sup>-30</sup> cm<sup>6</sup>s<sup>-1</sup> and 9.5x10<sup>-30</sup> cm<sup>6</sup>s<sup>-1</sup> with He and N<sub>2</sub> as the third body respectively [15]. Whilst these association rates are small, they can be important in some ionised gases, and the adduct ions NO<sup>+</sup>CO<sub>2</sub> are also seen in SIFT-MS at a low level [16]. The similar association reaction of O<sub>2</sub><sup>+</sup> with CO<sub>2</sub> has a very much smaller rate coefficient [17] and so the adduct ion O<sub>2</sub><sup>+</sup>CO<sub>2</sub> is not seen in SIFT-MS spectra and cannot be exploited to analyse CO<sub>2</sub>.

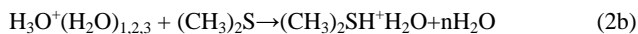
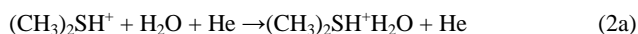
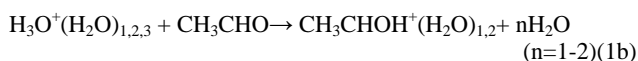
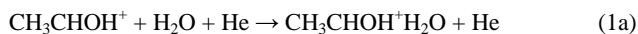
The purpose of the present paper is to explain how AA, CO<sub>2</sub> and DMS can be analysed by SIFT-MS when these three compounds coexist in humid air samples. Ultimately, this can only be achieved to an acceptable accuracy for each compound when both H<sub>3</sub>O<sup>+</sup> and NO<sup>+</sup> reagent ions are used for the analysis. Thus, kinetics library entries have been constructed for each of these compounds involving both H<sub>3</sub>O<sup>+</sup> and NO<sup>+</sup> for AA and CO<sub>2</sub>, and NO<sup>+</sup> only for DMS [18]. It is worth recognizing that if a higher resolution analytical mass spectrometer was available in the SIFT-MS instrument, for example a SIFT-TOF-MS, then, in principle, the various "isobaric ions" at nominally the same *m/z* could be separated and analysed, but the TOF variants have yet to

be demonstrated as useful real time analysers of trace compounds.

## 2. BASIC GAS PHASE ION CHEMISTRY AND MASS SPECTRA

### 2.1. H<sub>3</sub>O<sup>+</sup> analytical reactions

With AA and DMS the major reaction process is exothermic proton transfer, producing the primary protonated parent molecules AAH<sup>+</sup> and DMSH<sup>+</sup> respectively. These ions can form hydrates in humid samples either by three-body association reactions (direct clustering) with abundant H<sub>2</sub>O molecules or in ligand switching reactions between the hydrated hydronium ions H<sub>3</sub>O<sup>+</sup>(H<sub>2</sub>O)<sub>1,2,3</sub> that are inevitably formed in the helium carrier gas of the SIFT-MS:



Note that DMSH<sup>+</sup> only forms significant fractions of the monohydrate. Thus, the characteristic product ions are at *m/z*, 45, 63, 81 for AA, and at *m/z* 63 and 81 for DMS.

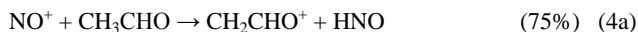
For CO<sub>2</sub>, the only reaction that occurs with H<sub>3</sub>O<sup>+</sup> under the low energy conditions in SIFT-MS is the three-body association, which results in the primary product ion H<sub>3</sub>O<sup>+</sup>CO<sub>2</sub> at *m/z* 63:

All the ions formed in reaction (1), (2) and (3) are seen in the composite SIFT-MS spectrum in Fig.(1a), which is the result of the analysis of headspace containing a mixture of these three compounds. Clearly the ions in these mass spectra are both primary products and their hydrates and all need to be considered for accurate analyses, as mentioned in the previous section.

### 2.2. NO<sup>+</sup> analytical reactions.

NO<sup>+</sup> can undergo a variety of reactions with VOCs, notably charge transfer producing the parent cation M<sup>+</sup>, hydride ion transfer producing (M-H)<sup>+</sup> ions and three-body association producing NO<sup>+</sup>M adduct ions [4, 19, 20]. There are examples of all three processes in the reactions of NO<sup>+</sup> with AA, CO<sub>2</sub> and DMS.

The AA reaction results in two product ions, thus:



The rates of three-body ion-molecule association reactions are to some degree dependent on the temperature and pressure (number density) of the carrier gas atoms or molecules, which in SIFT-MS is largely the He carrier gas, but to some extent the molecules of the air introduced as the sample to be analysed. So, the branching ratio of the reactions, as indicated in percentages in reaction (4), relates to the particular conditions under which SIFT-MS analyses are performed using the *Profile 3* instrument—

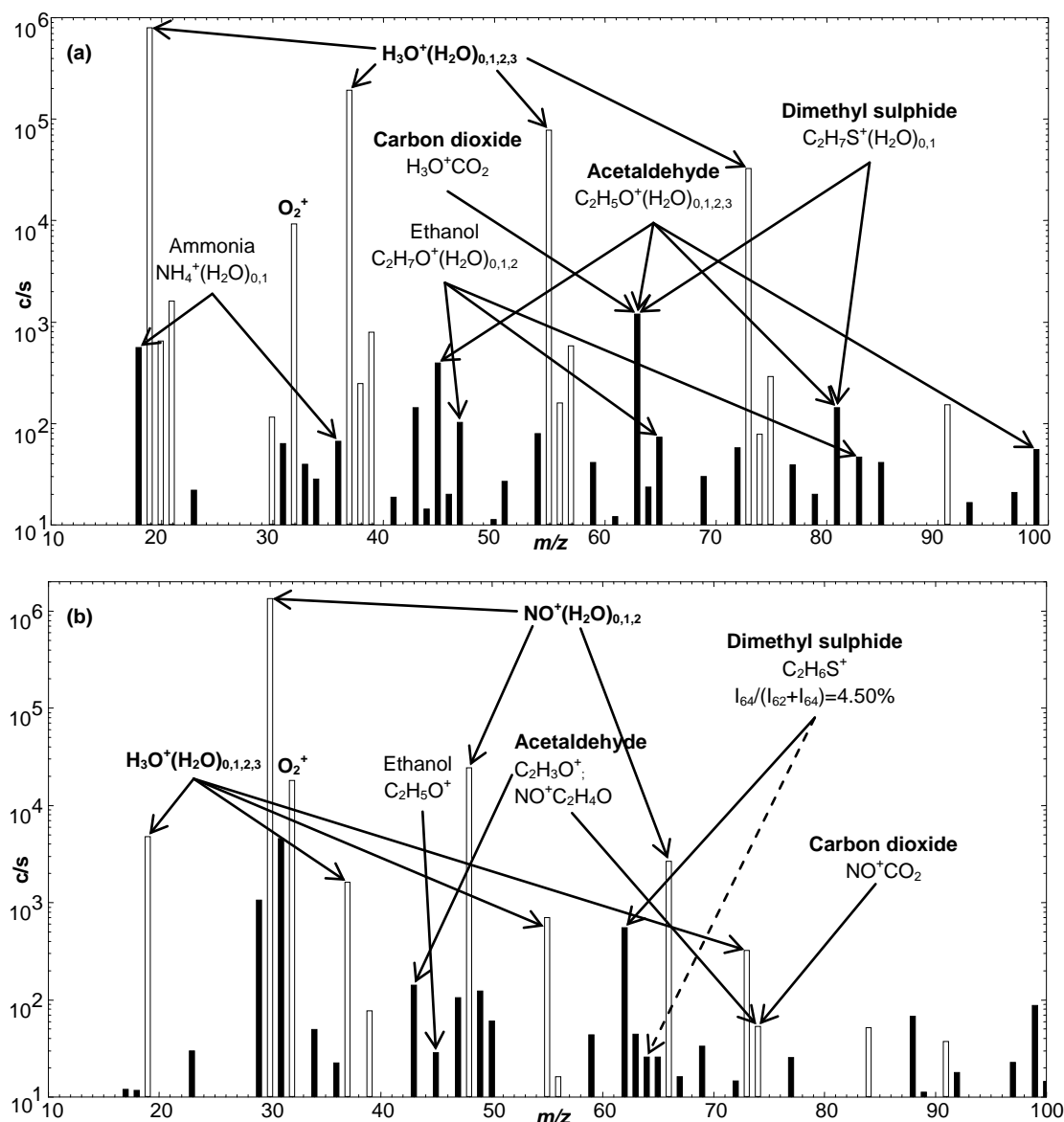


**Fig. (1).** SIFT-MS 'composite' mass spectra (ion counts-per-second, c/s, against mass-to-charge ratio,  $m/z$ ), obtained using (a)  $\text{H}_3\text{O}^+$ ; and (b)  $\text{NO}^+$  precursor ions, showing the combined analyses of  $\text{CO}_2$ , acetaldehyde and dimethyl sulphide, as obtained for humid air samples.

about 1 Torr pressure at room temperature (95% He, 5% air). So the characteristic product ions appear at  $m/z$  values of both 43 and 74.

The reaction of  $\text{NO}^+$  with  $\text{CO}_2$  also results in an adduct ion  $\text{NO}^+\text{CO}_2$  also at an  $m/z$  74 [16]:



This three-body reaction is somewhat slower than the analogous reaction of  $\text{H}_3\text{O}^+$  with  $\text{CO}_2$ , and the product  $\text{NO}^+\text{CO}_2$  adduct ion reacts rapidly with  $\text{H}_2\text{O}$  molecules via ligand switching:



This represents a rapid loss of the  $m/z$  74 adduct ion and it must be accounted for when using the production of  $\text{NO}^+\text{CO}_2$  via reaction (5) to analyse  $\text{CO}_2$  in humid mixtures (see later).

Now, by virtue of the low ionisation energy of DMS molecules (8.8 eV [21]), charge transfer occurs in its reaction with  $\text{NO}^+$  (recombination energy 9.26 eV [21]), thus:



The parent cation, so formed, does not associate with  $\text{H}_2\text{O}$  molecules at a significant rate; hence, this cation at  $m/z$  62 is ideal for the analysis of DMS in humid mixtures. So the characteristic product ions involved in the analysis of AA and DMS occur at both  $m/z$  43 and 74 for AA and only 62 for DMS. These product ions are seen in the composite spectrum in Fig. (1b), which results from the analysis using  $\text{NO}^+$  reagent ions of a mixture of these three compounds in air.

A note concerning the overlap of characteristic product ions with the isotopologues of the  $\text{H}_3\text{O}^+$  hydrates that are always

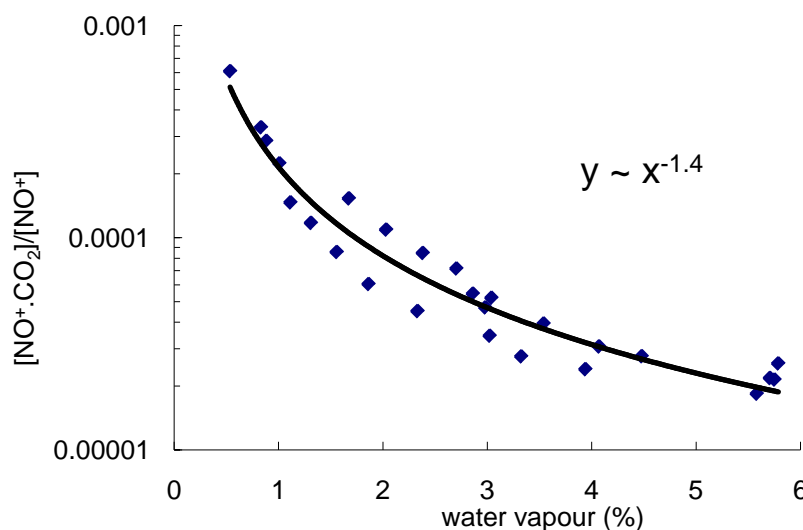


**Fig. (2).** Change of the relative count rate of  $\text{NO}^+\text{CO}_2$  with the humidity of the sample due to the switching reaction of this adduct ion with  $\text{H}_2\text{O}$  in SIFT-MS. The power law indicated can be used to account for this change and it is implemented in the latest versions of *Profile 3* SIFT-MS software (Trans Spectra Limited, UK, SIFT-MS software version 3.1.375 or later versions) using library entries from Table 2.

present in the mass spectra when using both  $\text{H}_3\text{O}^+$  and  $\text{NO}^+$  reagent ions (see Fig. (1)). In particular, the  $\text{H}_3\text{O}^+(\text{H}_2\text{O})_3$  ion at  $m/z$  73 has  $^{17}\text{O}$  and D isotopologues at  $m/z$  74, which can interfere with the analysis of acetaldehyde if the isobaric  $\text{NO}^+\text{AA}$  adduct is used in the analysis. This is only a serious interference at very low sample AA concentrations and very high humidity, when the  $m/z$  74 ion should be avoided for the analysis of AA using  $\text{NO}^+$  reagent ions. In the analysis of DMS, the  $^{34}\text{S}$  isotopologues of  $\text{DM}^{34}\text{SH}^+$  at  $m/z$  65 are seen when using  $\text{H}_3\text{O}^+$  reagent ions, and the isotopologue  $\text{DM}^{34}\text{S}^+$  at  $m/z$  64 is seen when using  $\text{NO}^+$  reagent ions (see Fig. (1b)). These isotopologues are a positive help when analysing organosulphur compounds.

So, in summary, in this scenario there are two undisturbed characteristic product ions that can be used for the analysis of AA, viz.  $m/z$  45 using  $\text{H}_3\text{O}^+$ , and  $m/z$  43 using  $\text{NO}^+$ . For DMS there is one undisturbed characteristic product ion at  $m/z$  62 when using  $\text{NO}^+$  reagent ions. For  $\text{CO}_2$  analysis in SIFT-MS, the only reagent ion that has been used to date is  $\text{H}_3\text{O}^+$  which forms the characteristic product ion at  $m/z$  63, but this is seriously disturbed in the presence of relatively large fractions of either AA or DMS. So it has been necessary to use the methods indicated in the subtraction methods outlined in the Introduction to be able to estimate  $\text{CO}_2$  concentrations. However, we describe later how  $\text{CO}_2$  concentrations can be estimated using  $\text{NO}^+$  reagent ions.

Finally, in this section, a note of caution is necessary. Clearly, in some complex mixtures there may be present significant concentrations of other VOCs whose characteristic analytical ions can disturb the simple scenario described above. For example, when methanol co-exists with DMS then the characteristic product ion for its reaction at  $m/z$  62 can be enhanced due to the production of the adduct ion  $\text{NO}^+\text{CH}_3\text{OH}$  also with  $m/z$  62, formed in the very slow association reaction of  $\text{NO}^+$  with  $\text{CH}_3\text{OH}$ . This would only be important at high methanol concentrations especially since the  $\text{NO}^+\text{CH}_3\text{OH}$  adduct ion is lost rapidly by ligand switching with  $\text{H}_2\text{O}$  molecules. Also, the use of ions at  $m/z$  43 in analyses must always be treated circumspectly,

because ions at  $m/z$  43 are quite commonly produced in reactions of aldehydes, ketones, carboxylic acids and esters with  $\text{NO}^+$  and  $\text{O}_2^{+\bullet}$  ions [4, 19, 22]. All of this indicates that some understanding of the major components of a mixture to be analysed and an appreciation of their ion chemistry with the reagent ion chosen can ensure that serious errors of analysis are avoided.

### 3. ANALYSES OF AA, DMS AND $\text{CO}_2$ IN COMBINATIONS; KINETICS LIBRARY ENTRIES

#### 3.1. Analysis of AA in the presence of $\text{CO}_2$ and DMS

We have treated the analysis of AA using  $\text{H}_3\text{O}^+$  reagent ions in detail previously [13, 19]. In brief, because of the overlap of the characteristic ions of AA and  $\text{CO}_2$  at  $m/z$  63, it has been necessary to exclude these  $m/z$  63 ions from the analysis of AA and to include only the characteristic AA ions at  $m/z$  45 and 81. Now, in the presence also of DMS, the hydrated  $\text{DMSH}^+$  ions at  $m/z$  81 must also be excluded. Thus, the analysis must be accomplished using only  $m/z$  45 ions, but account must be taken of the likely production of  $m/z$  45 ions by the reaction of “impurity”  $\text{O}_2^{+\bullet}$  ions with any ethanol in the sample to be analysed [13], which commonly occurs when analysing biogenic samples. As the fraction of  $m/z$  45 product changes with humidity, the concentration of AA must be calculated from the ratio of  $m/z$  45 to the sum of the precursor ions and their hydrates multiplied by factors obtained from fitting reference experimental data [13, 23]. An appropriate kinetics library entry for this analysis is given in the left column of Table 1, where the ethanol concentration in the sample being analysed is obtained from the  $m/z$  83 protonated ethanol dihydrate[24]. Fortunately, exclusion (filtering) of  $\text{O}_2^{+\bullet}$  when injecting  $\text{H}_3\text{O}^+$  in most SIFT-MS instruments is good ( $\text{O}_2^{+\bullet}$  signal < 1% of the  $\text{H}_3\text{O}^+$  signal) and so this correction for “impurity”  $\text{O}_2^{+\bullet}$  ions is very small. We have tested this experimentally and even for ethanol levels exceeding several

parts-per-million by volume, *ppmv*, in the sample to be analysed,

**Table 1.** SIFT-MS kinetics library entries for the determination of the concentrations of acetaldehyde (AA) and DMS in humid samples using  $\text{H}_3\text{O}^+$  and  $\text{NO}^+$  reagent ions. See the text for further explanation.<sup>a</sup>

Acetaldehyde45( $\text{H}_3\text{O}^+$ )	acetaldehydeC88 ( $\text{NO}^+$ )	DMS( $\text{NO}^+$ )
5 precursors	3 precursors	3 precursors
19 3.7e-9 1.0	30 3.4e-9 1.0	30 2.2e-9 1.0
37 3.0e-9 -1.0	48 3.0e-9 -1.0	48 2.0e-9 -1.0
55 2.7e-9 0.0	66 2.7e-9 0.0	66 1.9e-9 0.0
73 2.6e-9 0.0	32 3.7e-9 1.0	1 products
32 3.7e-9 1.0	2 products	62 1.04
2 products	43 1.33	
45 1.1	88 -100.9	
83 -100.5		
	acetaldehydeC58 ( $\text{NO}^+$ )	
	3 precursors	
	30 3.4e-9 1.0	
	48 3.0e-9 -1.0	
	66 2.7e-9 0.0	
	2 products	
	43 1.33	
	58 -0.67	

<sup>a</sup>The precursor rows contain mass-to-charge ratios  $m/z$ , rate coefficient  $k$  and the precursor ion factor  $f_i$ . The product ion rows contain mass-to-charge ratio  $m/z$  and the product ion factor  $f_p$ .

the apparent acetaldehyde increase above that obtained at near zero ethanol concentration is insignificant when calculated using the library entry given in the left column of Table 1 as Acetaldehyde45( $\text{H}_3\text{O}^+$ ). However, when the ethanol level is  $> 100$  *ppmv*, special care would have to be taken (calibration of a specific instrument under exact conditions) before analysing *ppbv* concentrations of acetaldehyde.

A value of the factor  $f_p$  more negative than -100 acts as a trigger for the analytical software to carry out the subtraction of overlapping product ion formed by an “impurity ion” listed as the last item in the precursors section of the entry, in this case  $m/z$  32, according to the equation given in [13]. The portion of the value of  $f_p$  in excess of -100 is used as a correction coefficient  $f_m$ . For example, where  $f_m = 0.5$  in the Acetaldehyde45( $\text{H}_3\text{O}^+$ ) entry, the correction is  $-0.5[83][32]/[19]$ , where the numbers in square brackets indicate the count rates at the three  $m/z$  values given.

Additionally, it is now possible to use  $\text{NO}^+$  reagent ions for AA analysis. In this case, as indicated above by reaction (4), the characteristic ions are at  $m/z$  43, which is the  $\text{CH}_3\text{CO}^+$  ion, and at  $m/z$  74, which is the  $\text{NO}^+$ AA adduct ion. The good news is that the  $\text{CH}_3\text{CO}^+$  ion does not form an adduct with  $\text{H}_2\text{O}$  molecules and so the  $m/z$  43 ion signal level is not influenced by the humidity of the sample; the bad news is that  $\text{CH}_3\text{CO}^+$  is a major (40%) product ion of the reaction of  $\text{O}_2^{+\bullet}$  ions with acetone,  $\text{CH}_3\text{COCH}_3$ , which is very often present in biogenic air/vapour samples, the other product ion of the  $\text{O}_2^{+\bullet}$ /acetone reaction being the parent acetone cation at  $m/z$  58 (60%) [19]. However, the filtering out of  $\text{O}_2^{+\bullet}$  when injecting  $\text{NO}^+$  ions in SIFT-MS is usually very good with the “impurity”  $\text{O}_2^{+\bullet}$  ions representing  $< 1\%$  of the injected  $\text{NO}^+$  ions, so unless the acetone is present at a concentration more than 100 times that of AA, it will not offer a

serious problem to the analysis of AA. Even so, the presence of acetone can be accounted for by producing a suitable kinetics library entry for AA analysis using  $\text{NO}^+$  reagent ions that only utilizes the  $m/z$  43 ion and excludes, but accounts for, the  $m/z$  74 ion, as can be seen by the two entries given in the centre column of Table 1. In these library entries the contribution to  $m/z$  43 due to the presence (concentration) of acetone can be corrected for by using the  $m/z$  58 ion formed by the “impurity”  $\text{O}_2^{+\bullet}$  ions as an indicator, given in Table 1 as AcetaldehydeC58( $\text{NO}^+$ ), and alternatively using the  $\text{NO}^+\text{CH}_3\text{COCH}_3$  adduct ion at  $m/z$  88 that is the primary product of the  $\text{NO}^+$  reaction with acetone [19, 20], given in Table 1 as AcetaldehydeC88( $\text{NO}^+$ ). When  $m/z$  88 is used to estimate the acetone concentration, the contribution of the  $\text{O}_2^{+\bullet}$  / acetone reaction to  $m/z$  43 is proportional to the ratio of count rates of the  $\text{O}_2^{+\bullet}$  impurity ions to the count rate of the  $\text{NO}^+$  precursor ions multiplied by the count rate of the  $m/z$  88 ions. Again, we have experimentally checked the efficacy of these library entries by measuring AA concentrations with varying acetone concentration and it is seen that even at acetone concentrations of a few *ppmv* (much higher than in healthy human breath [25, 26]), the apparent increase in the derived AA concentration, as calculated using both library entries, is not greater than a few *ppbv*. Nevertheless, this must be accounted for if the very low AA concentrations in human breath (typically a few *ppbv* [27, 28]) are to be accurately measured.

### 3.2. Analysis of DMS in the presence of $\text{CO}_2$ and AA

This analysis has an insurmountable problem when using  $\text{H}_3\text{O}^+$  reagent ions, because there is overlap of the product ions  $\text{DMSH}^+$  at  $m/z$  63 both with  $\text{AAH}^+\text{H}_2\text{O}$  and  $\text{H}_3\text{O}^+\text{CO}_2$  ions, and the hydrate  $\text{DMSH}^+\text{H}_2\text{O}$  ion at  $m/z$  81 with the hydrate  $\text{AAH}^+(\text{H}_2\text{O})_2$  ion. In principle, the  $\text{DM}^{34}\text{SH}^+$  isotopologue ion at  $m/z$  65 could be used for the analysis of DMS, but this overlaps with  $\text{C}_2\text{H}_5\text{OH}_2^+\text{H}_2\text{O}$ , the monohydrate of protonated ethanol; as mentioned previously, ethanol is a common constituent of biogenic samples. So, the only recourse is to use  $\text{NO}^+$  reagent ions for DMS analysis when the characteristic product ion is  $\text{DMS}^+$  at  $m/z$  62 (see reaction (7)), which is a unique product ion within the context of this study. Fortunately, the  $\text{DMS}^+$  parent cation does not readily form a hydrate and so the count rate of this ion is not influenced by the humidity of the sample. The kinetics library entry for the analysis of DMS using  $\text{NO}^+$  reagent ions, is therefore very simple (using a coefficient 1.04 to account for the isotopic abundance of the  $^{32}\text{S}$  isotope), given as DMS( $\text{NO}^+$ ) in the right column of Table 1.

### 3.3. Analysis of $\text{CO}_2$ in the presence of AA and DMS

The analysis of  $\text{CO}_2$  using  $\text{H}_3\text{O}^+$  reagent ions in the presence of AA has effectively been dealt with in Section 3.1. It is straightforward when the  $\text{CO}_2$  levels are within the range 1% to 5% (which are typical at biological samples and exhaled breath) as long as the AA concentration is not large too ( $< 100$  *ppbv*). However,  $\text{CO}_2$  analysis using  $\text{H}_3\text{O}^+$  reagent ions is challenging if the DMS concentration exceeds about 100 *ppbv*, and the quantification becomes increasingly uncertain as the DMS concentration increases further. Then only an approximation to the  $\text{CO}_2$  concentration can be made and even this is only possible, because of the fortunate circumstance that the ratios of the characteristic product ion signals at  $m/z$  81 to  $m/z$  63 are

different for the reactions of  $\text{H}_3\text{O}^+$  with AA and with DMS. Then, in principle, by measuring these ratios it is mathematically

possible

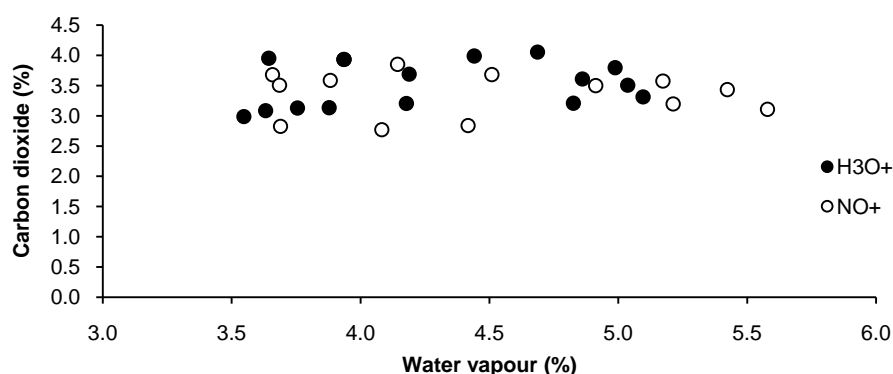


**Fig.(3).** Plot showing the carbon dioxide concentration (given in percentage units), measured using  $\text{H}_3\text{O}^+$  (closed circles) and  $\text{NO}^+$  (open circles) reagent ions, with the humidity of the air sample was altered. The carbon dioxide/air mixture was prepared at a constant concentration of 3.5%  $\text{CO}_2$  (typical of exhaled breath concentration in the resting state).

to calculate three independent concentrations (AA, DMS and  $\text{CO}_2$ ) from the three signal levels at  $m/z$  45, 63 and 81. Such a calculation is implemented in the left column in Table 2, where it is accepted that the ion count ratio for the characteristic product ions of DMS  $[81]/[63] = 1/6$  at 5% absolute humidity and a sample flow rate of 27 mL/min at standard temperature and pressure (STP). Since this ratio is sample flow rate and humidity dependent, it needs to be precisely determined in a separate experiment under the actual conditions of a specific study. Similarly, the coefficient for the  $m/z$  45 product ion must be adjusted according to the actual ratios of  $[45]:[63]:[81]$  obtained for the  $\text{H}_3\text{O}^+$  reaction with AA at varying humidity and sample flow rate [13]. It is clear that this approach can result in only approximate analyses.

**Table 2.** SIFT-MS kinetics library entries for the determination of the concentrations of  $\text{CO}_2$  in the presence of AA and DMS in humid samples using  $\text{H}_3\text{O}^+$  and  $\text{NO}^+$  reagent ions.

$\text{CO}_2\text{-corrDMS-AA}(\text{H}_3\text{O}^+)^a$	$\text{CO}_2(\text{NO}^+)^a$
4 precursors	3 precursors
19 $3\text{e-}15$ 1.0	30 $1.5\text{e-}15$ 1.0
37 $3\text{e-}15$ 1.0	48 $1.5\text{e-}15$ 1.0
55 $3\text{e-}15$ 1.0	66 $1.5\text{e-}15$ 1.0
73 $3\text{e-}15$ 1.0	3 products
3 products	74 1.0
63 1.0	73 -0.0029
45 1.5	43 -0.33
81 -6	

<sup>a</sup>Note that the order of the library entries is important to trigger the inclusion of the power law calculation in the Profile 3 SIFT-MS software and must be as given in this table.

However, as mentioned previously,  $\text{NO}^+$  ions slowly associate with  $\text{CO}_2$  molecules (reaction (5)), a process that is important in the terrestrial ionosphere [14, 15], and that the resulting  $\text{NO}^+\text{CO}_2$  adduct ions at  $m/z$  74 react with  $\text{H}_2\text{O}$  molecules by ligand switching resulting in  $\text{NO}^+\text{H}_2\text{O}$  ions at  $m/z$  48 (reaction (6)). The latter ion is also formed by direct association between  $\text{NO}^+$  ions and  $\text{H}_2\text{O}$  molecules and, as such, is always present in SIFT-MS spectra when  $\text{NO}^+$  is the reagent ion used to analyse humid samples. Both the  $m/z$  48 and 74 ions can be seen in the spectrum in Fig.(1b). The question is “can the  $m/z$  74 ion be used to

estimate the concentration of  $\text{CO}_2$ ?”. The answer is a qualified yes providing that the  $^2\text{H}$  and  $^{17}\text{O}$  isotopologues of  $\text{H}_3\text{O}^+(\text{H}_2\text{O})_3$  at  $m/z$  74 and the switching reaction of  $\text{NO}^+\text{CO}_2$  with the  $\text{H}_2\text{O}$  molecules present (governed by the sample humidity) are taken into account. To this end, a simple experiment has been carried out to study the rate of loss of the  $\text{NO}^+\text{CO}_2$  adduct ion with  $\text{H}_2\text{O}$  molecules under SIFT-MS conditions and the results obtained are shown in Fig. (2). The loss of the  $m/z$  74  $\text{NO}^+\text{CO}_2$  ions with increasing humidity is very clear, the signal level of this adduct ion decreasing by about a factor of 100 as the humidity increases from near zero to 6% of water vapour by volume that is typical of exhaled breath. Using these experimental data, which collectively describe the formation rate of the analytical adduct ion as obtained from the known rate coefficient for the association reaction (5) and its loss by the aforementioned switching reaction (6), an estimate of the  $\text{CO}_2$  concentration can be obtained. It is also essential to account for the overlap at  $m/z$  74 of the isobaric  $^2\text{H}$  and  $^{17}\text{O}$  isotopologues of  $\text{H}_3\text{O}^+(\text{H}_2\text{O})_3$  (using the known ratio of  $[74]/[73]$  for these ions in water vapour [29]) and for the overlap with the  $\text{NO}^+\text{AA}$  product of the AA reaction (using the known  $[74]/[43]$  ratio for these products given in reaction (3)). It is worthy of note that these corrections are of the order of 10% under typical humidity conditions of 3-5%. Thus, a suitable kinetics library entry is given in the right column of Table 2. The power-law correction shown in Fig. (2) is applied by the SIFT-MS analytical software to account for the loss of product ions in a fashion similar to that implemented for  $\text{CO}_2$  quantification by  $\text{H}_3\text{O}^+$ [12].

Using the kinetics library entries given in Table 2, we have analysed air samples containing  $\text{CO}_2$  at levels commonly met in exhaled breath using both  $\text{H}_3\text{O}^+$  and  $\text{NO}^+$  reagent ions at varying humidity, and sample data are shown in Fig.(3). The scatter in the data is due almost entirely to the small count rates of the analytical adduct ions  $\text{H}_3\text{O}^+\text{CO}_2$  and  $\text{NO}^+\text{CO}_2$ , which are the results of the low rate coefficients of the three-body reactions (3) and (5) and the effects of their reactions with  $\text{H}_2\text{O}$ . The count rates of these analytical ions would be greater should the count rates of the precursor (reagent) ions be increased above the current  $10^6$  ions per second, and efforts are now being made to achieve such increases. Given the current limitations on these ion



count rates, the agreement between the CO<sub>2</sub> concentrations as determined using the two analytical ions is reasonable, and

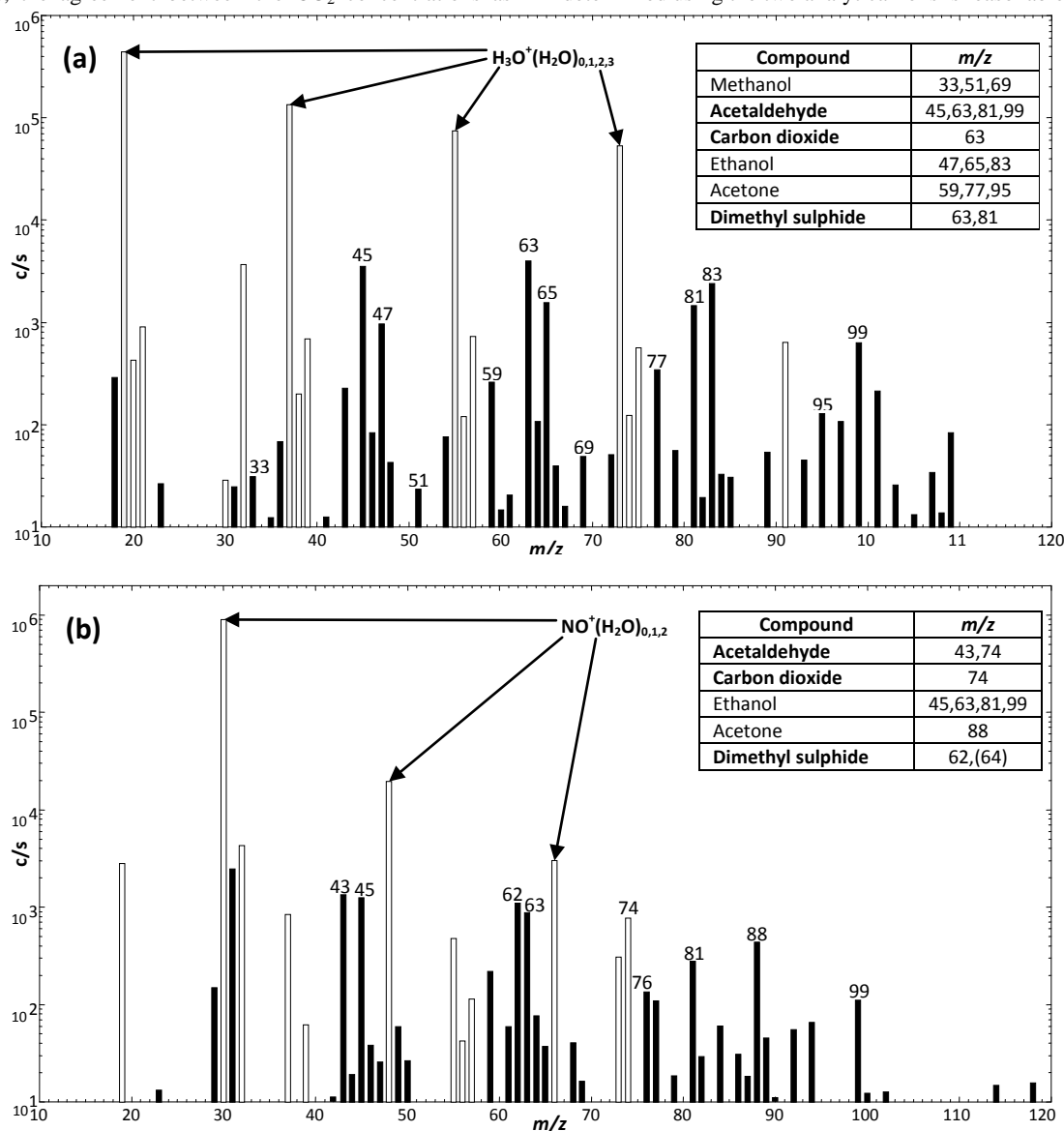


**Fig. (4).** SIFT-MS mass spectra (counts-per-second, c/s, against mass-to-charge ratio, m/z) obtained using (a) H<sub>3</sub>O<sup>+</sup> and (b) NO<sup>+</sup> precursor ions, showing the analysis of the headspace of an *E. coli* culture in DMEM, supplemented with 10% v/v foetal bovine serum, 2mM L-glutamine and 0.001% v/v dimethyl sulphoxide, DMSO. The dimethyl sulphide, DMS, is formed from the DMSO by bacterial reductase enzymes [32]. The m/z values of the identifiable compounds are indicated above the relevant peaks, and assigned to the neutral compounds from which they originate in the inset tables.

sufficient for the analysis of most biological samples, especially when it is considered that the CO<sub>2</sub> measurements are carried out simultaneously with other VOCs that are often present at the ppbv level [1, 30].

#### 4. SAMPLE SIFT-MS MASS SPECTRA OBTAINED FOR A BACTERIAL CULTURE HEADSPACE

To exemplify the data that is obtained when analysing the headspace of cell cultures, an analysis was performed of the headspace of a culture of the bacterium *E. coli* JM109. In this case, 1mL of *E. coli* suspension (in lysogeny broth) was added to 24 mL of Dulbecco's modified Eagle medium, DMEM, inside a

150 mL glass bottle, together with the addition of a small amount (0.001%) of dimethylsulphoxide, DMSO, that is commonly used as a cryopreservant for cell lines [31], and sealed overnight at 37°C. SIFT-MS analytical spectra obtained using both H<sub>3</sub>O<sup>+</sup> and NO<sup>+</sup> reagent ions are shown in Fig.(4). Note the appearance of the characteristic analyte product ions for AA, CO<sub>2</sub> and DMS, as indicated in the inset tables. The (very volatile) DMS originates from the reduction of the (less volatile) DMSO by the action of the bacterial cellular enzymes [32]. From these full scan spectra, which identify the analytical ions, analyses can be obtained using the multiple ion monitoring mode of SIFT-MS [23] together with the kinetics library entries for each compound given in Tables 1 and 2, as appropriate.

## 5. SUMMARY AND CONCLUDING REMARKS

The discussion above concerning the ion chemistry and mass spectrometry involved in the SIFT-MS investigation of the potential problems and pitfalls in the simultaneous analysis of acetaldehyde (AA) carbon dioxide (CO<sub>2</sub>) and dimethyl sulphide (DMS) when all three compounds are present in a humid air sample, indicates that separate analyses of each of them can be achieved using a combination of H<sub>3</sub>O<sup>+</sup> and NO<sup>+</sup> reagent ions. The analyses of both AA, which can be achieved independently using both reagent ions, and DMS using NO<sup>+</sup> reagent ions are robust. Analysis of CO<sub>2</sub> is robust in the presence of AA alone, but CO<sub>2</sub> analysis in the presence of DMS is inaccurate unless the DMS level is below about 100 ppbv. Whilst the experiments have been carried out on one type of SIFT-MS instruments, the ion chemistry described and the general principles of proposed approaches to analyses are relevant to any SIFT-MS instrument.

In exhaled breath, the CO<sub>2</sub> concentration lies within the 3–6% level and normally the AA and DMS levels are at the 10 ppbv level or less, at which the concentrations of all three compounds can be achieved reasonably accurately in real time using SIFT-MS. The headspace air/vapour above bacterial cultures is richer in these organic compounds, as can be seen in Fig. (4), and so this needs to be carefully considered when assessing the accuracy of their analyses.

## Acknowledgements

The contribution of the co-authors was as follows: David Smith designed the study and drafted the paper; Thomas W.E. Chippendale performed the experiments, collected and assessed the data; Patrik Španěl contributed to the study design and the data analysis and interpretation.

## References

- [1] Smith, D.; Španěl, P., Ambient analysis of trace compounds in gaseous media by SIFT-MS. *Analyst* **2011**, *136*, 2009–2032.
- [2] Španěl, P.; Smith, D., Progress in SIFT-MS; breath analysis and other applications. *Mass Spectrom. Rev.* **2011**, *30*(2), 236–267.
- [3] Smith, D.; Španěl, P., Selected ion flow tube mass spectrometry (SIFT-MS) for on-line trace gas analysis. *Mass Spectrom. Rev.* **2005**, *24*(5), 661–700.
- [4] Španěl, P.; Smith, D., A selected ion flow tube study of the reactions of NO<sup>+</sup> and O<sub>2</sub><sup>+</sup> ions with some organic molecules: The potential for trace gas analysis of air. *J. Chem. Phys.* **1996**, *104*(5), 1893–1899.
- [5] Sule-Suso, J.; Pysanenko, A.; Španěl, P.; Smith, D., Quantification of acetaldehyde and carbon dioxide in the headspace of malignant and non-malignant lung cells in vitro by SIFT-MS. *Analyst* **2009**, *134*(12), 2419–2425.
- [6] Chippendale, T. W. E.; Španěl, P.; Smith, D., Time-resolved selected ion flow tube mass spectrometric quantification of the volatile compounds generated by *E. coli* JM109 cultured in two different media. *Rapid Commun. Mass Spectrom.* **2011**, *25*(15), 2163–2172.
- [7] Shestivska, V.; Nemec, A.; Drevinek, P.; Sovova, K.; Dryahina, K.; Španěl, P., Quantification of methyl thiocyanate in the headspace of *Pseudomonas aeruginosa* cultures and in the breath of cystic fibrosis patients by selected ion flow tube mass spectrometry. *Rapid Commun. Mass Spectrom.* **2011**, *25*(17), 2459–2467.
- [8] Thorn, R. M. S.; Reynolds, D. M.; Greenman, J., Multivariate analysis of bacterial volatile compound profiles for discrimination between selected species and strains in vitro. *J. Microbiol. Methods* **2011**, *84*(2), 258–264.
- [9] Scotter, J. M.; Allardyce, R. A.; Langford, V.; Hill, A.; Murdoch, D. R., The rapid evaluation of bacterial growth in blood cultures by selected ion flow tube-mass spectrometry (SIFT-MS) and comparison with the BacT/ALERT automated blood culture system. *J. Microbiol. Methods* **2006**, *65*(3), 628–631.
- [10] Allardyce, R. A.; Hill, A. L.; Murdoch, D. R., The rapid evaluation of bacterial growth and antibiotic susceptibility in blood cultures by selected ion flow tube mass spectrometry. *Diagn. Microbiol. Infect. Dis.* **2006**, *55*(4), 255–261.
- [11] Ikezoe, Y.; Matsuoka, S.; Takebe, M.; Viggiano, A., *Gas phase ion-molecule reaction rate constants through 1986*. Maruzen: Tokyo, 1987.
- [12] Smith, D.; Pysanenko, A.; Španěl, P., The quantification of carbon dioxide in humid air and exhaled breath by selected ion flow tube mass spectrometry. *Rapid Commun. Mass Spectrom.* **2009**, *23*(10), 1419–1425.
- [13] Španěl, P.; Smith, D., Quantification of trace levels of the potential cancer biomarkers formaldehyde, acetaldehyde and propanol in breath by SIFT-MS. *J. Breath Res.* **2008**, *2*, 046003.
- [14] Smith, D.; Španěl, P., Ions in the terrestrial atmosphere and in interstellar clouds. *Mass Spectrom. Rev.* **1995**, *14*(4–5), 255–278.
- [15] Smith, D.; Adams, N. G.; Grief, D., Implications of some laboratory determinations of NO<sup>+</sup> reaction-rates to cluster ion formation in D-region. *Journal of Atmospheric and Terrestrial Physics* **1977**, *39*(4), 513–521.
- [16] Španěl, P.; Smith, D., Influence of weakly bound adduct ions on breath trace gas analysis by selected ion flow tube mass spectrometry (SIFT-MS). *Int. J. Mass Spectrom.* **2009**, *280*(1–3), 128–135.
- [17] Adams, N. G.; Bohme, D. K.; Dunkin, D. B.; Fehsenfeld, F. C.; Ferguson, E. E., Flowing afterglow studies of formation and reactions of cluster ions of O<sub>2</sub><sup>+</sup>, O<sub>2</sub><sup>+</sup>, and O<sup>+</sup>. *The Journal of Chemical Physics* **1970**, *52*(6), 3133–3140.
- [18] Pysanenko, A.; Španěl, P.; Smith, D., A study of sulfur-containing compounds in mouth-and nose-exhaled breath and in the oral cavity. *J. Breath Res.* **2008**, *2*, 046004.
- [19] Španěl, P.; Ji, Y. F.; Smith, D., SIFT studies of the reactions of H<sub>3</sub>O<sup>+</sup>, NO<sup>+</sup> and O<sub>2</sub><sup>+</sup> with a series of aldehydes and ketones. *Int. J. Mass Spectrom.* **1997**, *165*, 25–37.
- [20] Fairley, D. A.; Milligan, D. B.; Freeman, C. G.; McEwan, M. J.; Španěl, P.; Smith, D., Competitive association and charge transfer in the reactions of NO<sup>+</sup> with some ketones: a selected ion flow drift tube study. *Int. J. Mass Spectrom.* **1999**, *193*(1), 35–43.
- [21] Lias, S. G., Ionization Energy Evaluation. In *NIST Chemistry WebBook, NIST Standard Reference Database Number 69*, Linstrom, P. J.; Mallard, W. G., Eds. National Institute of Standards and Technology: Gaithersburg, 2010.
- [22] Španěl, P.; Smith, D., SIFT studies of the reactions of H<sub>3</sub>O<sup>+</sup>, NO<sup>+</sup> and O<sub>2</sub><sup>+</sup> with a series of volatile carboxylic acids and esters. *Int. J. Mass Spectrom.* **1998**, *172*(1–2), 137–147.
- [23] Španěl, P.; Dryahina, K.; Smith, D., A general method for the calculation of absolute trace gas concentrations in air and breath from selected ion flow tube mass spectrometry data. *Int. J. Mass Spectrom.* **2006**, *249*, 230–239.
- [24] Španěl, P.; Smith, D., Advances in on-line absolute trace gas analysis by SIFT-MS. *Current Analytical Chemistry* **2012**, *This issue*, In press.
- [25] Španěl, P.; Dryahina, K.; Rejskova, A.; Chippendale, T. W. E.; Smith, D., Breath acetone concentration; biological variability and the influence of diet. *Physiol. Meas.* **2011**, *32*(8), N23–N31.
- [26] Smith, D.; Španěl, P.; Fryer, A. A.; Hanna, F.; Ferns, G. A. A., Can volatile compounds in exhaled breath be used to monitor glycaemic control in diabetes mellitus? *Journal of Breath Research* **2011**, *5*(2), 022001.
- [27] Wang, T.; Pysanenko, A.; Dryahina, K.; Španěl, P.; Smith, D., Analysis of breath, exhaled via the mouth and nose, and the air in the oral cavity. *J. Breath Res.* **2008**, *2*, 037013.
- [28] Turner, C.; Španěl, P.; Smith, D., A longitudinal study of ethanol and acetaldehyde in the exhaled breath of healthy volunteers using selected-ion flow-tube mass spectrometry. *Rapid Commun. Mass Spectrom.* **2006**, *20*(1), 61–68.

- 
- [29]Španěl, P.; Shestivska, V.; Chippendale, T. W. E.; Smith, D., Determination of the Deuterium Abundances in Water from 156 to 10,000 ppm by SIFT-MS. *J. Am. Soc. Mass Spectrom.* **2011**,22(1), 179-186.
- [30]Smith, D.; Španěl, P., Direct, rapid quantitative analyses of BVOCs using SIFT-MS and PTR-MS obviating sample collection. *TRAC-Trends in Analytical Chemistry* **2011**,30(7), 945-959.
- [31]Lovelock, J. E.; Bishop, M. W. H., Prevention of Freezing Damage to Living Cells by Dimethyl Sulphoxide. *Nature* **1959**,183(4672), 1394-1395.
- [32]Zinder, S. H.; Brock, T. D., Dimethyl Sulphoxide Reduction by Micro-organisms. *Journal of General Microbiology* **1978**,105(2), 335-342.

**A5. A study of enzymatic activity in cell cultures *via* the analysis of volatile biomarkers**

Chippendale TWE, Hu B, El Haj AJ, Smith D. *Analyst* 2012, 137:4677-4685.

Cite this: DOI: 10.1039/c2an35815h

www.rsc.org/analyst

PAPER

# A study of enzymatic activity in cell cultures *via* the analysis of volatile biomarkers

Thomas W. E. Chippendale,<sup>†</sup> Bin Hu,<sup>†</sup> Alicia J. El Haj<sup>‡</sup> and David Smith<sup>‡,\*</sup>

Received 18th June 2012, Accepted 21st August 2012

DOI: 10.1039/c2an35815h

Aldehyde dehydrogenase (ALDH) enzymes are responsible for the metabolism of aldehydes, including acetaldehyde (AA), and are linked to disease. We describe a method to study ALDH activity in cell cultures involving the measurement of AA concentrations in the gas/vapour phase. This has been achieved using selected ion flow tube mass spectrometry (SIFT-MS), developed for the rapid quantification of trace gases in humid media. Human cells of the hepG2 hepatocellular carcinoma cell line and primary bone marrow-derived mesenchymal stem cells (hMSCs) depleted AA from the culture media, but the application of ALDH inhibitors diethylaminobenzaldehyde (DEAB) and disulfiram (DSF), suppressed this depletion or in some cases resulted in elevated AA concentrations. Further, the cells were shown to reduce the dimethyl sulphoxide (DMSO) to dimethyl sulphide, which is mediated by methionine sulfoxide reductase A (MsrA) enzymes. Interestingly, this process was also inhibited by DEAB and DSF. The results of this study indicate that SIFT-MS gas phase analysis could be applied to the study of volatile metabolites of intracellular enzyme reactions, this having potential utility in disease research and drug discovery.

## Introduction

The toxic volatile compound acetaldehyde (AA) is an intermediary of human ethanol metabolism; the proposed mechanism being that ethanol is oxidised to AA, which is then further oxidised to acetate *via* enzyme-mediated reactions.<sup>1</sup> However, AA may also be formed by alternative mechanisms, including lipid peroxidation.<sup>2</sup> Aldehyde dehydrogenase (ALDH) enzymes are thought to be primarily responsible for the oxidation/detoxification of aldehydes, including AA, in conjunction with the coenzyme nicotinamide adenine dinucleotide (NAD<sup>+</sup>), to form the corresponding carboxylic acids. There are 19 ALDH isozymes expressed in human cells, which have varying reaction efficiencies depending on the aldehyde substrate present and some also have other functions unrelated to aldehyde oxidation. ALDH2 has by far the greatest affinity and reaction efficiency for AA,<sup>3</sup> although ALDH1B1 may also be involved in its metabolism.<sup>4</sup> These 2 mitochondrial enzymes are expressed in numerous tissues of the body, but are most prevalent in the liver.<sup>4</sup>

ALDH deficiencies have been linked to the development of numerous diseases including Parkinson's disease,<sup>5</sup> pyridoxine-dependent epilepsy,<sup>6</sup> Sjögren–Larsson syndrome,<sup>6</sup> as well as some which are also partially linked to the presence of AA, such as alcoholic liver disease,<sup>7,8</sup> ethanol-induced cancers,<sup>6</sup> ischaemic tissue

diseases<sup>9</sup> and Alzheimer's disease.<sup>10</sup> In spite of this, disulfiram (DSF; trade-name Antabuse), an ALDH inhibitor, has been prescribed as a treatment for alcohol abuse, causing greatly increased concentrations of AA in the blood and contributing to an extended “hangover” effect. The drug has also been proposed as a treatment for cocaine addiction.<sup>11</sup> On the other hand, high ALDH expression has been associated with heightened metastatic potential in breast,<sup>12</sup> prostate<sup>13</sup> and pancreatic<sup>14</sup> cancer stem cells *in vitro* and has also been shown to play a role in drug resistance.<sup>15,16</sup> Furthermore, *in vitro*<sup>17</sup> and *in vivo*<sup>18</sup> studies suggest that the aforementioned ALDH inhibitor, DSF, may contribute to future anticancer therapies. Heightened ALDH activity is also an important marker for some stem cells, such as haematopoietic stem cells.

*In vitro* analyses of ALDH activity are commonly performed on solutions containing ALDH, NAD<sup>+</sup> and a suitable aldehyde substrate, by measuring the change in the absorbance of solutions at 340 nm, which provides an indication of the amount of NADH produced from the enzyme reactions.<sup>3,4</sup> This method of analysis has been widely used in the study of individual enzymes present in cell lysates, but is not useful for analysing metabolism in live cells, and cannot provide direct information on substrates. More recently, a flow cytometry-based assay has been developed, *viz.* ALDEFLUOR® (STEMCELL Technologies Inc.), for the selection of so-called ALDH<sup>br</sup> (ALDH-bright) cells, including haematopoietic stem cells<sup>19</sup> from a mixed population, employing the ALDH inhibitor diethylaminobenzaldehyde (DEAB) as a control. This technique has also been used to identify differences in the levels of ALDH expression in a number of lung cancer cell

Institute for Science and Technology in Medicine, Keele University, Stoke-on-Trent, Staffordshire, UK. E-mail: d.smith@bemp.keele.ac.uk

<sup>†</sup> TWEC and BH contributed equally to this work.

<sup>‡</sup> AJEH and DS are joint senior authors.

lines, which, it is hypothesised, may be due to the stem cell-like properties of some cancer cell lines.<sup>20</sup> It has also found utility in identifying and separating populations of cells based on their ALDH expression levels, but it is not designed for *in vitro* analyses of ALDH-mediated metabolism and enzyme kinetics.

Several gas/vapour phase mass spectrometry techniques have been used to analyse the headspaces of a number of cancer-derived and non-cancerous primary and transformed human cell types cultured *in vitro*, with AA commonly observed. AA was seen to have been produced by human lung cancer cell lines CALU-1 and SK-MES, relative to their respective media, by Smith and co-workers, using selected ion flow tube mass spectrometry (SIFT-MS), a real-time trace gas analysis technique.<sup>21</sup> Numerous similar studies have since shown the compound to be either produced<sup>22–24</sup> or consumed<sup>22,24–26</sup> by various cell types. Noteworthy is the consistency of a headspace analysis study in which it was found that BEAS2B produced AA, and A549 removed AA from their respective media<sup>24</sup> with the previously mentioned ALDEFLUOR study in which it was found that these cell types contained very low (0.3%) and very high (94%) ALDH expression levels respectively.<sup>20</sup> These results indicate that the production/consumption of AA from the headspace of a cell culture is correlated with the levels of ALDH expression and/or activity within the cells. This relationship is explored further in the present study using SIFT MS.

In the present study, we investigate the activities of intracellular enzymes within two cell types, specifically the effects of the enzyme inhibitors DEAB and DSF on AA present in cultures of immortalised hepatocellular carcinoma cell line (hepG2) and a primary human bone marrow derived mesenchymal stem cell (hMSC). This has been achieved using SIFT-MS, which allows real time absolute quantification of volatile compounds present in the headspace of cell cultures at concentrations down to parts-per-billion by volume (ppbv), with no requirement for repeated calibration. During the course of these experiments, it was observed that the solvent used to dissolve the inhibitor compounds, dimethyl sulphoxide (DMSO), was reduced to volatile dimethyl sulphide (DMS) by both cell types. Thus, the potential inhibitory effects of DEAB and DSF on this reduction reaction have also been studied using SIFT-MS to analyse DMS in the gas/vapour phase above the cell cultures.

## Experimental procedures

### Cell cultures

Human mesenchymal stem cells, hMSCs, are a primary cell type, and were isolated from a bone marrow aspirate sample (27 years old male; Lonza, US) using the plastic-adherence methodology and the hepG2 cells are of a human hepatocellular carcinoma cell line (Eton Bioscience, US), a cell line commonly used for the study of liver function. In both cases, the cells were cultured to confluence in Dulbecco's modified Eagle's medium (DMEM; Lonza, UK), supplemented with 10% v/v foetal bovine serum (FBS; Lonza, UK), 50 U mL<sup>-1</sup> penicillin–streptomycin (Lonza, UK) and 2 mM L-glutamine (Lonza, UK). The hMSCs additionally contained 1%v/v non-essential amino acids. The hMSCs were not cultured beyond passage number 4, whereas the well-differentiated hepG2 cells were analysed before passage number 20.

### Sample preparation

The ALDH inhibitors DEAB (Sigma, UK) and disulfiram (DSF; Sigma, UK) were dissolved in DMSO (Sigma, UK). DMSO was selected to be the common solvent for the inhibition experiments, because it has a relatively low vapour pressure (1.8 mbar at 37 °C) and thus was not expected to interfere significantly with headspace analyses (further explanation below). The inhibitor solutions were then added to volumes of medium so that the final DMSO concentration was always 0.1% v/v (or ~14 500 μM). In some experiments, inhibitors were added to hMSCs during routine culture, some 24 hours prior to proceeding to the next phase of the analysis, but this pre-treatment was not employed in the hepG2 experiments.

It is important to note that maximum concentration of DSF in a DMSO solution is 20 mM, which imposed a limit on the maximum concentration in the cultures (0.1% v/v) of 20 μM. The most obvious alternative solvent to DMSO would have been ethanol, but a concentration of 0.1% v/v ethanol in the liquid phase would equate to a vapour phase concentration of around 200 ppmv at 37 °C, assuming a Henry's Law coefficient<sup>27</sup> of 71 mol kg<sup>-1</sup> bar<sup>-1</sup>, and this would have seriously interfered with the SIFT-MS measurements because of the ability of ethanol molecules at this concentration to totally deplete the precursor ions on which SIFT-MS analyses depend.<sup>28</sup> The importance of precursor ions in the analysis is explained further in the SIFT-MS section below.

The method used for the preparation of cell cultures for SIFT-MS headspace analysis was adapted from the previous studies published in 2003 (ref. 21) and 2009 (ref. 22). On the evening prior to the analysis, the cells were removed from the tissue culture flasks using trypsin, counted using a haemocytometer, and suspended in fresh DMEM media containing the ALDH inhibitor where appropriate, inside 150 mL glass bottles. HEPES buffer (Sigma, UK) was added to each cell suspension/media volume to a final concentration of 10 mM in order to ensure that the pH of the sample did not change significantly overnight. The headspace of each bottle was purged with dry cylinder air before the bottles were finally sealed with metal caps, which incorporate rubber septa, and placed inside an incubator to be held at 37 °C for around 16 hours/overnight.

### SIFT-MS analysis

The methodology of SIFT-MS analyses for the sampling and quantification of compounds in the headspace of liquid samples has been described in detail previously.<sup>21,22,27–32</sup> Briefly, the contained headspace of a sealed 150 mL glass bottle, held at 37 °C, is sampled *via* a hypodermic needle, which penetrates a septum at the bottle cap, allowing the gas–vapour mixture to flow directly into the flow tube of the SIFT-MS instrument.<sup>27</sup> The flow rate of the sample into the instrument is controlled by a heated calibrated capillary and is approximately 40 mL min<sup>-1</sup> so the typical headspace volume of 135 mL can be sampled for about 30 seconds before the pressure in the bottle is significantly reduced. This flow rate is sufficiently small that the pressure reduction in the sealed bottle is only small and insufficient to significantly distort the analyses. This phenomenon has been discussed in a previous publication.<sup>27</sup> The trace compounds of the sample headspace are ionised by the appropriate precursor/reagent ion species, which

are simultaneously injected into the helium-buffered reaction flow tube of the instrument. The precursor ions, which are always  $\text{H}_3\text{O}^+$ ,  $\text{NO}^+$  or  $\text{O}_2^+$ , do not react significantly with the major components of air in the headspace sample, minimising interference from such compounds as nitrogen, oxygen and argon, and the resulting product ions are characteristic of the trace volatile analyte molecules. The product ions and the precursor ions are then analysed by a quadrupole mass spectrometer/detection system. Throughout the present study the instrument was operated in the multiple ion monitoring (MIM) mode, during which the desired precursor ion and its hydrates,<sup>33</sup> and the characteristic product ions, are continuously monitored. This system, in combination with the previously compiled kinetics data for the reactions between the precursor ions and neutral molecules,<sup>34,35</sup> rapidly allows the simultaneous absolute quantification of the concentrations of several selected volatile compounds of interest. The simultaneous detection and analysis of AA and DMS in a mixture presents a peculiar problem to SIFT-MS because of the overlap of characteristic product ions on which the analysis depends. However, the ion chemistry involved has been studied in detail and the kinetics database entries required for the accurate analyses of these two compounds by SIFT-MS have been constructed by following the guidelines given by previous studies.<sup>34,35</sup> In brief, AA was analysed using  $\text{H}_3\text{O}^+$  precursor ions and the unique protonated AA characteristic product ion at  $m/z$  45, as described in detail in a recent paper.<sup>36</sup> Since protonated DMS forms a monohydrate at  $m/z$  81, the dihydrate of protonated AA could not be used as an analytical ion for AA in the presence of DMS, as has been used previously.<sup>35</sup> The unambiguous analysis of DMS in the presence of AA was achieved using  $\text{NO}^+$  precursor ions, again, as discussed in ref. 34 and 36.

### Viability assay

In order to assess any changes in the viability of hepG2 cells due to the method of analysis, which requires the cells to be sealed inside a glass bottle for around 16 hours, cells were cultured to near-confluence using the untreated medium described earlier, and observed using a live-dead staining (Sigma, UK), and confocal microscopy.  $1.5(10^7)$  cells were suspended in 15 mL of DMEM medium containing 200  $\mu\text{M}$  DEAB or 20  $\mu\text{M}$  DSF, prepared as described previously, as well as an untreated sample with no inhibitors or DMSO present. The cell-suspensions were then sealed inside 150 mL glass bottles and incubated at 37 °C for 16 hours. The suspensions were then removed from the bottles and assessed by the same live-dead staining.

To test the affects of the ALDH inhibitors on cell viability, hepG2 cells and hMSCs were cultured to near-confluence in 96-well plates in their respective media, and treated with ALDH inhibitors for 16 hours. An ATPlite kit (Perkin-Elmer, UK) was used to quantify the ATP concentrations, according to the manufacturer's instructions. A Synergy 2 spectrophotometer (BioTek, UK) was employed to detect luminescence levels.

## Results

### Analysis of the background culture media headspace

A first stage in these studies was to establish the background concentrations of the common metabolites in the headspace of

the DMEM medium that was used exclusively in these cell culture studies. Thus, the concentrations of acetone and ethanol, which have previously been shown to largely originate from the foetal bovine serum (FBS),<sup>22</sup> as well as methanol, were routinely measured as reference controls, alongside acetaldehyde (AA) and DMS, which were the primary focus of this study. The potential influence of DMSO, DEAB and DSF additions to the DMEM medium was assessed. Table 1 indicates the headspace concentrations of the volatile compounds in DMEM media control samples with and without the addition of the varying concentrations of DMSO, DEAB and DSF. As can be seen, there is no discernible change in the headspace concentrations due to the addition of the three compounds beyond the spread in the measured values.

### AA measurements in the headspace of HepG2 cultures

**Removal of AA from DMEM medium by cellular action.** An initial probing experiment was conducted in which pure AA was added to 50 mL of the composite DMEM culture medium alone contained in three of our standard 150 mL bottles containing 20 million hepG2 cells prior to the 16-hour incubation period at 37 °C. Identical medium samples without cells were also analysed (as described above) to obtain the starting (background) headspace AA concentration. The starting AA concentrations were measured as 59, 396 and 990 parts-per-billion by volume (ppbv), or 0.4, 2.8 and 7.2  $\mu\text{M}$  in the liquid phase, which were reduced by approximately 90% in the presence of the 20 million hepG2 cells, to 20, 48 and 118 ppbv respectively. The headspace concentrations of acetone, ethanol and methanol were unchanged by the presence of the added AA, the measured mean values, in ppbv, being 264 (274); ethanol 208 (212); and methanol 73 (67), the concentration without cells shown in parentheses.

The loss of AA from the DMEM medium was also investigated as the number of hepG2 cells in the medium was varied, beginning at the low AA level in 15 mL of medium that is partly due only to the presence of the FBS. The results of these studies are illustrated in Fig. 1a over the wide range of cell numbers from  $1(10^4)$  through  $3(10^7)$  and following 16 hours incubation at 37 °C. The initial headspace concentration of AA of about 120 ppbv is rapidly reduced to almost background levels for about  $1(10^6)$  cells, which rapidly levels off with increasing cell numbers up to  $3(10^7)$  and asymptotically approaches zero ppbv. This trend can be qualitatively explained by following Michaelis-Menton enzyme kinetics,<sup>1</sup> which has been used here to produce a model plot of the AA headspace concentration at the different cell numbers covered in this study. This model assumes that AA formation and loss is entirely due to the ethanol metabolism pathway: ethanol  $\rightarrow$  AA  $\rightarrow$  acetate, which is further assumed to proceed entirely by the actions of alcohol dehydrogenases -1B1, -1C1, -1C2 and aldehyde dehydrogenases ALDH1B1 and ALDH2. The implication of this metabolic pathway is that AA is constantly produced, and at the same time removed by the aforementioned enzymes. The Michaelis-Menton constants ( $K_M$ ) and maximum enzyme reaction rates ( $V_{\text{max}}$ ) values were obtained from the literature.<sup>3,4,37</sup> Thus, assuming initial concentrations of 500 ppbv (44  $\mu\text{M}$ , liquid phase) ethanol and 100 ppbv (0.7  $\mu\text{M}$ , liquid phase) AA in the medium, and that each hepG2 cell contains 5000 combined alcohol dehydrogenase -1B1, -1C1,



**Table 1** SIFT-MS measurements of the headspace concentrations of acetone, ethanol, methanol, AA and DMS measured in non-treated (NT) DMEM medium, as well as medium containing 0.1% v/v DMSO (141 000  $\mu\text{M}$ ) alone, and with dissolved diethylaminobenzaldehyde (DEAB; 200  $\mu\text{M}$ ) or disulfiram (DSF; 20  $\mu\text{M}$ ), following 16 hours sealed incubation with no cells present. All headspace concentrations are given in parts-per-billion by volume (ppbv). The instrumental error is typically within 10% (see Smith and Španěl, 2011 (ref. 32)), except in the case of DMS, which was present at concentrations which are approaching the limit of detection of the SIFT-MS instrument

	Compound concentration (M)	Headspace concentrations (ppbv)				
		Acetone	Methanol	Ethanol	AA	DMS
NT	—	190	248	483	104	13
DMSO	$1.4 \times 10^{-2}$	181	242	554	109	33
DEAB	$2.0 \times 10^{-4}$	203	259	421	106	12
DSF	$2.0 \times 10^{-5}$	173	263	478	104	18
Mean	—	187	253	484	106	19

-1C2 molecules and 8000 combined ALDH1B1 and ALDH2 molecules, then  $10^6$  cells are calculated to consume 80% (net) of the AA from the culture medium over 16 hours, but only 1% of the ethanol. In this way the variation in AA headspace concentration can be obtained for other cell numbers and the dashed plot in Fig. 1a is a representation of the predicted variation. This approach assumes that vapour phase/liquid phase equilibrium is established and that Henry's Law applies to this complex system (Henry's Law coefficients have been derived previously in

SIFT-MS experiments<sup>27</sup>). As can be seen, the model plot approximately follows the data points from which we conclude that enzymatic activity is responsible for the loss of AA from the medium. Finally, it should be appreciated that the Henry's Law coefficients for ethanol and AA are greatly different at 37 °C, favouring the partition of AA into the headspace by a factor of about 12 times.<sup>27</sup> Hence, the change in the ethanol headspace concentration for the observed changes in the AA headspace concentration will be relatively small and not discernible within the measurement uncertainty.

**Inhibition of ALDH with DEAB.** In order to investigate the loss of AA *via* enzymatic processes, experiments were carried out in which the ALDH inhibitor DEAB was added at different concentrations to the DMEM medium containing  $1.5(10^7)$  hepG2 cells and the combinations were incubated for 16 hours at 37 °C after which the headspace AA concentrations were measured using SIFT-MS. The results obtained are shown in Fig. 2a, where a general increase in the AA concentration is seen with increasing DEAB in the cell culture media; the rate of increase apparently slowing down at the higher DEAB concentrations.

Headspace AA concentrations were also measured in the presence of a fixed concentration of DEAB as the number of cells in the medium was varied. For these studies a mid-range concentration of DEAB of 200  $\mu\text{M}$  was chosen from a consideration of the data in Fig. 2a and the cell number was varied

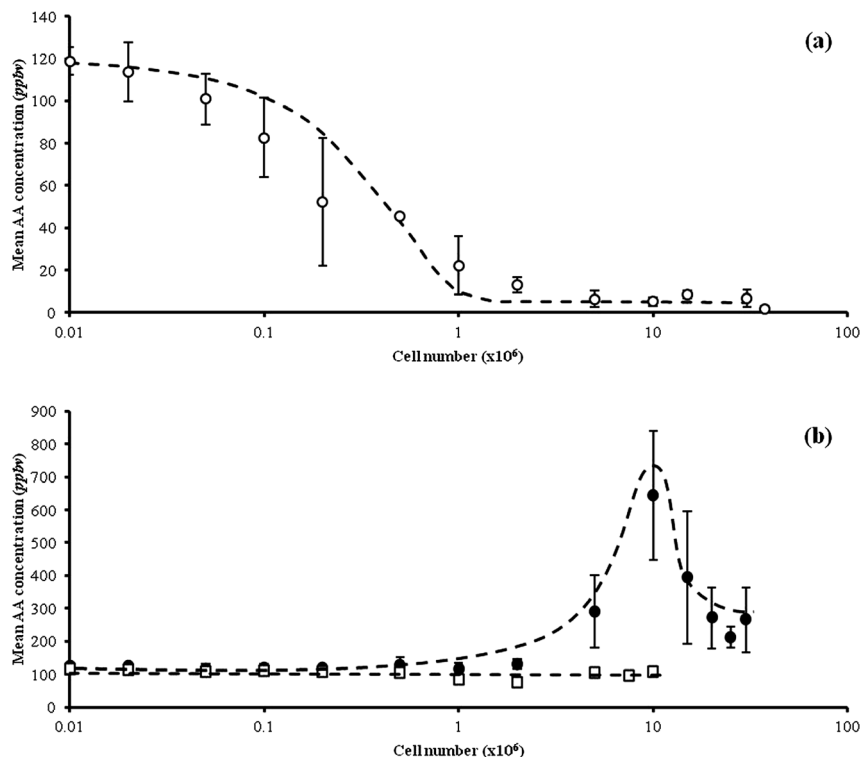


**Fig. 1** Plots showing the AA concentrations, given in parts-per-billion by volume (ppbv), measured in the headspaces hepG2 cell cultures, against the cell number, following a 16-hour incubation period at 37 °C. The cells were contained in 15 mL volumes of DMEM medium, inside sealed 150 mL glass bottles for the duration of this period. In (a), the cells were not treated with ALDH inhibitors (open circles), and the dashed line displays the results of a mathematical model, based on Michaelis–Menton enzyme kinetics (explanation in Results section). In (b), the cells were treated with 200  $\mu\text{M}$  DEAB (closed circles) or 20  $\mu\text{M}$  DSF (open squares) for 16 hours prior to the analysis. All experiments were performed in duplicate and the bars indicate the range of the obtained values. Note the change of scale of the y-axes.



between  $1(10^4)$  and  $5(10^6)$ . The results of these experiments are given in Fig. 1b. The first point to notice is that there is not a reduction in the AA concentration even at the lowest cell number as is seen in the data in Fig. 1a; in fact, there is a small increase compared to the DMEM medium alone. Then as the cell number approaches  $1(10^6)$  a clear increase in the headspace AA occurs and a peak of around 600 ppbv ( $4\text{ }\mu\text{M}$  in the liquid phase) is apparent at about  $1(10^7)$  cells with a subsequent reduction as the cell number is further increased. It is worthy of note that in these DEAB intervention experiments the acetone, methanol and ethanol present in the headspace of each cell culture did not change with cell number.

**Inhibition of ALDH with disulfiram.** Similar experiments to those above were carried out to study the influence of the enzyme inhibitor disulfiram (DSF) on AA production/loss. The DSF was added to the cell cultures at a maximal concentration of  $20\text{ }\mu\text{M}$  (see below in the Sample preparation section). Then the headspace AA concentrations were measured for hepG2 cell cultures over the cell number range from  $1(10^4)$  to  $1(10^7)$  and the results are shown in Fig. 1b. It is clear that no increase in the AA levels occurs; rather a small, continuous decrease from the DMEM headspace levels is observed and not the small but certain increase seen for DEAB addition over the same cell number range. However, this is likely due to the much lower concentration of DSF that was possible compared to that for DEAB (see Sample preparation section).

## Dimethyl sulphide (DMS) measurements in HepG2 cultures

**DMSO reduction to DMS by cellular action and inhibition by DEAB and DSF.** It was observed during the experiments that, following overnight incubation, DMS was present in the headspaces of the cell-containing samples at parts-per-million by volume (ppmv) levels where 0.1% v/v DMSO was initially present in the medium as a solvent or control. This translates to liquid-phase concentrations of  $>300\text{ nM}$ , by Henry's Law. Thus, the effects of ALDH inhibitors DEAB and DSF on the  $\text{DMSO} \rightarrow \text{DMS}$  reduction reactions in hepG2 cells were simultaneously investigated with the AA measurements. As before, the first experiment involved varying the DEAB concentration (dissolved in 0.1% v/v DMSO) in cell cultures containing  $1.5(10^7)$  hepG2 cells. The results of these experiments are shown in Fig. 2b, where it can be seen that from 0 to  $25\text{ }\mu\text{M}$  DEAB, there is a 30% decline in headspace DMS, but little further reduction with increasing DEAB concentration.

The influence of cell numbers on the DMS production from DMSO, and on the inhibitory effects of DEAB, were also investigated. As before, the DEAB concentration was  $200\text{ }\mu\text{M}$  in all samples, with the cell numbers varied. The plot shown in Fig. 3a provides further evidence that DEAB inhibits DMS production. At cell numbers less than  $5(10^5)$ , when only DMSO is present and the ALDH inhibitors are absent, DMS production is negligible (1 ppbv or less in the headspace), but between  $5(10^5)$  and  $5(10^6)$ , the DMS concentration clearly increases. However, when  $200\text{ }\mu\text{M}$  DEAB is also present, DMS production is clearly

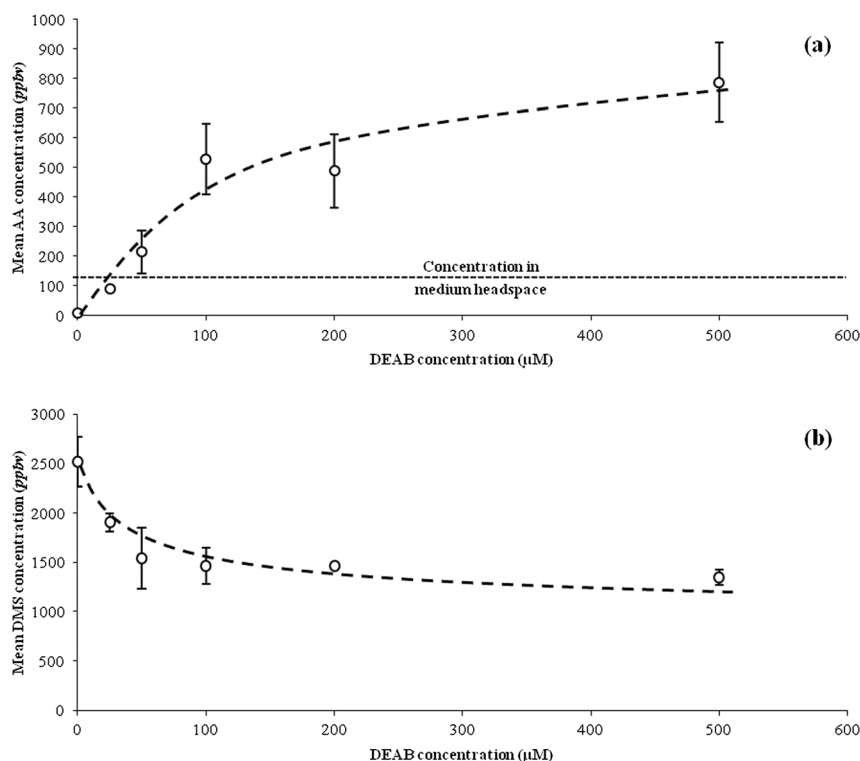


**Fig. 2** Plots showing the measured headspace concentrations of AA (a) and DMS (b), in parts-per-billion by volume (ppbv), against the liquid phase DEAB concentration in cultures containing  $1.5(10^7)$  hepG2 cells in 15 mL of DMEM medium. The DEAB was dissolved in 0.1% v/v DMSO in all experiments. In samples of the medium alone, with no cells, no DMSO and no inhibitor compounds present, the AA concentration was measured to be 130 ppbv, as is indicated with the labelled, short-dashed line, and the measured DMS concentration was 10 ppbv. The long dashed curve is an "eye ball" variation following the experimental points.

reduced and at cell numbers less than  $5(10^6)$  cells there is little production of DMS above the level appropriate to the zero DEAB situation.

For cell numbers greater than  $5(10^6)$  up to  $3(10^7)$ , DMS production continues to increase for both the zero DEAB situation (labelled DMSO) and for the  $200\ \mu\text{M}$  DEAB situation, but inhibition still occurs by the DEAB, as can be seen in Fig. 3b. The DMS concentration appears to increase with cell number in a linear fashion, and the slope of the line declines by about 30% in the presence of the DEAB. A similar level of reduction is observed in the headspace concentration of DMS when DEAB is present, as shown in Fig. 2b. These experiments were conducted from the same “stock” of cells, on the same day (*i.e.* not independent experiments).

When  $20\ \mu\text{M}$  DSF is added, no DMS production is observed, as can also be seen in Fig. 3a. Thus, both DEAB and DSF are able to inhibit the reduction of DMSO to DMS by hepG2 cells.

### Headspace analyses of human mesenchymal stem cell cultures

As a comparison with the hepG2 cell line, similar experiments (see section: Sample preparation) were conducted using primary human bone marrow-derived mesenchymal stem cells (hMSCs). Thus, cultures of approximately  $5(10^6)$  hMSCs were in this case pre-treated for 24 hours during routine tissue flask culture with DEAB and DSF at the liquid concentrations given in Table 2. The results of these exploratory experiments, also given in

Table 2, suggest that only DEAB is an effective inhibitor of ALDH in the hMSCs, under these conditions, and it is also effective at preventing DMS production from DMSO, particularly at the higher DEAB concentration of  $500\ \mu\text{M}$ . DSF, on the other hand, apparently has little or no effect on the ability of the hMSCs to metabolise AA, but it has an inhibiting effect on DMS production from DMSO, although the lower concentration of DSF, relative to the DEAB experiments, may again be a contributing factor to the observed metabolism of AA.

### Assessment of viability in HepG2 and hMSC cultures

The potential effects of the overnight incubation in the sealed bottle on the viability of the hepG2 were observed using live-dead staining, the resulting images being shown in Fig. 4a–d. Here it is clear that the method of keeping the cells sealed for a period of 16 hours, with and without the presence of DEAB or DSF, caused little or no decline in the viability of the hepG2 cells cultured. The effects of treating the cells with the ALDH inhibitors on the viabilities of hepG2 and hMSC cells were also assessed and the resulting luminescence measurements are shown in Fig. 4e and f. These indicate that the inhibitors had no clear affect on the viability of either cell type. However, we have not thoroughly investigated the affects of this protocol of analysis on the condition of the cells, and it is surely true that these adherent cell types will initially proliferate at a decreased rate on transfer to suspension culture conditions and will tend to form

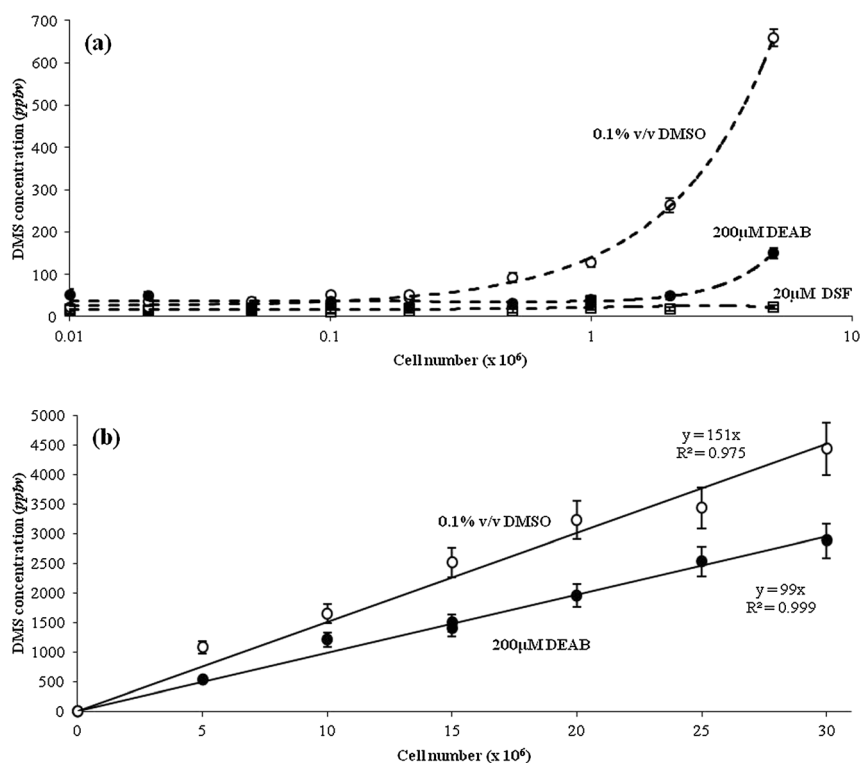


**Fig. 3** Plots showing the headspace DMS concentrations against the numbers of hepG2 cells in DMEM media containing 0.1% v/v DMSO (open circles),  $200\ \mu\text{M}$  DEAB (closed circles) and  $20\ \mu\text{M}$  DSF (open squares). The results were obtained from two independent experiments, which, for clarity, are presented on 2 separate plots by the number of cells present as follows: (a)  $1(10^4)$  to  $5(10^6)$  cells; and (b) 0 to  $3(10^7)$  cells. Note that the  $x$ -axis in (a) is presented on a logarithmic scale, whereas in (b) the scale is linear. The concentration of DMS measured in the headspace of the DMEM medium alone was approximately 10 ppbv in both situations.

**Table 2** AA and DMS concentrations measured in the headspace of hMSCs cultures (in glass bottles sealed by septa) containing typically 5 million cells in 10 mL of DMEM, following 24 hours pre-treatment and a further 16 hours of sealed incubation at 37 °C in the presence of DEAB or DSF. All samples contained 0.1% v/v DMSO (14 500 µM) with the exception of the non-treated cell-containing sample (NT). The mean headspace concentrations of acetaldehyde and DMS in medium without any cells were 89 ± 37 and 6 ± 4 ppbv respectively

Sample	Compound concentration (µM)	AA (ppbv)		DMS (ppbv)	
NT	—	1	9	11	3
DMSO	14 500	6	12	3016	963
DEAB	100	83	171	2269	1756
	200	76	162	2050	1524
	500	120	205	585	934
DSF	10	44	7	29	1067
	20	10	4	878	927

aggregates. These could affect cell behaviour. The essential point is that the cells were all exposed to ostensibly identical conditions, and the inhibitory affects of DEAB and DSF were clear.

## Discussion

This study has described how SIFT-MS can be used to non-invasively identify and accurately quantify volatile metabolite compounds present in the headspace above immortalised cell lines and primary derived cell cultures and thereby analyse metabolic processes occurring *in vitro*. Crucially, it was observed that the hepG2 cells, specifically the functional ALDH present within the cells, metabolised the AA, effectively removing it from the medium. However, when the ALDH enzyme inhibitor DEAB was present in the cell cultures the headspace AA increased, seemingly because the DEAB concentration was sufficient to inhibit the action of the cellular ALDH in removing AA, according to the general equation below.



On the other hand, alcohol dehydrogenase was not inhibited in producing AA, and consequently the liquid phase/vapour phase AA increases. This explains why DEAB appeared to cause the accumulation of AA, as opposed to simply preventing the loss of the compound, as was the case for DSF. The spread in the AA levels measured in each experiment are presumably due to batch-to-batch variations in the cell status (cell cycle), which are likely linked to enzyme expression levels.<sup>38</sup> That the AA level does not fall at the lower cell numbers (see Fig. 1a) is the result of the inhibiting effect of the DEAB molecules. At the highest cell densities the ALDH molecular density could become excessive leaving the DEAB insufficient to prevent the loss of AA, which is seen to decrease towards the initial DMEM value. In short, the accumulation and loss of AA in this way is the key to understanding the form of the data curve shown in Fig. 1b. It is worth mentioning that acetic acid can be quantified by SIFT-MS,<sup>39</sup> but because the pH of the cell culture media (typically 7.5) any acetic

acid formed exists largely as non-volatile acetate ions. However, several biogenic molecular species, including methanol, ethanol, acetone and AA were observed in the headspace of the DMEM medium used exclusively for these studies. Acetone and ethanol were previously reported to originate largely in the FBS, which is routinely added to the cultures.<sup>22</sup> The presence of these compounds was confirmed in these latest studies.

The reduction of DMSO to DMS by the hepG2 cells was observed, which was apparently also inhibited by the presence of DEAB and DSF in the hepG2 cell cultures, which, to the authors' knowledge has not been reported previously. It has previously been reported that DMSO can be reduced by the actions of the enzyme methionine sulfoxide reductase A (MsrA).<sup>40–42</sup> The presence of this enzyme in the hepG2 cells and hMSCs used in this study has been confirmed by quantitative real-time polymerase chain reaction (PCR) (data not shown). It is possible that DEAB and DSF directly inhibited the actions of the cellular MsrA, for example by interacting with the cysteine residues of the enzyme active site.<sup>43</sup> Alternatively, the inhibitors could have indirectly affected the activity of this enzyme by causing aldehyde concentrations to increase in the media, although no linear relation is evident from the plots in Fig. 1b and 3. MsrA is believed to protect tissue from oxidative damage, and may be related to the ageing process. Diminished MsrA activities have also been reported in the brains of Alzheimer's disease patients,<sup>44</sup> and there is evidence to suggest that the enzyme protects dopaminergic cells from Parkinson's disease-related damage.<sup>45</sup> To the authors' knowledge, the possibility of a link between ALDH/AA and MsrA function/activity levels has not been reported in the literature. This may have implications for the use of DSF (Antabuse) for the treatment of alcohol and cocaine addictions, mentioned previously.<sup>11</sup> Also, given that ALDH has also been linked with the development of both

Parkinson's<sup>5</sup> and Alzheimer's<sup>10</sup> diseases, these findings may be significant in the pathology of these diseases.

In summary, we have demonstrated that SIFT-MS can be used for the measurement of volatile compounds emitted by cell cultures, and that these measurements can be used to study cellular activity, including that of specific intracellular enzymes, and even enzyme kinetics. The scope of this technique is not limited to the study of AA metabolism by ALDH, as is demonstrated by the finding that the cell-types studied both reduced DMSO to DMS. Provided that the substrates and/or products of enzymatic reactions are volatile, the described techniques could certainly be applied for the analysis of the metabolic activity of other cell types, including microbial cells and animal cells, which can also be used to study time variations in volatile compound emissions and hence to follow the course of cellular activity and responses to chemical stimuli. Also, as is mentioned in the Introduction, toxic AA and ALDH deficiencies have been

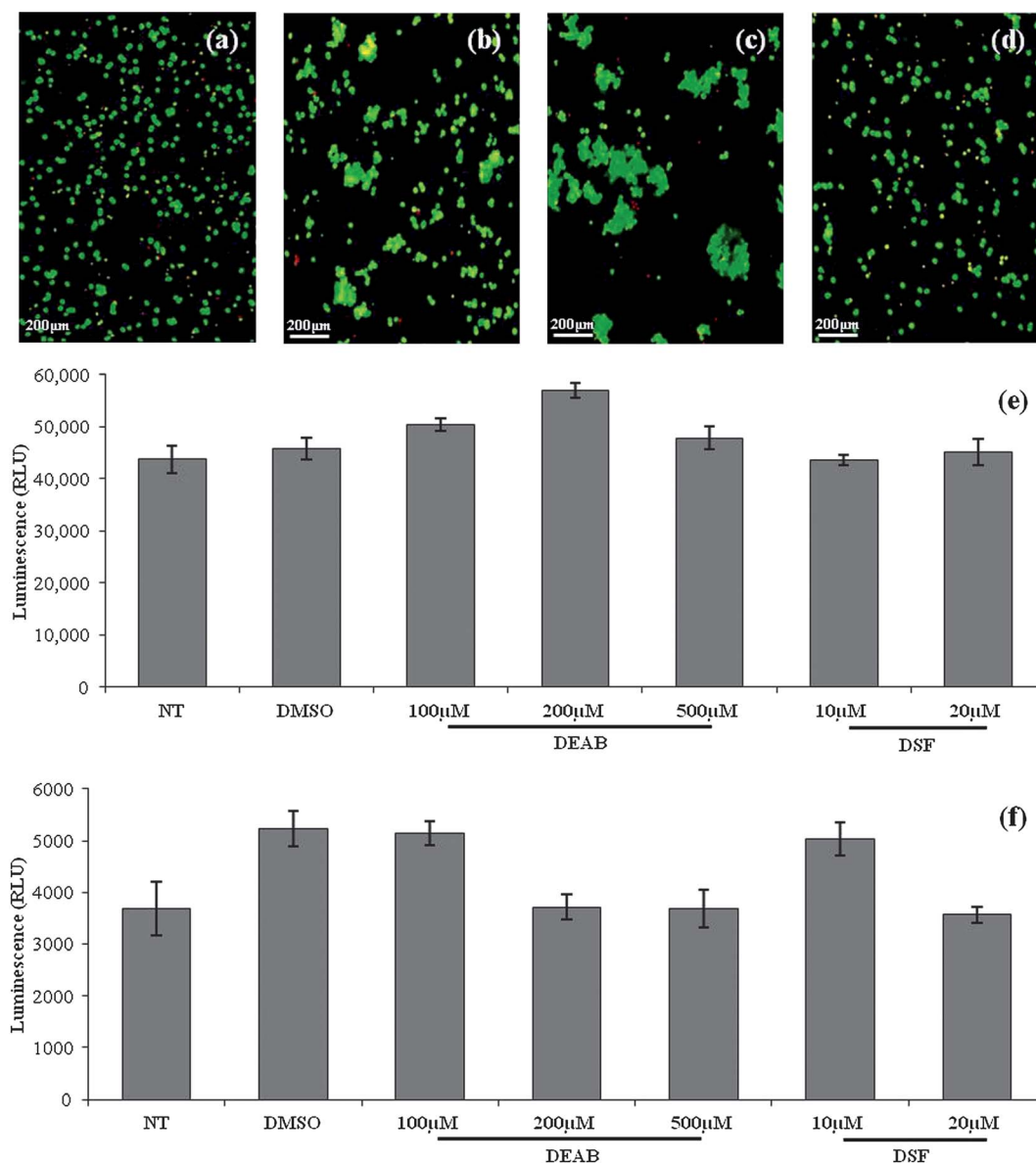


**Fig. 4** Microscopy images of hepG2 cells (a) prior to and (b–d) following overnight incubation inside sealed glass bottles. The cells in (a) and (b) were not treated with ALDH inhibitors, whereas in (c) and (d) 200  $\mu$ M DEAB and 20  $\mu$ M DSF were added to the contained medium respectively. The results of ATPLite assays conducted on hepG2 (e); and hMSC (f), are also shown. The results were obtained following culture under normal conditions (non-treated; NT) or following 16 hours of treatment with 0.1% v/v DMSO, or with ALDH inhibitors: DEAB or DSF. The inhibitor concentrations are indicated on the x-axis where appropriate. The data is presented as the mean  $\pm$  standard error ( $N = 8$ ).

linked to numerous diseases, such as ethanol-induced cancers,<sup>6</sup> alcoholic liver disease<sup>7</sup> and ischaemic tissue diseases.<sup>9</sup> The simple, rapid and non-invasive analytical methods described in this study could surely find utility in drug screening, which could aid in the treatment or prevention of these and other diseases.

## Acknowledgements

We gratefully acknowledge the funding provided by the EPSRC Doctoral Training Centre programme, BBSRC.

## References

- J. T. Berg and L. Stryer, *Biochemistry*, W. H. Freeman and Company, New York, USA, 2002.
- D. Conklin, R. Prough and A. Bhatnagar, *Mol. BioSyst.*, 2007, **3**, 136–150.
- M. F. Wang, C. L. Han and S. J. Yin, *Chem.–Biol. Interact.*, 2009, **178**, 36–39.
- D. Stagos, Y. Chen, C. Brocker, E. Donald, B. C. Jackson, D. J. Orlicky, D. C. Thompson and V. Vasiliou, *Drug Metab. Dispos.*, 2010, **38**, 1679–1687.
- D. Galter, S. Buervenich, A. Carmine, M. Anvret and L. Olson, *Neurobiol. Dis.*, 2003, **14**, 637–647.
- J. S. Moreb, *Curr. Stem Cell Res. Ther.*, 2008, **3**, 237–246.
- C. J. Eriksson, *Alcohol.: Clin. Exp. Res.*, 2001, **25**, 15S–32S.
- T. Mello, E. Ceni, C. Surrenti and A. Galli, *Mol. Aspects Med.*, 2008, **29**, 17–21.
- H. S. White, L. Smith, T. Gentry and A. E. Balber, *J. Stem Cell Res. Ther.*, 2011, **S1**, DOI: 10.4172/2157-7633.S1-001.
- S. Ohta, I. Ohsawa, K. Kamino, F. Ando and H. Shimokata, *Ann. N. Y. Acad. Sci.*, 2004, **1011**, 36–44.

- 11 K. M. Carroll, L. R. Fenton, S. A. Ball, C. Nich, T. L. Frankforter, J. Shi and B. J. Rounsaville, *Arch. Gen. Psychiatry*, 2004, **61**, 264–272.
- 12 P. Marcato, C. A. Dean, D. Pan, R. Araslanova, M. Gillis, M. Joshi, L. Helyer, L. Pan, A. Leidal, S. Gujar, C. A. Giacomantonio and P. W. K. Lee, *Stem Cells*, 2011, **29**, 32–45.
- 13 C. Yu, Z. Yao, J. Dai, H. Zhang, J. Escara-Wilke, X. Zhang and E. T. Keller, *In Vivo*, 2011, **25**, 69–76.
- 14 M. P. Kim, J. B. Fleming, H. Wang, J. L. Abbruzzese, W. Choi, S. Kopetz, D. J. McConkey, D. B. Evans and G. E. Gallick, *PLoS One*, 2011, **6**, e20636.
- 15 J. S. Moreb, D. Mohuczy, B. Ostmark and J. R. Zucali, *Cancer Chemother. Pharmacol.*, 2007, **59**, 127–136.
- 16 J. S. Moreb, D. Ucar, S. Han, J. K. Amory, A. S. Goldstein, B. Ostmark and L. J. Chang, *Chem.-Biol. Interact.*, 2012, **195**, 52–60.
- 17 D. Cen, D. Brayton, B. Shahandeh, F. L. Meyskens and P. J. Farmer, *J. Med. Chem.*, 2004, **47**, 6914–6920.
- 18 S. S. Brar, C. Grigg, K. S. Wilson, W. D. J. Holder, D. Dreau, C. Austin, M. Foster, A. J. Ghio, A. R. Whorton, G. W. Stowell, L. B. Whittall, R. R. Whittle, D. P. White and T. P. Kennedy, *Mol. Cancer Ther.*, 2004, **3**, 1049–1060.
- 19 M. V. Lioznov, P. Freiburger, N. Kroger, A. R. Zander and B. Fehse, *Bone Marrow Transplant.*, 2005, **35**, 909–914.
- 20 J. S. Moreb, J. R. Zucali, B. Ostmark and N. A. Benson, *Cytometry, Part B*, 2007, **72B**, 281–289.
- 21 D. Smith, T. Wang, J. Sulé-Suso, P. Španěl and A. J. El Haj, *Rapid Commun. Mass Spectrom.*, 2003, **17**, 845–850.
- 22 J. Sulé-Suso, A. Pysanenko, P. Španěl and D. Smith, *Analyst*, 2009, **134**, 2419–2425.
- 23 H. W. Shin, B. Umber, S. Meinardi, S. Y. Leu, F. Zaldivar, D. Blake and D. Cooper, *J. Transl. Med.*, 2009, **7**, 31.
- 24 C. Brunner, W. Szymczak, V. Hollriegel, S. Mortl, H. Oelmez, A. Bergner, R. M. Huber, C. Hoeschen and U. Oeh, *Anal. Bioanal. Chem.*, 2010, **397**, 2315–2324.
- 25 W. Filipiak, A. Sponring, T. Mikoviny, C. Ager, J. Schubert, W. Miekisch, A. Amann and J. Troppmair, *Cancer Cell Int.*, 2008, **8**, 17.
- 26 A. Sponring, W. Filipiak, T. Mikoviny, C. Ager, J. Schubert, W. Miekisch, A. Amann and J. Troppmair, *Anticancer Res.*, 2009, **29**, 419–426.
- 27 P. Španěl, A. M. Diskin, S. M. Abbott, T. Wang and D. Smith, *Rapid Commun. Mass Spectrom.*, 2002, **16**, 2148–2153.
- 28 K. Dryahina, F. Pehal, D. Smith and P. Španěl, *Int. J. Mass Spectrom.*, 2009, **286**, 1–6.
- 29 D. Smith and P. Španěl, *Mass Spectrom. Rev.*, 2005, **24**, 661–700.
- 30 P. Španěl, K. Dryahina and D. Smith, *Int. J. Mass Spectrom.*, 2006, **249–250**, 230–239.
- 31 T. W. E. Chippendale, P. Španěl and D. Smith, *Rapid Commun. Mass Spectrom.*, 2011, **25**, 2163–2172.
- 32 D. Smith and P. Španěl, *Analyst*, 2011, **136**, 2009–2032.
- 33 P. Španěl and D. Smith, *J. Phys. Chem.*, 1995, **99**, 15551–15556.
- 34 P. Španěl and D. Smith, *Int. J. Mass Spectrom.*, 1998, **176**, 167–176.
- 35 P. Španěl and D. Smith, *J. Breath Res.*, 2008, **2**, 046003.
- 36 D. Smith, T. W. E. Chippendale and P. Španěl, *Curr. Anal. Chem.*, in press.
- 37 S. L. Lee, H. T. Shih, Y. C. Chi, Y. P. Li and S. J. Yin, *Chem.-Biol. Interact.*, 2011, **191**, 26–31.
- 38 M. D. C. Córdoba-Pedregosa, J. M. Villalba, D. González-Aragón, R. I. Bello and F. J. Alcaín, *Anticancer Res.*, 2006, **26**, 3535–3540.
- 39 A. Pysanenko, P. Španěl and D. Smith, *Int. J. Mass Spectrom.*, 2009, **285**, 42–48.
- 40 J. Moskovitz, H. Weissbach and N. Brot, *Proc. Natl. Acad. Sci. U. S. A.*, 1996, **93**, 2095–2099.
- 41 H. Weissbach, L. Resnick and N. Brot, *Biochim. Biophys. Acta Protein Proteomics*, 2005, **1703**, 203–212.
- 42 G. H. Kwak, S. H. Choi, J. R. Kim and H. Y. Kim, *BMB Rep.*, 2009, **42**, 580–585.
- 43 W. T. Lowther, N. Brot, H. Weissbach, J. F. Honek and B. W. Matthews, *Proc. Natl. Acad. Sci. U. S. A.*, 2000, **97**, 6463–6468.
- 44 S. P. Gabbita, M. Y. Aksenov, M. A. Lovell and W. R. Markesbery, *J. Neurochem.*, 1999, **73**, 1660–1666.
- 45 F. Liu, J. Hindupur, J. L. Nguyen, K. J. Ruf, J. Zhu, J. L. Schieler, C. C. Bonham, K. V. Wood, V. J. Davisson and J. C. Rochet, *Free Radical Biol. Med.*, 2008, **45**, 242–255.

**A6. Time-resolved selected ion flow tube mass spectrometric quantification of the volatile compounds generated by *E. coli* JM109 cultured in two different media**

Chippendale TWE, Španěl P, Smith D. *Rapid Commun Mass Spectrom* 2011, 25:2163-2172.



Rapid Commun. Mass Spectrom. 2011, 25, 2163–2172  
(wileyonlinelibrary.com) DOI: 10.1002/rcm.5099

# Time-resolved selected ion flow tube mass spectrometric quantification of the volatile compounds generated by *E. coli* JM109 cultured in two different media

Thomas W. E. Chippendale<sup>1</sup>, Patrik Španěl<sup>1,2\*</sup> and David Smith<sup>1</sup>

<sup>1</sup>Institute for Science and Technology in Medicine, School of Medicine, Keele University, Thornburrow Drive, Hartshill, Stoke-on-Trent ST4 7QB, UK

<sup>2</sup>J. Heyrovský Institute of Physical Chemistry, Academy of Sciences of the Czech Republic, Dolejškova 3, 182 23, Prague 8, Czech Republic

Preliminary measurements have been made of the volatile compounds emitted by the bacterium *E. coli* JM109 cultured in the commonly used media Dulbecco's modified Eagle's medium (DMEM) and lysogeny broth (LB) using selected ion flow tube mass spectrometry, SIFT-MS, as a step towards the real time, non-invasive monitoring of accidental infections of mammalian cell cultures. In one procedure, the culture medium alone and the *E. coli* cells/medium combination were held at 37°C in bottles sealed with septa for a given time period, usually overnight, to allow the bacterium to proliferate, after which the captured headspace was analysed directly by SIFT-MS. Several compounds were seen to be produced by the *E. coli* cells that depended on the liquid medium used: when cultured in DMEM, copious amounts of ethanol, acetaldehyde and hydrogen sulphide were produced; in LB ammonia is the major volatile product. In a second procedure, to ensure aerobic conditions prevailed in the cell culture, selected volatile compounds were monitored by SIFT-MS in real time for several hours above the open-to-air *E. coli*/DMEM culture held at close to 37°C. The temporal variations in the concentrations of some compounds, which reflect their production rates in the culture, indicate maxima. Thus, the maxima in the ethanol and acetaldehyde production are a reflection of the reduction of glucose from the DMEM by the vigorous *E. coli* cells and the maximum in the hydrogen sulphide level is an indication of the loss of the sulphur-bearing amino acids from the DMEM. Serendipitously, emissions from DMEM inadvertently infected with the bacterium *C. testosteroni* were observed when large quantities of ammonia were seen to be produced. The results of this preliminary study suggest that monitoring volatile compounds might assist in the early detection of bacterial infection in large-scale bioreactors. Copyright © 2011 John Wiley & Sons, Ltd.

There is a growing interest in identifying and quantifying volatile compounds that are emitted from mammalian and bacterial cell cultures *in vitro*, since these may assist in diagnosing and monitoring related diseased states *in vivo*, for example via breath analysis and urine headspace analysis. Additionally, if volatile biomarkers of the early onset of infection in large-scale industrial bioreactors<sup>[1]</sup> could be identified, especially by real-time continuous monitoring, then this could be of great value economically. It is with these uses in mind, especially breath analysis for clinical diagnosis and therapeutic monitoring, that we have developed selected ion flow tube mass spectrometry, SIFT-MS.<sup>[2–4]</sup> With SIFT-MS, analyses of single exhalations of breath can be carried out obviating sample collection with all the disadvantages this brings, making SIFT-MS a valuable technique for ambient gas analysis.<sup>[5]</sup> The development of SIFT-MS and its application to breath analysis and in other areas of research by several research groups are summarized in recent review papers.<sup>[6,7]</sup>

Relevant to the present paper are the previous SIFT-MS pilot studies of the volatile organic compounds, VOCs, released by two cancer cell lines (CALU-1 and SKMES) cultured *in vitro*<sup>[8]</sup> which showed that both emit acetaldehyde in amounts in close proportion to the number of cells in the medium, in this case DMEM (Dulbecco's modified Eagle's medium) supplemented with 10% (v/v) FBS (foetal bovine serum). More recently, we have extended this work by quantifying both acetaldehyde and carbon dioxide in the headspace of malignant and non-malignant lung cell lines *in vitro*, recognising that some acetaldehyde, ethanol and acetone were released by the FBS into the cell culture headspace.<sup>[9]</sup> It was seen in this study that one of the non-malignant cell lines actually removed acetaldehyde from the DMEM/FBS, a feature that we see again in our most recent studies of mesenchymal stem cells.

The focus of the present study was to extend the mammalian (human) cell culture work to the study of the volatile compounds emitted by microbial cultures. Our first entry into this topic involved a study of the VOCs released by the bacterium *Pseudomonas aeruginosa*, PA, present in the sputum from cystic fibrosis patients when cultured on blood agar and *Pseudomonas*-selective media plates. Ammonia, acetonitrile, ethanol, dimethyl disulphide and hydrogen cyanide, HCN, were detected and quantified by SIFT-MS.<sup>[10]</sup>

\* Correspondence to: P. Španěl, J. Heyrovský Institute of Physical Chemistry, Academy of Sciences of the Czech Republic, Dolejškova 3, 182 23, Prague 8, Czech Republic.  
E-mail: spanel@jh-inst.cas.cz

Subsequently, HCN was detected in the exhaled breath of children suffering from cystic fibrosis<sup>[11]</sup> and this offers the opportunity to monitor the presence of *PA* in the airways and its eradication by therapy.

There have been few studies of microbial cultures in the liquid medium phase; microbial studies have focused mostly on foods,<sup>[12]</sup> sewage<sup>[13]</sup> and agriculture.<sup>[14]</sup> A recent study using proton transfer reaction mass spectrometry, PTR-MS, of microbial volatile metabolites<sup>[15]</sup> indicated that three bacterial species and one fungus could be distinguished by the relative amounts of product ions tentatively related to the released methanol, ethanol, acetaldehyde, indole and 2-butanone. There has also been some SIFT-MS work to detect and identify VOC emissions from medically important fungi.<sup>[16]</sup> Six different fungi were cultured in five different media and varying concentrations of ethanol, acetaldehyde, acetone, methanethiol and 2-butanone were observed. An important observation is that the compounds detected varied both for the type of fungus and medium that was used to culture them. Similar work has also been carried out using SIFT-MS to identify the VOCs produced by different bacteria,<sup>[17]</sup> and to compare the speed with which bacterial infections could be identified with an automated blood culture system.<sup>[18]</sup> SIFT-MS was shown to be capable of identifying almost all species of bacteria included in the study after 8 h of incubation, several hours earlier than the automated system. In two of these studies,<sup>[16,17]</sup> the headspace concentrations of some of the detected compounds were quantified using only crude rating systems based on the counts-per-second of their product ions. In a more recent study, multivariate analysis was used to treat SIFT-MS data in order to distinguish between different species and strains of bacteria cultured using tryptone-yeast extract medium.<sup>[19]</sup>

Following 5 h of culture, this revealed that almost all cell populations were distinguishable in clearly defined populations on a multidimensional scaling plot, and this differentiation improved when data obtained after a further 24 h of culture were analysed. A study has been carried out of the emission of volatile compounds from *Bacillus cereus* and *PA* contaminations in Chinese hamster ovary (CHO) cell perfusion bioreactor cultures using a gas sensor array. Unidentified volatile compounds produced a response of the sensor 10 h before the presence of the infecting microorganisms could be detected by changes in pH and the concentration of dissolved oxygen.<sup>[20]</sup> This work is perhaps indicative of the potential value of early identification of microbial infections in bioreactor cultures to industry.

The present pilot study is intended to point the way to the proper identification and quantification by SIFT-MS of volatile compounds emitted by various bacteria cultured in various liquid media and ultimately to facilitate the recognition of the onset of bacterial infection of cell cultures. In this initial study we chose to investigate in detail the time profiles of the concentrations of VOCs released by a defined strain of bacterium *Escherichia coli* (*E. coli*) cultured in two commonly used media and to complement the results with analyses of VOC emissions from a medium, DMEM, unintentionally infected with the bacterium *Comamonas testosteroni*.

## EXPERIMENTAL

### SIFT-MS

The SIFT-MS analytical technique for sampling liquid headspace has been described in detail in several research and review papers,<sup>[6,7,9,21–23]</sup> and need not be repeated here. It is

**Table 1.** List of the precursor ions and the primary product ions together with their mass-to-charge ratio,  $m/z$ , and those of their hydrates, as used for the compound analyses reported in this paper

Compound	Precursor ions ( $m/z$ )	Simplest product ion	$m/z^a$
Water vapour	$H_3O^+(H_2O)_{0,1,2,3}$ (19, 37, 55, 73)	$H_3O^+(H_2O)$	37, 55, 73
Ammonia		$NH_4^+$	18, 36, 54
Methanol		$CH_5O^+$	33, 51, 69
Hydrogen sulphide		$H_3S^+$	35
Acetaldehyde		$C_2H_5O^+$	45, 63, 81
Ethanol		$C_2H_7O^+$	47, 65, 83
Methanethiol		$CH_5S^+$	49, 67, 85
Acetone		$C_3H_7O^+$	59, 77, 95
Propanol		$C_3H_7^+$	43
Dimethyl disulphide		$C_2H_7S_2^+$	95 (97)
Acetone	$NO^+(H_2O)_{0,1,2}$ (30, 48, 66)	$NO^+C_3H_6O$	88
Butanone		$NO^+C_4H_8O$	102
Dimethyl disulphide		$C_2H_6S_2^+$	94 (96)
Ammonia	$O_2^+$ (32)	$NH_3^+$	17, 35
Dimethyl disulphide		$C_2H_6S_2^+$	94 (96)

<sup>a</sup>The  $m/z$  values of the isotopologues of the sulphur-containing compounds are indicated in parentheses. The relative contributions of the precursor ions,  $H_3O^+(H_2O)_{1,2,3}$ , to the analysis of each compound, either by proton transfer or ligand switching, is dependent on the reaction energetics.<sup>[24]</sup> The judicious choice of precursor ion minimises ambiguity that can result in the overlap of different product ions with the same  $m/z$  value. For example, for the analysis of propanol, only the characteristic ion at  $m/z$  43 is used to avoid overlaps with the characteristic ions of the isobaric acetic acid and methyl formate; see the text for further explanation.



sufficient to say that the analysis of the captured headspace of liquid cell cultures is achieved by penetrating the septum that seals the glass bottle containing the medium/cell/bacterial culture with a hypodermic needle connected directly to the sample inlet port of the SIFT-MS instrument.<sup>[23]</sup> There is minimum dead space volume and so the response of the system is very rapid. The glass bottles have a volume of about 200 mL and the volume of medium/cells was standardised at 25 mL. The sampling flow rate was approximately 40 mL/min, and so the headspace volume was sufficient to allow a 1-min analysis time without appreciably lowering the pressure in

the bottle that results from the sampling process. In a subsequent experiment, after recognising the virility of *E. coli* cells, the headspace of the bacterial culture was analysed when open to the atmosphere for the reason alluded to in the next section.

The appropriate precursor (reagent) ion was chosen (from either  $\text{H}_3\text{O}^+$ ,  $\text{NO}^+$  or  $\text{O}_2^+$ ) and the SIFT-MS instrument was operated in the full scan (FS) mode in which an analytical mass spectrum was acquired over a chosen range of mass-to-charge ratio,  $m/z$ , when the spectrum (see examples later) provided the information from which the volatile compounds

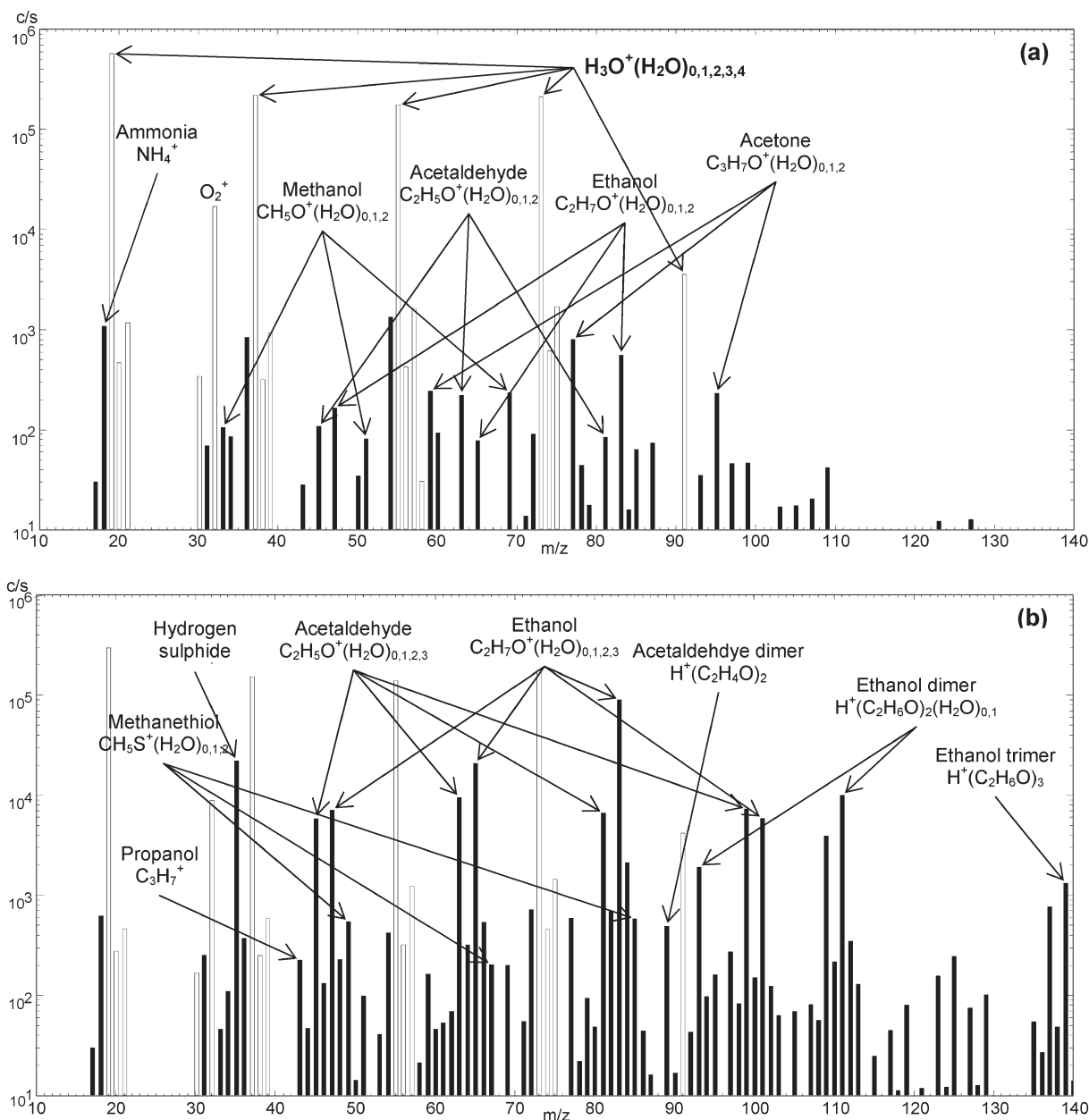


**Figure 1.** SIFT-MS spectra (counts-per-second, c/s, against mass-to-charge ratio,  $m/z$ ) obtained using  $\text{H}_3\text{O}^+$  precursor ions for the analysis of the captured (contained) headspace of (a) 25 mL of DMEM supplemented with 10% (v/v) FBS and 2 mM L-glutamine and (b) 24 mL of the same medium with 1 mL of highly concentrated *E. coli* cells in LB medium following overnight incubation at 37°C of both the medium and the medium/cells culture. Only the positively identified major compounds are indicated.

in the headspace of the liquid were identified and approximately quantified. The instrument can then be operated in the multiple ion monitoring (MIM) mode in which the appropriate primary precursor ion and its hydrates<sup>[24]</sup> and characteristic product ions and their hydrates of chosen volatile compounds (see Table 1) are selectively monitored and this provides a more accurate quantification than does the FS mode of data acquisition.

### Preparation of bacterial cultures

The JM109 strain of *E. coli* used throughout this pilot study is widely used for producing large amounts of a specific gene, which can be transfected into mammalian cells (genetic modification) to elicit a desired response, such as increased production of a particular protein.<sup>[25,26]</sup> These *E. coli* cells (originally purchased from Stratagene, now Agilent) were initially cultured overnight at 37°C in lysogeny broth (LB), which contained no glucose, using a shaker flask system in which the culture was open to the atmosphere. In this way the cells reached a high number density, and based on optical density measurements using a 600 nm wavelength, the high density suspensions were estimated to contain 1.5–2.0 billion cells per millilitre. 1 mL samples of this medium/cell composite were transferred to the sample bottles containing 24 mL of either DMEM (Sigma-Aldrich) supplemented with 10% (v/v) FBS and 2 mM L-glutamine or LB. The bottles were sealed by a septum and incubated overnight at 37°C. The following morning the cell density had clearly increased in both samples and, in addition, the DMEM/cell culture, which contained a phenol red indicator, had changed to a yellow colour, indicating a reduction of the pH of the sample.

LB is a nutritionally rich medium primarily used for bacterial growth. There are several common formulations of LB, but they generally share a similar composition of ingredients used to promote growth, including nitrogenous peptides formed from the enzymatic digestion of casein (collectively known as tryptone), vitamins, trace elements and minerals.

DMEM, on the other hand, is commonly used in mammalian cell culture, and the high glucose (4.5 g/L) variant was used throughout this work. Its other components include a host of inorganic salts, amino acids and vitamins. As we show below, the different compositions of these two media result in the production of very different major volatile compounds.

An important comment is now in order regarding incubation of the bacterial cultures in the sealed bottles. This procedure was previously investigated very thoroughly for our previous cell culture work.<sup>[8,9]</sup> The malignant and non-malignant mammalian cells that we have worked with are not vigorous and during overnight (about 1000 min) culture the production of volatiles is relatively slow, and the consequential loss of oxygen from the sealed headspace is not sufficient to transit from aerobic to anaerobic conditions; significantly, after culture the cell viability was always around 95%. However, as expected, the bacterial cells are much more vigorous and can consume the enclosed oxygen more quickly. It is difficult to model the oxygen loss but it does seem likely that its partial pressure will fall during an overnight incubation period so the conditions might become somewhat hypoxic and the metabolism of the bacteria may begin to switch from aerobic to anaerobic. Thus, as explained in the previous section, the real-time production of volatile compounds was investigated in the headspace above the bacterial cultures when open to the atmosphere.

## RESULTS

### *E. coli* cultured in DMEM

In all these measurements the headspace of the medium alone (also held at 37°C overnight in a sealed bottle) was analysed, immediately followed by the analysis of medium/bacterial culture headspace. Sample FS spectra obtained using H<sub>3</sub>O<sup>+</sup> precursor ions are shown in Fig. 1. These spectra were obtained by scanning the analytical mass spectrometer three consecutive times each for 20 s. The FS spectrum obtained

**Table 2.** Concentrations of various compounds (in parts-per-billion, ppb) as measured by SIFT-MS in the captured headspace above different concentrations of growing cultures of *E. coli* JM109 in DMEM with 10% FBS (v/v) and 2 mM L-glutamine

Compound	Primary precursor ion	<i>E. coli</i> added (mL) <sup>a</sup>		
		0	1	5
Methanol	H <sub>3</sub> O <sup>+</sup>	270	280	300
Hydrogen sulphide		10	1000	37,000
Acetaldehyde		150	10,000	16,000
Ethanol		600	37,000	67,000
Methanethiol		10	350	1500
Propanol		50	160	150
Acetone	NO <sup>+</sup>	420	380	250
Dimethyl disulphide		10	500	1000
Ammonia	O <sub>2</sub> <sup>+</sup>	700	700	600

<sup>a</sup>The bacteria were first cultured overnight in shaker flasks containing LB, resulting in a highly concentrated cell suspension the following morning. A volume of this suspension, indicated in the top row of the table, was then added to bottles containing DMEM so that the final volume was always 25 mL. These *E. coli*/DMEM suspensions were cultured overnight and analysed in the morning. Note that there is not a simple relationship between the initial number of *E. coli* cells and the headspace concentrations of the volatile compounds.

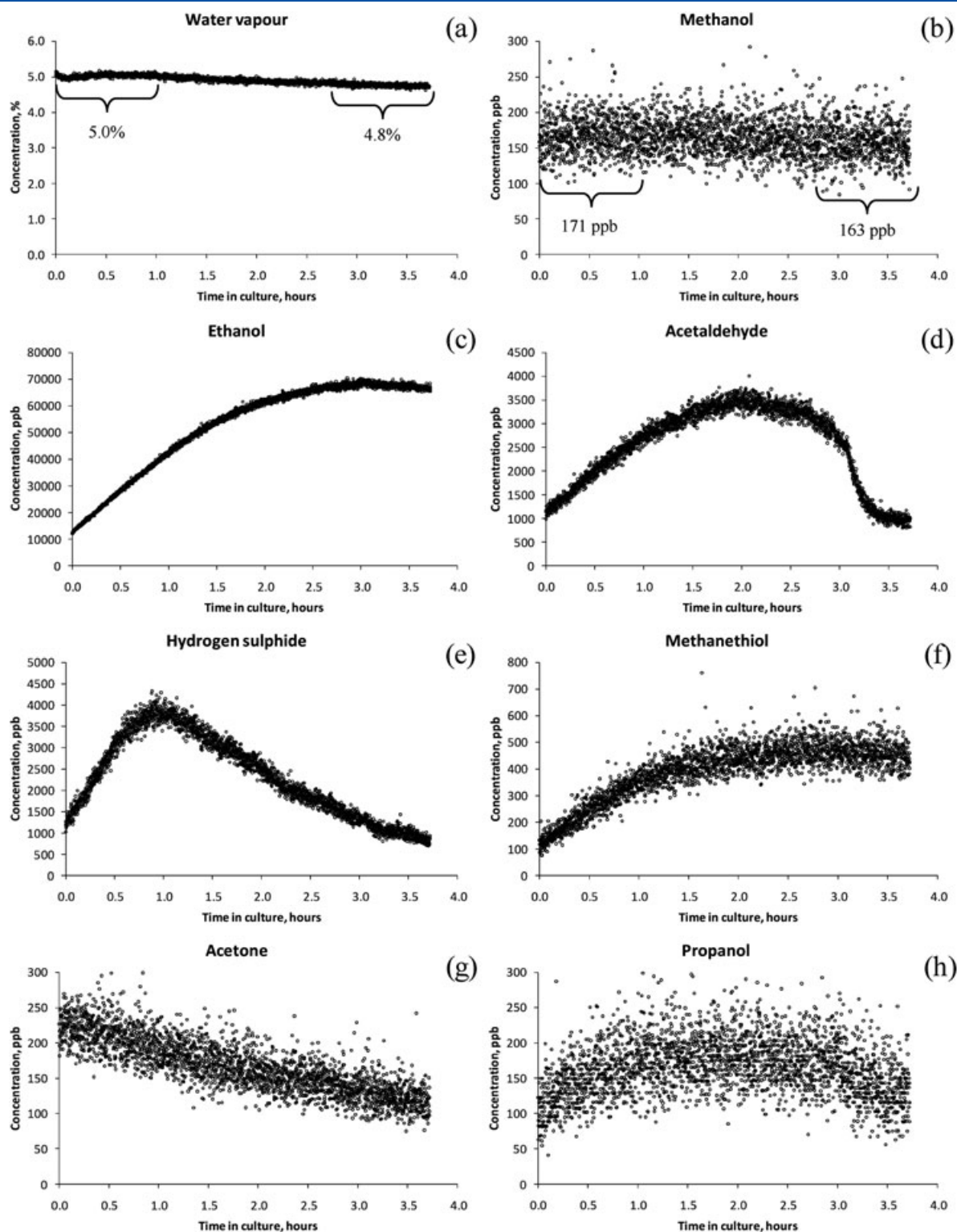


**Figure 2.** Plots of concentration (parts-per-billion, ppb) against time (h) for several compounds emitted from 15 mL of DMEM, supplemented with 10% (v/v) FBS and 2 mM L-glutamine, together with 10 mL of LB medium that contained approximately 15–20 billion *E. coli* cells cultured over a 4-h period near 37°C in an open glass bottle of volume 200 mL, as measured by SIFT-MS using the  $\text{H}_3\text{O}^+$  precursor ion: (a) water vapour; (b) methanol; (c) ethanol; (d) acetaldehyde; (e) hydrogen sulphide; (f) methanethiol; (g) acetone; and (h) propanol. The mean absolute concentrations of water vapour (in percentage, %) and methanol (ppb) are also shown in (a) and (b), respectively, for the first and last hour of the experiment, which both indicate about a 5% decline from the starting measurement over the course of the analysis due to a minor detuning of the analytical mass spectrometer over the 4-h time period. Note the very large number of data points (about 2700) on each plot. See the text for a discussion of these data. Note the larger statistical scatter of the data for the lower compound concentrations.

on analysing the headspace of the medium alone is shown in Fig. 1(a) and that for the medium/cells culture is shown in Fig. 1(b). Clearly, the major peaks in these spectra are the hydronium ion and its hydrates at  $m/z$  values of 19, 37, 55, 73 and 91; the relative signal levels (ion count rates) of these ions provides the absolute humidity of the headspace gas,<sup>[27]</sup> which is typically close to 5%. The smaller peaks in the medium headspace spectrum are characteristic of ethanol (concentration of 500 ppb), acetaldehyde (150 ppb), acetone (500 ppb) and ammonia (700 ppb). It is understood that these compounds originate from the FBS that is added to the DMEM, as mentioned above.

Now compare the spectrum in Fig. 1(a) with that obtained for the analysis of the medium/cell culture in Fig. 1(b) and notice the relatively intensive peaks at an  $m/z$  value of 35, undoubtedly due to the presence of hydrogen sulphide,  $H_2S$ <sup>[28]</sup> (present at the high concentration of about 50 parts-per-million, ppm), and those at  $m/z$  45, 63 and 81, which are due to acetaldehyde (about 10 ppm) and  $m/z$  47, 65 and 83 due to ethanol (about 100 ppm). The concentration of ethanol is so high that the proton-bound dimer and trimer ions of this compound are clearly present,<sup>[21]</sup> as indicated in Fig. 1(b), as is the proton-bound dimer ion of acetaldehyde. Also seen on this spectrum is methanethiol ( $m/z$  49, 67 and 85). Measurements with two different numbers of *E. coli* cells (assessed by adding different volumes of a stock suspension of these bacterial cells to fresh DMEM, maintaining the total volume at 25 mL; actual numbers of cells not determined) gave the results seen in Table 2. Note that there is not a simple relationship between the compound headspace concentrations and the five-fold increase in cells numbers. The fractional increase in ethanol and acetaldehyde is much less than five times and this we judge to be due to the depletion of the glucose from the medium, which is the metabolic source of these compounds (see also Fig. 2). There is also evidence to suggest that propanol and dimethyl disulphide are produced in smaller quantities, although accurate analyses, especially of low level compounds, might be influenced by the extremely high ethanol and acetaldehyde concentrations. These compounds are further discussed below.

In view of the very large concentrations of the captured major headspace compounds, the cultures were set up again in the glass bottles (10 mL of *E. coli* broth added to 15 mL of DMEM) and placed into the temperature enclosure at 37°C. The open neck of the bottle was positioned close to a small hole in the wall of the enclosure (and therefore at a somewhat lower temperature than 37°C) and the needle normally used to penetrate the septum was placed a few centimetres inside the bottle allowing the headspace to be continuously sampled and analysed for several chosen compounds using the MIM mode of data acquisition for about 4 h. In this way there was a free flow of air into the bottle, and free flow of trace compounds out of the bottle could take place principally by diffusion, since the headspace was not agitated. The number of precursor and characteristic product ions that had to be sampled amounted to 25 in this particular MIM mode study. This meant that each compound under analysis was sampled every 5 s, which in the approximately 14 000 s of observation realised about 2700 data points (analyses) for each compound. The very interesting results of the time variation of the headspace concentrations of the individual compounds are shown in Fig. 2.

Note in Fig. 2(a) the constancy of the water vapour pressure at about 5% over the total observational period, this being equivalent to a temperature of about 35°C. The measurement of the expected steady water vapour level is an indicator of the instrument stability. Notice in Fig. 2(b) that the methanol concentration is also closely invariant over the observational period at a concentration of 180 ppb with a standard deviation, SD, of 52 ppb. Its origin is the FBS supplement in the DMEM medium and so *E. coli* JM109 in DMEM does not generate methanol (but some fungi do so, as mentioned in the last section of this paper).

Ethanol is the most abundant compound present in the open headspace, as expected in view of the data presented in Table 2 that relates to the contained headspace. Its concentration increases as the *E. coli* cell numbers grow reaching a zenith at the end of the observational period when it begins to fall, again presumably due to the depletion of the glucose in the medium (see Fig. 2(c)). The acetaldehyde concentration also increases and reaches its zenith earlier than that for ethanol and its reduction is faster, reflecting a common origin (glucose) of these related compounds. Notice that its maximum concentration of 3.5 ppm is 3–4 times lower than its value reached in the contained headspace (Fig. 2(d) and Table 2). This is explained by the high volatility of acetaldehyde, which is more than ten times greater than that of ethanol, as reflected in the much greater Henry's Law coefficient.<sup>[23]</sup>

A similar situation pertains to the very volatile hydrogen sulphide,  $H_2S$ , the concentration of which peaks earlier and declines more quickly than that of the acetaldehyde, and can be seen to reach a maximum of about 4 ppm, some ten times lower than the contained concentration (see Fig. 2(e) and Table 2). The origin of the  $H_2S$  is assumed to be the sulphur-bearing amino acids present in the DMEM (L-cysteine and L-methionine), which is relatively quickly consumed by the *E. coli* cells. The concentration reached by the methanethiol, about 500 ppb, is several times lower than that in the contained headspace (Fig. 2(f) and Table 2).

The acetone headspace concentration apparently reduces during the period of the observations (see Fig. 2(g)). The origin of the acetone is the FBS in the DMEM. This loss can either be due to evaporative loss from the medium or that the *E. coli* cells are actually using it as a source of energy. Loss due to consumption seems unlikely, because of the approximate constancy of the acetone above the contained medium alone and the cell cultures (see Table 2). There is an indication that propanol is produced in the cell cultures, as seen in Fig. 2(h) and Table 2. The concentration of propanol was evaluated using the  $m/z$  43 product ion only.<sup>[29]</sup> The protonated propanol ion at  $m/z$  61 was avoided, because of the potential overlap with the protonated ions of the isobaric compounds methyl formate and acetic acid,<sup>[30]</sup> made very necessary because of the presence of a small concentration of acetic acid (100 ppb), as indicated by  $m/z$  90 product ions when  $NO^+$  was used to analyse the headspace.

### *E. coli* culture in LB

As before, the headspace of the LB medium alone (also held at 37°C overnight in a sealed bottle) was analysed, immediately followed by the analysis of medium/bacterial culture headspace. Sample FS spectra obtained using  $H_3O^+$  precursor



ions are shown in Fig. 3, that for the headspace of the medium alone in Fig. 3(a) and that for the LB medium/cell culture in Fig. 3(b). Clearly, the major peaks in these spectra are the hydronium ion and its hydrates; the smaller peaks in the medium headspace spectrum are characteristic of ethanol (300 ppb), acetaldehyde (600 ppb), ammonia (400 ppb) and acetone (340 ppb).

Now compare the spectrum in Fig. 3(a) with that obtained for the analysis of the medium/cell culture in Fig. 3(b) and notice the very large peaks at  $m/z$  values of 18, 36 and 54, undoubtedly due to ammonia,  $\text{NH}_3$  (present at relatively large concentration of 50 ppm),<sup>[31]</sup> and those smaller but

significant peaks at  $m/z$  values of 49, due to methanethiol, and  $m/z$  95 and 97, due to the  $^{32}\text{S}$  and  $^{34}\text{S}$  isotopologues of dimethyl disulphide,  $(\text{CH}_3)_2\text{S}_2$ . In one experiment a stock suspension of *E. coli* was diluted to different cell concentrations in LB on the morning of the experiment and incubated for ~2 h in sealed bottles. The cell concentrations varied from no *E. coli* (neat LB), through 20%, 40%, 60%, 80% and 100% of stock solution in the same total volume of 25 mL. The contained headspace ammonia concentration was found to increase rapidly beyond the 40% stock solution (10 mL), as can be seen in Table 3, ranging from about 4 ppm to some 50 ppm. Also shown in Table 3 are the headspace

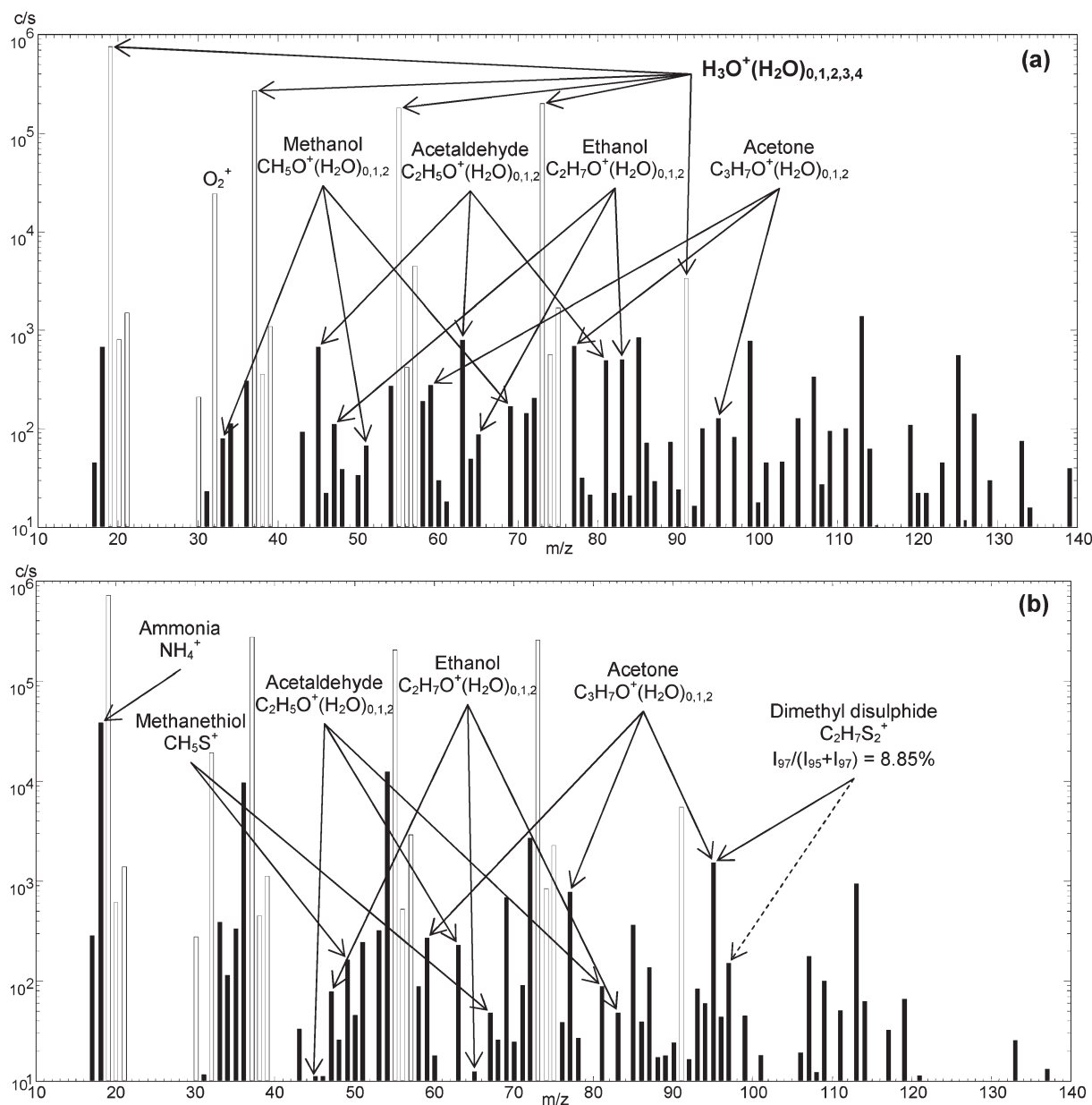


**Figure 3.** SIFT-MS spectra (counts-per-second, c/s, against mass-to-charge ratio,  $m/z$ ) obtained using  $\text{H}_3\text{O}^+$  precursor ions for the analysis of the captured (contained) headspace of (a) 25 mL of LB culture medium and (b) a highly concentrated suspension of *E. coli* in LB that had been cultured at 37°C for a total of 4 days prior to analysis. Only the positively identified major compounds are indicated. Dimethyl disulphide is identified by the abundance ratio of its characteristic isotopologue ions at  $m/z$  values of 95 and 97. Only the positively identified major compounds are indicated.

concentrations of several other compounds in the LB headspace alone (0 mL) and in the LB/*E. coli* cultures.

It is worthy of note that the detection of dimethyl disulphide, DMDS, using  $\text{H}_3\text{O}^+$  precursor ions, which would result in characteristic product ions  $m/z$  values of 95 and 97 (protonated  $(\text{CH}_3)_2^{32}\text{S}_2$  and  $(\text{CH}_3)_2^{32}\text{S}^{34}\text{S}$ ), can be confused by the presence of acetone, because an overlap occurs with the di-hydrate of protonated acetone,  $\text{CH}_3\text{COCH}_3\text{H}^+(\text{H}_2\text{O})_2$ , that also appears at  $m/z$  95. Fortunately, this overlap can be avoided by using  $\text{NO}^+$  or  $\text{O}_2^+$  precursor ions to analyse DMDS that produce characteristic product ions at  $m/z$  values of 94 and 96.

#### DMEM infected with the bacterium *Comamonas testosteroni*

During the course of this preliminary work in our laboratory it was reported by a colleague that a particular batch of DMEM was apparently infected. A colour change towards yellow of the phenol red indicator, present in the DMEM, can indicate infection if such results in a lowering of the pH, but this did not occur. In this case infection was suspected due to the cloudy appearance of the liquid. So the DMEM was assayed in the local microbiology laboratory and found to be infected with *Comamonas testosteroni*, a gram-negative soil bacterium. Headspace analysis of this infected DMEM showed the presence of large concentrations of ammonia, smaller concentrations of acetone,  $\text{CH}_3\text{SH}$ ,  $(\text{CH}_3)_2\text{S}_2$  and even a trace of butanone, as shown in Fig. 4 and Table 4. Interestingly, this bacterium appeared to remove acetaldehyde from the medium in common with some mammalian cells.<sup>[9]</sup> Note the consistency in the concentrations of the various compounds in the medium headspace given in Tables 2 and 4, even though the medium samples were taken from different batches.

## SUMMARY AND CONCLUDING REMARKS

This study reveals the clear differences between the volatile compounds produced by a single species and strain of the bacterium *E. coli* JM109, as cultured in two different media. Perhaps this is not surprising given that the bacterium must feed on the constituents of the medium and this must reflect

the products of this metabolism. Nevertheless, we could not have predicted that  $\text{H}_2\text{S}$  would be a major compound formed in DMEM by this strain of *E. coli* whereas when this bacterium is cultured in LB that  $\text{NH}_3$  is copiously produced. The headspace concentrations are such that they are readily detected and analysed by SIFT-MS when the culture is open to ambient air and a ready supply of oxygen is available. Indeed, this study shows that several volatile compounds at widely different concentrations can be detected simultaneously on-line and in real time, the data flow being so great that the kinetics of production of these volatile compounds in the cultures and the reflected emissions into the headspace (gas phase) can be accurately studied. The quality of the data is such that when there is some doubt in the designation of a particular product ion then isotopic analysis involving  $^{13}\text{C}/^{12}\text{C}$  and  $^{34}\text{S}/^{32}\text{S}$  can be carried out as an additional check.

However, it must be stressed that the headspace concentrations we have obtained for each volatile compound are clearly subject to variable parameters that we have not accounted for or carefully controlled in detail, in particular the concentration (numbers) of the cells in each medium/cell sample. Therefore, the volatile compound concentrations given are only intended to show that the emissions are high enough to be readily identified and quantified by SIFT-MS and that these several compounds can be used to monitor suspensions of growing cells. It is certain that these bacterial cells are emitting other VOCs that have not been seriously searched for in this preliminary study.

The experiments described in this short report can clearly be used to 'fingerprint' the characteristic volatile emissions from any bacterium cultured in any sustainable medium. This work was initiated by the desire to explore the value of real-time SIFT-MS analyses of the headspace of large-scale bioreactors as a check of microbial infection. The limited work we have carried out on analysing the headspace of cultured mammalian cells, malignant and non-malignant, has shown that ammonia, hydrogen sulphide and organosulphur compounds are not generated in large amounts, whereas these compounds are generated by *E. coli* and *C. testosteroni* in culture. During the course of this initial investigative study some volatile compounds emitted and consumed by uncharacterised fungal infections of cell culture media have been seen. Thus, it is apparent that acetone, acetaldehyde and ethanol are often consumed by fungi; copious amounts of

**Table 3.** Concentrations of various compounds (in parts-per-billion, ppb) as measured by SIFT-MS in the captured headspace above different concentrations of growing cultures of *E. coli* JM109 in lysogeny broth, LB

Compound	Primary precursor ion	<i>E. coli</i> added (mL) <sup>a</sup>					
		0	5	10	15	20	25
Acetaldehyde	$\text{H}_3\text{O}^+$	600	170	320	360	110	20
Ethanol		200	3000	3100	2300	900	70
Acetone		340	390	400	450	430	400
Ammonia	$\text{O}_2^+$	1700	1400	1300	5200	19,000	50,000
Dimethyl disulphide		20	30	110	140	60	140

<sup>a</sup>The bacteria were first cultured overnight in shaker flasks containing LB, resulting in a suspension containing approximately 1.5–2.0 billion cells/mL the following morning. A volume of this suspension, indicated in the top row of the table, was then added to bottles containing fresh medium, so that the final volume was always 25 mL. Note the massive increase in the ammonia, the obvious decrease in the ethanol and acetaldehyde concentration with increasing cell number and the constancy of the acetone.

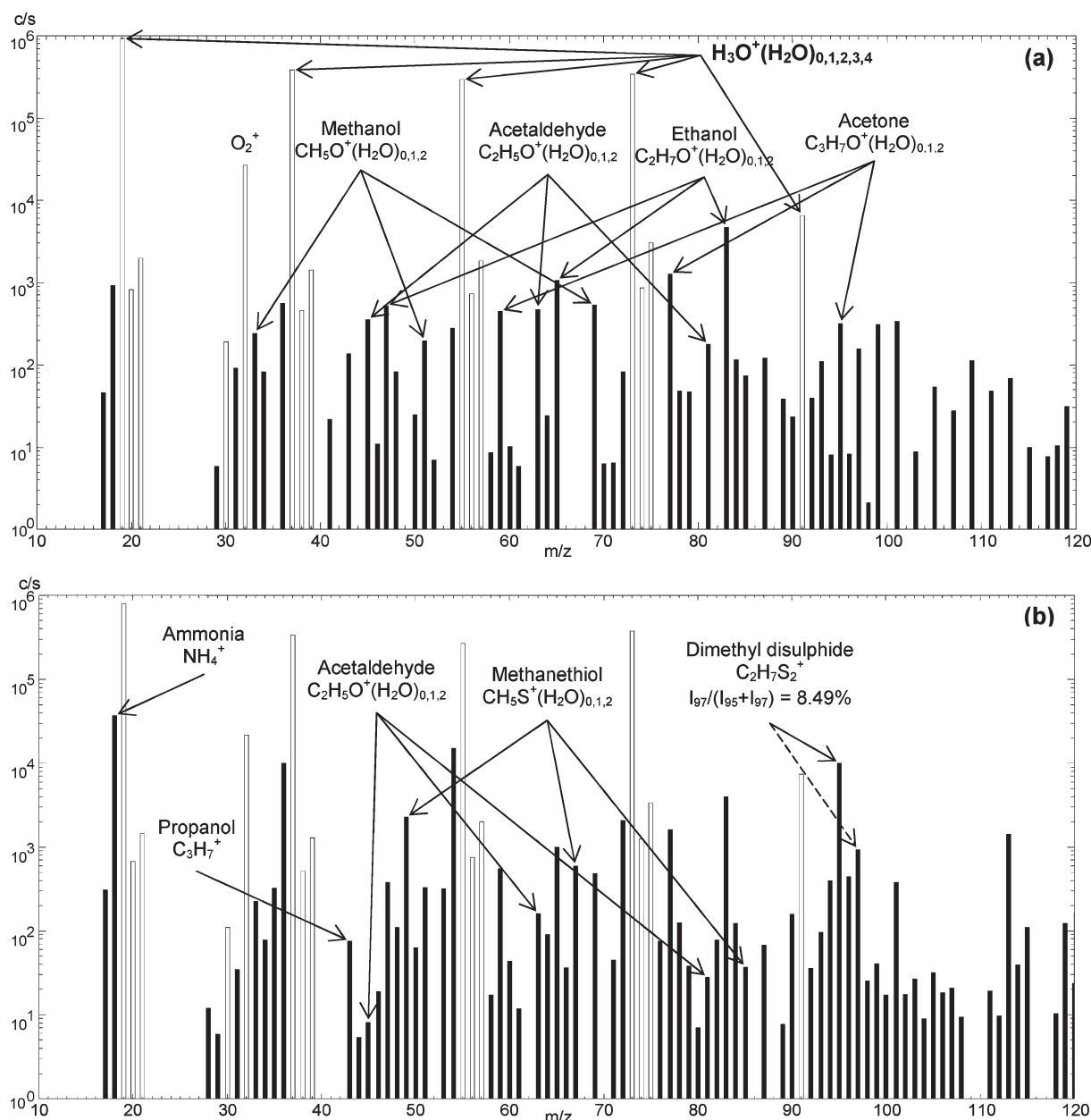


**Figure 4.** SIFT-MS spectra (counts-per-second, c/s, against mass-to-charge ratio,  $m/z$ ) obtained using  $\text{H}_3\text{O}^+$  precursor ions for the analysis of the captured (contained) headspace of (a) DMEM supplemented with 10% (v/v) FBS and 2 mM L-glutamine and (b) the same medium that had become infected with a bacterium identified as *Comamonas testosteroni*. Only the positively identified major compounds are indicated. Dimethyl disulphide is again identified by the abundance ratio of its characteristic isotopologue ions at  $m/z$  values of 95 and 97.

**Table 4.** Concentrations of selected compounds (in parts-per-billion, ppb) measured in the headspaces of two samples of DMEM supplemented with 10% FBS and 2 mM L-glutamine, one of which was known to be infected with the bacterium *C. testosteroni*

Compound	Primary precursor ions	DMEM control	DMEM infected with <i>C. testosteroni</i>
Ammonia	$\text{H}_3\text{O}^+$	300	13,200
Methanol		260	310
Hydrogen sulphide		0	200
Acetaldehyde		140	0
Ethanol		1400	1400
Methanethiol	$\text{NO}^+$	10	760
Acetone		220	330
Butanone		0	40
Dimethyl disulphide		10	2500

methanol were produced by one fungus and ammonia by another. Emissions such as these have been seen before, for example, methanol production by *Trametes versicolor* has been detected by gas chromatography,<sup>[32]</sup> and ammonia production by *Colletotrichum coccodes* has been detected by liquid-phase photometric analysis.<sup>[33]</sup> This work and our observations indicate that the use of SIFT-MS for real-time monitoring of large-scale bioreactors may assist in the detection of bacterial and fungal infection, which could be of real benefit to industry.

## Acknowledgements

We wish to thank to Alicia El Haj and Chris Hewitt for their contributions to the study of mammalian cell cultures. We gratefully acknowledge financial support by EPSRC (DTC regenerative medicine) and GACR (Project No. 203/09/0256).

## REFERENCES

- [1] R. Portner, S. Nagel-Heyer, C. Goepfert, P. Adamietz, N. M. Meenen. *J. Biosci. Bioeng.* **2005**, *100*, 235.
- [2] P. Španěl, D. Smith. *Rapid Commun. Mass Spectrom.* **1999**, *13*, 585.
- [3] P. Španěl, S. Davies, D. Smith. *Rapid Commun. Mass Spectrom.* **1999**, *13*, 1733.
- [4] D. Smith, P. Španěl, T. A. Holland, W. Al Singari, J. B. Elder. *Rapid Commun. Mass Spectrom.* **1999**, *13*, 724.
- [5] D. Smith, P. Španěl. *Analyst* **2011**, *136*, 2009.
- [6] P. Španěl, D. Smith. *Mass Spectrom. Rev.* **2011**, *30*, 236.
- [7] D. Smith, P. Španěl. *Mass Spectrom. Rev.* **2005**, *24*, 661.
- [8] D. Smith, T. S. Wang, J. Sule-Suso, P. Španěl, A. El Haj. *Rapid Commun. Mass Spectrom.* **2003**, *17*, 845.
- [9] J. Sule-Suso, A. Pysanenko, P. Španěl, D. Smith. *Analyst* **2009**, *134*, 2419.
- [10] W. Carroll, W. Lenney, T. S. Wang, P. Španěl, A. Alcock, D. Smith. *Pediatr. Pulmonol.* **2005**, *39*, 452.
- [11] B. Enderby, D. Smith, W. Carroll, W. Lenney. *Pediatr. Pulmonol.* **2009**, *44*, 142.
- [12] D. Ercolini, F. Russo, A. Nasi, P. Ferranti, F. Villani. *Appl. Environ. Microbiol.* **2009**, *75*, 1990.
- [13] P. Pierucci, E. Porazzi, M. P. Martinez, F. Adani, C. Carati, F. M. Rubino, A. Colombi, E. Calcaterra, E. V. Chemosphere **2005**, *59*, 423.
- [14] D. N. Miller, V. H. Varel. *J. Anim. Sci.* **2001**, *79*, 2949.
- [15] M. Bunge, N. Araghipour, T. Mikoviny, J. Dunkl, R. Schnitzhofer, A. Hansel, F. Schinner, A. Wisthaler, R. Margesin, T. D. Mark. *Appl. Environ. Microbiol.* **2008**, *74*, 2179.
- [16] J. M. Scotter, V. S. Langford, P. F. Wilson, M. J. McEwan, S. T. Chambers. *J. Microbiol. Methods* **2005**, *63*, 127.
- [17] R. A. Allardyce, V. S. Langford, A. L. Hill, D. R. Murdoch. *J. Microbiol. Methods* **2006**, *65*, 361.
- [18] J. M. Scotter, R. A. Allardyce, V. Langford, A. Hill, D. R. Murdoch. *J. Microbiol. Methods* **2006**, *65*, 628.
- [19] R. M. S. Thorn, D. M. Reynolds, J. Greenman. *J. Microbiol. Methods* **2011**, *84*, 258.
- [20] T. Bachinger, U. Riese, R. K. Eriksson, C. F. Mandenius. *Biosens. Bioelectron.* **2002**, *17*, 395.
- [21] K. Dryahina, F. Peהל, D. Smith, P. Španěl. *Int. J. Mass Spectrom.* **2009**, *286*, 1.
- [22] P. Španěl, K. Dryahina, D. Smith. *Int. J. Mass Spectrom.* **2006**, *249*, 230.
- [23] P. Španěl, A. M. Diskin, S. M. Abbott, T. S. Wang, D. Smith. *Rapid Commun. Mass Spectrom.* **2002**, *16*, 2148.
- [24] P. Španěl, D. Smith. *J. Phys. Chem.* **1995**, *99*, 15551.
- [25] S. Shima, J. Kato, Y. Igarashi, T. Kodama. *J. Ferment. Bioeng.* **1989**, *68*, 75.
- [26] J. Shiloach, J. Kaufman, A. S. Guillard, R. Fass. *Biotechnol. Bioeng.* **1996**, *49*, 421.
- [27] P. Španěl, D. Smith. *Rapid Commun. Mass Spectrom.* **2001**, *15*, 563.
- [28] P. Španěl, D. Smith. *Rapid Commun. Mass Spectrom.* **2000**, *14*, 1136.
- [29] P. Španěl, D. Smith. *J. Breath Res.* **2008**, *2*, 046003.
- [30] A. Pysanenko, P. Španěl, D. Smith. *Int. J. Mass Spectrom.* **2009**, *285*, 42.
- [31] P. Španěl, S. Davies, D. Smith. *Rapid Commun. Mass Spectrom.* **1998**, *12*, 763.
- [32] M. G. Paice, I. D. Reid, R. Bourbonnais, F. S. Archibald, L. Jurasek. *Appl. Environ. Microbiol.* **1993**, *59*, 260.
- [33] N. Alkan, O. Davydov, M. Sagi, R. Fluhr, D. Prusky. *Mol. Plant-Microbe Interact.* **2009**, *22*, 1484.



## Appendix B. Typical operating conditions of the SIFT-MS instrument

**Table 27.** Typical values for selected working parameters of the *Profile 3* SIFT-MS instrument used throughout this study.

Parameter	Symbol	Typical value	Unit	Reference
Flow tube (reaction) length	$l$	50	mm	[36]
End correction factor	$\varepsilon$	20	mm	[66]
Flow tube diameter	$d_t$	10	mm	[76]
Injection orifice diameter	$O_2$	1.0-2.0	mm	[36]
Ion sampling orifice diameter	$O_3$	0.3	mm	[36]
Reaction time	$t$	$5 \times 10^{-4}$	s	[36]
Bulk velocity	$v_g$	$10^4$	$\text{cm.s}^{-1}$	
Precursor ion velocity	$v_i$	$1.5 \times 10^4$	$\text{cm.s}^{-1}$	[35]
Carrier gas flow rate	$\phi_C$	11.0	$\text{Torr.l.s}^{-1}$	
		820	ml/min	
Sample flow rate	$\phi_{A,M}$	0.32	$\text{Torr.l.s}^{-1}$	
		24	ml/min	
Helium number density	[He]	$3 \times 10^{16}$	$\text{cm}^{-3}$	[145]
Flow tube pressure	$P_g$	1.0	Torr	[36]
Ion source pressure		0.5	Torr	
Precursor ion filter pressure		$10^{-4}$	Torr	[202]
Downstream mass spectrometer pressure		$10^{-4}$	Torr	
Gas temperature	$T_g$	300	K	[36]

The carrier gas flow rate,  $\phi_C$ , is approximated from the measured sample flow rate,  $\phi_{A,M}$ , using the relation:  $\phi_{A,M} = 0.1\phi_C$  [36].